

# LOAN DOCUMENT

PHOTOGRAPH THIS SHEET

①

INVENTORY

AD-A252 284



DTIC ACCESSION NUMBER

LEVEL

Proceedings of the 15th Annual Gravity  
Gradiometry Conference Vol. 2

DOCUMENT IDENTIFICATION

11-13 Feb 87

DISTRIBUTION STATEMENT A

Approved for public release:  
Distribution Unlimited

DISTRIBUTION STATEMENT

ACCESSION FOR

NTIS GRA&I  
DTIC TRAC  
UNANNOUNCED  
JUSTIFICATION



BY Per Vol. 1

DISTRIBUTION/

AVAILABILITY CODES

DISTRIBUTION

AVAILABILITY AND/OR SPECIAL

A-1

DISTRIBUTION STAMP



DTIC  
ELECT  
JUN 24 1992  
S C D

DATE ACCESSIONED

DATE RETURNED

92-16510



DATE RECEIVED IN DTIC

REGISTERED OR CERTIFIED NUMBER

PHOTOGRAPH THIS SHEET AND RETURN TO DTIC-FDAC

H  
A  
N  
D  
L  
E  
  
W  
I  
T  
H  
  
C  
A  
R  
E

AD-A252 284



Proceedings

of the

Fifteenth Annual Gravity Gradiometry Conference

United States Air Force Academy  
Colorado Springs, Colorado

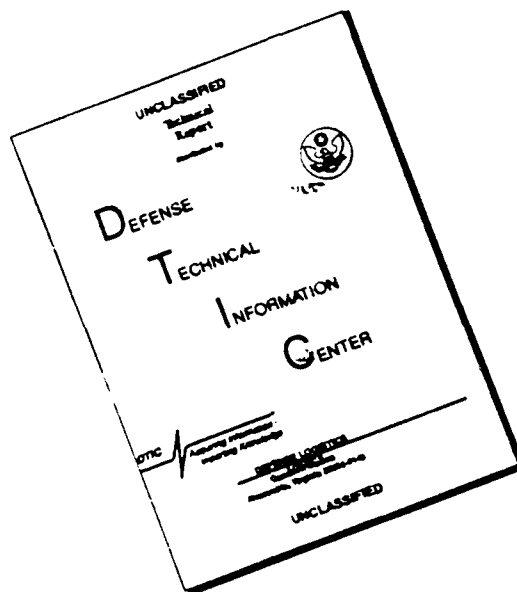
11-13 February 1987

VOLUME II

Compiled By:

Capt Vishnu V. Nevrekar, USAF  
Earth Sciences Division  
USAF Geophysics Laboratory  
Hanscom AFB, MA 01731

# DISCLAIMER NOTICE



THIS DOCUMENT IS BEST QUALITY AVAILABLE. THE COPY FURNISHED TO DTIC CONTAINED A SIGNIFICANT NUMBER OF PAGES WHICH DO NOT REPRODUCE LEGIBLY.

ABOUT THESE PROCEEDINGS.....

Due to the large number of papers presented at the Conference, I have divided the proceedings into two manageable volumes. At the beginning of each volume is a list of all papers contained in both volumes, in actual order of presentation at the Conference. This is also the sequence of the published papers within these proceedings.

For the sake of completeness, both volumes contain the Attendees List, Conference Agenda, Lists of Papers, Conference History, Acknowledgments and this explanation.

Every paper is preceded by an abstract in a standard format. Some papers may also have the original abstract included. Further, you may recall the Q&A session we had at the end of each presentation. In cases where a technical interchange did take place, the questions and answers are documented at the end of each pertinent paper. Every paper did not have a Q&A session, and I have included all Q&A sheets that were handed to me at the end of each presentation. Except for a few minor editorial changes, the information on these sheets has not been significantly altered. Obviously, these sheets are as "good" as the inputs you provided.

In summary, I hope the above explanation was helpful. I have done what I consider to be a thorough job of collecting and checking all the information for these proceedings. Errors will occur, however, and while I will entertain any comments and criticisms on this issue, these proceedings will stand as published.

Thank you for your participation, and your patience!

Capt Vishnu V. Nevrekar  
Earth Sciences Division  
USAF Geophysics Laboratory  
Hanscom AFB, MA 01731

November 1987

ABOUT THE GRAVITY GRADIOMETRY CONFERENCE .....

The First Gravity Gradiometry Conference was held at the Air Force Cambridge Research Laboratory (AFRL, now AFGL) in 1973. Its purpose was to provide a forum to evaluate and compare the efforts of three vendors (Charles Stark Draper Lab, Hughes Research Lab and Bell Aerospace Textron) in still-emerging areas of gravity gradiometry. About 15 people attended, most of them from the companies mentioned above or the Terrestrial Sciences Division at AFRL. In contrast, the 1987 Conference had a guest list of 70 plus attendees, with participation from academia (foreign and domestic), private industry and government. The papers presented were not restricted to gradiometry alone. Indeed, the scope of this annual event has broadened considerably since 1973.

With the exception of the first two conferences, all the others have been held at the US Air Force Academy in Colorado Springs, Colorado. The Geodesy and Gravity Branch of the Earth Sciences Division of the Air Force Geophysics Laboratory (AFGL), Hanscom AFB, Massachusetts, has always organized the event, which usually takes place around the second week in February. This trend is expected to continue.

If you are not already on our mailing list and would like to attend the 1988 Conference, or if you have any questions, please write to:

Ms Claire McCartney  
AFGL/LW  
Hanscom AFB, MA 01731

Due to space constraints, we restrict the size of our Conferences to about 75 people. Attendance will generally be on a "first-come, first-served basis" once the completed registration forms are returned to us. We shall mail these forms later this year.

While we have a limited number of copies of the proceedings for non-attendees of the 1987 Conference, copies of proceedings for prior years are not available. Also, we appreciate any comments or suggestions you may have regarding this document.

## ACKNOWLEDGMENTS

We couldn't possibly organize a conference the scope and size of our forum without some very diligent "behind-the-scenes" work by a few outstanding individuals. We would like to recognize their efforts and thank them for their support throughout the planning and execution of the 1987 Gradiometry Conference.

We are indebted to the Directorate of Protocol at the US Air Force Academy for allowing us to host the Conference there these past 13 years. Ms Nancy Gass was the liaison officer from the Directorate, and we gratefully acknowledge her assistance in handling all the conference arrangements, including hotel accomodation for the attendees, transportation for the Conference and NORAD/CSOC tours, luncheons during the conference and the "mixers" later in the evening, all of which were set up with great skill and professionalism.

Also, we acknowledge the outstanding efforts of TSgt Kent Droz, USAF, of the Community Relations Division at HQ NORAD, who arranged tours of the Cheyenne Mountain Complex (CMC) and the Consolidated Space Operations Center (CSOC) at Falcon AFS. These tours gave the conference attendees a first-hand look at the complex space defense environment.

Next, we thank all the speakers for taking the time to compile and present their papers for the benefit of the Conference attendees. As always, the broad mix of topics went a long way towards making the Conference an intellectually stimulating event. Indeed, the high quality of the research material presented "made" this Conference.

Finally, we thank Col J.R. Johnson, then Commander, AFGL, Dr Donald H. Eckhardt, Director, Earth Sciences Division and Dr Thomas P. Rooney, Chief, Geodesy and Gravity Branch, without whose support and guidance this Conference could not have been held.

Alphabetical Listing of Conference Participants

<u>Name</u>	<u>Organization</u>
*Georges Balmino	C.N.E.S./Bureau Gravimetrique International (FR)
Anthony Barringer	Barringer Resources, Inc
*Hans Baussus Von Luetzow	US Army Engineer Topographic Laboratory
Don Benson	Dynamics Research Corporation
Ed Biegert	Shell Development Corporation
John Binns	BP Minerals International, Ltd (UK)
*Sam Bose	Applied Science Analytics, Inc
*Carl Bowin	Woods Hole Oceanographic Institution
John Brozena	Naval Research Laboratory
Marcus Chalona	US Naval Oceanographic Office
Lindrith Cordell	US Geological Survey
Ronald Davis	Northrop Electronics Division
Mark Dransfield	University of Western Australia (AUS)
Donald Eckhardt	USAF Geophysics Laboratory
Michael Ellett	USAF Space Division
Harry Emrick	Consultant
John Fett	La Coste and Romberg Gravity Meters, Inc
Charles Finley	National Aeronautics and Space Administration
Thomas Fischetti	Technology Management Consultants, Inc
James Flx	Teledyne Geotech
Guy Flanagan	Standard Oil Production Company
*Rene Forsberg	Geodetic Institute (DEN)
Capt Terry Fundak	USAF Geophysics Laboratory
*David Gleason	USAF Geophysics Laboratory
Rob Goldsborough	USAF Geophysics Laboratory

<u>Name</u>	<u>Organization</u>
*John Graham	Defense Mapping Agency
Andrew Grierson	Bell Aerospace Textron
Michael Hadfield	Honeywell, Inc
Richard Hansen	Colorado School of Mines
Chris Harrison	Geodynamics Corporation
Ray Hassanzadeh	McDonnell Douglas
*Warren Heller	The Analytic Sciences Corporation
Howard Heuberger	Johns Hopkins University
George Hinton	Consultant
Albert Hsui	USAF Geophysics Laboratory
Gene Jackson	McDonnell Douglas
Christopher Jekeli	USAF Geophysics Laboratory
*Albert Jircitano	Bell Aerospace Textron
Col J.R. Johnson	Commander, USAF Geophysics Laboratory
J. Edward Jones	USAF Intelligence Service
J. Latimer	Johns Hopkins University
Andrew Lazarewicz	USAF Geophysics Laboratory
Thomas Little	US Naval Oceanographic Office
*Dan Long	Eastern Washington University
James Lowery III	Rockwell International
Charles Martin	University of Maryland Research Foundation
*Bahram Mashhoon	University of Missouri
*Ernest Metzger	Bell Aerospace Textron
*M. Vol Moody	University of Maryland
*Ian Moore	University of Queensland (AUS)
1Lt Vishnu Nevrekar	USAF Geophysics Laboratory
*Ho Jung Paik	University of Maryland

<u>Name</u>	<u>Organization</u>
Maj John Prince	USAF Office of Scientific Research
*Richard Rapp	Ohio State University
Richard Reineman	GWR Instruments
*Jean-Paul Richard	University of Maryland
Thomas Rooney	USAF Geophysics Laboratory
Alan Rufty	Naval Surface Weapons Center
Alton Schultz	AMOCO Production Company
*Michael Sideris	University of Calgary (CAN)
Ted Sims	Naval Surface Weapons Center
Randall Smith	Defense Mapping Agency
*David Sonnbend	CALTECH/Jet Propulsion Laboratory
Milton Trageser	Charles Stark Draper Laboratory
Gary Tuck	University of Queensland (AUS)
Herbert Valliant	LaCoste and Romberg Gravity Meters, Inc
Robert Valska	Defense Mapping Agency
*Frank van Kann	University of Western Australia (AUS)
Richard Wold	TerraSense, Inc
Robert Ziegler	Defense Mapping Agency
*Alan Zorn	Dynamics Research Corporation
Paul Zucker	Johns Hopkins University

\* Denotes Speaker at Conference

Fifteenth Gravity Gradiometer Conference  
United States Air Force Academy  
Colorado Springs, Colorado

CONFERENCE AGENDA

Tuesday, 10 February 1987

1900 - 2200 - Pre-Conference Get-Together at Hilton Inn  
Early Registration

Wednesday, 11 February 1987

0700 - Depart Hilton Inn for Fairchild Hall

0730 - Registration - 3rd floor Fairchild Hall, South End

0745 - Welcome/Introduction - Capt Terry J. Pundak

0815 - Presentation by Dr. Georges Balmino of the ONERA (Office National  
d'Etudes et de Recherches Aerospatiales).

"GRADIO Project: A SGG Mission Based on Microaccelerometers"

0845 - Presentation by Dr. G. Ian Moore of the University of Queensland.

"A Mercury Manometer Gravity Gradiometer"

0900 - Presentation by Mr. Ernest H. Metzger of Bell Aerospace Textron.

"Bell Aerospace Gravity Gradiometer Survey System (GGSS) - Program  
Review"

0925 - Presentation by Dr. Frank J. van Kann of the University of Western  
Australia.

"A Prototype Superconducting Gravity Gradiometer for Geophysical  
Exploration"

0952 - Presentation by Dr. Warren G. Heller of The Analytic Sciences Corp.

"Gravity Gradiometer Survey System (GGSS) Data Processing and Data  
Use"

1016 - Break

1035 - Presentation by Mr. Al Jircitano of Bell Aerospace Textron.

"Self-Gradient Calibration of the GGSS in a C-130 Aircraft"

- 1058 - Presentation by Dr. Sam C. Bose of Applied Sciences Analytics, Inc.  
"Gravity Gradiometer Data Processing Using the Karhunen-Loeve Method"
- 1120 - Presentation by Mr. David M. Gleason of the Air Force Geophysics Laboratory.  
"Numerically Deriving the Kernels of an Integral Predictor Yielding Surface Gravity Disturbance Components from Airborne Gradient Data"
- 1130 - Presentation by Mr. Al Jircitano of Bell Aerospace Textron.  
"Stage II Simulation Results Using the NSWC Synthetic Gravity Field"
- 1150 - Depart Fairchild Hall for USAFA Noncommissioned Officers' (NCO) Club
- 1200 - Lunch - USAFA NCO Club
- 1245 - Depart NCO Club for Fairchild Hall
- 1330 - Presentation by Dr. Richard H. Rapp of Ohio State University.  
"Gradient Information in New High Degree Spherical Harmonic Expansions"
- 1354 - Presentation by Mr. John J. Graham of the Defense Mapping Agency Aerospace Center.  
"The Effect of Topography on Airborne Gravity Gradiometer Data"
- 1357 - Presentation by Mr. Mike Sideris of the University of Calgary.  
"Effect of Terrain Representation, Grid Spacing, and Flight Altitude on Topographic Corrections for Airborne Gradiometry"
- 1417 - Presentation by Dr. Rene Forsberg of Geodetic Institute (Denmark) (Currently at the University of Calgary, Canada).  
"Topographic Effects in Airborne Gravity Gradiometry"
- 1434 - Presentation by Dr. Alan H. Zorn of Dynamics Research Corporation.  
"Observability of Laplace's Equation Using a Torsion-Type Gravity Gradiometer"
- 1510 - Break
- 1530 - Presentation by Dr. Carl Bowin of Woods Hole Oceanographic Institute.  
"Ratios of Gravity Gradient, Gravity, and Geoid for Determination of Crustal Structure"

1550 - Presentation by Dr. Rene Forsberg of Geodetic Institute (Denmark).

"Combining Gravity Gradiometry with Other Exploration  
Methods for Geophysical Prospecting"

1600 - Presentation by Dr. Rene Forsberg of Geodetic Institute (Denmark).

"Computation of the Gravity Vector from Torsion Balance Data in S.  
Ohio"

1615 - Presentation by Dr. Hans Baussus von Luetzow of the U.S. Army  
Engineer Topographic Laboratories.

"Estimation of Gravity Vector Components from Bell Gravity Gradiometer  
and Auxiliary Data under Consideration of Topography and Associated  
Analytical Upward Continuation Aspects"

1635 - Depart Fairchild Hall for the Hilton Inn

1700 - Reception - Hilton Inn

Thursday, 12 February 1987

0700 - Depart Hilton Inn for Fairchild Hall

0755 - Presentation by Dr. M. Vol Moody of the University of Maryland.

"Development of A Three-Axis Superconducting Gravity Gradiometer  
and a Six-Axis Superconducting Accelerometer"

0835 - Presentation by Dr. Bahram Mashhoon of the University of Missouri-  
Columbia.

"The Gravitational Magnetic Field of the Earth and the Possibility  
of Measuring It Using an Orbiting Gravity Gradiometer"

0905 - Presentation by Dr. Ho Jung Paik of the University of Maryland.

"Tests of General Relativity in Earth Orbit Using a Superconducting  
Gravity Gradiometer"

0928 - Presentation by Dr. Dave Sonabend of Jet Propulsion Laboratory.

"Magnetic Isolation - Closing the Loop"

0941 - Presentation by Dr. Dan Long of Eastern Washington University.

"Laboratory G(R) Experiment - Progress Report"

1004 - Break

- 1030 - Cheyenne Mountain Complex Overview  
Briefing by Maj Bill Carver, USAF  
(Chief, NORAD Presentations Division).
- 1110 - Form Groups A & B
- 1115 - Depart Fairchild Hall for USAFA NCO Club
- 1130 - Lunch - USAFA NCO Club
- 1200 - Depart USAF Academy for Falcon Air Force Station
- 1245 - Arrive Falcon AFS for briefing on 2nd Space Wing  
Tour of the Consolidated Space Operations Center (CSOC)

(Group A)

- 1415 - Depart CSOC for Cheyenne Mountain Complex (CMC)
- 1500 - Arrive CMC
- 1505 - Security in-processing and process through metal detector
- 1525 - Travel
- 1530 - Tour NORAD Command Post  
Tour Industrial Area
- 1620 - Travel/question and answer session
- 1630 - Depart for Hilton Inn
- 1715 - Arrive Hilton Inn

(Group B)

- 1415 - Depart USAF Academy for Peterson Air Force Base (AFB)
- 1445 - Arrive Peterson AFB museum
- 1600 - Depart Peterson AFB for Hilton Inn
- 1630 - Arrive Hilton Inn

Friday, 13 February 1987

- 0800 - Tour of JILA, Boulder, Colorado

Papers included in VOLUME I of the Conference Proceedings

1. \*Dr. Georges Balmino, C.N.E.S./Bureau Gravimetrique International, France  
Dr. Alain Bernard, ONERA (Office National d'Etudes et de Recherches  
Aerospaciales, France)  
Dr. Pierre Touboul, ONERA, France

"GRADIO Project: A SGG Mission Based on  
Microaccelerometers"

2. \*Dr. G. Ian Moore, University of Queensland, Australia  
Dr. Frank D. Stacey, University of Queensland, Australia  
Dr. Gary J. Tuck, University of Queensland, Australia  
Dr. Barry D. Goodwin, University of Queensland, Australia

"A Mercury Manometer Gravity Gradiometer"

3. Mr. Louis L. Pfohl, Bell Aerospace Textron  
\*Mr. Ernest Metzger, Bell Aerospace Textron

"Bell Aerospace Gravity Gradiometer Survey  
System (GGSS) - Program Review"

4. \*Dr. Frank J. van Kann, et al, University of Western Australia

"A Prototype Superconducting Gravity  
Gradiometer for Geophysical Exploration"

5. \*Dr. Warren G. Heller, The Analytic Sciences Corporation

"Gravity Gradiometer Survey System (GGSS)  
Data Processing and Data Use"

6. Dr. W. John Hutcheson, Bell Aerospace Textron  
(Paper presented by Mr. Al Jircitano of Bell Aerospace Textron)

"Self-Gradient Calibration of the GGSS  
in a C-130 Aircraft"

7. \*Dr. Sam C. Bose, Applied Science Analytics, Inc  
Mr. Glenn E. Thobe, Applied Science Analytics, Inc

"Gravity Gradiometer Data Processing Using  
the Karhunen-Loeve Method"

\* Denotes Speaker at Conference

8. \*Mr. David M. Gleason, Air Force Geophysics Laboratory

"Numerically Deriving the Kernels of an Integral  
Predictor Yielding Surface Gravity Disturbance  
Components from Airborne Gradient Data"

9. Dr. W. John Hutcheson, Bell Aerospace Textron  
(Paper presented by Mr. Al Jircitano of Bell Aerospace Textron)

"Stage II Simulation Results Using  
the NSWC Synthetic Gravity Field"

10. \*Dr. Richard H. Rapp, Ohio State University

"Gradient Information in New High  
Degree Spherical Harmonic Expansions"

Papers included in VOLUME II of the Conference Proceedings

1. \*Mr. John J. Graham, Defense Mapping Agency Aerospace Center  
Mr. Joseph L. Toohey, Defense Mapping Agency Aerospace Center  
  
"The Effect of Topography on Airborne  
Gravity Gradiometer Data"
2. Dr. Klaus-Peter Schwarz, University of Calgary, Canada  
\*Mr. M.G. Sideris, University of Calgary, Canada  
Dr. I.N. Tziavos, University of Calgary, Canada  
(Dr. Tziavos on leave from the University of Thessaloniki, Greece)  
  
"Effect of Terrain Representation, Grid Spacing, and  
Flight Altitude on Topographic Corrections for  
Airborne Gradiometry"
3. \*Dr. Rene Forsberg, Geodaetisk Institut, Denmark  
  
"Topographic Effects in Airborne Gravity Gradiometry"
4. \*Dr. Alan H. Zorn, Dynamics Research Corporation  
  
"Observability of Laplace's Equation Using  
a Torsion-Type Gravity Gradiometer"
5. \*Dr. Carl Bowin, Woods Hole Oceanographic Institute  
  
"Ratios of Gravity Gradient, Gravity, and Geoid  
for Determination of Crustal Structure"
6. Dr. Anthony A. Vassiliou, University of Calgary, Canada  
(Paper presented by Dr. Rene Forsberg, Geodaetisk Institut, Denmark)  
  
"Combining Gravity Gradiometry with other  
Exploration Methods for Geophysical Prospecting "
7. Dr. D. Arabelos, University of Thessaloniki, Greece  
Mr. Christian Tscherning, Geodaetisk Institut, Denmark  
(Paper presented by Dr. Rene Forsberg, Geodaetisk Institut, Denmark)  
  
"Computation of the Gravity Vector from Torsion  
Balance Data in Southern Ohio"

\* Denotes Speaker at Conference

8. \*Dr. Hans Baussus von Luetzow, US Army Engineer Topographic Laboratory  
"Estimation of Gravity Vector Components from Bell Gravity  
Gradiometer and Auxiliary Data under Consideration of  
Topography and Associated Analytical Upward Continuation  
Aspects"
9. Dr. H. A. Chan, University of Maryland  
Dr. Q. Kong, University of Maryland  
\*Dr. M. Vol Moody, University of Maryland  
Dr. H. J. Paik, University of Maryland  
Mr. J. W. Parke, University of Maryland  
"Development of a Three-Axis Superconducting Gravity  
Gradiometer and a Six-Axis Superconducting Accelerometer"
10. \*Dr. Bahram Mashhoon, University of Missouri-Columbia  
"The Gravitational Magnetic Field of the Earth and  
the Possibility of Measuring it Using an Orbiting  
Gravity Gradiometer"
11. \*Dr. Ho Jung Paik, University of Maryland  
"Tests of General Relativity in Earth Orbit  
Using a Superconducting Gravity Gradiometer"
12. \*Dr. Dave Sonabend, Jet Propulsion Laboratory  
Mr. A. Miguel San Martin, Jet Propulsion Laboratory  
"Magnetic Isolation-Closing the Loop"
13. \*Dr. Dan Long, Eastern Washington University  
"Laboratory G(R) Experiment - Progress Report"

PROCEEDINGS  
OF THE  
FIFTEENTH GRAVITY GRADIOMETRY CONFERENCE

VOL II PAPERS

THE EFFECT OF TOPOGRAPHY  
ON AIRBORNE GRAVITY GRADIOMETER DATA

by

Mr. John J. Graham  
Mr. Joseph L. Toohey

Defense Mapping Agency Aerospace Center  
3200 South Second Street  
St Louis MO 63118-3399

ABSTRACT

The reduction and conversion of airborne gravity gradiometer data to ground level estimates of the gravity disturbance vector is currently of considerable interest in support of short wavelength gravity modeling. A pressing problem is the need for an accurate procedure for the downward continuation of data acquired at altitude by the airborne Gravity Gradiometer Survey System (GGSS). As part of ongoing investigations, a prism method has been used to calculate the effect of topography on the gravity disturbance vector and the five independent second-order gravity gradients. Calculations of the contribution of topography to the magnitudes of these gravimetric parameters were made at both surface and elevated points in the Wichita Mountains of Oklahoma. Computations were made utilizing Digital Terrain Elevation Data (DTED) with an assumed constant density of 2.67 grams/centimeters<sup>3</sup> for the topographic masses. Results are presented which reflect the use of DTED sets of different horizontal extent and grid interval.

THE EFFECT OF TOPOGRAPHY  
ON  
AIRBORNE GRAVITY GRADIOMETER DATA

by  
John J. Graham  
&  
Joseph L. Toohey

Presented To  
Fifteenth Annual Gravity Gradiometry Conference  
United States Air Force Academy  
Colorado Springs, Colorado  
11-12 February 1987

Defense Mapping Agency Aerospace Center  
3200 South Second Street  
St. Louis, Missouri 63118-3399

## ABSTRACT

The reduction and conversion of airborne gravity gradiometer data to ground level estimates of the gravity disturbance vector is currently of considerable interest in support of short wavelength gravity modeling. A pressing problem is the need for an accurate procedure for the downward continuation of data acquired at altitude by the Airborne Gravity Gradiometer Survey System (GGSS). As part of ongoing investigations, a prism method has been used to calculate the effect of topography on the gravity disturbance vector and the five independent second-order gravity gradients. Calculations of the contribution of topography to the magnitudes of these gravimetric parameters were made at both surface and elevated points in the Wichita Mountains of Oklahoma. Computations were made utilizing Digital Terrain Elevation Data (DTED) with an assumed constant density of 2.67 grams/centimeters<sup>3</sup> for the topographic masses. Results are presented which reflect the use of DTED sets of different horizontal extent and grid interval.

# THE EFFECT OF TOPOGRAPHY ON AIRBORNE GRAVITY GRADIOMETER DATA

## I. INTRODUCTION

The field testing of the airborne Gravity Gradiometer Survey System (GGSS), being built by Bell Aerospace/Textron for the Defense Mapping Agency, is scheduled to commence before midyear. Therefore, methods for validation of the system's ability to map the local gravity field to high detail through gravity gradient measurements and their subsequent downward continuation/conversion into surface gravity disturbance components are of pressing interest. Validation can in-part be accomplished by estimating the influence of local topography on the radial disturbance, the deflection components, and the second-order gravity gradients at both surface and aloft stations. This report summarizes the results of computing topographic terrain effects from the topography above mean sea level. The terrain effects are calculated on the basis of homogeneous rectangular prisms which model the terrain masses with an assumed constant density.

The surface computation points coincide with two astro-geodetic stations located in the Wichita Mountains of Oklahoma. One is near Sunset Peak and the other is on Mount Scott as shown in Figure 1. Terrain effects were computed at these surface stations and at points directly overhead at altitude 5000 feet above the geoid. Digital Terrain Elevation Data (DTED) supplied the topographic model needed to compute the terrain effects. The main goal of the study was to determine which DTED field should make up an inner grid zone and to what radial extent outward. There was also a need to establish the coarsest DTED representation permissible for the outer zone and its span of coverage for adequate modeling of the local terrain effects on selective gravimetric quantities.

## II. DISCUSSION

### a. Objective

A major part of the short wavelength variation of the gravity field in a local area is due to topography. Therefore, especially in mountainous areas, one would anticipate the need for the best available topographic elevation data in the immediate vicinity of a computation point. At some further distance beyond this, a coarser terrain representation could be utilized to make the computational process more efficient with a minimal effect on results. With this premise, terrain effects were computed for the stations shown in Figure 1 to establish the radius of an inner zone for 3" point DTED which is our finest grain DTED. The computations also allow the determination of the largest mean DTED representation that is permissible for an outer zone and its span of coverage for adequate modeling of the local terrain effects on selective gravimetric quantities. These quantities include the radial gravity disturbance, the deflection of the vertical components, and the second-order gravity gradients. Inner zone modeling with mean DTED will indicate whether there is a need for the exclusive use of point DTED for this area. Insight into upward continuation effects is afforded with the inclusion of aloft computation points.

## b. Method of Analysis

A modified version of the Rene Forsberg prism program was run to compute the topographic terrain effects. The program is discussed in Reference 1. The right-handed coordinate system was centered at each computation station with X pointing east, Y pointing north, and Z pointing up. Prisms were formed from the geoid base up to the DTED topography of an assumed density of  $2.67 \text{ gm/cm}^3$  as illustrated in Figure 2. The integration was performed numerically using the distances from station coordinates to the eight corners of each prism. The surface station height was offset 1 cm to avoid the central prism from being automatically eliminated from the program and to avoid the station from being located within the central prism boundaries.

## c. DTED Fields Used

A 3" point DTED field was built around the stations from the same data that DMAAC sent to Bell Aerospace/Textron. Also created were 9", 12", 15", 30", 1', and 3' mean fields from the 3" point data. When using both an inner field and an outer field around a station, the prisms must properly fit together. If the inner field is the 3" DTED, then the outer mean field must be a multiple of 6" for the prisms to fit together.

## d. Formulation

Terrain mass modeling is accomplished with homogeneous rectangular prisms in the calculations. Gravitational formulas for such prisms are known from MacMillan's work on potential theory in Reference 2. The prism dimensions for this study were controlled by the description of the topography. Figure 3 shows the indefinite integral solutions that are used to compute exact values for ten gravimetric quantities at the computation point P in Figure 2 for a single prism. When the separation between a prism and the computation point permits, approximate prism formulations are used instead of the exact ones. Figure 4 gives details on how a series expansion for a prism's potential may be derived by formulating the reciprocal distance "r" as an infinite series in terms of the Legendre polynomials. Using only the first few terms of the potential series, all desired gravity quantities may be found by simple differentiation. The exact formulation is normally used for the central prism while approximate formulation is used for all remaining prisms to obtain the desired gravity quantities.

# III. RESULTS

## a. Tabular Output

Tables 1 and 2 show the effects of topographic modeling by different DTED fields within a 12' radius about the two surface stations. The various terrain fields used were 3", 9", 12", 15", 30", 1', and 3' DTED. The same investigation is repeated in Tables 3 and 4 for the computation

points at elevation 5000 feet above the geoid and directly overhead the ground stations. Terrain effect variations due to unit step increases over the interval, 6' to 13', in the radius of a central zone of 3" point DTED are shown in Tables 5 and 6 for the ground level stations. In the remaining tables, terrain effects are accounted for by employing the 3" point DTED in an inner zone and one of the mean DTED fields in an outer zone. It was discovered that the prism program requires the outer grid field to be a multiple of 6" for the prisms to properly fit together. This is the same as saying that if one extends the 3" field, then the outer mean field grid points must coincide with a 3" point. Examples of outer fields would then be 12", 30", 1', and 3'.

Tables 7 and 8 indicate variation in terrain effects caused by mean DTED representations in an outer zone of radius 30' and an inner zone radius of 12'. The means considered for the outer zone terrain modeling were 12", 30", 1' and 3' DTED. Each table displays results for one of the surface points, Sunset Peak or Mount Scott, and the related overhead point. Tables 9 and 10 reflect the usage of 1' mean DTED in two expanded outer zones, one of radius 2° and the other 2.5° with an inner zone radius of 12'. These are again composite tables for a pair of ground/aloft stations. For the ground level stations, Tables 11 and 12 indicate terrain variations due to inner zone modeling with different radial extents over the interval 1' to 10' while the outer 1' DTED zone was extended out to a radius of 2.5°. Tables 13 and 14 are composite tables for a pair of ground/aloft stations where the terrain modeling was accomplished by an inner region of 3" point DTED and an outer zone of 3' mean DTED. The radii of the inner and outer regions were 5' and 2.5°, respectively, in one case while 6' and 3° in another.

#### b. Analysis

From Tables 1-4 the pronounced decline in the ground elevation at Mount Scott with the increasingly smoother DTED modeling in a 12' central zone indicates steeper terrain here than near Sunset Peak. A 200 meter change in elevation occurred when the 1' DTED field was used instead of the best 3" point DTED representation. Tables 1 and 2 clearly show the need for the best DTED modeling in the immediate vicinity of each ground station as large gradient variations resulted even with the 9" mean DTED field. The same requirement applies to the aloft stations even though the variations are not as striking due to attenuation effects with altitude. Tables 5-6 show diminishing contributions from successive additions of 1' bandwidths of 3" point DTED to a central zone with an initial radius of 6'. The aggregate contribution of the seven 1' bands is between -23 E and -25 E on Tzz and 11-13 E on Txx and Tyy. These tables also show that the off-diagonal gradients experienced magnitude changes of less than 1 E.

Later tables will indicate an improbable need for continuance of best terrain modeling beyond the 6' radius. From Tables 7-8 the inclusion of an outer band, extending from 12' to 30', has an impact of approximately -12 E on Tzz, 5-7 E on Txx and Tyy, and between -0.02 E and 0.7 E on the off-diagonal gradients irrespective of terrain modeling by 12", 30", 1', or 3' mean DTED. This beckons the use of either the 1' or 3' mean DTED field for outer zone modeling. Tables 9 and 10 show that outer zone

modeling with the 1' mean DTED field must extend to  $2.5^{\circ}$  for the diagonal gradients to exhibit satisfactory convergence. For all cases, the span of 1' mean DTED from  $30'$  to  $2.5^{\circ}$  contributes between  $-6$  E and  $-7$  E to  $T_{zz}$  with approximately  $-0.5$  E of that coming from the band  $2^{\circ}$ - $2.5^{\circ}$ . This same half-degree width band accounts for less than  $0.4$  E to the  $T_{xx}$  and  $T_{yy}$  values. Even less contribution to the results would be expected from any band beyond  $2.5^{\circ}$  due to the nature of the kernel functions. With entries in Tables 9-10 as benchmarks, results in Tables 11-12 show that the inner grid radius for the 3" point DTED may be reduced to at least  $5'$  or  $6'$  for a  $2.5^{\circ}$  outer radius with the gradient changes being  $0.24$  E or less in absolute value. Comparing Tables 13-14 with Tables 11-12 shows that outer zone modeling, from  $5'$  to  $2.5^{\circ}$  with 3' mean DTED instead of 1' mean DTED, causes gradient changes with magnitudes no greater than  $0.41$  E. Selection of the larger mean field would reduce computer processing time in that fewer prisms are needed. It should be noted that each table contains results for the gravity disturbance and deflection of the vertical components that the reader may examine. The deflection components were more affected by distant topographic masses than the radial gravity disturbance.

When an outer grid is used, the inner grid values are extended further than they were in Tables 1 through 4. For instance when the 3' field was the outer grid and the inner radius was  $5'$  as in Table 13, the portion of fine grid used in computations agrees with that of the  $8'$  radius of Table 5. Another example is when the 1' field was the outer grid and the inner radius was  $6'$  as in Table 11. This agrees with the portion of fine grid used in computations for the  $7'$  radius of Table 5. The inner field is then extended by one unit of the outer grid spacing to form prisms that fit next to the prisms from the outer field. This explains why the outer grid must be a multiple of  $6''$  for the prisms to fit together. This also explains the increase in number of prisms for Tables 7 and 8. The 3" field was extended further out by  $1'$  and  $3'$  which caused an increase in number of prisms. However, as one increases the outer radius to  $3^{\circ}$ , a decrease in number of prisms would be seen by using a  $3'$  outer mean field rather than an outer field of higher density. Computer time is thus reduced by using the  $3'$  outer field.

#### IV. CONCLUSIONS AND FUTURE CONSIDERATIONS

The inner field must be the 3" point DTED with an inner radius of at least  $5'$ . The outer field may be 3' mean DTED with an outer radius of at least  $2.5^{\circ}$ . If the field is big enough it would be advisable to use an outer radius of  $3^{\circ}$  and an inner radius of  $6'$  in general. This would allow convergence of the topographic terrain effects within acceptable limits. The 3" inner grid contributes the major portions of the gradient values which means that the 3" elevations near the station coordinates must be as accurate as possible. An inner grid that is a less dense mean field would not yield the proper elevations near the station. The outer grid may be thought of as fine-tuning the values until convergence is achieved within acceptable limits. The 3" DTED tapes are written in  $3'$  blocks which makes it convenient to form  $3'$  mean DTED fields for the outer grid.

One must consider the computer time saved by using 3' mean DTED fields for the outer grid as large numbers of stations are computed. The number of prisms is cut down without sacrificing accuracy. About 90 seconds of CPU time is added per station with 3' mean DTED out to a radius of 3° and 3" point DTED out to a radius of 6'. The radial gravity disturbance and second-order gradients converged within desired limits. The deflection components will not converge as the outer grid radial extent is increased. Conversion of the deflections into the other two disturbance components does not give near the magnitude of the radial disturbance. We see the high frequency nature of the second-order gradients by their rapid convergence. The much lower frequency nature of the deflection components will not allow convergence in the computation of the terrain effects.

In the future it would be desirable to augment the analysis with more stations in the Wichita mountains. The spectral characteristics and covariance functions for both local topography and terrain effects should be defined. Terrain effect computation by the FFT method may be investigated in the future for reduction of computer processing time. Comparisons of GGSS gradiometry data against gradients derived from DTED fields will need to be made. It would be desirable to incorporate error propagation into the topographic terrain effects programs as errors in the DTED and density assumption become better defined. A major goal is to be able to add long and intermediate wavelength information to terrain effects for prediction of more accurate gravimetric quantities.

#### REFERENCES

1. Forsberg, Rene: A Study of Terrain Reductions, Density Anomalies and Geophysical Inversion Methods in Gravity Field Modelling; OSU Report No. 355, April, 1984
2. MacMillan, William Duncan: The Theory of Potential; Dover Publications, Inc., New York, New York; 1958

TOPOGRAPHIC TERRAIN EFFECTS  
IN THE WICHITA MOUNTAINS  
ON THE TOPOGRAPHIC SURFACE  
AND AT 5000 FT ABOVE THE GEOID

OBJECTIVE

DETERMINE DTED FIELD REPRESENTAION NEEDED FOR  
CONVERGENCE OF LOCAL TOPOGRAPHIC TERRAIN EFFECTS  
ON THE RADIAL GRAVITY DISTURBANCE, DEFLECTION  
COMPONENTS, AND SECOND-ORDER GRADIENT COMPONENTS

STUDY AREA

WICHITA MOUNTAINS OF OKLAHOMA/ASTRO-GEODETIC  
STATIONS LOCATED AT SUNSET PEAK AND MOUNT SCOTT

Sunset Peak:  $34^{\circ} 44'N$ ,  $98^{\circ} 48'W$

Mount Scott:  $34^{\circ} 44'N$ ,  $98^{\circ} 31'W$

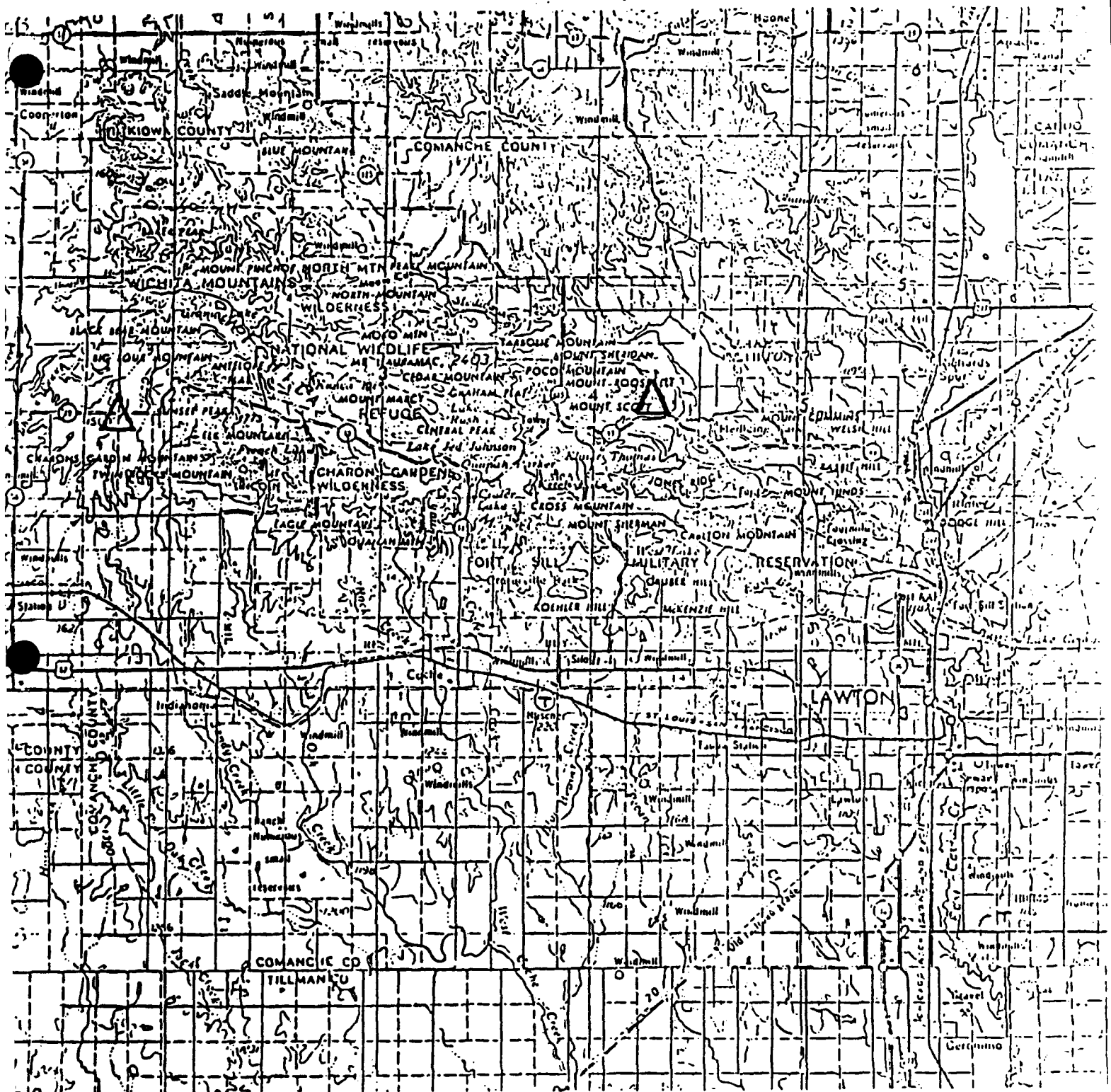


FIGURE 1. Area of Topographic Terrain Analysis - Wichita Mountains

## METHOD OF ANALYSIS

MODIFIED FORSBERG PRISM PROGRAM BASED ON EXACT FORMULATION FOR CENTRAL PRISM AND APPROXIMATE FORMULATION FOR REMAINING PRISMS WITHIN RADII

## DTED FIELDS USED

3" POINT DATA AND MEAN FIELDS OF THE 3" DATA FORMED INTO 9" , 12" , 15" , 30" , 1' , AND 3' GRIDS

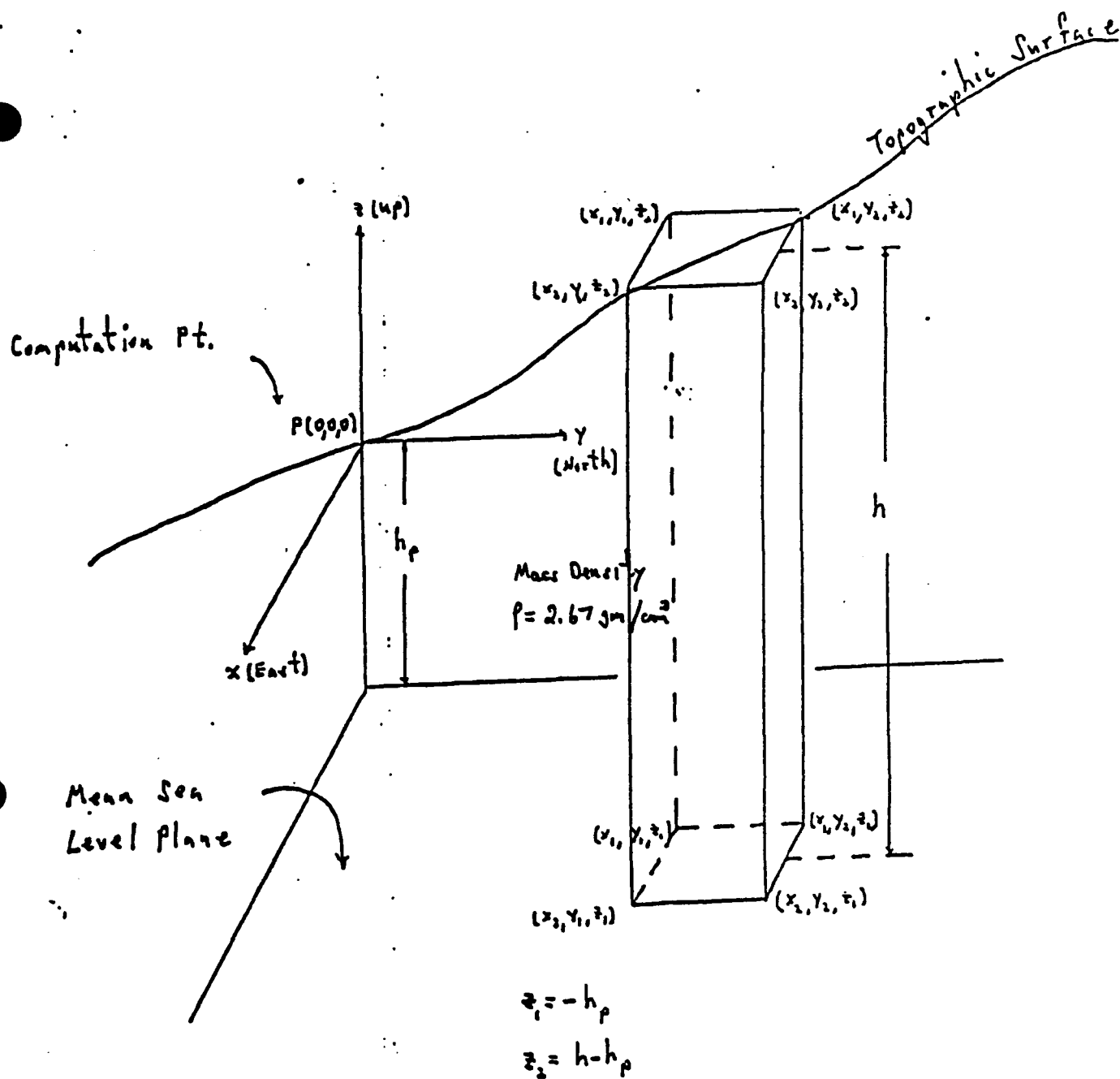


FIGURE 2. Prism Modeling of Terrain Masses

$$T_i(P) = K \rho \left\{ \left\{ \left\{ F_i(x, y, z) \right\}_{z_1}^{z_2} \right\}_{y_1}^{y_2} \right\}_{x_1}^{x_2} \right\}$$

WHERE  $F_i(x, y, z)$  IS THE SOLUTION OF THE INDEFINITE INTEGRAL

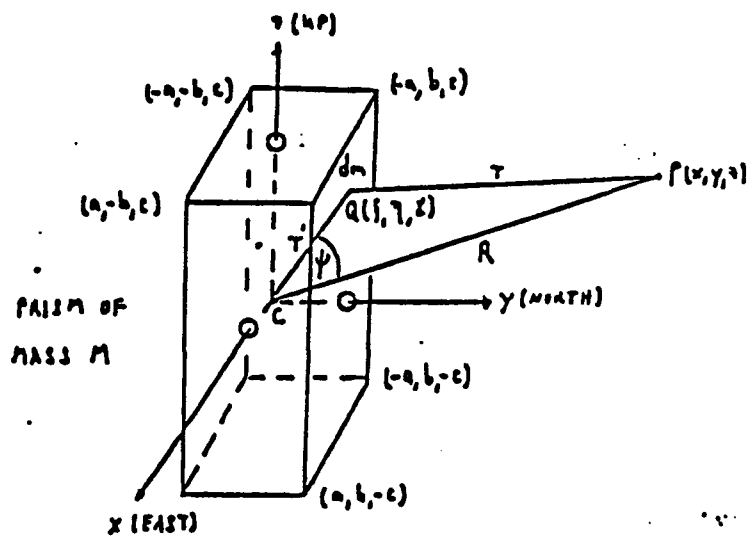
$$F_i(x, y, z) = \int \int \int h_i(x, y, z) dz dy dx$$

# GRAVITY QUANTITIES AND FUNCTIONAL EXPRESSIONS

INDEX $i$	$T_i(P)$	$h_i(x, y, z)$	$F_i(x, y, z)$
1	$T(P)$	$1/r$	$xy \ln(z+r) + xz \ln(y+r) + yz \ln(x+r) - \frac{1}{2} \left[ x^2 \tan^{-1} \left\{ \frac{yz}{xr} \right\} + y^2 \tan^{-1} \left\{ \frac{xz}{yr} \right\} + z^2 \tan^{-1} \left\{ \frac{xy}{zr} \right\} \right]$
2	$S_3(P)$	$-z/r^3$	$x \ln(y+r) + y \ln(x+r) - z \tan^{-1} \left\{ \frac{xy}{zr} \right\}$
3	$\xi(P)$	$-\frac{1}{6} \frac{y}{r^3}$	$z \ln(x+r) + x \ln(z+r) - y \tan^{-1} \left\{ \frac{xz}{yr} \right\}$
4	$\eta(P)$	$-\frac{1}{6} \frac{x}{r^3}$	$y \ln(z+r) + z \ln(y+r) - x \tan^{-1} \left\{ \frac{yz}{xr} \right\}$
5	$T_{xx}(P)$	$\frac{3x^2 - r^2}{r^5}$	$-\tan^{-1} \left\{ \frac{yz}{xr} \right\}$
6	$T_{yy}(P)$	$\frac{3y^2 - r^2}{r^5}$	$-\tan^{-1} \left\{ \frac{xz}{yr} \right\}$
7	$T_{zz}(P)$	$\frac{3z^2 - r^2}{r^5}$	$-\tan^{-1} \left\{ \frac{xy}{zr} \right\}$
8	$T_{xy}(P)$	$\frac{3xy}{r^5}$	$\ln(z+r)$
9	$T_{yz}(P)$	$\frac{3yz}{r^5}$	$\ln(y+r)$
10	$T_{zx}(P)$	$\frac{3xz}{r^5}$	$\ln(x+r)$

$$r = (x^2 + y^2 + z^2)^{1/2}$$

FIGURE 3. Exact Prism Formulation for Different Gravimetric Quantities



$$r = [(x-x)^2 + (y-y)^2 + (z-z)^2]^{1/2}$$

$$R = [x^2 + y^2 + z^2]^{1/2}$$

$$\Delta x = a$$

$$\Delta y = b$$

$$\Delta z = c$$

$$M = \rho a b c$$

$$\text{POTENTIAL: } T(x, y, z) = k \rho \int_{-c}^c \int_{-b}^b \int_{-a}^a \frac{1}{r} dx dy dz$$

SUBSTITUTION OF

$$\frac{1}{r} = \sum_{n=0}^{\infty} \frac{(r')^n}{R^{n+1}} P_n(\cos \psi) \quad \text{AND} \quad r' \cos \psi = (x^2 + y^2 + z^2)/R$$

LEADS TO THE SERIES APPROXIMATION

$$T(x, y, z) = k M \left[ \frac{1}{R} + \frac{1}{2R^3} \{ (2\Delta x^2 - \Delta y^2 - \Delta z^2) x^2 + (-\Delta x^2 + 2\Delta y^2 - \Delta z^2) y^2 \right. \\ \left. + (-\Delta x^2 - \Delta y^2 + 2\Delta z^2) z^2 \} + \frac{1}{24R^5} \{ \alpha_1(\Delta x, \Delta y, \Delta z) x^4 \right. \\ \left. + \alpha_2(\Delta x, \Delta y, \Delta z) y^4 + \alpha_3(\Delta x, \Delta y, \Delta z) z^4 + \dots + \alpha_4(\Delta x, \Delta y, \Delta z) x^2 z^2 \right. \\ \left. + \dots \right]$$

FIGURE 4. Approximative Prism Formulation of Potential T

RESULTS OBTAINED FROM MODIFIED  
FORSBERG PRISM PROGRAM USING  
VARIOUS DTED FIELDS AS INPUT

TABLE 1

SUNSET PEAK EFFECTS USING ONLY INNER RADIUS OF 12'  
AND STATION ELEVATION LOCATED ON TERRAIN SURFACE

FIELD	STN ELV (meters)	DTM ELV	DG (mgals)	KSI (arc secs)	ETA	PRISMS
3"	483	483	53.47	-1.49	-1.02	220303
9"	485	485	53.71	-1.46	-1.12	24580
12"	487	487	53.92	-1.44	-1.15	13877
15"	488	488	54.03	-1.44	-1.20	8924
30"	485	485	53.71	-1.34	-1.27	2316
60"	486	486	53.82	-1.32	-1.25	664

FIELD	Txx	Tyy	Tzz ( units in eotvos)	Txy	Txz	Tyz
3"	11.67	-14.11	2.44	31.51	-2.37	-1.19
9"	-32.68	-9.91	42.59	15.88	1.12	-0.12
12"	-43.78	-17.85	61.62	13.14	0.77	-0.50
15"	-15.88	-31.46	47.35	12.78	0.09	-0.42
30"	-13.78	-23.94	37.72	6.87	-0.10	-0.19
60"	-13.15	-12.00	25.15	0.79	-0.03	0.01

TABLE 2

MOUNT SCOTT EFFECTS USING ONLY INNER RADIUS OF 12'  
AND STATION ELEVATION LOCATED ON TERRAIN SURFACE

FIELD	STN ELV (meters)	DTM ELV	DC (mgals)	KSI (arc secs)	ETA	PRISMS
3"	701	701	71.94	-0.83	1.85	220303
9"	680	680	70.54	-0.18	1.48	24580
12"	663	663	69.31	0.11	1.35	13277
15"	643	643	67.90	0.26	1.38	8924
30"	580	580	62.87	0.49	1.61	2316
60"	499	499	55.08	0.19	2.04	664

FIELD	Txx	Tyy	Tzz ( units in eotvos)	Txy	Txz	Tyz
3"	-371.29	-371.17	742.46	-106.74	-12.48	-6.68
9"	-279.98	-349.15	629.13	-52.65	-26.52	27.72
12"	-178.41	-370.19	548.60	-52.64	-13.92	45.39
15"	-166.81	-245.44	412.24	-57.75	-4.06	24.71
30"	-48.27	-214.42	262.68	-55.98	5.05	26.15
60"	-28.51	-30.14	58.64	-7.95	1.14	0.96

TABLE

SUNSET PEAK EFFECTS USING ONLY INNER RADIUS OF 12'  
AND STATION ELEVATION 5000 FT ABOVE MEAN SEA LEVEL

FIELD	STN ELV (meters)	DTM ELV.	DG (mgals)	KSI (arc secs)	ETA	PRISMS
3"	1524	483	50.84	-1.24	-1.05	220303
9"	1524	485	50.87	-1.23	-1.06	24580
12"	1524	487	50.87	-1.22	-1.06	13877
15"	1524	488	50.88	-1.22	-1.06	8924
30"	1524	485	50.91	-1.18	-1.08	2316
60"	1524	486	51.00	-1.14	-1.10	664

FIELD	Txx	Tyy	Tzz ( units in eotvos)	Txy	Txz	Tyz
3"	-10.88	-13.99	24.88	4.48	-5.66	-7.95
9"	-10.92	-14.05	24.97	4.45	-5.95	-7.70
12"	-10.93	-14.11	25.04	4.42	-6.10	-7.59
15"	-10.96	-14.10	25.06	4.38	-6.22	-7.51
30"	-10.76	-14.05	24.81	3.96	-6.62	-7.17
60"	-11.32	-14.30	25.62	3.51	-7.09	-7.05

TABLE 4

MOUNT SCOTT EFFECTS USING ONLY INNER RADIUS OF 12'  
AND STATION ELEVATION 5000 FT ABOVE MEAN SEA LEVEL

FIELD	STN ELV	DTM ELV	DG	KSI	ETA	PRISMS
	(meters)	(mgals)	(arc secs)			
3"	1524	701	51.67	-0.71	1.76	220303
9"	1524	680	51.69	-0.63	1.73	24580
12"	1524	663	51.68	-0.60	1.71	13877
15"	1524	643	51.63	-0.57	1.71	8924
30"	1524	580	51.35	-0.43	1.66	2316
60"	1524	499	49.99	-0.32	1.63	664

FIELD	Txx	Tyy	Tzz	Txy	Txz	Tyz
			( units in eotvos)			
3"	-33.38	-51.51	84.89	-3.56	19.03	-4.61
9"	-31.60	-50.30	81.90	-3.49	16.34	1.42
12"	-30.50	-49.45	79.95	-3.59	15.29	3.93
15"	-29.31	-48.16	77.47	-3.61	14.86	5.93
30"	-24.03	-42.22	66.25	-3.07	13.32	12.80
60"	-17.26	-22.94	40.20	-0.11	14.64	13.60

SUNSET PEAK EFFECTS USING ONLY 3" INNER FIELD  
AND STATION ELEVATION LOCATED ON TERRAIN SURFACE

RADIUS	STN ELV	DTM ELV	DC	KSI	ETA	PRISMS
	(meters)	(mgals)	(arc secs)			
6'	483	483	52.85	-1.04	-0.75	55147
7'	485	485	53.02	-1.15	-0.84	75042
8'	487	487	53.15	-1.25	-0.91	97969
9'	488	488	53.26	-1.32	-0.95	123966
10'	485	485	53.34	-1.38	-0.98	153028
11'	486	486	53.41	-1.44	-1.00	185130
12'	486	486	53.47	-1.49	-1.02	220303
13'	486	486	53.52	-1.54	-1.04	258546

RADIUS	Txx	Tyy	Tzz	Txy	Txz	Tyz
			( units in eotvos)			
6'	-0.38	-25.12	25.50	30.74	-2.37	-1.18
7'	3.09	-21.80	18.71	31.03	-2.37	-1.18
8'	5.69	-19.41	13.72	31.19	-2.37	-1.18
9'	7.67	-17.60	9.93	31.29	-2.37	-1.19
10'	9.26	-16.19	6.93	31.36	-2.37	-1.19
11'	10.58	-15.05	4.47	31.44	-2.37	-1.19
12'	11.67	-14.11	2.44	31.51	-2.37	-1.19
13'	12.58	-13.33	0.75	31.58	-2.37	-1.19

TABLE 6

MOUNT SCOTT EFFECTS USING ONLY 3" INNER FIELD  
AND STATION ELEVATION LOCATED ON TERRAIN SURFACE

RADIUS	STN ELV (meters)	DTM ELV (meters)	DG (mgals)	KSI (arc secs)	ETA	PRISMS
6'	701	701	70.85	-0.27	1.24	55147
7'	701	701	71.16	-0.40	1.36	75042
8'	701	701	71.39	-0.52	1.47	97969
9'	701	701	71.57	-0.62	1.58	123966
10'	701	701	71.72	-0.70	1.68	153028
11'	701	701	71.84	-0.77	1.77	185130
12'	701	701	71.94	-0.83	1.85	220303
13'	701	701	72.02	-0.88	1.91	258546

RADIUS	Txx	Tyy	Tzz units in eotvos	Txy	Txz	Tyz
6'	-382.47	-381.84	764.31	-105.94	-12.58	-6.58
7'	-379.31	-378.59	757.90	-106.03	-12.55	-6.61
8'	-377.04	-376.19	753.23	-106.20	-12.52	-6.64
9'	-375.18	-374.44	749.61	-106.37	-12.51	-6.65
10'	-373.62	-373.10	746.72	-106.51	-12.50	-6.66
11'	-372.35	-372.03	744.38	-106.64	-12.49	-6.67
12'	-371.29	-371.17	742.46	-106.74	-12.48	-6.68
13'	-370.40	-370.46	740.86	-106.80	-12.47	-6.68

TABLE 7

SUNSET PEAK EFFECTS USING A 3" INNER FIELD OF 12'  
RADIUS AND A VARIABLE OUTER FIELD WITH A RADIUS OF 30'

FIELD	STM ELV (meters)	DTM ELV (meters)	DC (mgals)	KSI (arc secs)	ETA	PRISMS
12"	483	483	53.93	-2.07	-0.81	352933
30"	483	483	53.93	-2.07	-0.81	300082
1'	483	483	53.93	-2.07	-0.81	307791
3'	483	483	53.94	-2.04	-0.79	356794
12"	1524	483	52.61	-1.82	-0.83	352933
30"	1524	483	52.61	-1.82	-0.83	300082
1'	1524	483	52.61	-1.82	-0.84	307791
3'	1524	483	52.62	-1.79	-0.81	356794

FIELD	Txx	Tyy	Tzz ( units in eotvos )	Txy	Txz	Tyz
12"	17.56	-8.12	-9.44	31.76	-2.25	-1.21
30"	17.93	-8.14	-9.79	31.76	-2.31	-1.20
1'	17.80	-8.13	-9.68	31.76	-2.28	-1.21
3'	17.82	-8.11	-9.71	31.74	-2.28	-1.21
12"	-4.32	-8.09	12.41	4.74	-5.65	-8.04
30"	-4.30	-8.09	12.40	4.74	-5.65	-8.04
1'	-4.28	-8.09	12.37	4.73	-5.65	-8.04
3'	-4.23	-8.08	12.30	4.71	-5.65	-8.03

TABLE 8

MOUNT SCOTT EFFECTS USING A 3" INNER FIELD OF 12'  
RADIUS AND A VARIABLE OUTER FIELD WITH A RADIUS OF 30'

FIELD	STN ELV (meters)	DTM ELV (mgals)	DG	KSI (arc secs)	ETA PRISMS
12"	701	701	72.65	-1.40	2.25 352933
30"	701	701	72.65	-1.39	2.25 300082
1'	701	701	72.65	-1.38	2.25 307791
3'	701	701	72.65	-1.34	2.26 356794
12"	1524	701	53.36	-1.27	2.15 352933
30"	1524	701	53.36	-1.27	2.15 300082
1'	1524	701	53.36	-1.26	2.15 307791
3'	1524	701	53.37	-1.22	2.16 356794

FIELD	Txx	Tyy	Tzz ( units in eotvos )	Txy	Txz	Tyz
12"	-364.17	-365.78	729.95	-106.72	-12.19	-6.63
30"	-364.44	-365.76	730.20	-106.76	-12.31	-6.65
1'	-364.32	-365.77	730.08	-106.73	-12.26	-6.64
3'	-364.27	-365.76	730.03	-106.73	-12.25	-6.63
12"	-26.91	-46.09	72.99	-3.69	19.13	-4.69
30"	-26.91	-46.08	72.99	-3.68	19.11	-4.69
1'	-26.91	-46.08	72.98	-3.67	19.12	-4.69
3'	-26.88	-46.07	72.96	-3.67	19.12	-4.69

TABLE 9

SUNSET PEAK EFFECTS USING A 3" INNER FIELD WITH A 12' RADIUS AND A 1' OUTER FIELD WITH A VARIABLE RADIUS

RADIUS	STN ELV (meters)	DTM ELV (meters)	DG (mgals)	KSI (arc secs)	ETA	PRISMS
120'	483	483	54.76	-3.54	1.48	359412
150'	483	483	55.02	-3.70	2.50	390382
120'	1524	483	54.11	-3.29	1.46	359412
150'	1524	483	54.43	-3.45	2.47	390382

RADIUS	Txx	Tyy	Tzz	Txy	Txz	Tyz
		(	units in eotvos )			
120'	21.22	-5.04	-16.18	31.54	-2.26	-1.22
150'	21.55	-4.85	-16.69	31.52	-2.25	-1.22
120'	-0.87	-5.01	5.88	4.52	-5.60	-8.08
150'	-0.54	-4.82	5.36	4.50	-5.58	-8.08

TABLE 10

MOUNT SCOTT EFFECTS USING A 3" INNER FIELD WITH A 12' RADIUS AND A 1' OUTER FIELD WITH A VARIABLE RADIUS

RADIUS	STN ELV (meters)	DTM ELV (meters)	DC (mgals)	KSI (arc secs)	ETA	PRISMS
120'	701	701	73.56	-2.73	4.27	359412
150'	701	701	73.81	-2.90	5.20	390382
120'	1524	701	54.77	-2.60	4.17	359412
150'	1524	701	55.06	-2.78	5.10	390382

RADIUS	Txx	Tyy	Tzz units in eotvos )	Txy	Txz	Tyz
120'	-361.12	-362.88	724.00	-106.99	-12.23	-6.66
150'	-360.82	-362.70	723.52	-107.01	-12.22	-6.66
120'	-23.72	-43.19	66.91	-3.93	19.16	-4.73
150'	-23.41	-43.02	66.43	-3.95	19.18	-4.73

TABLE 11

SUNSET PEAK EFFECTS USING A 1' OUTER FIELD WITH A 150' RADIUS AND 3" INNER FIELD WITH A VARIABLE RADIUS. THE STATION ELEVATION IS ON THE TERRAIN SURFACE

RADIUS	STN ELV (meters)	DTM ELV (meters)	DG (mgals)	KSI (arc secs)	ETA	PRISMS
1'	483	483	55.03	-3.59	2.45	90334
2'	483	483	55.02	-3.61	2.44	98115
3'	483	483	55.02	-3.62	2.45	109885
4'	483	483	55.02	-3.63	2.47	123850
5'	483	483	55.02	-3.65	2.48	145396
6'	483	483	55.02	-3.66	2.49	166543
10'	483	483	55.02	-3.70	2.50	299309

RADIUS	Txx	Tyy (	Tzz units in eotvos )	Txy	Txz	Tyz
1'	21.84	-5.15	-16.69	31.39	-2.27	-1.23
2'	22.36	-5.39	-16.97	31.28	-2.25	-1.23
3'	22.16	-5.30	-16.86	31.22	-2.25	-1.23
4'	21.95	-5.24	-16.71	31.34	-2.25	-1.23
5'	21.79	-5.03	-16.75	31.42	-2.25	-1.22
6'	21.69	-4.98	-16.71	31.43	-2.25	-1.22
10'	21.57	-4.86	-16.71	31.51	-2.25	-1.22

MOUNT SCOTT EFFECTS USING A 1' OUTER FIELD WITH A 150' RADIUS AND 3" INNER FIELD WITH A VARIABLE RADIUS, THE STATION ELEVATION IS ON THE TERRAIN SURFACE

RADIUS	STN ELV (meters)	DTM ELV (meters)	DG (mgals)	KSI (arc secs)	ETA	PRISMS
1'	701	701	73.85	-2.89	5.18	90334
2'	701	701	73.85	-2.89	5.22	98115
3'	701	701	73.83	-2.87	5.20	109885
4'	701	701	73.83	-2.86	5.21	123850
5'	701	701	73.82	-2.86	5.21	145396
6'	701	701	73.82	-2.87	5.20	166543
10'	701	701	73.81	-2.90	5.20	299809

RADIUS	Txx	Tyy	Tzz ( units in eotvos )	Txy	Txz	Tyz
1'	-361.73	-360.62	722.35	-105.67	-12.34	-6.62
2'	-359.97	-362.07	722.04	-106.62	-12.19	-6.68
3'	-360.67	-362.08	722.75	-106.76	-12.22	-6.65
4'	-360.58	-362.46	723.03	-106.81	-12.22	-6.65
5'	-360.64	-362.68	723.32	-106.86	-12.22	-6.65
6'	-360.70	-362.73	723.44	-106.89	-12.22	-6.66
10'	-360.82	-362.70	723.53	-106.99	-12.22	-6.66

TABLE 13

FINAL SUNSET PEAK EFFECTS USING A 3" INNER FIELD AND  
A 3' OUTER FIELD WITH BOTH RADII BEING VARIABLE

RADII	STN ELV (meters)	DTM ELV (meters)	DG (mgals)	KSI (arc secs)	ETA secs)	PRISMS
5', 150'	483	483	55.03	-3.56	2.51	90649
6', 180'	483	483	55.31	-3.77	3.45	121846
5', 150'	1524	483	54.45	-3.31	2.48	90649
6', 180'	1524	483	54.79	-3.52	3.42	121846

RADII	Txx	Tyy	Tzz ( units in eotvos )	Txy	Txz	Tyz
5', 150'	22.20	-5.44	-16.76	31.11	-2.24	-1.23
6', 180'	22.17	-4.83	-17.35	31.31	-2.23	-1.22
5', 150'	0.14	-5.40	5.26	4.09	-5.58	-7.98
6', 180'	0.12	-4.80	4.68	4.28	-5.60	-8.04

TABLE 14

FINAL MOUNT SCOTT EFFECTS USING A 3" INNER FIELD AND  
A 3' OUTER FIELD WITH BOTH RADII BEING VARIABLE

RADII	STN ELV (meters)	DTM ELV (meters)	DG (mgals)	KSI (arc secs)	ETA	PRISMS
5', 150'	701	701	73.83	-2.81	5.19	90649
6', 180'	701	701	74.10	-2.97	6.15	121846
5', 150'	1524	701	55.11	-2.69	5.09	90649
6', 180'	1524	701	55.39	-2.84	6.05	121846

RADII	Txx	Tyy	Tzz ( units in eotvos )	Txy	Txz	Tyz
5', 150'	-360.34	-362.80	723.14	-106.66	-12.22	-6.65
6', 180'	-360.40	-362.56	722.96	-106.69	-12.19	-6.65
5', 150'	-22.97	-43.12	66.08	-3.61	19.14	-4.69
6', 180'	-23.02	-42.88	65.90	-3.63	19.20	-4.69

## ANALYSIS OF RESULTS

- \* TERRAIN IS STEEPER AT MOUNT SCOTT THAN SUNSET PEAK
- \* THE INNER GRID MUST BE THE 3" POINT DATA TO OBTAIN PROPER TERRAIN ELEVATIONS AT THE STATION COORDINATES
- \* THE MAJOR CONTRIBUTION TO TERRAIN EFFECTS IS LOCATED VERY CLOSE TO THE STATION COORDINATES
- \* A 3' MEAN OUTER GRID GIVES SIMILAR RESULTS TO THOSE OBTAINED BY USING A FINER GRAIN OUTER GRID
- \* AN INNER GRID RADIUS OF 5' OR 6' IS VERY ACCEPTABLE FOR CONVERGENCE OF THE TERRAIN EFFECTS
- \* AN OUTER GRID RADIUS OF 150' OR 180' IS ADEQUATE FOR CONVERGENCE OF THE TERRAIN EFFECTS

### CONCLUSIONS FROM RESULTS

- \* THE INNER GRID MUST BE THE 3" POINT DTED FIELD
- \* THE OUTER FIELD MAY BE A 3' MEAN DTED FIELD
- \* THE INNER GRID RADIAL EXTENT SHOULD BE 5' OR 6'
- \* THE OUTER GRID RADIAL EXTENT SHOULD BE 150' OR 180'
- \* THE 3" FIELD CONTRIBUTES THE MAJOR CONTRIBUTION TO THE TOPOGRAPHIC TERRAIN EFFECTS
- \* THE DEFLECTION COMPONENTS WILL NOT CONVERGE AS THE OUTER GRID RADIAL EXTENT IS INCREASED
- \* THE RADIAL GRAVITY DISTURBANCE AND SECOND-ORDER GRADIENTS CONVERGE WITHIN DESIRED LIMITS
- \* VERY ACCURATE 3" DTED IS NEEDED FOR CONVERGENCE TO THE CORRECT TOPOGRAPHIC TERRAIN EFFECT VALUES

## FUTURE CONSIDERATIONS

- \* AUGMENT THE ANALYSIS WITH ADDITIONAL STATIONS IN THE WICHITA MOUNTAINS
- \* DETERMINE THE SPECTRAL CHARACTERISTICS AND THE COVARIANCE FUNCTIONS FOR BOTH LOCAL TOPOGRAPHY AND TERRAIN EFFECTS
- \* INVESTIGATE TERRAIN EFFECTS BY FFT METHOD TO MINIMIZE COMPUTER PROCESSING TIME
- \* COMPARE GGSS GRADIOMETRY DATA AGAINST THE GRADIENTS DERIVED FROM DTED FIELDS
- \* INVESTIGATE CONSEQUENCES OF TERRAIN ELEVATION INACCURACIES AND IMPROPER DENSITY MODELING
- \* PREDICT MORE ACCURATE GRAVITY QUANTITIES BY ADDING LONG AND INTERMEDIATE WAVELENGTH INFORMATION TO TOPOGRAPHIC TERRAIN EFFECTS

EFFECT OF TERRAIN REPRESENTATION, GRID SPACING,  
AND FLIGHT ALTITUDE ON TOPOGRAPHIC CORRECTIONS  
FOR AIRBORNE GRADIOMETRY

by

Klaus-Peter Schwarz  
Michael G. Sideris  
I.N. Tziavos

The University of Calgary  
2500 University Drive N.W.  
Calgary, Alberta  
CANADA T2N 1N4

ABSTRACT

The fast Fourier transform (FFT) algorithm is used to efficiently compute terrain corrections for airborne gravity gradients. The formulation of the equations is given in detail, deriving the spectra of the gradient components of the gravitational tensor directly from the spectrum of the gravitational potential. The terrain is represented by either line masses or by prisms. Results of the method are given for a very rough digital terrain field in the Kananaskis area. Comparisons of the terrain corrections in common points for grid spacings of 0.1, 0.2, 0.3, 0.4, 0.5 and 1 km are made using the line mass and prism representation of the terrain, for two different flight altitudes. Results indicate that for a flight height of 1 km above the terrain, a 0.5 km x 0.5 km grid of elevations is adequate for an RMS accuracy of 1 Eotvos, while to retain this accuracy for a flight height of 0.6 km a grid spacing of about 0.25 km is required.

**EFFECT OF TERRAIN  
REPRESENTATION, GRID SPACING,  
AND FLIGHT ALTITUDE ON  
TOPOGRAPHIC CORRECTIONS FOR  
AIRBORNE GRADIOMETRY**

**BY**

**I.N. TZIAVOS\*, M.G. SIDERIS AND K.P. SCHWARZ**

**THE UNIVERSITY OF CALGARY  
DEPARTMENT OF SURVEYING ENGINEERING  
CALGARY, ALBERTA, CANADA**

**\* On leave from  
THE UNIVERSITY OF THESSALONIKI  
DEPARTMENT OF GEODESY AND SURVEYING  
THESSALONIKI, GREECE**

**Presented at " The 15th Gravity Gradiometer Conference ", Colorado Springs, Feb. 11-13, 1987**

# **NEED FOR ACCURATE TERRAIN CORRECTIONS**

## **MAIN SOURCES OF NOISE ( instrument independent)**

- Topographical noise
  - Due to surface topography
  - Can be minimized using DEMs and DTMs
- Geological noise
  - Due to density variations in the upper crust
  - Additional information needed for its estimation
- High frequency effects "filtered out" by flight altitude

## **REQUIRED TERRAIN CORRECTION ACCURACY**

- 1 E RMS or better at flight altitude
- Depends on
  - Terrain sampling rate (grid spacing)
  - Terrain representation (prisms or point heights)
  - Flight altitude
  - (Extent and topographic features of the area)

## **FFT EVALUATION MOST CONVENIENT**

- Fastest approach for large data files
- Availability of DEMs
- Homogeneous coverage in results
- Spectral analysis and interpretation

# **OBJECTIVES**

## **DERIVATION OF CONVENIENT COMPUTATIONAL FORMULAS**

- 2D convolution integrals  
Fast evaluation using 2D FFT routines
- Relationship between spectra of prisms and point heights

## **ESTIMATE THE EFFECT OF GRID SPACING**

- 0.1km x 0.1km grid results used as control values
- 0.2km, 0.3km, . . . , 1km grid results compared to those of 0.1km grid for 1.1km flight altitude ( $z_f = 1.1\text{km}$ )

## **ESTIMATE THE EFFECT OF TERRAIN REPRESENTATION**

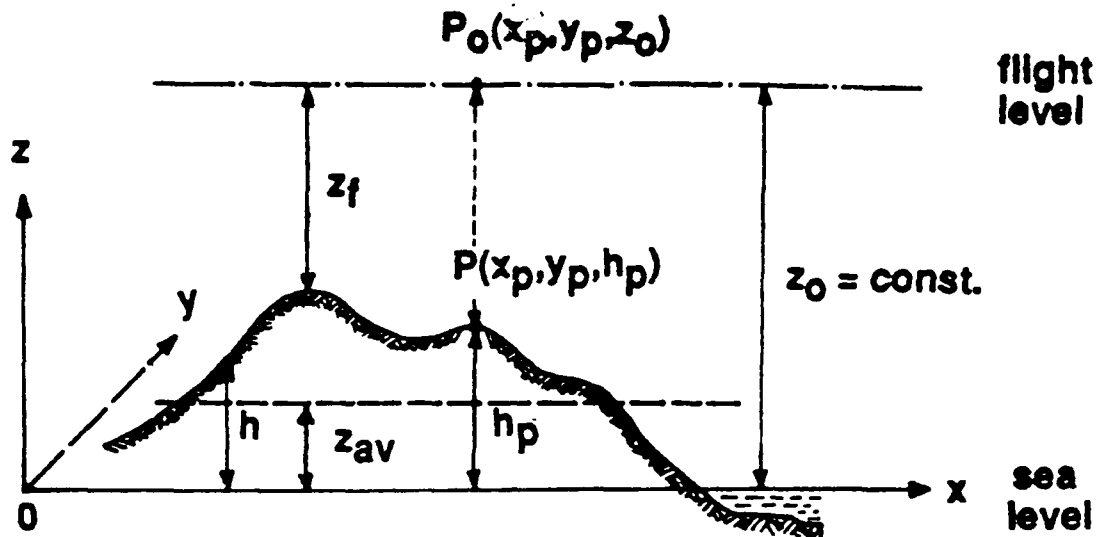
- Prism representation results versus point height results
- Comparison for a grid spacing of 1km and  $z_f = 1.1\text{km}$

## **ESTIMATE THE EFFECT OF FLIGHT ALTITUDE**

- $z_f = 1.1\text{km}$  and  $z_f = 0.6\text{km}$  were used
- Comparison for various grid spacings

**PROPOSE THE GRID SPACING AND TERRAIN REPRESENTATION NECESSARY FOR A 1E OR BETTER RMS ACCURACY AT FLIGHT LEVEL**

## COMPUTATIONAL FORMULAS



POTENTIAL OF TOPOGRAPHY AT  $P_0$

$$V(x_p, y_p, z_0) = G_p \int \int \int_0^h \frac{dx dy dz}{E [s^2 + (z - z_0)^2]^{1/2}}, \quad s^2 = (x - x_p)^2 + (y - y_p)^2 \quad (1)$$

### GRAVITY TERRAIN CORRECTION AT $P_0$

$$t(x_p, y_p, z_0) = - \frac{\partial V(x_p, y_p, z_0)}{\partial z_0} = G_p \int \int \int_0^h \frac{z - z_0}{E [s^2 + (z - z_0)^2]^{3/2}} dx dy \quad (2)$$

- Series expansion of (2) around  $z_{av}$ , neglecting orders higher than 2nd, gives in convolution form

$$t(x_p, y_p, z_0) = - 2\pi G_p z_{av} + G_p [h_1(x_p, y_p) * k_1(x_p, y_p) + h_2(x_p, y_p) * k_2(x_p, y_p)] \quad (3)$$

( = Bouguer affect + effect of residual topography )

$$\begin{aligned}
h_1(x,y) &= h(x,y) - z_{av} , & h_2(x,y) &= [h(x,y) - z_{av}]^2 \\
k_1(x,y) &= -(z_0 - z_{av}) / [x^2 + y^2 + (z_0 - z_{av})^2]^{3/2} \\
k_2(x,y) &= 1/2 [x^2 + y^2 + (z_0 - z_{av})^2]^{3/2} \\
&\quad - 3(z_0 - z_{av})^2 / [x^2 + y^2 + (z_0 - z_{av})^2]^{5/2}
\end{aligned} \tag{4}$$

- FFT evaluation of (3) :  $t_z(x_p, y_p, z_0) = F^{-1}\{TZ(u,v)\}$  (5)

$$\begin{aligned}
TZ(u,v) &= F\{t_z(x_p, y_p, z_0)\} = -2\pi G\rho z_{av}\delta(u,v) \\
&\quad + G\rho [H_1(u,v) K_1(u,v) + H_2(u,v) K_2(u,v)]
\end{aligned} \tag{6}$$

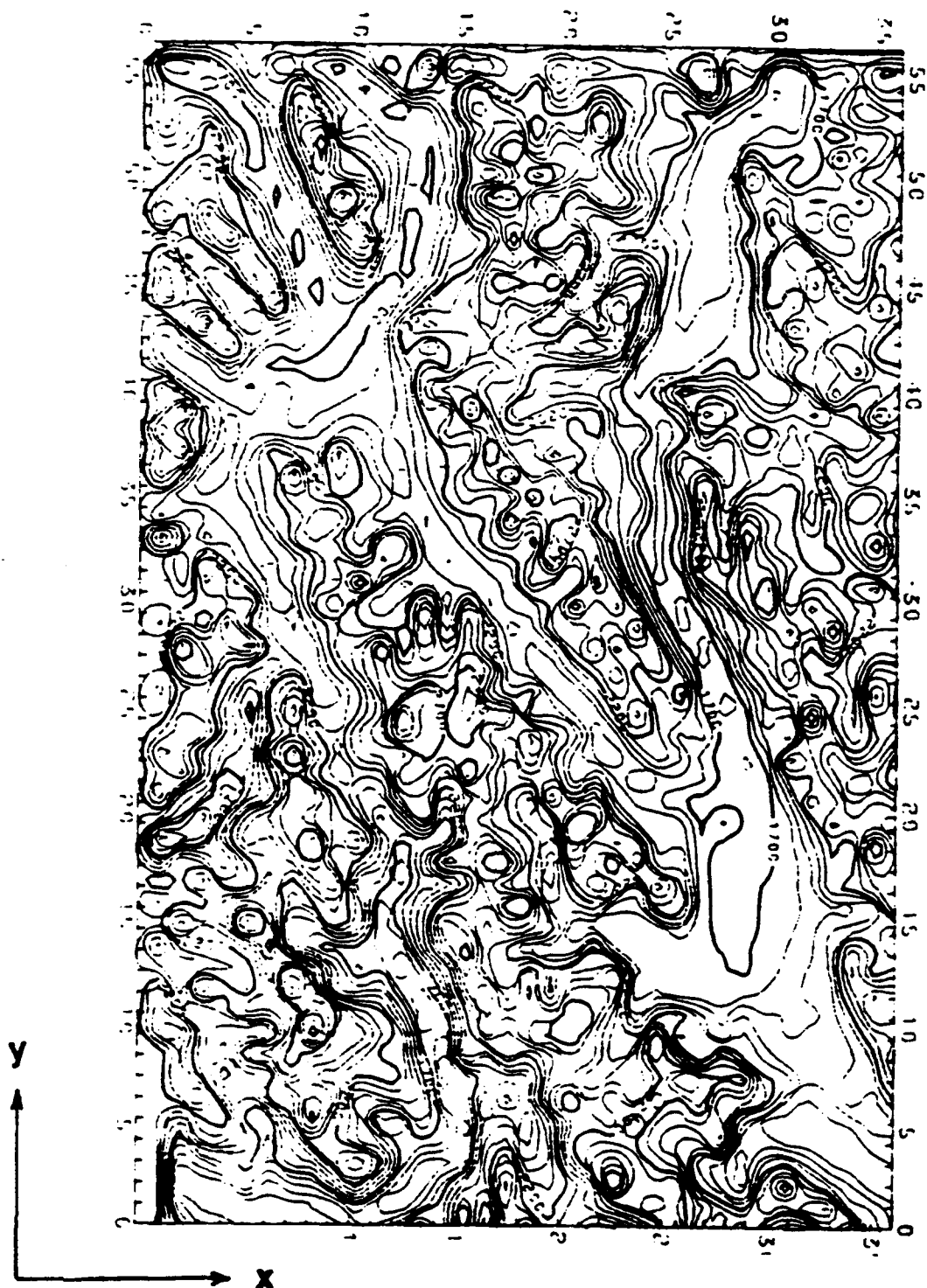
$$\begin{aligned}
H_1(u,v) &= F\{h_1(x,y)\} , & H_2(u,v) &= F\{h_2(x,y)\} \\
K_1(u,v) &= F\{k_1(x,y)\} = -2\pi e^{-2\pi q(z_0 - z_{av})} \\
K_2(u,v) &= F\{k_2(x,y)\} = -2\pi^2 q e^{-2\pi q(z_0 - z_{av})}
\end{aligned} \tag{7}$$

**GRADIENT TENSOR COMPONENTS AS DERIVATIVES OF  $t_z$  OR  $t$**

$$\begin{aligned}
t_{zx}(x,y) &= F^{-1}\{TZX(u,v)\} , & TZX(u,v) &= 2\pi i u TZ(u,v) \\
t_{zy}(x,y) &= F^{-1}\{TZY(u,v)\} , & TZY(u,v) &= 2\pi i v TZ(u,v) \\
t_{zz}(x,y) &= F^{-1}\{TZZ(u,v)\} , & TZZ(u,v) &= 2\pi q TZ(u,v) \\
t_{xx}(x,y) &= F^{-1}\{TXX(u,v)\} , & TXX(u,v) &= -2\pi u^2 q^{-1} TZ(u,v) \\
t_{xy}(x,y) &= F^{-1}\{TXY(u,v)\} , & TXY(u,v) &= -2\pi u v q^{-1} TZ(u,v) \\
t_{yy}(x,y) &= F^{-1}\{TYY(u,v)\} , & TYY(u,v) &= -2\pi v^2 q^{-1} TZ(u,v)
\end{aligned} \tag{8}$$

$$TXX(u,v) + TYY(u,v) + TZZ(u,v) = 0 \quad \text{or} \quad -u^2 - v^2 + q^2 = 0 \tag{9}$$

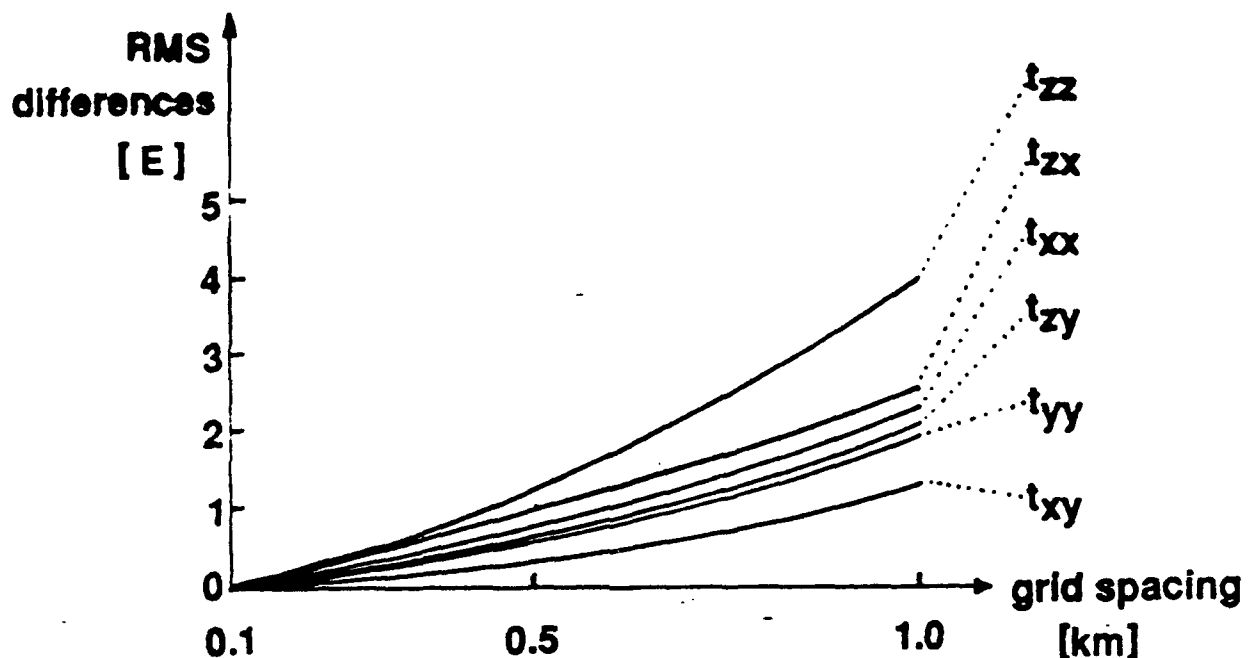
# 2D PLOT OF THE TEST AREA 1km x 1km DTM



**STATISTICAL ANALYSIS OF TOPOGRAPHY AND TERRAIN  
CORRECTIONS IN THE 36 km x 56 km TEST AREA OF ROUGH  
TOPOGRAPHY USING A 0.1km x 0.1km GRID OF POINT HEIGHTS**

Statistics	Topo- graphy	$\Delta g$ corr.		Corr. for $t_{ij}$ at $z_o = 4.5$ km ( $z_f = 1.1$ km)					
		z=hp	z=z <sub>o</sub>	t <sub>xx</sub>	t <sub>xy</sub>	t <sub>xz</sub>	t <sub>yy</sub>	t <sub>yz</sub>	t <sub>zz</sub>
	meters	mgal		Eotvos					
min	1378.0	-313.1	46.6	-76.7	-40.7	-74.9	-45.9	-62.8	-129.7
max	3413.0	-141.0	14.6	72.0	38.9	82.4	70.5	69.2	86.5
mean	2129.6	-226.7	-15.1	0.0	0.3	4.6	0.8	-3.5	-0.8
s. d.	350.2	37.3	12.2	35.7	14.6	37.2	18.5	23.9	45.5
RMS	2158.2	229.7	19.4	35.7	14.6	37.5	18.5	24.1	45.5

## EFFECT OF GRID SPACING ( USING POINT HEIGHTS AND $z_f = 1.1\text{km}$ )



- z-components more sensitive than the horizontal
- Effect on the horizontal components dependent on the terrain frequency content along the x and y-direction
- 1km grid insufficient for  $< 1E$  RMS accuracy
- 0.5km grid sufficient for  $< 1E$  RMS accuracy
- 0.25km - 0.35km grid spacing necessary for  $< 0.5 E$  RMS accuracy
- Bias always  $< 1E$  for 1km grid  
 $< 0.35 E$  for 0.5 km grid

# EFFECT OF TERRAIN REPRESENTATION ( FOR $z_f = 1.1\text{km}$ )

DIFFERENCES BETWEEN THE RESULTS FROM PRISMS AND FROM  
POINT HEIGHTS AT FOR A 1km x 1km GRID

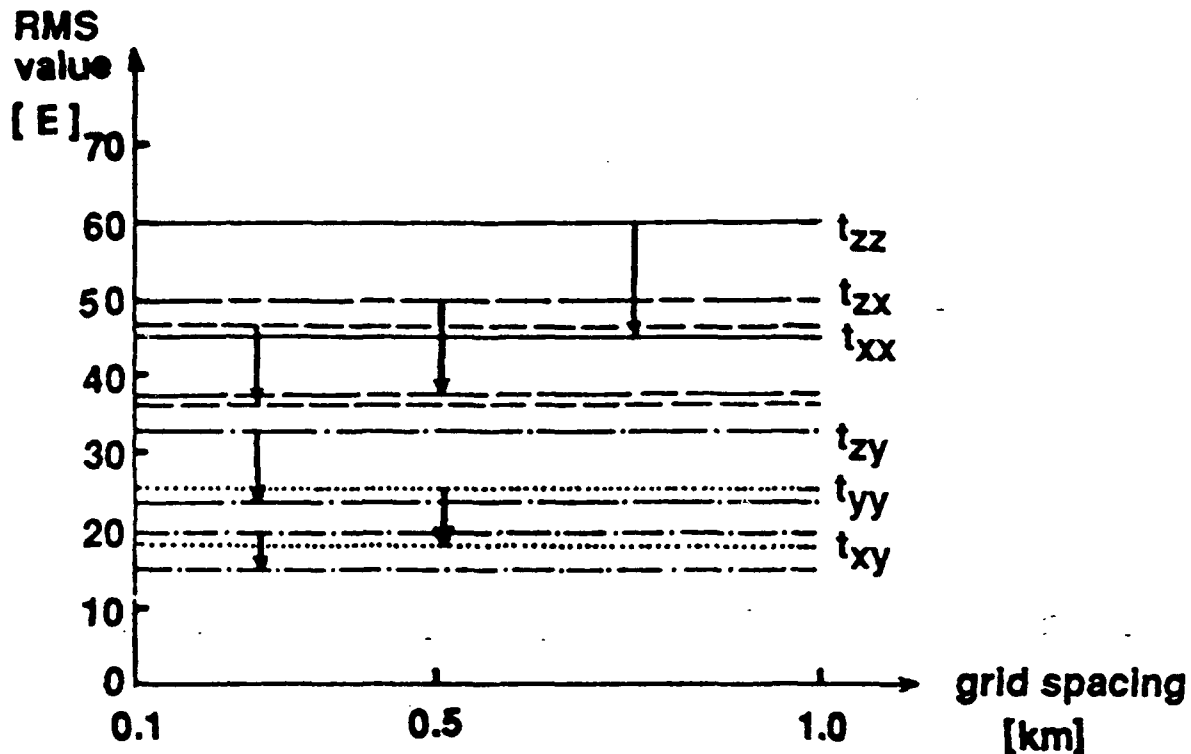
Terrain correction differences, in E , for $t_{ij}$ at $z_f = 1.1\text{km}$						
Statistics	$t_{xx}$	$t_{xy}$	$t_{xz}$	$t_{yy}$	$t_{yz}$	$t_{zz}$
min	-6.2	-1.5	-7.0	-1.6	-2.1	-7.3
max	6.5	1.1	8.1	1.5	1.6	6.5
mean	0.4	0.0	0.5	0.0	0.0	-0.4
s . d .	3.5	0.4	3.5	0.5	0.6	3.6
RMS	3.5	0.4	3.5	0.5	0.6	3.6

- If  $\overline{TZ}(u,v)$  is the spectrum of  $t_z(x,y)$  computed from prisms and  $TZ(u,v)$  is the spectrum computed from point heights , then

$$\overline{TZ}(u,v) = \frac{\sin(u\pi\Delta x)}{u\pi\Delta x} \frac{\sin(v\pi\Delta y)}{v\pi\Delta y} TZ(u,v) \quad (10)$$

- Prism representation has smoothing effect on high frequencies
- x-components more affected than the y-components because this particular terrain has more high frequency content in the x-direction
- Differences of up to a few E are to be expected in the more sensitive components

## EFFECT OF FLIGHT ALTITUDE (USING POINT HEIGHTS)



high values :  $z_f = 0.6\text{km}$  ( $z_0 = 4\text{km}$ ) ; low values :  $z_f = 1.1\text{km}$  ( $z_0 = 4.5\text{km}$ )

- Attenuation stronger for z-components
- x-components attenuated more than y-components due to unisotropic terrain frequency distribution
- Attenuation independent of grid spacing
- Accuracy of results dependent on grid spacing / altitude ratio  
0.25km grid to be used with  $z_f = 0.6\text{km}$  above very rough terrain for  $< 0.5\text{ E}$  RMS accuracy

# **CONCLUSIONS**

## **TERRAIN CORRECTIONS NEEDED TO CORRECT FOR THE " TOPOGRAPHIC NOISE " ON THE MEASURED GRADIENTS**

**REQUIRED ACCURACY AT FLIGHT LEVEL :  $0.5 \text{ E} - 1\text{E}$**

- Depends on
  - Grid spacing
  - Terrain representation
  - Flight altitude
- Effects on horizontal components depend on terrain frequency content along the x and y-direction

### **GRID SPACING**

- Affects more the z-components
- Accuracy decreases with increase of grid spacing

### **TERRAIN REPRESENTATION**

- Point and prism results can differ by a few E RMS
- Prism representation is more accurate

### **FLIGHT ALTITUDE**

- Stronger attenuation for z-components
- Attenuation effect rather insensitive to grid spacing

## **RECOMMENDATIONS**

### **FFT TECHNIQUES RECOMMENDED FOR THE COMPUTATIONS**

- Convenient formula derivations in the spectral domain
- Speed, easy handling of large data sets
- Homogeneous coverage
- Frequency domain analysis and interpretation of data and results

**FOR  $z_f = 1.1\text{km}$  AND  $z_f = 0.6\text{km}$  ,  $0.5\text{ km}$  AND  $0.25\text{ km}$  GRID SPACINGS RESPECTIVELY ARE NECESSARY FOR  $< 1\text{E}$  RMS ACCURACY**

**$\Delta x / z_f = 1 / 3$  appears to be a good choice**

**ACCURACY EFFECT OF HIGHER THAN 2nd ORDER TERMS IN THE EQUATIONS TO BE INVESTIGATED**

# TOPOGRAPHIC EFFECTS IN AIRBORNE GRAVITY GRADIOMETRY

by

Rene Forsberg  
Geodaetisk Institut  
Gamlehave Alle 22  
2920 Charlottenlund  
Denmark

## ABSTRACT

The gravitational signal due to terrain masses will play a dominant role in airborne gravity gradiometer surveys over mountainous areas. The variations in the gravity gradient tensor elements may easily attain magnitudes of several hundred Eotvos units, thus being much larger than typical signals associated with possible geophysical structures of interest.

To smooth the gradient field and enhance "geological" gravity gradient anomalies, the gravitational "noise" caused by the topography may be attenuated using available digital terrain models, from which the elements of the terrain - induced gradient tensor may be computed efficiently at aircraft altitude using either space domain (integration) or frequency domain (FFT) methods.

In the paper, both of these computation methods are outlined and compared, and typical magnitudes of the effects are illustrated by examples from the Rocky Mountains. In general, statistics of the gradient variations may be inferred rather easily from empirical ACF parameters of the topographic heights, and the paper concludes with a number of such examples for areas of different types, from lowlands to high mountains, yielding useful "hand rules" for the gravity gradient terrain effects in future gravity gradiometer surveys in particular areas.

# TOPOGRAPHIC EFFECTS IN AIRBORNE GRAVITY GRADIOMETRY

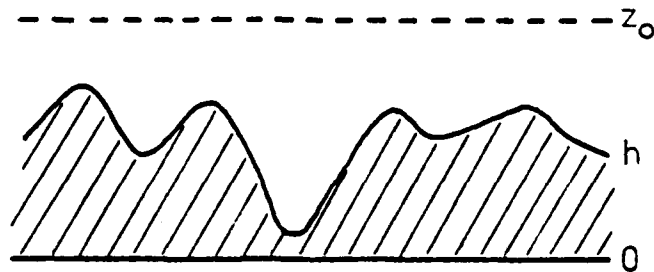
*Rene Forsberg*

*Danish Geodetic Institute*

## Overview of talk:

- why terrain reductions?
- practical computations (integration  
or fit methods)
- examples: New Mexico and Colorado
- covariance analysis

TERRAIN REDUCTION: REMOVAL OF GRAVITATIONAL SIGNAL DUE  
TO TOPOGRAPHY IN A CONSISTENT MANNER



0 GEOPHYSICAL EXPLORATION

- ENHANCE GEOLOGICAL SIGNAL
- EXAMPLE: SIGNAL 10-20 E, TOPOGRAPHY 50-100E

0 GEODETIC GRAVITY FIELD MODELLING

- MORE SMOOTH FIELD
- MORE STABLE DOWNWARD CONTINUATION
- REMOVE-RESTORE TECHNIQUE

0 LOCAL TERRAIN EFFECTS ON SECOND-ORDER GRADIENTS:

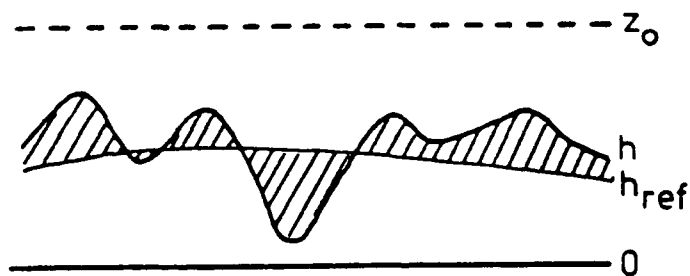
- MORE SMOOTH FIELD
- MORE STABLE DOWNWARD CONTINUATION
- REMOVE-RESTORE TECHNIQUE

0 LOCAL TERRAIN EFFECTS ON SECOND-ORDER GRADIENTS:

- VERY LARGE ON GROUND, REQUIRES VERY DETAILED HEIGHTS
- AIRBORNE GRADIOMETRY: ATTENUATION,

## 0 MODIFICATIONS FOR OPTIMAL GRAVITY FIELD MODELLING (COLLOCATION ETC.)

- IMPORTANT TO AVOID BIAS IN COMPUTED TERRAIN EFFECTS, ESPECIALLY FOR COMBINATION SOLUTIONS WITH TERRESTRIAL GRAVITY AND DEFLECTIONS.
- BIAS OCCUR IN  $T_{XX}$ ,  $T_{YY}$ , AND  $T_{ZZ}$  WHEN COMPUTATION AREA FINITE AND MEAN HEIGHT  $> 0$ !
- REMEDY: REFER TO MEAN HEIGHT OR USE ISOSTASY!
- BETTER REMEDY: RTM - RESIDUAL TERRAIN MODEL



### RTM ADVANTAGES:

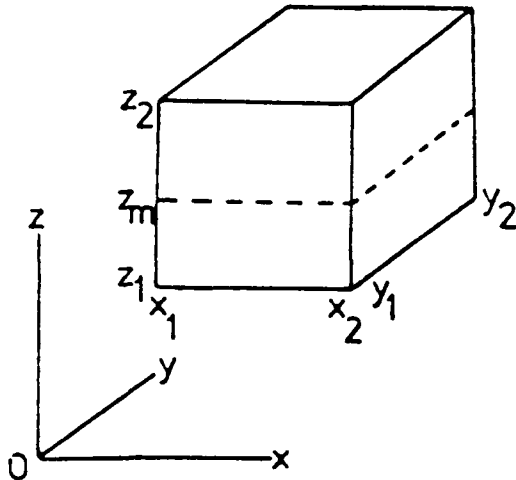
- HEIGHT DATA NEEDED FOR SMALLER AREA
- CONSISTENCY OF NEIGHBOURING SURVEYS
- CONSISTENCY IN PRISM AND FFT METHODS

# COMPUTATION METHODS:

## PRISM INTEGRATION AND FFT

### 1) PRISM METHOD

#### NUMERICAL METHOD



$$T_{zz} = G\rho \left[ \left[ -\arctan \frac{xy}{zr} \right]_{x_1}^{x_2} \left[ \right]_{y_1}^{y_2} \left[ \right]_{z_1}^{z_2} \right]$$

$$T_{xz} = G\rho \left[ \left[ \log(y+r) \right]_{x_1}^{x_2} \left[ \right]_{y_1}^{y_2} \left[ \right]_{z_1}^{z_2} \right]$$

APPROXIMATE FORMULAS (McMILLAN):

$$T = GM \left( \frac{1}{r} + \frac{1}{24r^5} f \right)$$

$$f = ax^2 + by^2 + cz^2, \quad a = 2\Delta x^2 - \Delta y^2 - \Delta z^2 \dots$$

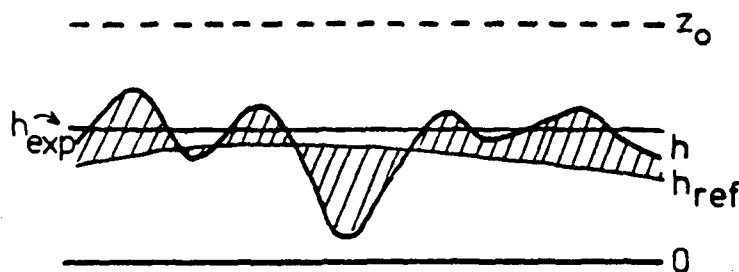
↓

$$T_{zz} = GM \left( \frac{3z^2 - r^2}{r^5} + \frac{1}{24r^5} \left[ \frac{35z^2f - 5r^2f}{r^4} - 20 \frac{cz^2}{r^2} + 2c \right] \right)$$

$$T_{xz} = GM \left( -\frac{3xz}{r^5} + \frac{1}{24r^5} \left[ \frac{35xz f}{r^4} - 10 \frac{(a+c)xz}{r^2} \right] \right)$$

IMPLEMENTATION: DETAILED / COARSE GRID, INNERZONE SPLINE,  
AUTOMATIC FORMULA SELECTION

## 2) FFT METHOD: PARKER EXPANSION



$$\tilde{T}(u,v) = 2\pi G \rho e^{-\omega(z_0 - z_{exp})} \sum_{n=1}^{\infty} \frac{\omega^{n-2}}{n!} F\{(h - z_{exp})^n - (h_{ref} - z_{exp})^n\}$$

FF: FOURIER TRANSFORMATION,  $\omega = (u^2 + v^2)^{\frac{1}{2}}$

GRADIENTS:

$$\begin{aligned} \tilde{T}_{xx} &= -u^2 \tilde{T} \\ \tilde{T}_{yy} &= -v^2 \tilde{T} \\ \tilde{T}_{zz} &= \omega^2 \tilde{T} \\ \tilde{T}_{xy} &= -uv \tilde{T} \\ \tilde{T}_{xz} &= -iu\omega \tilde{T} \\ \tilde{T}_{yz} &= -iv\omega \tilde{T} \end{aligned}$$

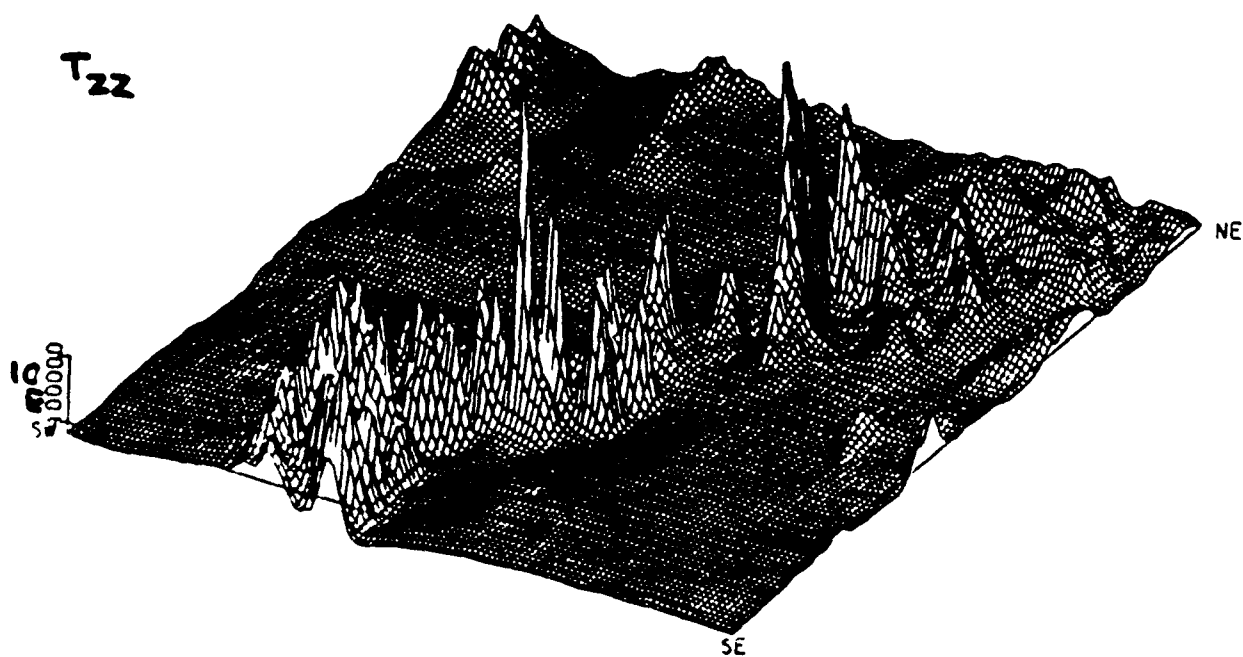
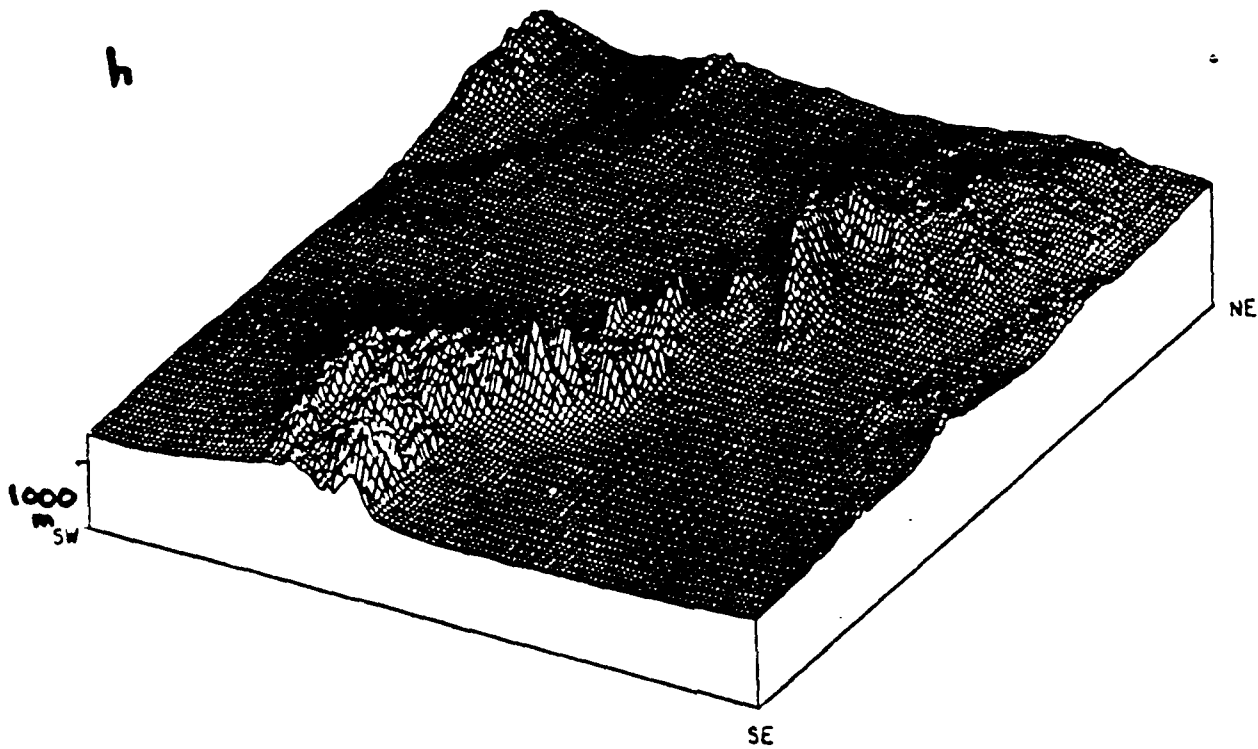
IMPLEMENTATION -H, H<sup>2</sup>, ... REAL TRANSFORMS

-COMPLEX FILTER INVERSE TRANSFORM: PAIRWISE RESULTS

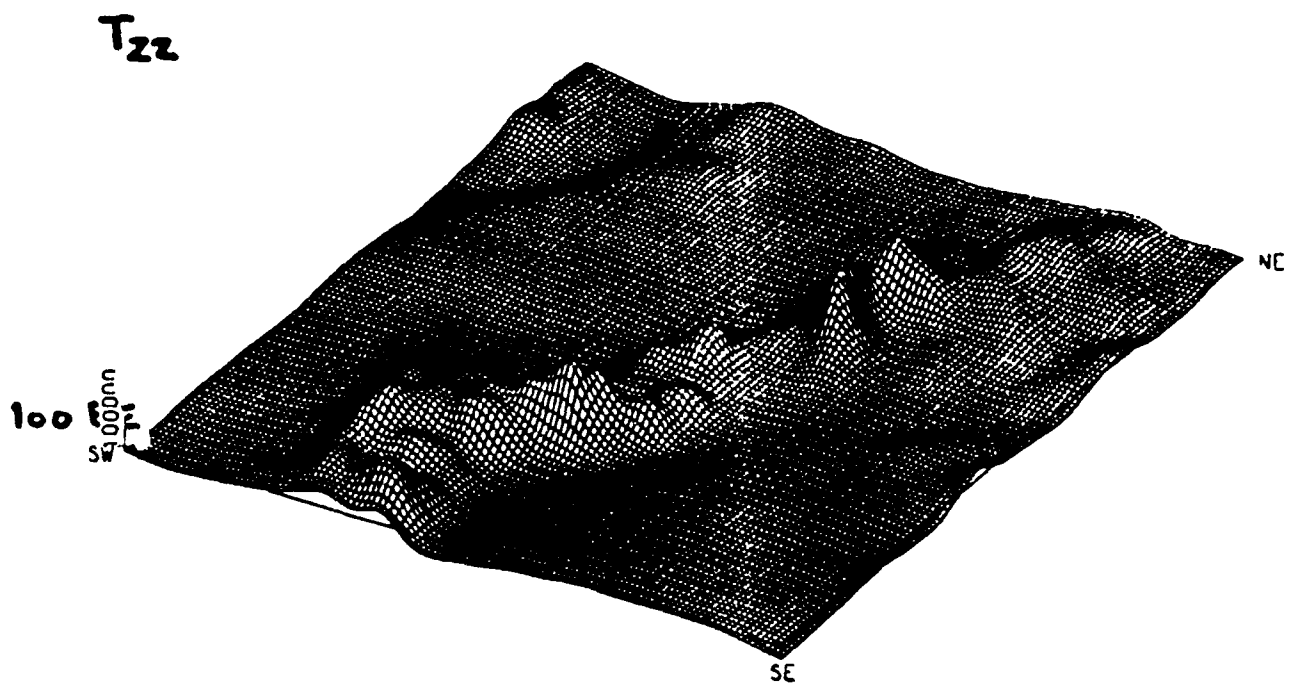
EXAMPLE: WHITE SANDS, NEW MEXICO

33°N - 34°N, 107°W - 106°W, ELEV. 3000 M.

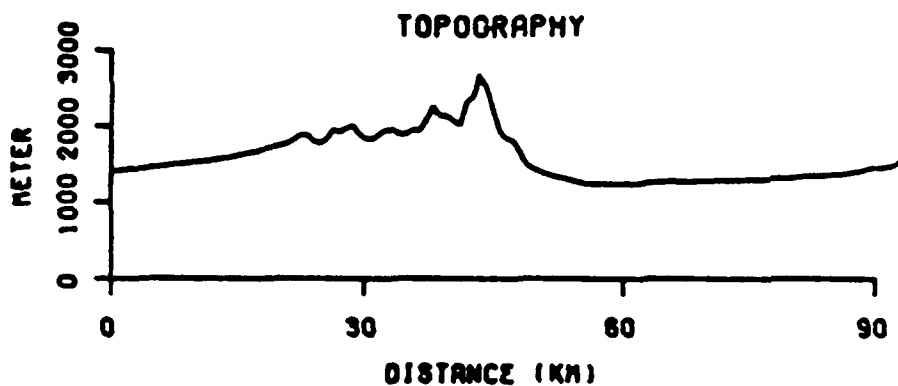
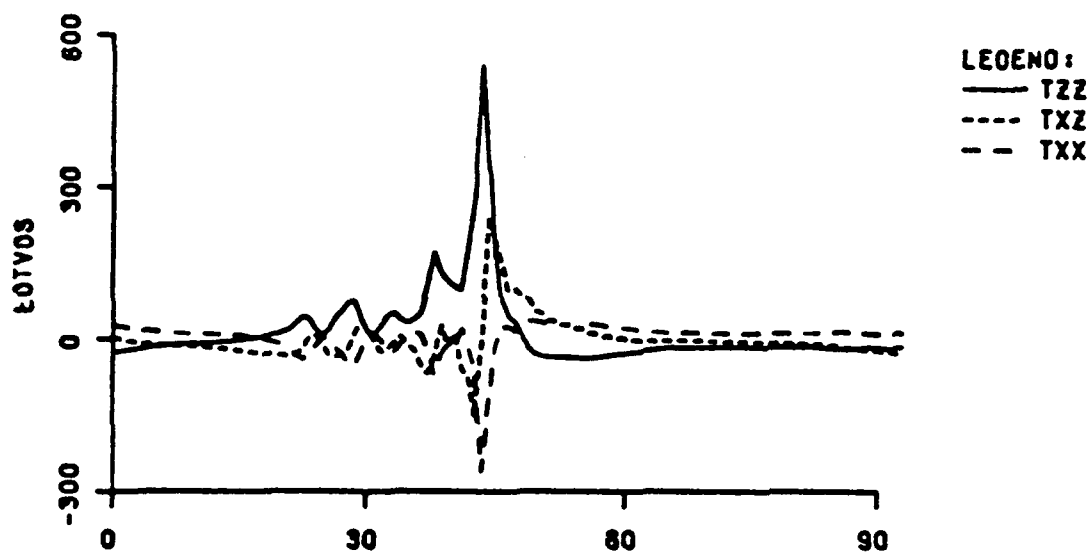
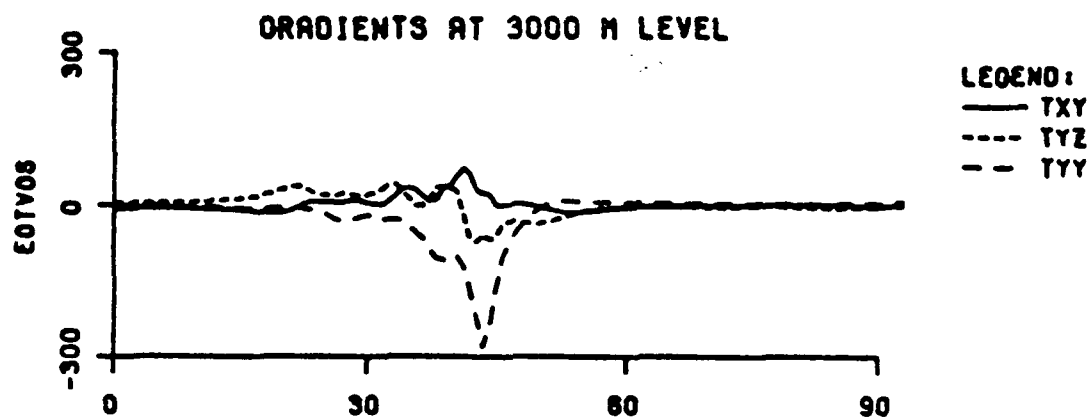
0.5' x 0.5' HEIGHT DATA, 192x192 POINT FFT, 30' RTM



INCREASING FLIGHT ALTITUDE: ELEVATION 5000 M.



PROFILE TEST: 33.3°N (PASSING 2680 M PEAK)



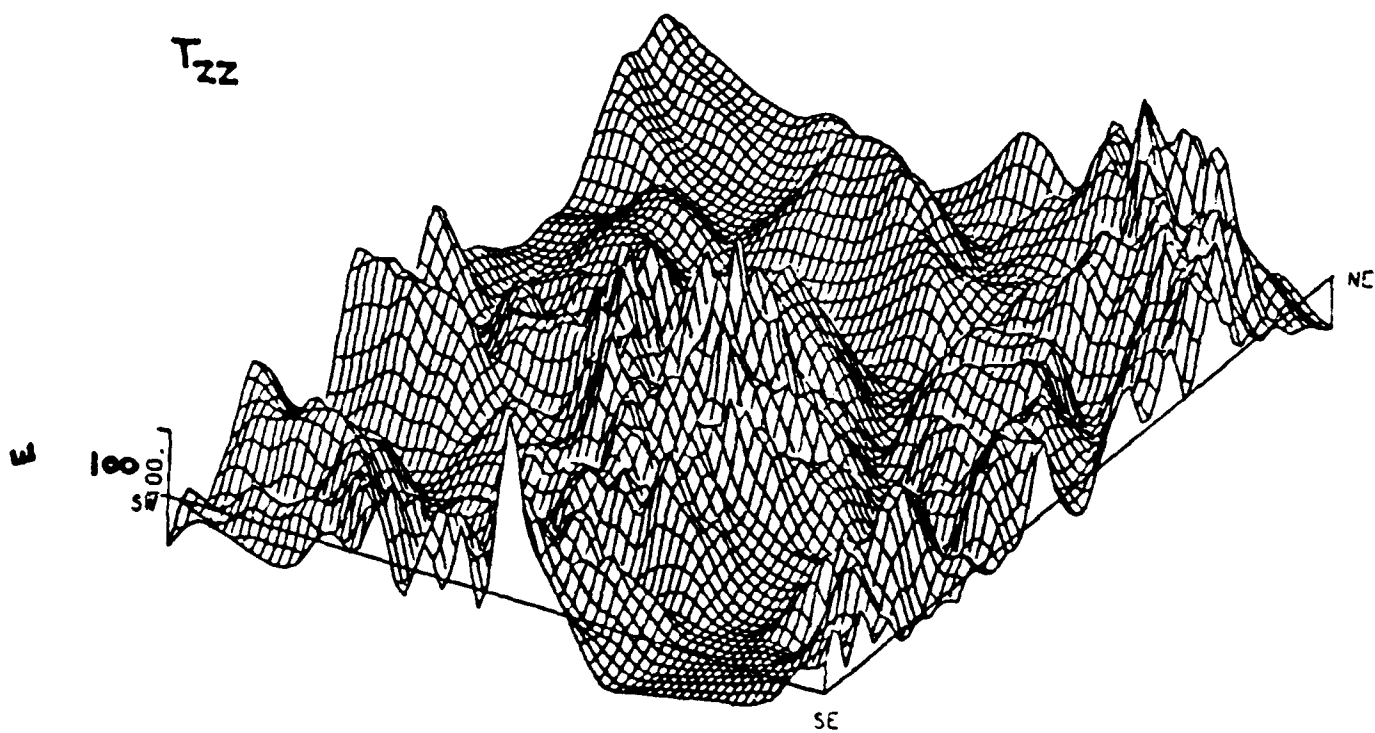
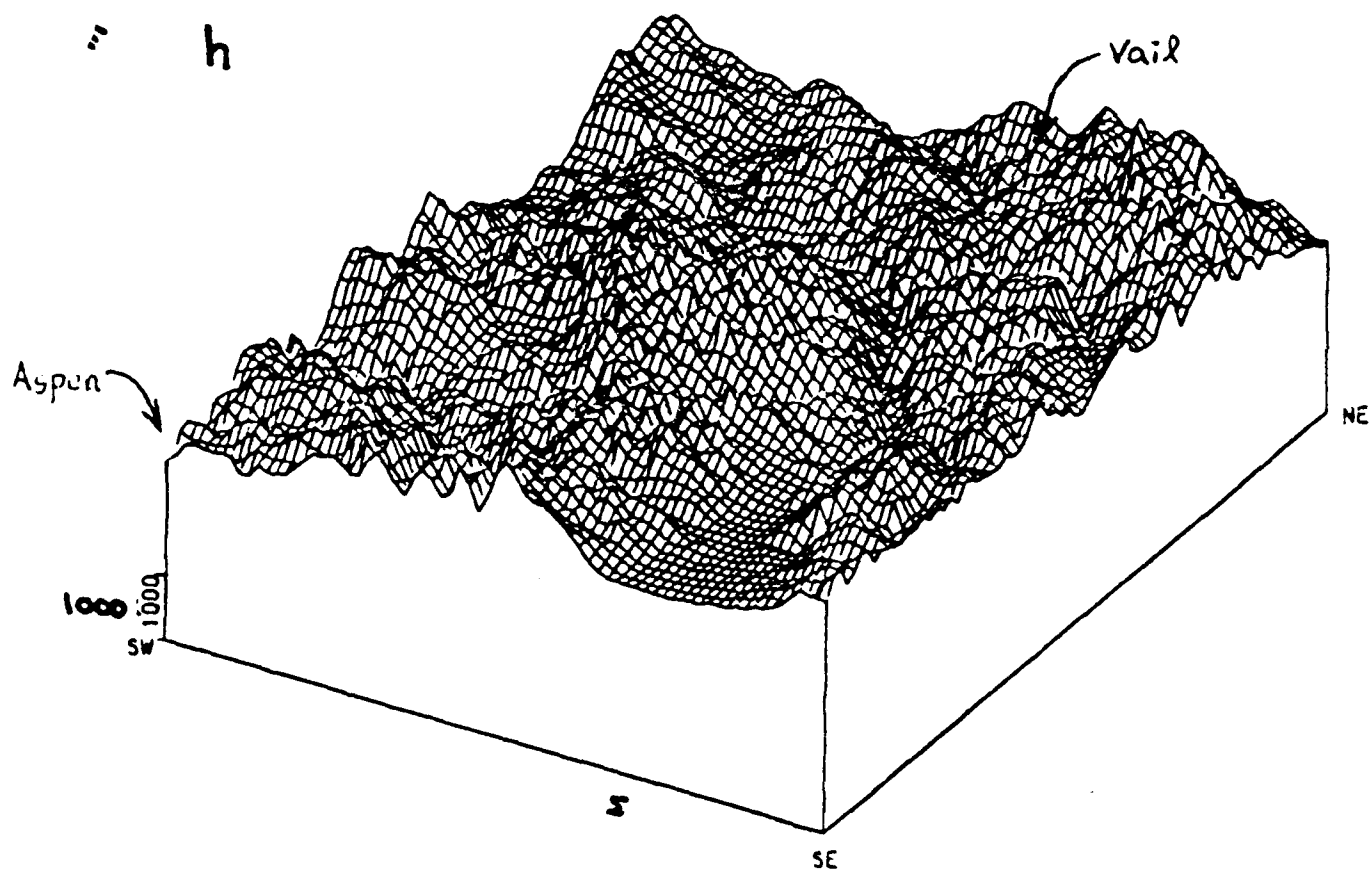
R.M.S. FIT PRISM ↔ FFT:  $T_{ZZ}$ : 1.9E,  $T_{XY}$ : 1.4E ( $n=8$ )

# EXAMPLE: CENTRAL COLORADO

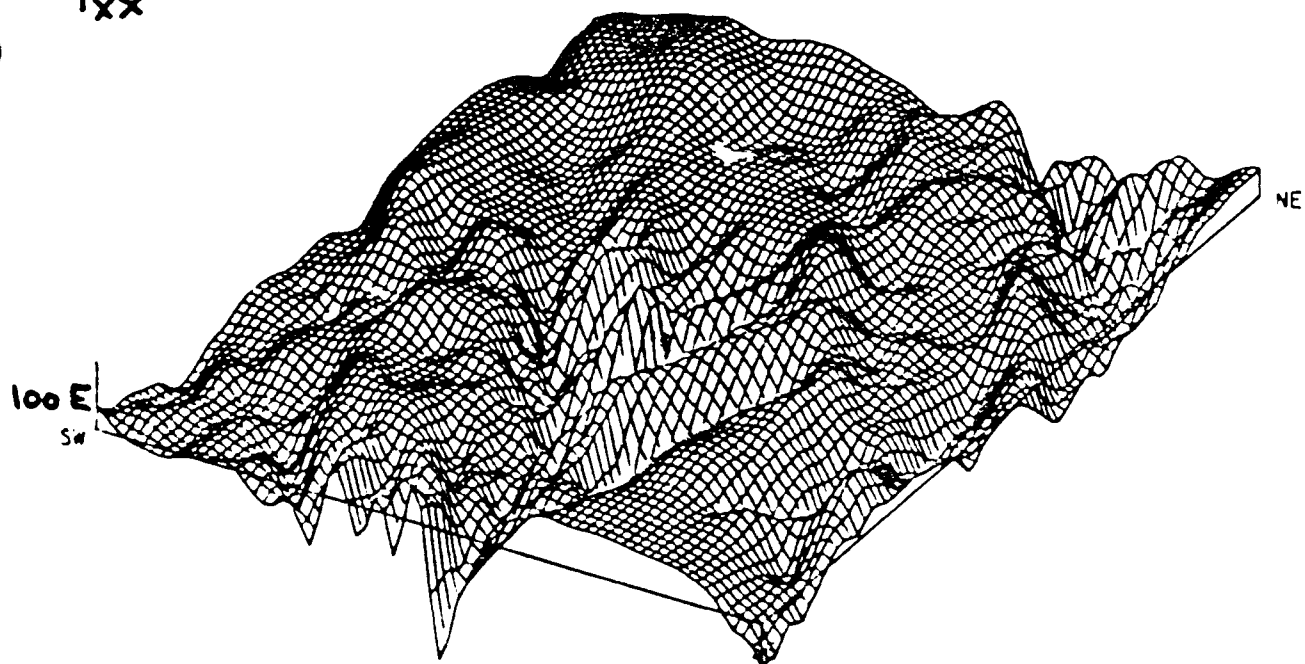
39°N - 40°N, 107°W - 106°W, ELEV. 4800 M.

FFT  
192x192; c

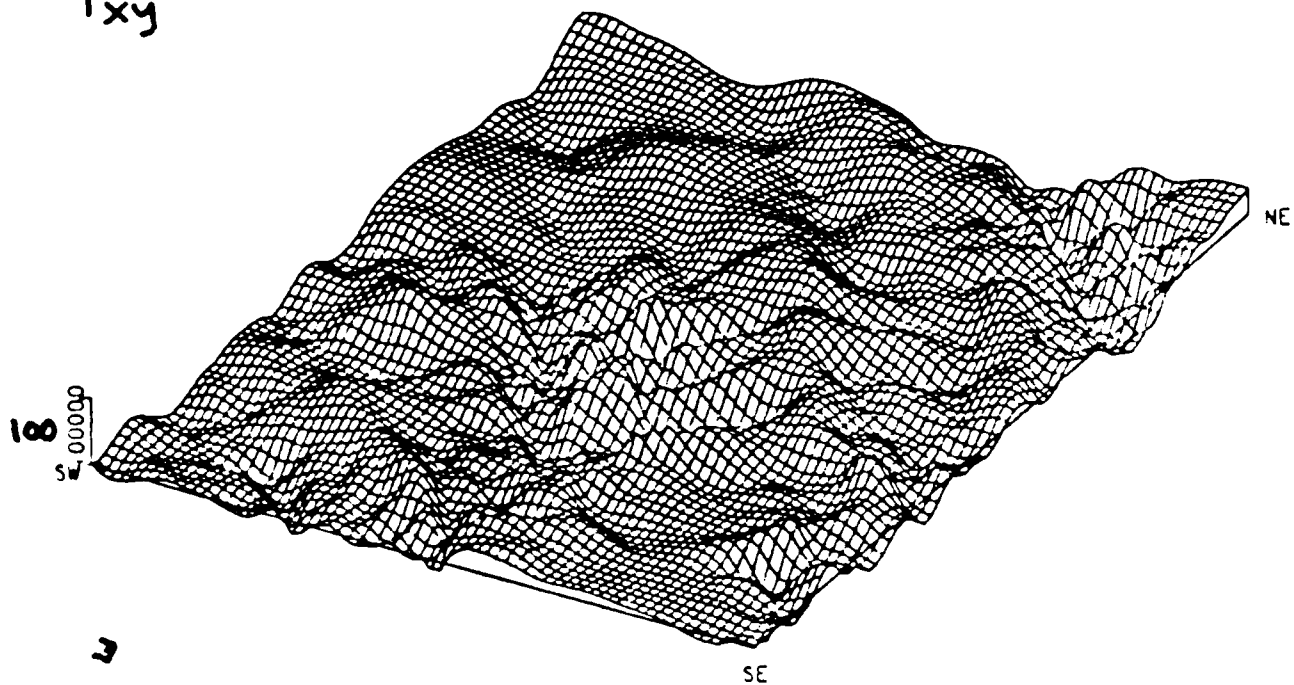
COMPARISON AREA FFT ↔ PRISM : 39.2 - 39.8, 106.8-105.2



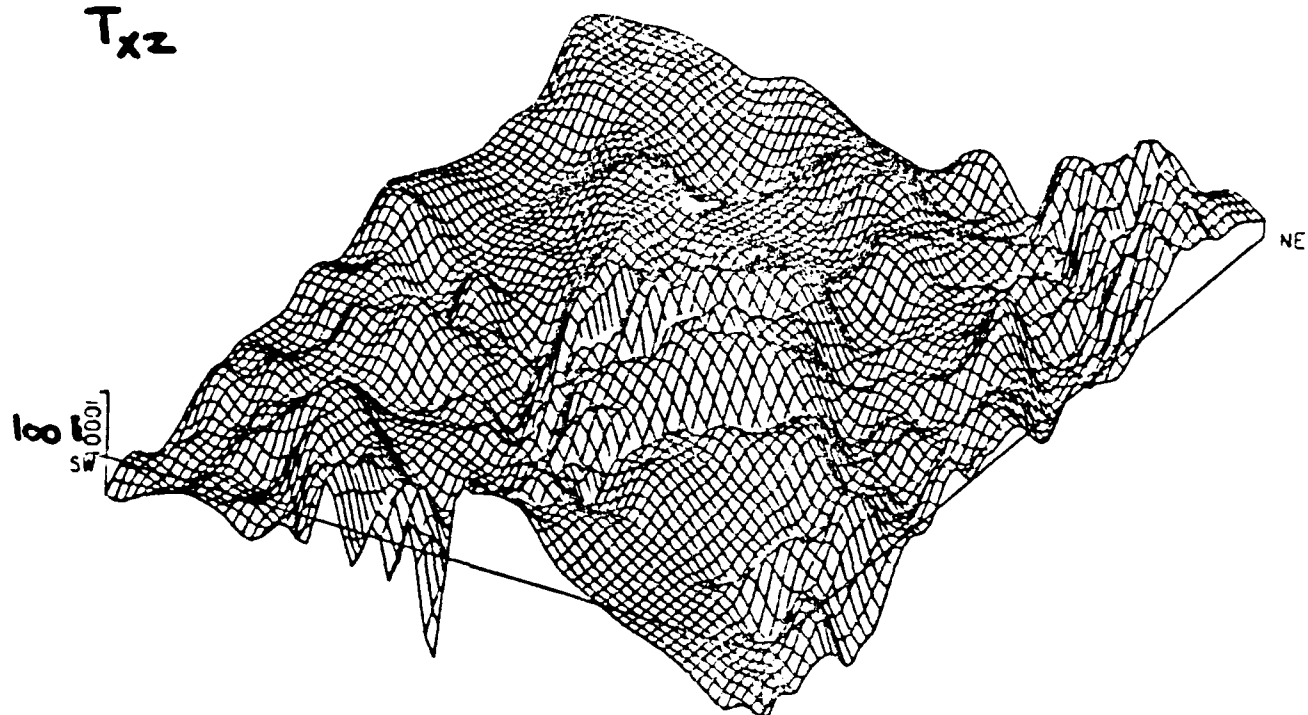
$T_{xx}$



$T_{xy}$



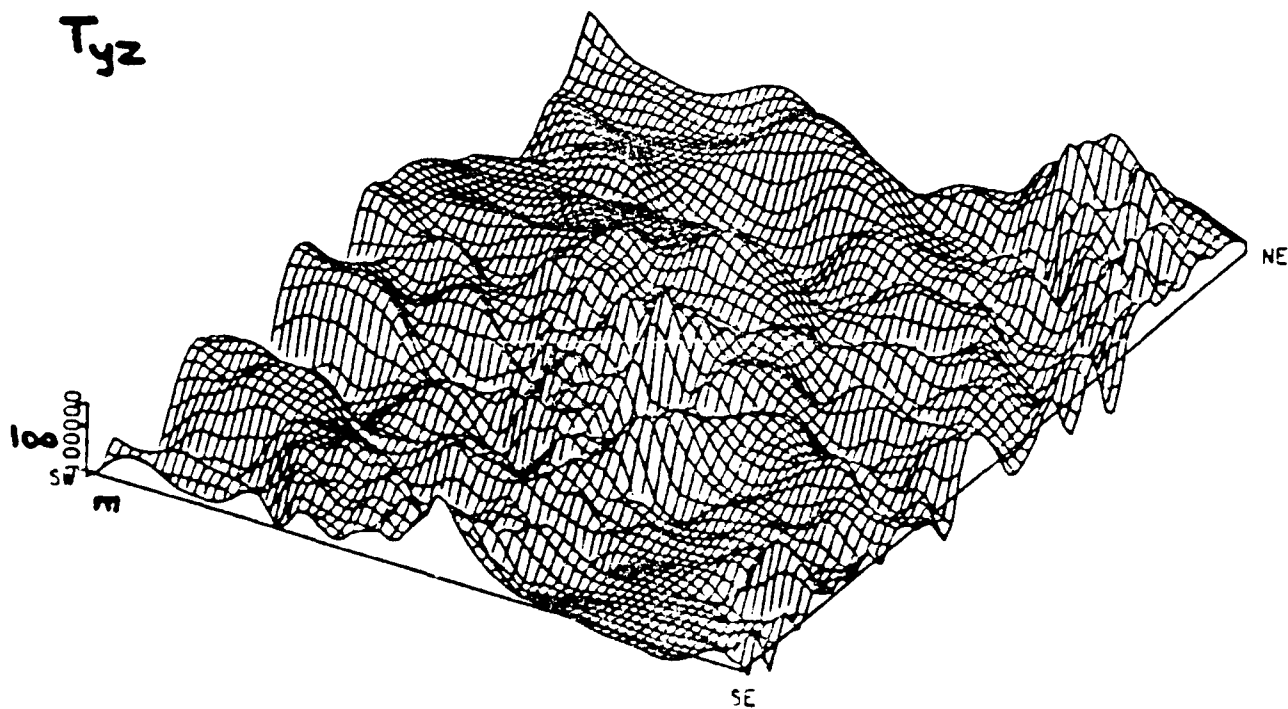
$T_{xz}$



DTM PLOT

Overheijning: 0.05  
 39.2 dg 39.8 dg  
 -106.8 dg -106.2 dg

$T_{yz}$



DTM PLOT 2 op12

Overheijning 0.05  
 39.2 dg 39.8 dg  
 -106.8 dg -106.2 dg

TABLE 1. COMPARISON TEST - 441 POINTS (EOTVOS)

			T <sub>XX</sub>	T <sub>YY</sub>	T <sub>ZZ</sub>	T <sub>XY</sub>	T <sub>XZ</sub>	T <sub>YZ</sub>
COMPUTED GRADIENTS	MEAN RMS	$\bar{x}$	-0.9	-0.6	1.4	-.9	-4.9	1.0
		$\sigma$	36.0	34.5	57.0	20.3	43.2	41.0
RMS DIFFERENCE FFT - PRISM (N=8)			0.6	0.5	0.9	0.5	.8	1.0

TABLE 2. DEPENDENCE ON NO. OF FFT EXPANSION TERMS

R.M.S. DIFFERENCE	$T_{ZZ}$	$T_{XY}$
N = 1	22.2	8.3
N = 3	5.5	1.6
N = 8	0.8	1.1
N = 15	0.9	0.6

## COVARIANCE ANALYSIS

- 0 TOPOGRAPHY ACF → GRAVITY ACF (FIRST ORDER PARKER)  
→ GRADIENT ACF AT ALTITUDE
- 0 SELECTED TOPOGRAPHY ACF: SINGLE DIFFERENCE LOGARITHMIC  
(FORSBERG, 1986)

$$C_{hh}(s) \sim -\log(D+r_D) + \log(T+r_T) \quad r_D = (s^2 + D^2)^{1/2}$$

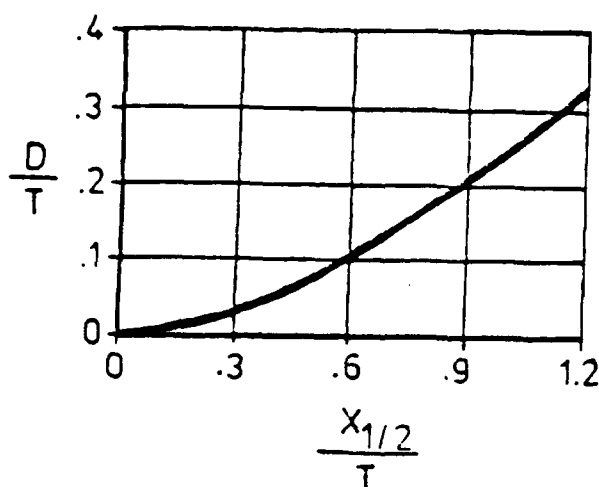
CONSISTENT GRAVITY ACF - CLOSED FORMULAS BOTH ON GROUND  
AND ALOFT. E.G.:

$$C_{gg}(s) \sim -\log(D+r_D) \Rightarrow C_{T_{zz}, T_{zz}} \sim \frac{D}{r_D^3}$$

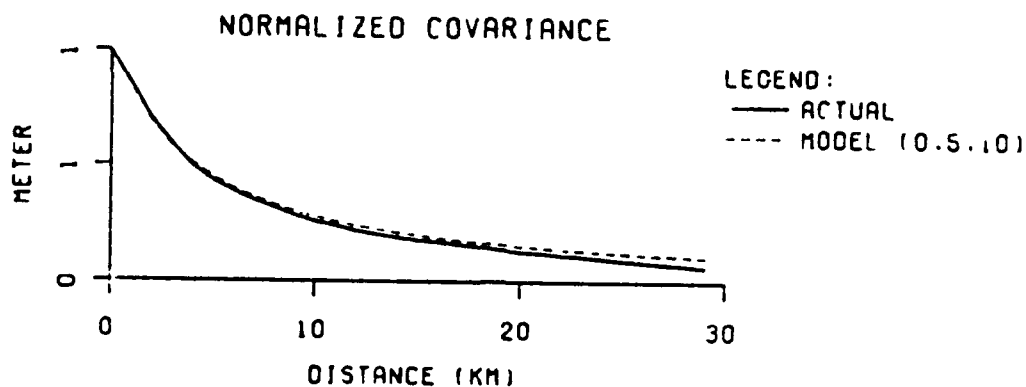
RESULT AT ELEVATION H:

$$\sigma_{zz}^2(H) = (2\pi G \rho)^2 \sigma_h^2 \frac{1}{\log \frac{T}{D}} \left( \frac{1}{(D+2H)^2} - \frac{1}{(T+2H)^2} \right)$$

T FIXED → D FUNCTION OF  $X_{1/2}$  FOR TOPOGRAPHY



0 TYPICAL GOOD FIT:  $T = 10$  KM,  $D = 0.5$  KM (JOTUNHEIMEN, NORWAY)



0 ANALYSIS  $\sigma_h$ ,  $x_{1/2}$  FOR SAMPLE AREAS (FFT),  $1^\circ$ RTM

$\rightarrow \sigma_{zz}$  AT 600 M CLEARANCE ELEV.

0 RELATIONSHIP OF VARIANCES:

$$\text{VAR}(T_{XX}) = \text{VAR}(T_{YY}) = \frac{3}{8} \text{VAR}(T_{ZZ})$$

$$\text{VAR}(T_{XZ}) = \text{VAR}(T_{YZ}) = \frac{1}{2} \text{VAR}(T_{ZZ})$$

$$\text{VAR}(T_{XY}) = \frac{1}{8} \text{VAR}(T_{ZZ})$$

0 COLORADO  
R.M.S. (E)

	$T_{XX}$	$T_{YY}$	$T_{ZZ}$	$T_{XY}$	$T_{XZ}$	$T_{YZ}$
ACTUAL	35	34	57	20	43	41
MODEL	38	38	62	22	44	44

SAMPLE AREA	AREA SIZE	HEIGHT SPACING	HIGHEST POINT	MEAN ELEVATION	RM (M)	$\lambda_k$ (KM)	RMS GRADIENT $\sigma_z$ (E)
SIERRA, NEVADA	1x1.2°	0.5'	4417	1607	785	11.3	68
CASCADES, WASH.	1x1.2°	-	4302	950	426	6.7	30
ROCKY MOUNTAIN, COLO.	-	-	4300	3005	426	6.5	50
SMOKY MOUNTAINS, TENN.	-	-	2025	750	305	7.6	50
WHITE SANDS REGION, NEW MEX.	-	-	3600	1583	217	11.7	23
SOUTHERN OHIO	-	-	400	255	45	9.3	10
JOTUNHEIMEN, NORWAY	120x120KM	1KM	2200	1140	304	4.1	34
HARDANGERVIDDIA, NORWAY	-	-	1000	1003	222	4.3	21
FINNMARK, NORWAY	-	-	1200	477	155	4.4	16
JAMESON LAND, EAST GREENLAND	15x15KM	100M	909	520	128	1.7	32
NORTH ZEALAND, DENMARK	15x20KM	-	80	35	14	2.2	5

## SUMMARY

- 0 TOPOGRAPHIC EFFECTS EFFECTIVELY HANDLED BY  
RTM - REDUCTION "REMOVE-RESTORE"
- 0 EFFECTS LARGE IN ALPINE REGIONS (UP TO 200-300E)
- 0 COMPUTATIONS BY FFT OR PRISM METHOD  
(HIGH-ORDER EXPANSION NECESSARY IN FFT)
- 0 EASY MAGNITUDE ESTIMATION FROM TOPOGRAPHY ACF,  
- RELATIVELY LARGE EFFECTS EVEN FOR LOWLANDS (DUE TO  
LOWER EFFECTIVE FLIGHT LEVEL)

TITLE OF PAPER: Topographic Effects in Airborne Gravity Gradiometry

SPEAKER: Rene Forsberg

QUESTIONS AND COMMENTS:

1. Question: Carl Bowin

It appears that your conversion of topography to gravity assumes the lack of compensation of the topography, hence the predicted gravity may be larger than observed.

Response:

Yes, but the computed gravity correlation is like a Bouguer correction.

(Carl Bowin: We do not measure a Bouguer anomaly, only the equivalent of the free-air anomaly).

OBSERVABILITY OF LAPLACE'S EQUATION USING  
A TORSION-TYPE GRAVITY GRADIOMETER

by

Alan H. Zorn  
Dynamics Research Corporation  
60 Frontage Road  
Andover, MA 01810

ABSTRACT:

The trace of the gravitation gradient tensor, theoretically zero, is not directly observable by a torsion-type gradiometer. However, changes in the trace are directly observable at track crossings by a moving-base torsion gradiometer. The practicality of measuring these trace changes is illustrated by covariance analysis of GGSS track crossings. The sensitivity of these results to flight conditions and noise model parameters is also presented.

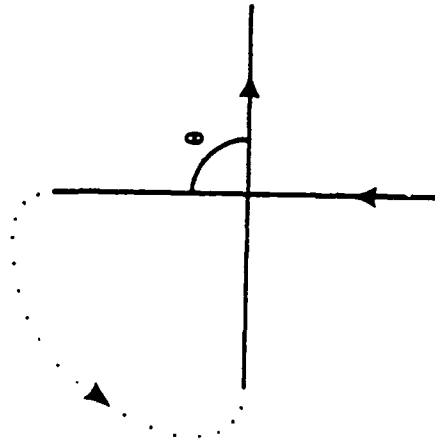
## **BASELINE CONDITIONS**

- **FLIGHT PARAMETERS**
  - **SPEED = 360 KM/HR**
  - **ALTITUDE = 600 M**
  - **RIGHT ANGLE TRACK CROSSING**
  - **TIME BETWEEN CROSSINGS = 6.5 MIN**
- **INSTRUMENTATION**
  - **3 GGI'S (ROTATING-ACCELEROMETER)**
  - **UMBRELLA FRAME**
  - **10-SEC AVERAGING/SAMPLING TIME**
  - **NO CAROUSELLING**



# COVARIANCE SIMULATION

- SIMULATION OF GGSS TRACK CROSSINGS



- QUANTITIES OF INTEREST:

$$\left. \begin{aligned} \lambda_N &= \frac{\partial}{\partial N} (T_{NN} + T_{EE} + T_{DD}) \\ \lambda_E &= \frac{\partial}{\partial E} (T_{NN} + T_{EE} + T_{DD}) \end{aligned} \right\} \text{AT TRACK INTERSECTION}$$

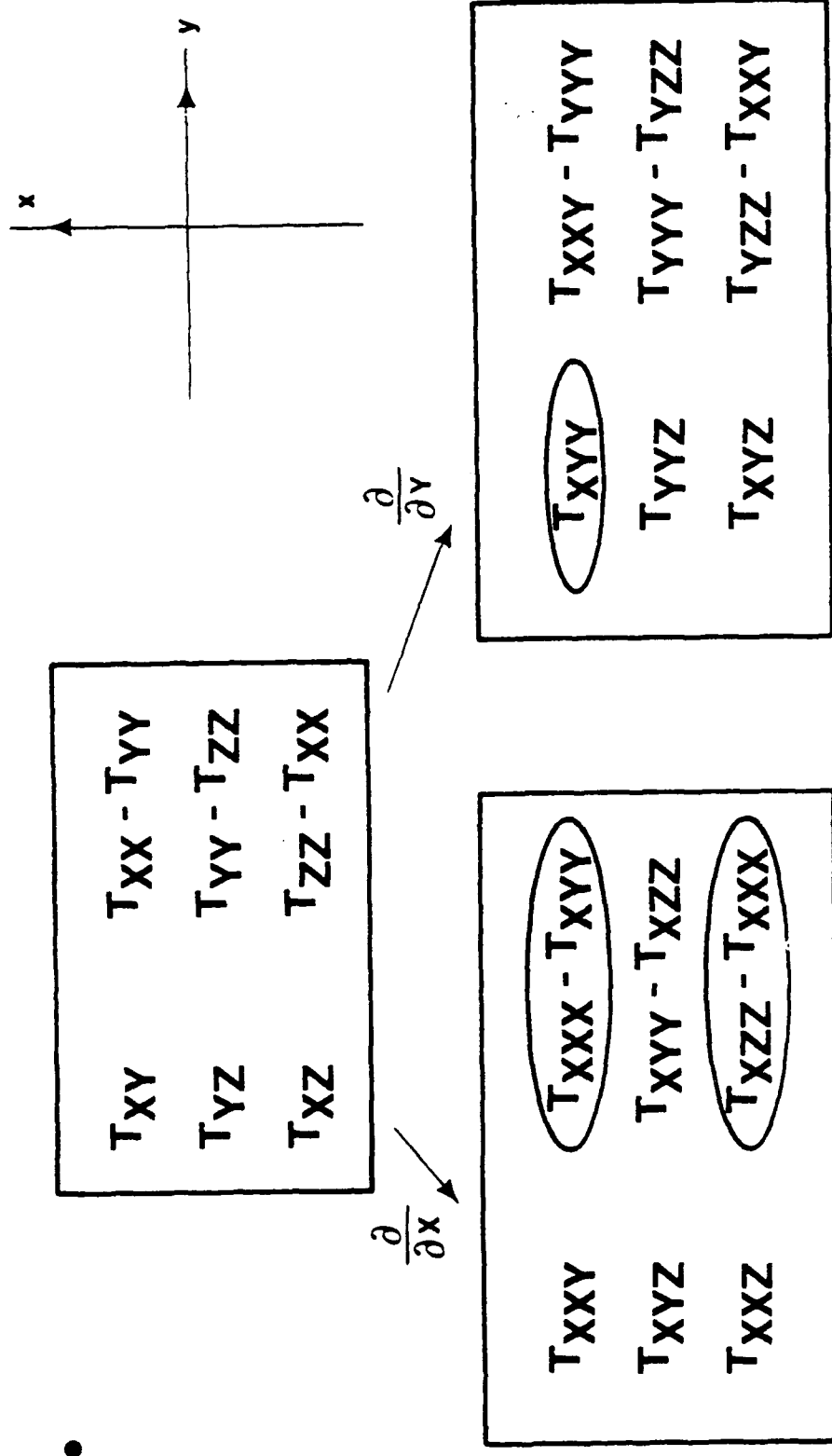
- KALMAN FILTER APPROACH — LARGE A PRIORI'S FOR ALL BIAS STATES

# TEXAS-OKLAHOMA AWN MODEL

- USED AS BASIS OF COMPARISON OF RMS GRAVITY FIELD VALUES IN FOLLOWING RESULTS
- NOT USED IN COVARIANCE SIMULATION — LAPLACE'S EQUATION IS BUILT INTO TEXAS-OKLAHOMA MODEL
- GRADIENT-DERIVATIVE FIELD VALUES:

TERM	RMS (E/KM)	
	AT SURFACE	AT 600 M
$T_{XXX}, T_{YYY}$	13.1	6.6
$T_{XXY}, T_{XYX}$	5.9	3.0
$T_{XZZ}, T_{YZZ}$	16.6	8.4
$T_{ZZZ}$	23.4	11.9

# DIFFERENTIATE OBSERVABLES AT TRACK CROSSING



- $\lambda_X = \frac{\partial \lambda}{\partial x} = T_{XXX} + T_{XYY} + T_{XZZ}$  IS OBSERVABLE
- SIMILARLY,  $\lambda_Y$  IS OBSERVABLE

## GRAVITY FIELD ASSUMPTIONS

- CONSERVATIVE FIELD
  - CANNOT GET TOO FAR WITHOUT THIS
- NOT NECESSARILY HARMONIC
  - $\lambda = 0$  IS NOT ASSUMED



# TORSION GRADIOMETER OBSERVABLES

- $$\begin{array}{cc} T_{XY} & T_{XX} - T_{YY} \\ T_{YZ} & T_{YY} - T_{ZZ} \\ T_{XZ} & T_{ZZ} - T_{XX} \end{array}$$

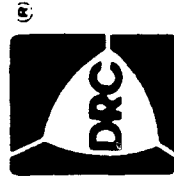
- ONLY FIVE INDEPENDENT COMBINATIONS

- $\lambda = T_{XX} + T_{YY} + T_{ZZ}$  NOT OBSERVABLE



- TREATMENT OF LAPLACE'S EQUATION:

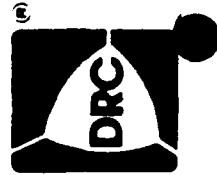
- USUAL ASSUMPTION:  $\lambda = 0$

- DON'T ASSUME  $\lambda = 0$  — HOW FAR CAN ONE GO WITHOUT THIS ASSUMPTION?



## GRADIOMETER TYPES

- TWO BASIC TYPES OF GRAVITY GRADIOMETER:
  - TENSION MEASURES DIAGONAL ELEMENTS OF GRADIENT TENSOR (EG -  $T_{XX}$ )  

  - TORSION MEASURES OFF-DIAGONAL ELEMENTS (EG -  $T_{XY}$ )  

- FUNDAMENTAL DIFFERENCE BETWEEN THESE TWO TYPES, WHEN MULTIPLE INSTRUMENTS USED IN SINGLE SYSTEM
  - TENSION GRADIOMETER MEASURES ALL SIX COMPONENTS OF SYMMETRIC GRADIENT TENSOR
  - TORSION GRADIOMETER MEASURES ONLY FIVE



## DEFINITIONS AND TERMINOLOGY

- $T$  = GRAVITATIONAL POTENTIAL
- $\Gamma = \begin{bmatrix} T_{XX} & T_{XY} & T_{XZ} \\ T_{YX} & T_{YY} & T_{YZ} \\ T_{ZX} & T_{ZY} & T_{ZZ} \end{bmatrix}$
- FURTHER DERIVATIVES DENOTED  $T_{XXX}$ ,  $T_{XXY}$ , ETC.
- $\lambda = \nabla^2 T = T_{XX} + T_{YY} + T_{ZZ}$
- LAPLACE'S EQUATION:  $\lambda = 0$



## WHY MEASURE SPACIAL DERIVATIVES OF $\lambda$ ?

- GRADIOMETER ERROR MODEL VALIDATION
- POTENTIAL FOR TEST OF LAPLACE'S EQUATION
  - UPWARD/DOWNWARD CONTINUATION
  - VARIATION OF GRAVITATIONAL CONSTANT
- GGSS MAKES MEASUREMENTS "FOR FREE"
  - THOUSANDS OF TRACK CROSSINGS
  - NO CHANGE IN SURVEY PLAN REQUIRED

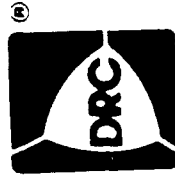


## OVERVIEW

- TORSION-TYPE GRADIOMETER NOT CAPABLE OF MEASURING TRACE OF GRADIENT TENSOR:

$$\lambda = T_{XX} + T_{YY} + T_{ZZ}$$

- MOVING-BASE TORSION GRADIOMETER CAN, HOWEVER, MEASURE SPACIAL DERIVATIVES OF  $\lambda$  AT TRACK CROSSINGS
- FEASIBILITY OF MEASURING THESE SPACIAL DERIVATIVES IS DEMONSTRATED FOR GGSS TRACK CROSSINGS
  - COVARIANCE SIMULATION
  - SENSITIVITY ANALYSIS



B-580U

# **OBSERVABILITY OF LAPLACE'S EQUATION USING A TORSION-TYPE GRAVITY GRADIOMETER**

*Presented At:*

**15TH GRAVITY GRADIOMETER CONFERENCE  
UNITED STATES AIR FORCE ACADEMY  
COLORADO SPRINGS, COLORADO**

**11-12 FEBRUARY 1987**

*Presented By:*

**DYNAMICS RESEARCH CORPORATION  
60 FRONTAGE ROAD  
ANDOVER, MASSACHUSETTS 01810  
(617) 475-9090**



# **ABSTRACT**

## **OBSERVABILITY OF LAPLACE'S EQUATION USING A TORSION-TYPE GRAVITY GRADIOMETER**

**ALAN ZORN  
DYNAMICS RESEARCH CORPORATION**

The trace of the gravitation gradient tensor, theoretically zero, is not directly observable by a torsion-type gradiometer. However, changes in the trace are directly observable at track crossings by a moving-base torsion gradiometer. The practicality of measuring these trace changes is illustrated by covariance analysis of GGSS track crossings. The sensitivity of these results to flight conditions and noise model parameters is also presented.

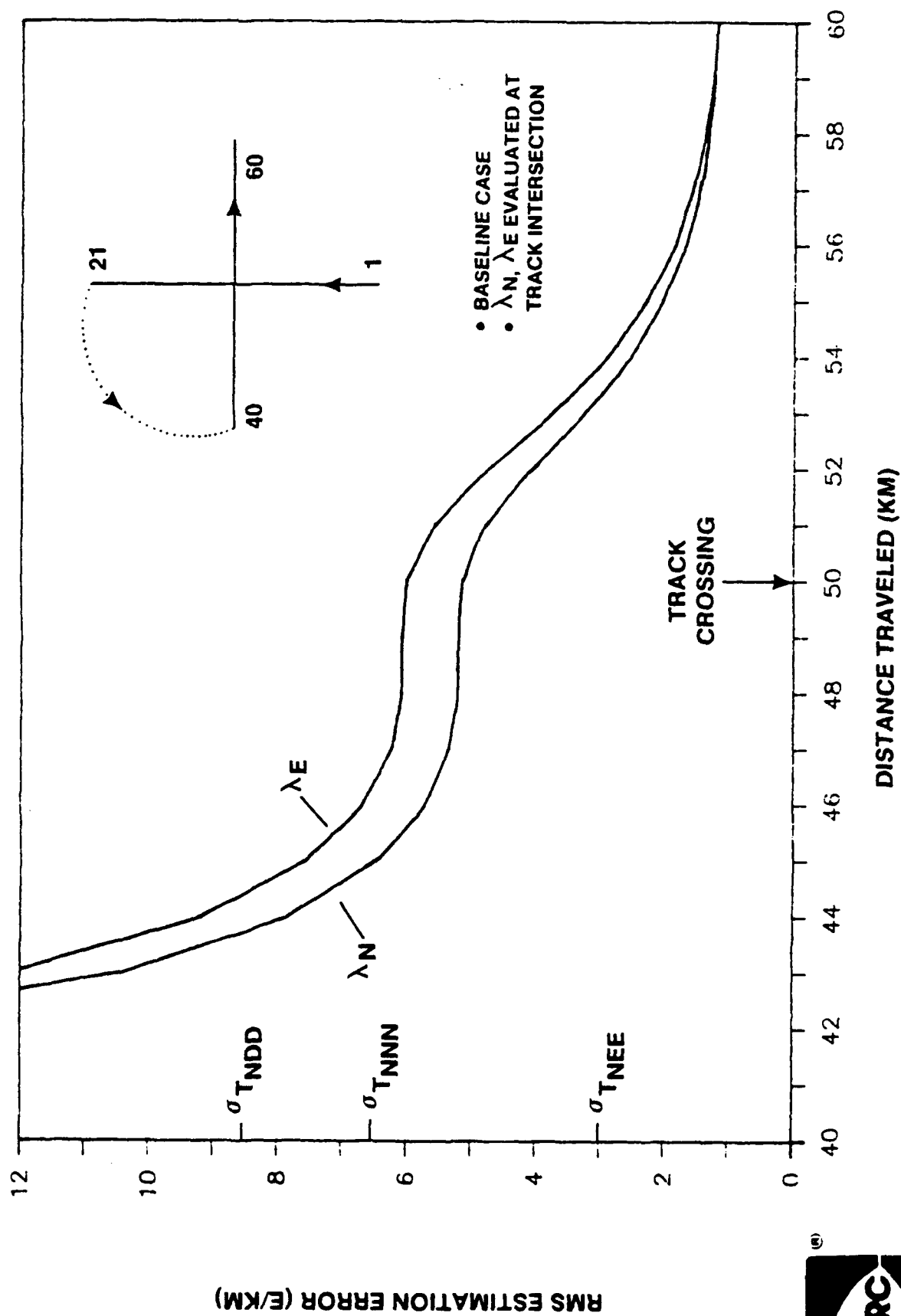


# BASELINE MODELS

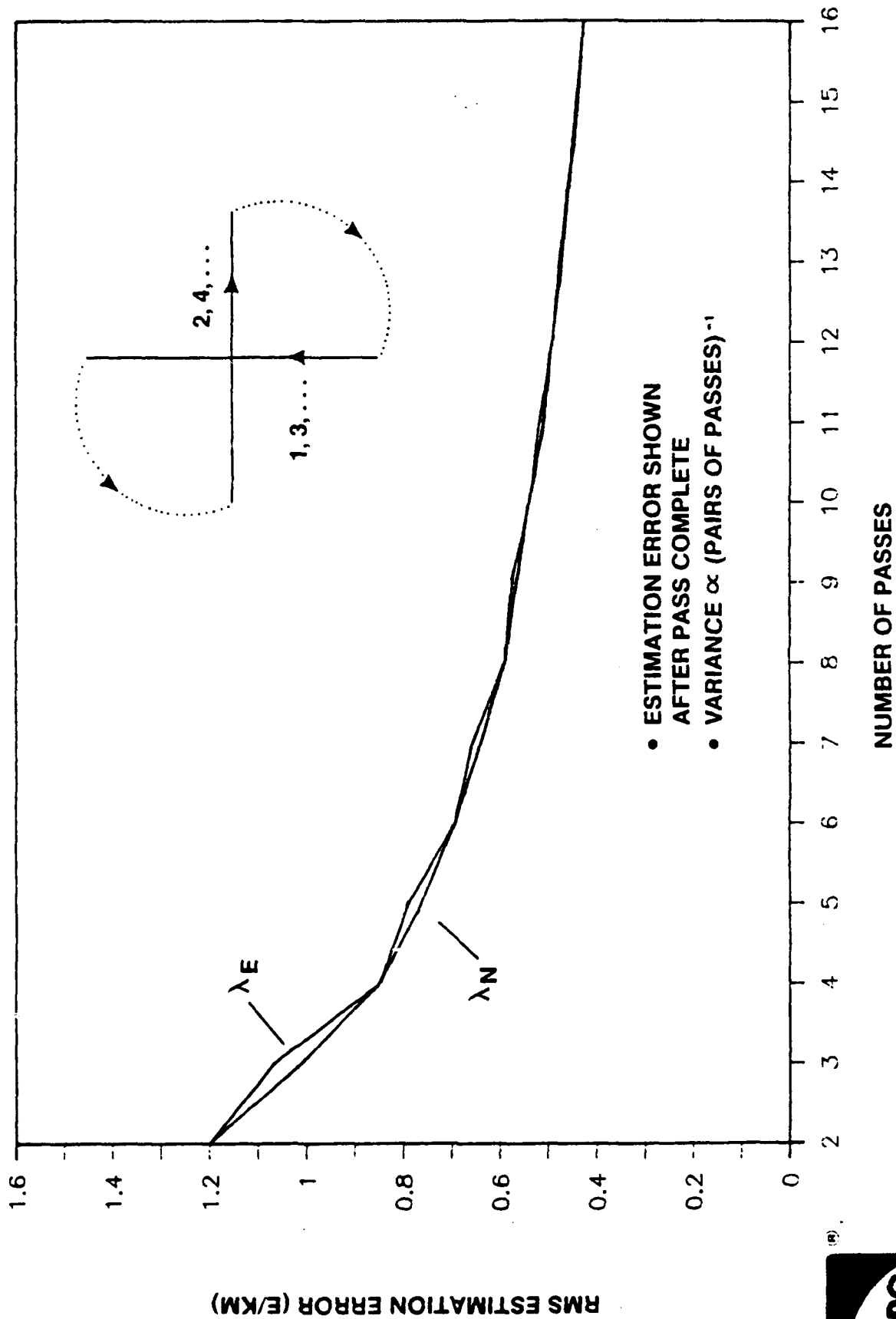
- INSTRUMENT ERROR MODEL
  - $\text{PSD} = \frac{A}{\omega^2} + B$
  - JORDAN PARAMETERS (3RD INTER SYMP ITSG)  
 $A = \pi \times 10^{-4} \text{ E}^2 - \text{rps}$        $B = 600 \text{ E}^2/\text{rps}$
  - BIAS AND RAMP
- GRAVITY FIELD MODEL
  - PARAMETRIC TENSOR EXPANSION OF POTENTIAL ABOUT TRACK INTERSECTION (TO ORDER 4)
  - LAPLACE'S EQUATION NOT ASSUMED
  - MODEL ASSUMED VALID TO A RADIUS OF 10 KM OF TRACK INTERSECTION
- RESULTS VALID WHEN GRAVITY FIELD DOESN'T CHANGE SUBSTANTIALLY OVER AVERAGING/SAMPLING DISTANCE



# SIMPLE TRACK CROSSING



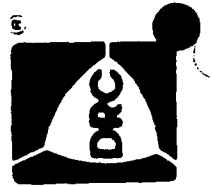
# MULTIPLE PASSES OVER SAME POINT



## SENSITIVITY ANALYSIS

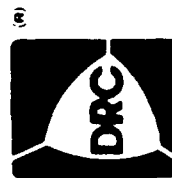
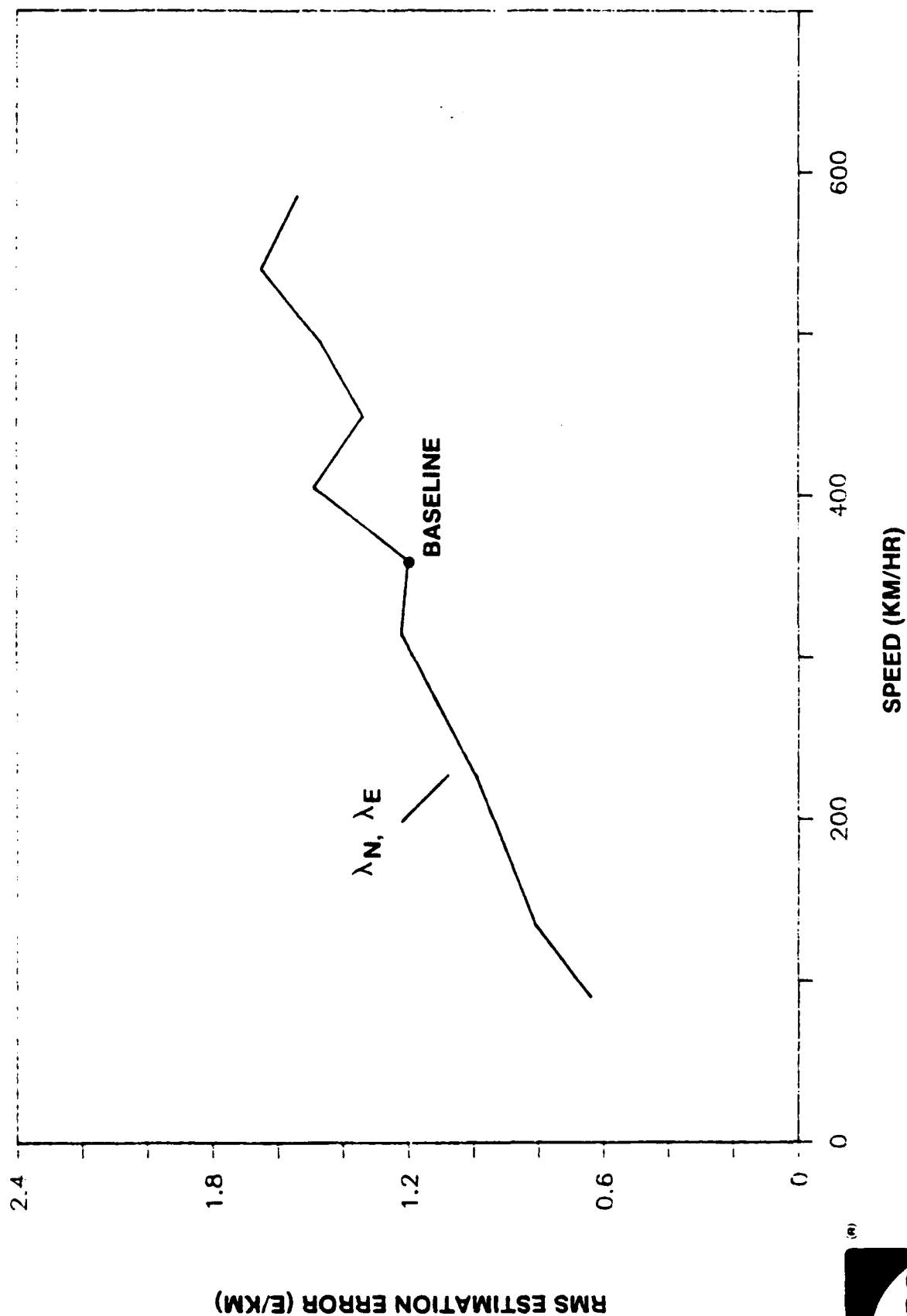
- DETERMINED SENSITIVITY OF RMS ESTIMATION ERROR IN  $\lambda_N$  AND  $\lambda_E$  TO VARIOUS SIMULATION PARAMETERS:

	INSENSITIVE TO:	SENSITIVE TO:
FLIGHT PARAMETERS	<ul style="list-style-type: none"> <li>• ALTITUDE</li> <li>• TIME BETWEEN TRACK CROSSINGS</li> </ul>	<ul style="list-style-type: none"> <li>• SPEED</li> <li>• ANGLE OF TRACK CROSSING</li> </ul>
INSTRUMENTATION	<ul style="list-style-type: none"> <li>• CAROUSELLING</li> <li>• AVERAGING/SAMPLING TIME</li> </ul>	
INSTRUMENT NOISE LEVELS	<ul style="list-style-type: none"> <li>• RED NOISE</li> <li>• BIAS</li> <li>• RAMP</li> </ul>	<ul style="list-style-type: none"> <li>• WHITE NOISE</li> </ul>

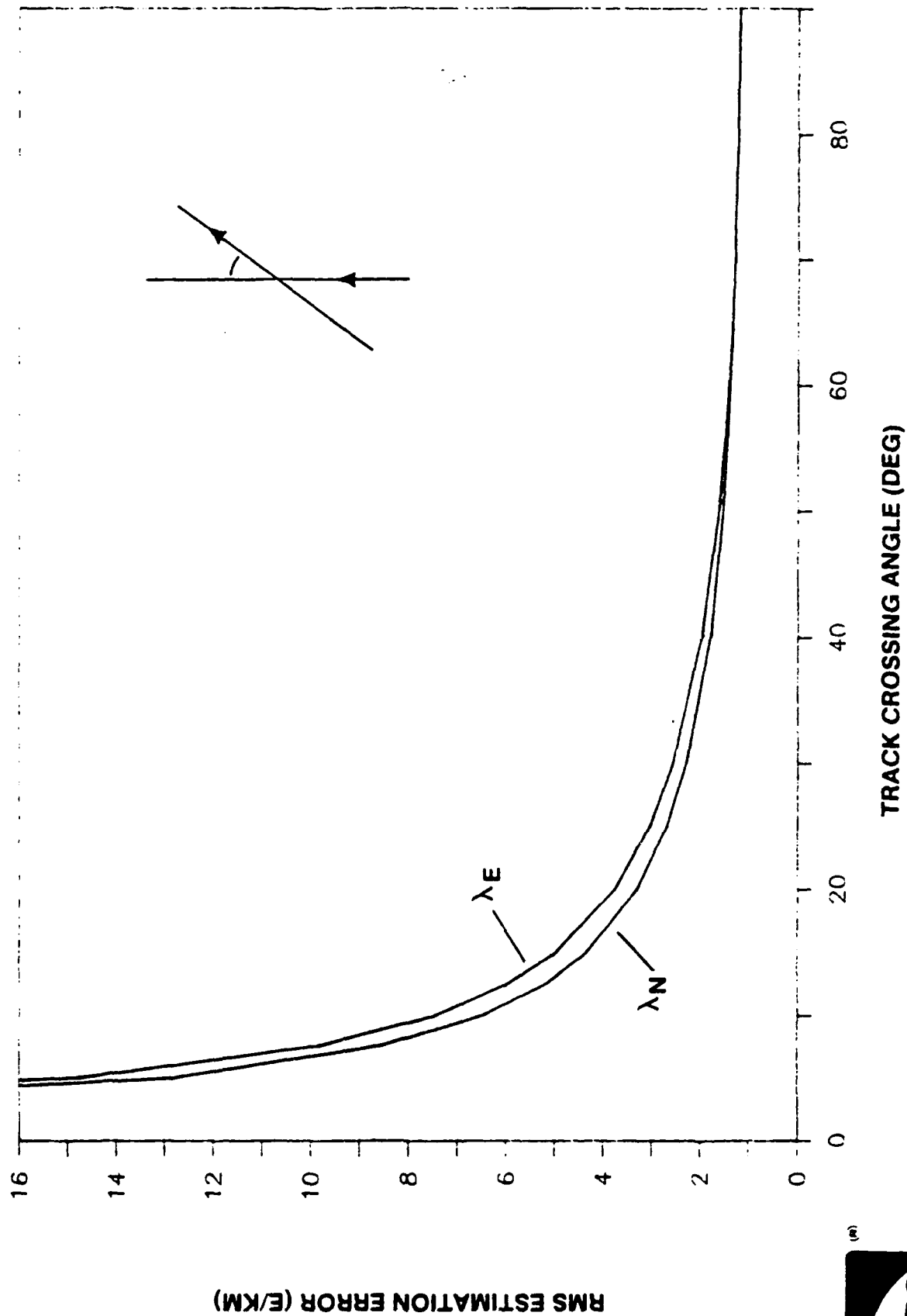


- SENSITIVITY CURVES FOLLOW

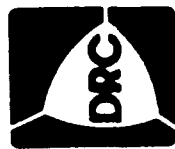
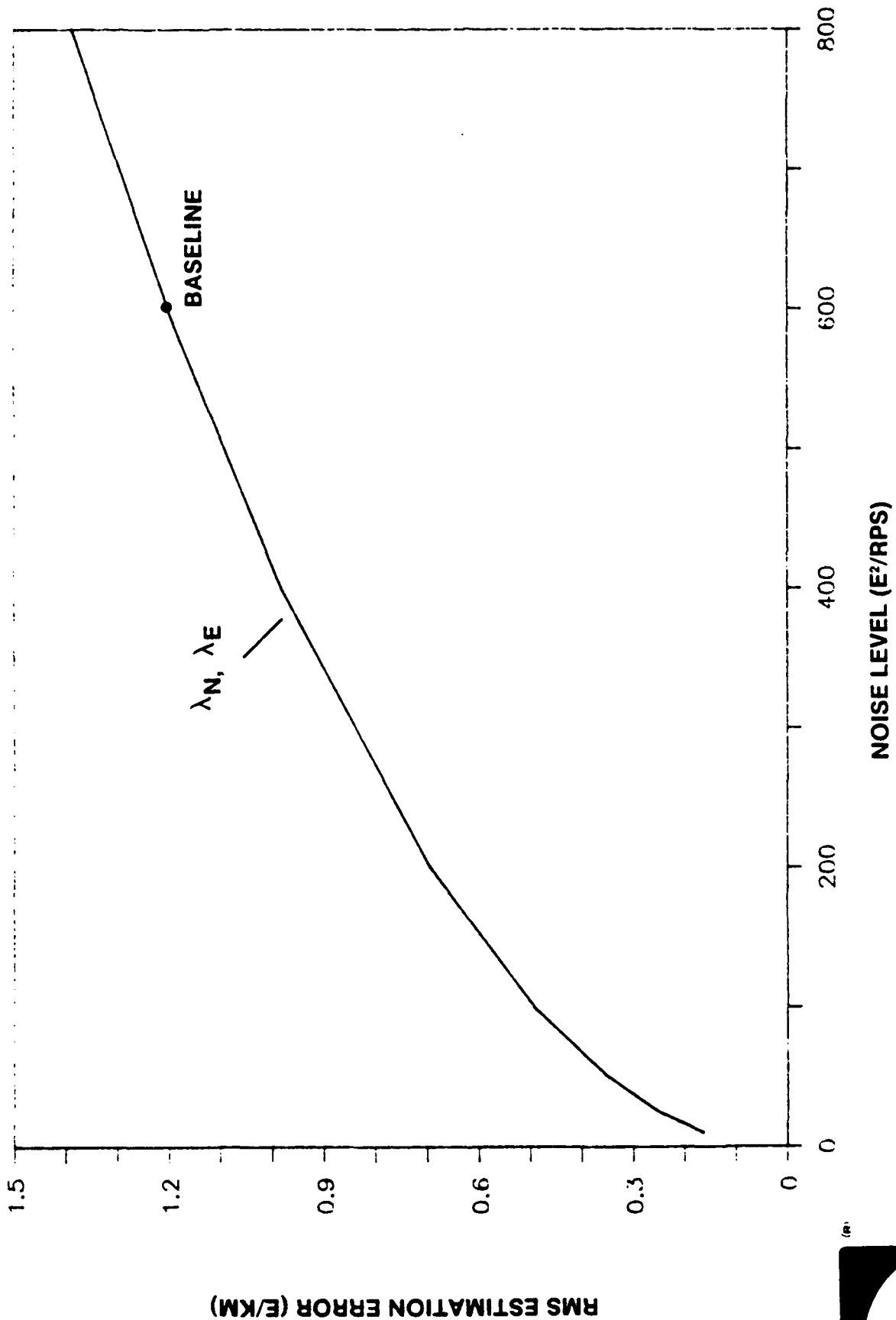
# SENSITIVITY TO AIRCRAFT SPEED



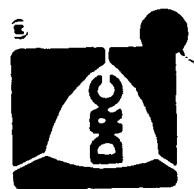
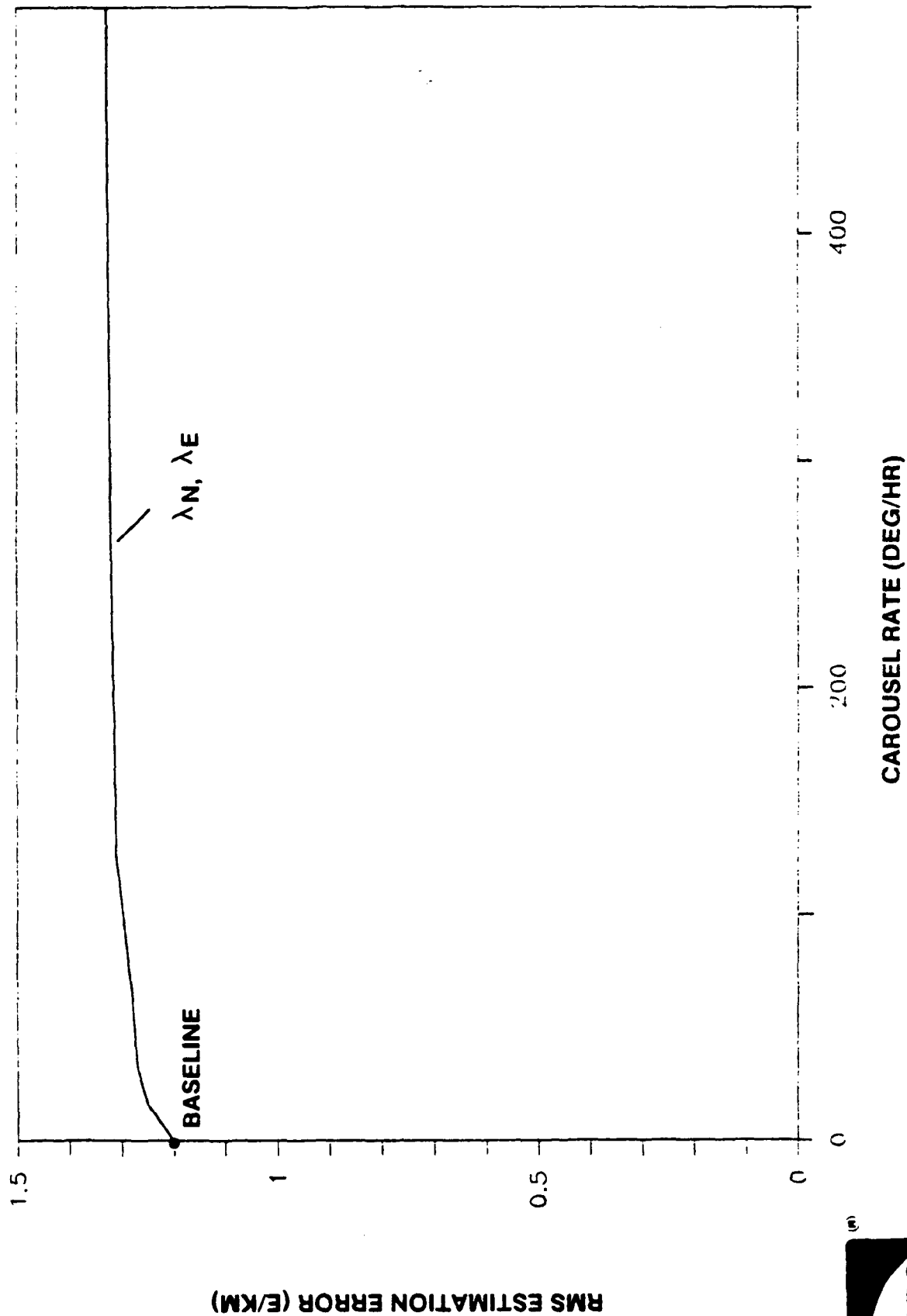
# SENSITIVITY TO TRACK CROSSING ANGLE



# SENSITIVITY TO WHITE NOISE

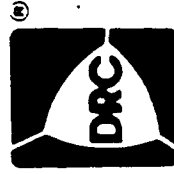


# SENSITIVITY TO CAROUSEL RATE



## SUMMARY AND CONCLUSIONS

- MOVING-BASE TORSION GRADIOMETER CAN MEASURE  $\lambda_N$  AND  $\lambda_E$  AT TRACK CROSSINGS
- FOR GGSS, CAN MEASURE  $\lambda_N$  AND  $\lambda_E$  TO 1.2 E/KM RMS AT SIMPLE TRACK CROSSINGS
- ACCURACY INCREASES WITH MULTIPLE PASSES OVER SAME POINT — AS IF PAIRS OF PASSES WERE INDEPENDENT SAMPLES
- ACCURACY MOST SENSITIVE TO INSTRUMENT WHITE NOISE
- NOT ASSUMING LAPLACE'S EQUATION UNTIL FINAL ANALYSIS GIVES CLEARER PICTURE OF GRADIOMETER MEASUREMENT SPACE AND CONSERVATIVE NATURE OF GRAVITY FIELD



TITLE OF PAPER: Observability of Laplace's Equation Using a Torsion-Type Gravity Gradiometer

SPEAKER: Alan H. Zorn

QUESTIONS AND COMMENTS:

1. Question: Dave Sonabend

Have you taken into account the errors in estimating the angular rate corrections to the gradiometer? For instance, gyro bias causes correlated errors in measuring  $\lambda$ .

Response:

Rate measurements are good enough for instruments used in aerial surveys.

2. Comment: Warren Heller

Dave's point was that your technique is a good way to test for gradiometer errors but that the instrumentation is not adequate for tests of inverse square law.

Response:

I am not advertising my idea as a test of the inverse square law.

3. Comment: Ho Jung Paik

Your signal for inverse square law test is of the order of  $GM/R^4$ , which is about 0.2 E/km. So the sensitivity of the gradiometer must be improved by at least a factor of 10 before you can have a test of the inverse square law.

Response:

My simulation of the Texas-Oklahoma area shows that the signal is about 5-10 E/km.

4. Question: Dan Long

I suggest there is more likelihood that  $\frac{d\lambda}{dZ}$  rather than  $\frac{d\lambda}{dN}$  or  $\frac{d\lambda}{dE}$  would show interesting results.

Response:

It is harder to measure  $\frac{d\lambda}{dZ}$ , but I see your point.

5. Question: Alan Rufty

Noise, as measured by the gradiometer, does not form a conservative field. How do you separate out the signal from the noise so that your assumption of a conservative field can be used?

Response:

If one knows something about the nature of the noise, then one can apply the conservative field assumption only to the signal. I do not assume that the noise is conservative.

6. Question: George F. Hinton

Shouldn't your method also be sensitive to the <sup>.. ..</sup>Eotvos effect?

Response:

No, I am taking this into account with my measurement of the velocity.

RATIOS OF GRAVITY GRADIENT, GRAVITY, AND GEOID  
FOR DETERMINATION OF CRUSTAL STRUCTURE

by

Carl Bowin  
Woods Hole Oceanographic Institution  
Woods Hole, MA 02543

ABSTRACT

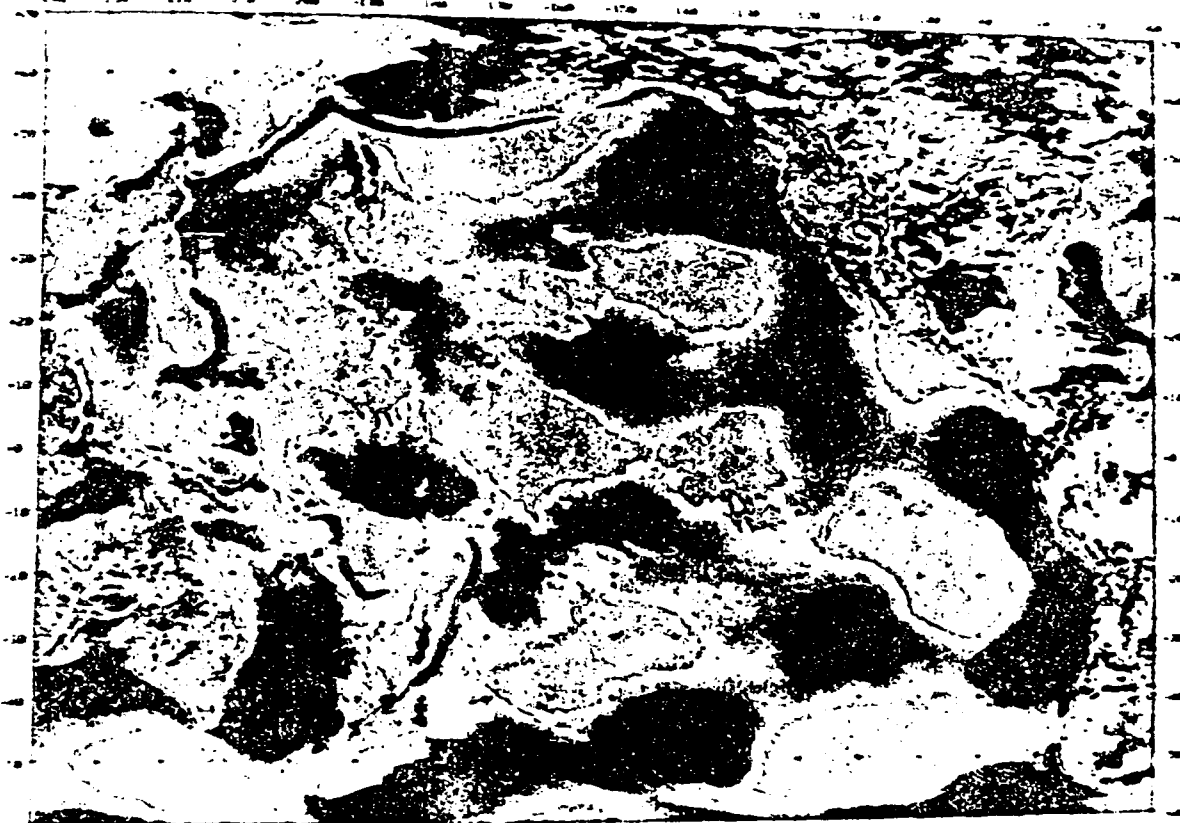
It has been shown (Bowin, 1983, 1985; Bowin et al., 1986) that the simple ratio of gravity to geoid anomalies at the center of a feature provides information comparable to that obtained by the Fourier transforming of either field, as well as to that obtained by other traditional spatial and frequency analysis methods. If perfectly accurate measurements of any one of the three fields - geoid, gravity, or vertical gravity gradient - were available over the entire earth's surface, no further observations would be necessary or useful. The other fields could be derived completely by either integration or differentiation. However, both caveats fail us in the real world: the existing data are neither perfectly accurate nor universal in coverage. Thus, for the immediate future, knowledge of the full spectrum of the Earth's gravity field will come from combinations of the various measurement types. In this presentation we summarize our ratio results to date, and indicate the utility of gravity gradient measurements to aid the determination of crustal structure and depth of causative mass anomaly sources.

Note: The following references include most of the illustrations used in Carl Bowin's talk at the 15th Gravity Gradiometry Conference. Also attached are copies of the new world residual geoid, gravity and vertical gravity gradient maps that were presented at the Conference (Figure 1, 2 and 3 respectively).

References:

- 1) Bowin, Carl, 1983. Depth of Principal Mass Anomalies Contributing to the Earth's Geoidal Undulations and Gravity Anomalies. *Marine Geodesy*, V.7, p.61-100.
- 2) Bowin, Carl, 1985. Global Gravity Maps and the Structure of Earth. IN: W.J. Hinze, ed., SEG Volume: Utility of Regional Gravity- and Magnetic- Anomaly Maps.
- 3) Bowin, Carl, 1986. Topography at the Core Mantle Boundary. *Geophysical Research Letters*, Vol. 13, No. 13, p.1513-1516.
- 4) Bowin, C., Edward Scheer, Woolcott Smith, 1986. Depth Estimates from Ratios of Gravity Geoid, and Gravity Gradient Anomalies. *Geophysics*, Vol. 51, No.1, p.123-136.

Figure 1. Residual Gold



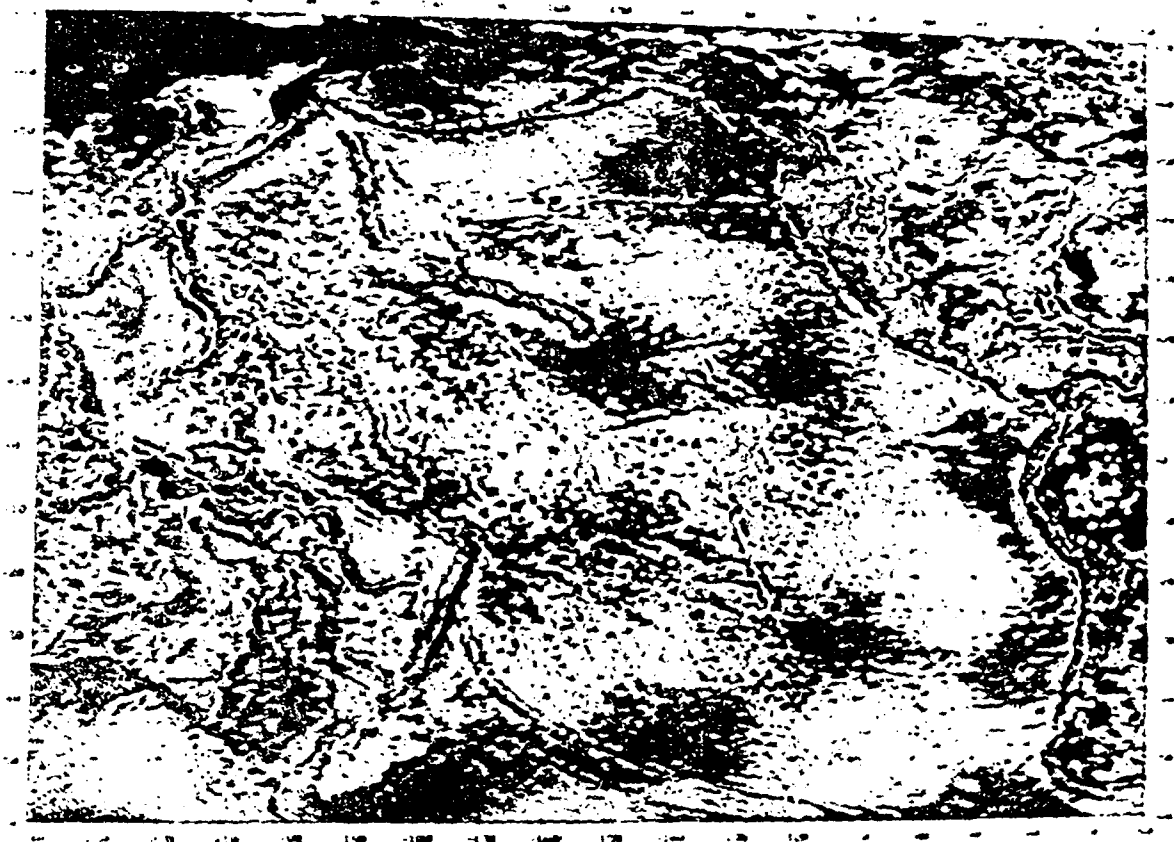


Figure 2. Residual Gravity

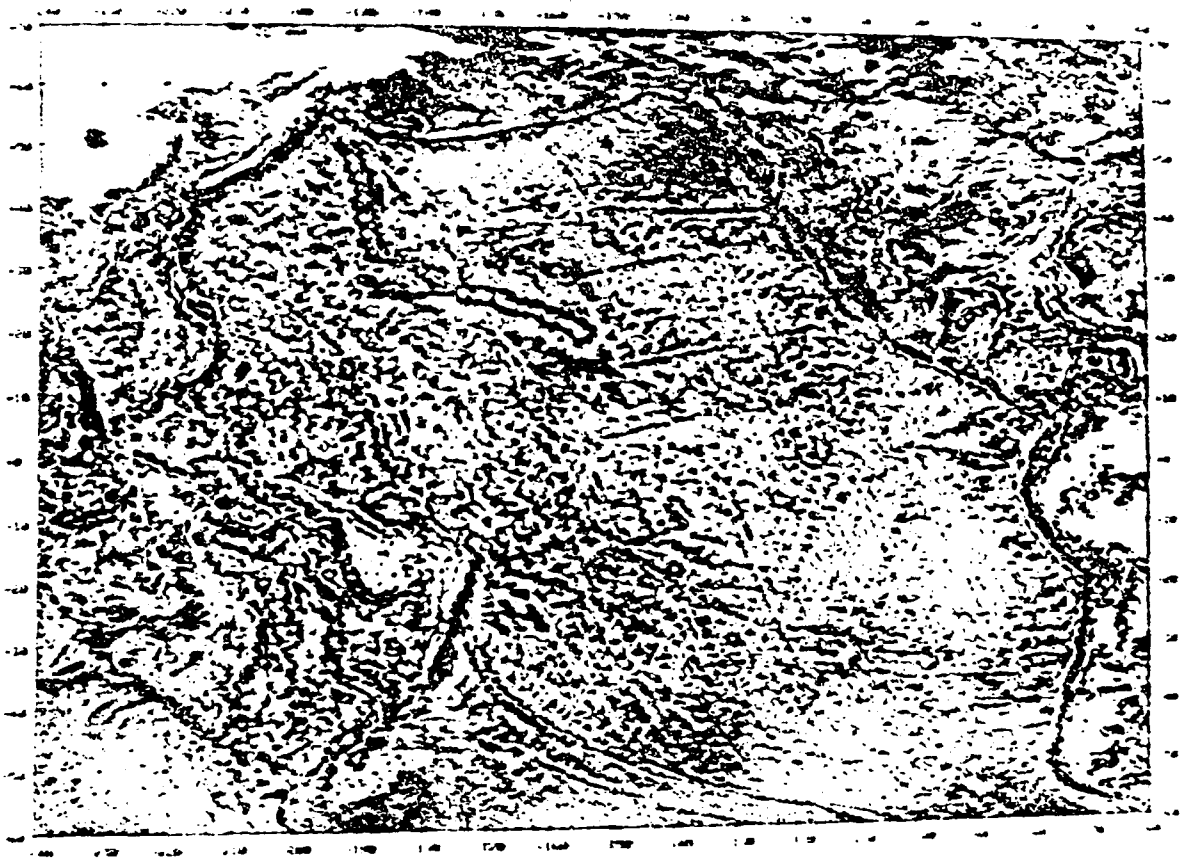


FIGURE 3. RESIDUAL VERTICAL GRAVITY GRADIENT

COMBINING GRAVITY GRADIOMETRY WITH OTHER  
EXPLORATION METHODS FOR GEOPHYSICAL PROSPECTING

by

Dr. Anthony A. Vassiliou  
Department of Surveying Engineering  
The University of Calgary  
2500 University Drive N.W.  
Calgary, Alberta  
CANADA T2N 1N4

ABSTRACT

The Parker-Oldenburg algorithm for fast computation of potential field anomalies is modified to allow for multilayer inversion of gravity data. First the algorithm is developed for the inversion of gravity anomaly data and then it is further extended to suit airborne gravity gradiometer data. It is shown that the use of gradiometer data is preferable to the use of gravity anomaly data for the computation of the anomalous density and topography of subsurface densities. The solution of the inverse gravity problem is constrained by density and if possible layer depth information. Density information can be obtained from borehole surveys or from computed compressional seismic velocities via a non-linear formula. Subsurface layer information can be obtained from inverted seismic reflection data. In addition to gravity gradiometer data, the same inversion algorithm can be employed to determine magnetic susceptibility for subsurface magnetized layers. Using aeromagnetic data the depth of these layers is determined by using the Spector-Grant spectral method.

COMBINING GRAVITY GRADIOMETRY WITH OTHER  
EXPLORATION METHODS FOR GEOPHYSICAL PROSPECTING

Anthony A. Vassiliou

Department of Surveying Engineering  
The University of Calgary  
2500 University Drive N.W.  
Calgary, Alberta

Paper presented at the 15th Gravity Gradiometer Conference  
Colorado Springs, U.S.A.  
February 11-12, 1987

Objective:      Develop a method to determine the anomalous density and depth of subsurface layers using gravity gradiometer data and incorporating information from other geophysical prospecting methods.

Content:

- Forward Parker's algorithm.
- Single layer inversion using gravity anomaly and gravity gradiometer data.
- Multilayer inversion with gravity anomaly and gradiometer data.
- Constraints on the multilayer inversion from other geophysical exploration methods.

# 1. Forward Parker's algorithm

If  $F\{ \}$  : Fourier transform of  $\{ \}$   
 $G$  : Newton's gravitational constant  
 $\rho(x,y)$  : density  
 $z_0$  : altitude at which gravity data are observed  
 $h(x,y)$  : layer topography  
 $T$  : anomalous gravity potential  
 $T_{ij}$  : second-order gradients of  $T$   
 $u, v$  : spatial frequencies in the two directions  
 $q$  :  $(u^2 + v^2)^{1/2}$

then:

$$F\{T(x,y)\} = 2\pi G e^{-2\pi q z_0} \sum_{n=1}^{\infty} \frac{(2\pi q)^{n-2}}{n!} F\{\rho(x,y) h^n(x,y)\}$$

$$F\{\Delta g(x,y)\} = -2\pi G e^{-2\pi q z_0} \sum_{n=1}^{\infty} \frac{(2\pi q)^{n-1}}{n!} F\{\rho(x,y) h^n(x,y)\}$$

$$F\{T_{xx}(x,y)\} = -2\pi G e^{-2\pi q z_0} \sum_{n=1}^{\infty} \frac{(2\pi q)^{n-1}}{n!} \frac{2\pi u^2}{q} F\{\rho(x,y) h^n(x,y)\}$$

$$F\{T_{yy}(x,y)\} = -2\pi G e^{-2\pi q z_0} \sum_{n=1}^{\infty} \frac{(2\pi q)^{n-1}}{n!} \frac{2\pi v^2}{q} F\{\rho(x,y) h^n(x,y)\}$$

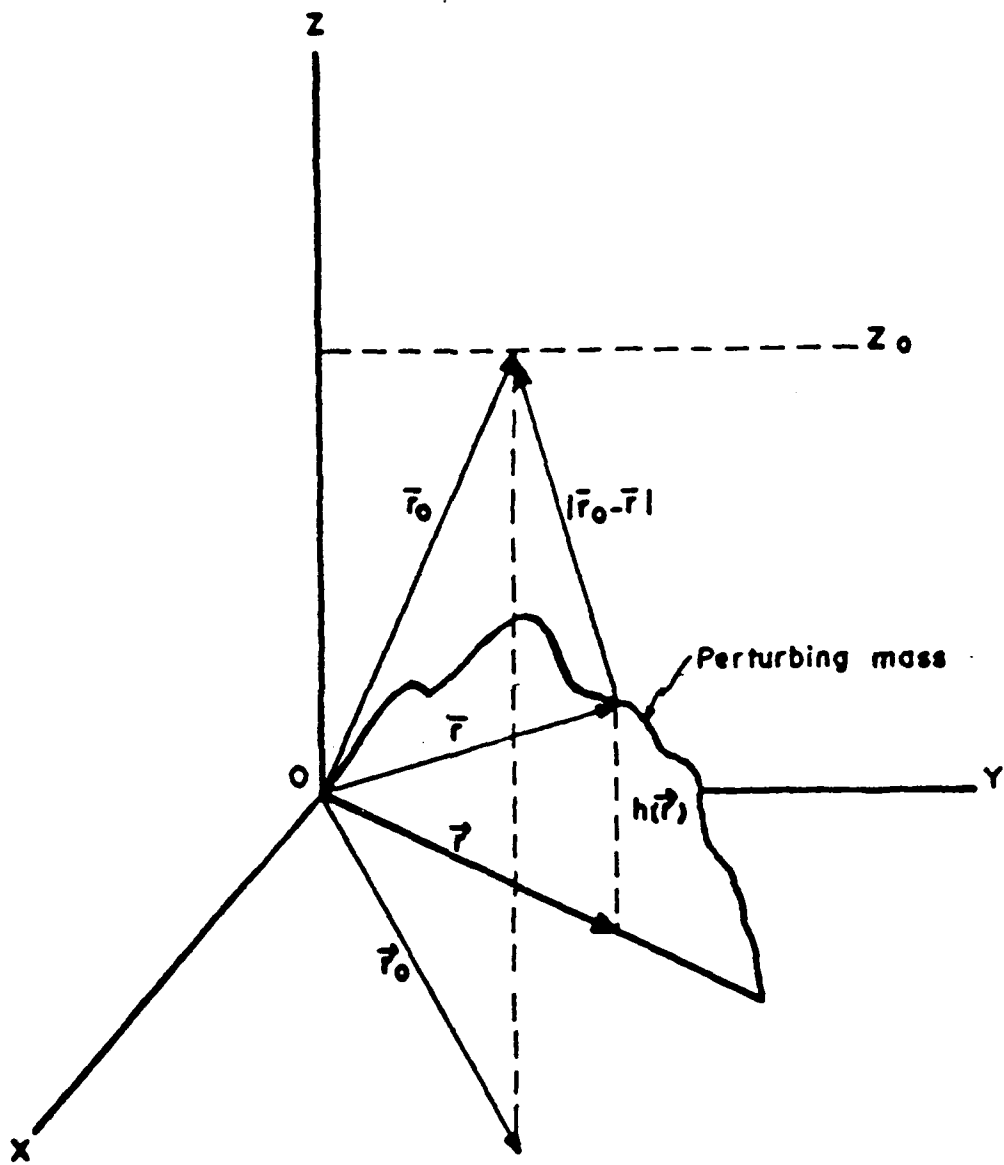
$$F\{T_{zz}(x,y)\} = 2\pi G e^{-2\pi q z_0} \sum_{n=1}^{\infty} \frac{(2\pi q)^n}{n!} F\{\rho(x,y) h^n(x,y)\}$$

$$F\{T_{xy}(x,y)\} = -2\pi G e^{-2\pi q z_0} \sum_{n=1}^{\infty} \frac{(2\pi q)^{n-1}}{n!} 2\pi uv F\{\rho(x,y) h^n(x,y)\}$$

$$F\{T_{xz}(x,y)\} = -2\pi G e^{-2\pi q z_0} \sum_{n=1}^{\infty} \frac{(2\pi q)^{n-1}}{n!} j 2\pi u F\{\rho(x,y) h^n(x,y)\}$$

$$F\{T_{yz}(x,y)\} = -2\pi G e^{-2\pi q z_0} \sum_{n=1}^{\infty} \frac{(2\pi q)^{n-1}}{n!} j 2\pi v F\{\rho(x,y) h^n(x,y)\}$$

$j$  is the imaginary unit.



## Single Layer Inversion

• Assume gravity anomaly data are available and have been corrected for any thin sediments or water overlying the layer. Also assume that the density varies in some smooth fashion reasonably known. Then the layer topography  $h(x,y)$  is determined from

$$F\{\rho(x,y)h(x,y)\} = - \frac{F\{\Delta g(x,y)\} e^{2\pi q z_0}}{2-G} - \sum_{n=2}^{\infty} \frac{(2\pi q)^{n-1}}{n!} F\{\rho(x,y)h^n(x,y)\} \quad (1)$$

• Use equation (1) in an iterative inversion. Start with some estimate of  $h(x,y)$  (probably given from borehole surveys), compute R.H.S. of (1) up to  $n=N$ , then compute L.H.S. and take its inverse 2-D FFT to get  $h(x,y)$ . Iterate to achieve convergence. The degree  $n=N$  up to which the sum in the R.H.S. of (1) is computed, is determined from the ratio  $(S_N/S_2) < 1.0 \times 10^{-3}$  (with  $S_n = (2\pi q)^{n-1}/n! F\{h^n(x,y)\rho(x,y)\}$ ). Convergence in the iterative algorithm is considered when the r.m.s. of the differences between two consecutive estimates of gridded  $h(x_i, y_k)$  is smaller than 0.3 m.

• Excessive noise amplification in downward continuation is prevented by low-pass filtering. For gravity anomaly profiles, it has been suggested by Oldenburg to use cutoff passband frequency  $u_p: 0.05 \leq u_p \leq 0.1$  (cycles/profile spacing) and edge of the stopband critical frequency  $0.15 \leq u_s \leq 0.25$ .

• For gravity gradiometer data higher limits for cutoff frequency  $u_p$  and stopband critical frequency  $u_s$  have to be used, due to their high frequency signature. Therefore less information will be smoothed out in the downward continuation.

• The iterative inversion algorithm expressed by equation (1) converges only for densities larger than a minimum density  $\rho_{\min}$ . It also converges for heights  $z_0 > \text{minimum } z_0$ . In short, convergence depends on the density contrast, depth of the subsurface layer and the passband; stopband frequencies of the low-pass filter.

### Single Layer Gravity Inversion (continued)

• Using gravity gradiometer data, we have six data sets instead of one to determine the subsurface layer topography. Thus the determination of  $h(x,y)$  is strengthened due to the additional information, and thus the solution becomes more reliable. The equations for the iterative inversion of  $h(x,y)$ , using gradients  $T_{ij}$  are derived from the forward Parker's algorithm in the same way as for the gravity anomaly data.

# Gravity Gradient Single Layer Inversion

• For simplicity assume  $T_{xz}(x,y)$ ,  $T_{yz}(x,y)$ ,  $T_{zz}(x,y)$  data.

• From the forward Parker's algorithm, after reconstructing the equations

$$F\{\rho_1(x,y)h_1(x,y)\} = - [F\{T_{xz}(x,y)\}/2\pi G]e^{2\pi qz_1} -$$

$$\sum_{n=2}^{\infty} \frac{(2\pi q)^{n-1}}{n!} j2\pi u F\{\rho_1(x,y)h_1^n(x,y)\}$$

$$F\{\rho_1(x,y)h_1(x,y)\} = - [F\{T_{yz}(x,y)\}/2\pi G]e^{2\pi qz_1} -$$

$$\sum_{n=2}^{\infty} \frac{(2\pi q)^{n-1}}{n!} j2\pi v F\{\rho_1(x,y)h_1^n(x,y)\}$$

$$F\{\rho_1(x,y)h_1(x,y)\} = - [F\{T_{zz}(x,y)\}/2\pi G]e^{2\pi qz_1} -$$

$$\sum_{n=2}^{\infty} \frac{(2\pi q)^n}{n!} F\{\rho_1(x,y)h_1^n(x,y)\}$$

• Iterate for each one of the  $T_{xz}$ ,  $T_{yz}$ ,  $T_{zz}$  data sets, to finally compute three sets of subsurface layer topography  $h_1(x,y)$ . Then combine the solutions for  $h_1(x,y)$  from  $T_{xz}$ ,  $T_{yz}$ ,  $T_{zz}$  using spectral weighting

$$F\{\hat{h}_1(x,y)\} =$$

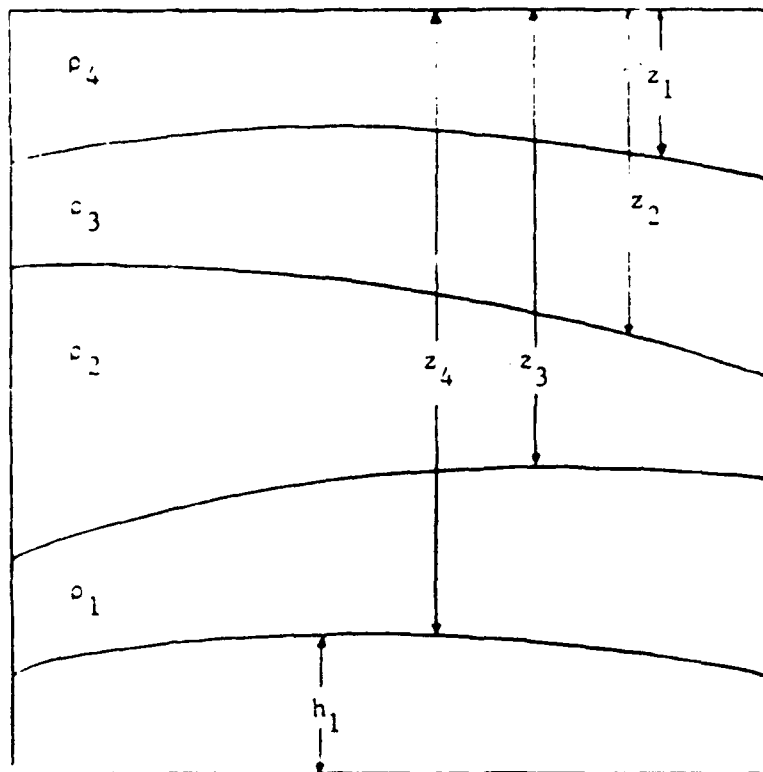
$$\frac{S_{h_{1,1}}(u,v)F\{h_{1,1}(u,v)\} + S_{h_{1,2}}(u,v)F\{h_{1,2}(u,v)\} + S_{h_{1,3}}(u,v)F\{h_{1,3}(u,v)\}}{S_{h_{1,1}}(u,v) + S_{h_{1,2}}(u,v) + S_{h_{1,3}}(u,v)}$$

where  $h_{1,1}$ ;  $h_{1,2}$ ;  $h_{1,3}$  ... solutions for  $h_1(x,y)$  from  $T_{xz}$ ,  $T_{yz}$ ,  $T_{zz}$  respectively

$S_{h_{1,1}}$ ;  $S_{h_{1,2}}$ ;  $S_{h_{1,3}}$  ... are the corresponding amplitude spectra.

• This iterative weighting procedure can be applied for more than three data sets.

## Multilayer Gravity Inversion



$$\sigma_i = \rho_{i-1} - \rho_i \quad (i=1,2,3,4)$$

density contrasts

• For simplicity we use gravity anomaly data. Assume a 4 layer model on top of which a layer (composed of sediments, water) with density  $\rho_4$  is located. The density and bedthickness of layers 1,2,3 are known. Determine the topography of the bottom layer  $h(x,y)$  having some knowledge of the density  $\rho$ .

• Use Parker's formula for more than one layer

$$F\{\Delta g(x,y)\} = 2\pi G \sum_{k=1}^4 e^{-2\pi q z_k} \sum_{n=1}^{\infty} \frac{(2\pi q)^{n-1}}{n!} F\{\sigma_k(x,y) h_k^n(x,y)\} \quad (2)$$

• Reconstruct the formula for multilayer inversion

$$F\{\sigma_1(x,y) h_1(x,y)\} =$$

$$- [F\{\Delta g(x,y) - \Delta g(x,y)_{\text{others}}\} / 2\pi G] e^{2\pi q z_1} - \sum_{n=2}^{\infty} \frac{(2\pi q)^{n-1}}{n!} F\{\sigma_1(x,y) h_1^n(x,y)\} \quad (3)$$

# Multilayer Gravity Inversion (continued)

with  $\Delta g(x,y)$  determined from  
others

$$P\{\Delta g(x,y)\}_{\text{others}} = -2\pi G \sum_{k=1}^4 e^{-2\pi q z_k} \sum_{n=1}^{\infty} \frac{(2\pi q)^{n-1}}{n!} P\{\sigma_k(x,y) h_k^n(x,y)\} \quad (4)$$

• Equation (3) is used in an iterative manner to solve for the unknown topography  $h_1(x,y)$ . Some apriori (or model) knowledge about  $h_1(x,y)$  is necessary. This knowledge will provide the depth  $z_1$ .

• The depth of each layer  $k, z_k$ , is then determined by

$$z_{k+1} = z_k - (\text{bed thickness})_{k+1} \quad (5)$$

• The values of  $h_1(x,y)$  vary at each iteration, thus the depths  $z_k$  need to be updated. Due to this updating, the gravity anomaly  $\Delta g(x,y)$  will  
others

vary as well. A reasonable starting model for  $\Delta g(x,y)$  would prob. bly be  
others

$$\Delta g(x,y)_{\text{others}} = \Delta g(x,y)_{\text{observed}} + \frac{\sum_{k=1}^4 \sigma_k(x,y)}{\sum_{k=1}^4 \sigma_k(x,y)} \quad (6)$$

• Combining equations (3), (4), (5), (6) an iterative procedure for computing the topography  $h_1(x,y)$  can be employed.

## Multilayer Gravity Gradient Inversion

- Assume for simplicity that only  $T_{xz}$ ,  $T_{yz}$ ,  $T_{zz}$  are available.
- From the multi-layer formulation of the forward Parker's algorithm we get after reconstruction of the formulas

$$F\{\sigma_1(x,y)h_1(x,y)\} = - \left[ \underset{\text{observed}}{F(T_{xz}(x,y))} - \underset{\text{others}}{T_{xz}(x,y)} \right] / 2\pi G e^{2\pi qz_1} - \sum_{n=2}^{\infty} \frac{(2\pi q)^{n-1}}{n!} j 2\pi u F\{\sigma_1(x,y)h_1^n(x,y)\}$$

$$F\{\sigma_1(x,y)h_1(x,y)\} = - \left[ \underset{\text{observed}}{F(T_{yz}(x,y))} - \underset{\text{others}}{T_{yz}(x,y)} \right] / 2\pi G e^{2\pi qz_1} - \sum_{n=2}^{\infty} \frac{(2\pi q)^{n-1}}{n!} j 2\pi v F\{\sigma_1(x,y)h_1^n(x,y)\}$$

$$F\{\sigma_1(x,y)h_1(x,y)\} = - \left[ \underset{\text{observed}}{F(T_{zz}(x,y))} - \underset{\text{others}}{T_{zz}(x,y)} \right] / 2\pi G e^{2\pi qz_1} - \sum_{n=2}^{\infty} \frac{(2\pi q)^n}{n!} F\{\sigma_1(x,y)h_1^n(x,y)\}$$

where  $\underset{\text{others}}{T_{xz}(x,y)}$ ,  $\underset{\text{others}}{T_{yz}(x,y)}$ ,  $\underset{\text{others}}{T_{zz}(x,y)}$  are the gradients  $T_{xz}$ ,  $T_{yz}$ ,  $T_{zz}$

computed from the other three layers.

- The same iteration procedure as for the gravity data has to be applied for gravity gradient data. To combine the solutions  $h_{1,1}$ ,  $h_{1,2}$ ,  $h_{1,3}$  for the subsurface topography from  $T_{xz}$ ,  $T_{yz}$ ,  $T_{zz}$  respectively we use a spectral weighting scheme as in the single layer case.

### Multilayer Gravity Gradient Inversion (continued)

- After stripping the overlying layers, single layer inversion has essentially to be performed. Deeper layer inversion can then be attempted by examining a lower frequency band.

- Again the advantage of using gravity gradiometer data is that five more data sets are available with higher frequency content. Thus the solution for  $h_1(x,y)$  is more reliable and more detailed for shallow depths.

## Constraints on Multilayer Gravity Inversion from Other Geophysical Methods

- The inverted surface need not be the bottom one, as long as information about the other layers is available.
- Densities from the other layers can be obtained from seismic data, or from borehole surveys. Borehole data will provide density information at two, or three points (maybe a few more) in the area of interest. Then the densities between these points can be assumed to vary linearly.
- Information about bedthickness for each of the other layers can be obtained from seismic reflection data or from well logs or from sonic logs.
- If detailed information about the shape of each layer is not available (as is often the case), then a reasonable approximation is that the topography of the other layers varies in the same way as the topography of the inversion subsurface.
- For the gravity correction due to the sedimentary layers, the density (for Western Canada), is taken from extensive density logging as

$$\rho = 2.266 + 0.146 z \pm 0.210 \text{ (gr/cm}^3\text{)} \quad (z: \text{ depth of sediments})$$

- Assuming known compressional (P-wave) velocities with depth, from seismic traveltime inversion, a reasonable density approximation can be obtained from the non-linear formula

$$\rho = 0.23 V^{0.25} \quad (V : \text{ P-wave seismic velocity})$$

- Information about densities can also be obtained from deconvolution of reflection seismograms and computed reflection coefficients. In this case the density or velocity for some layer should be known (not the upper sedimentary weathering layer though).

## Magnetic Data-Relation to Gravity Data

- For a constant ratio of density  $\rho$ , to magnetic susceptibility  $k$

$$T = \frac{\rho}{k} : \text{constant}$$

the magnetic anomalous potential  $W$  is related to the first order gradients of the anomalous gravity potential  $T$  by the Poisson's equation

$$W = - \frac{\underline{H}_0 \cdot \nabla T}{T \mu_0 G} \quad \text{with } \underline{H}_0 : \text{ magnetic field strength}$$
$$\mu_0 : \text{ magnetic permeability}$$

- A similar relation can be developed between the magnetic field anomaly  $B$  ( $B = -\nabla W$ ) and the second-order gradients of  $T$ . Inversion of magnetic anomaly data resembles very much the inversion of gravity gradiometer data.

- The anomaly in the direction of the perturbing field  $|\nabla B|$  is related to the magnetic susceptibility by the relation

$$F(|\Delta B|) = \frac{2\pi \underline{N}(u,v) q |\underline{H}_0| e^{-2\pi q z}}{\mu_0} \sum_{n=1}^{\infty} \frac{(2\pi q)^{n-1}}{n!} F(k(x,y) h^n(x,y))$$

where the dimensionless vector  $\underline{N}(u,v)$  is a function of magnetic declination  $D$  and magnetic inclination  $I$ .

- Information about the depths of the magnetized layers can be obtained from the PSD of aeromagnetic intensity data, by using the method developed by Spector and Grant.

## Conclusions

- Forward Parkers's algorithm can be used to invert gravity anomaly and gravity gradiometer data in an iterative mode.
- By using gravity gradiometer data, a solution can be obtained for the shallower layers with better detail than for deeper layers for which gravity anomaly data have to be used.
- Knowledge of depth and density of the overlying layers constrains the solution for the layer topography.
- Depth and density information about the subsurface layers can be obtained from either borehole surveys or inverted seismic reflection travelttime data, or from density logs or from sonic logs.
- The same algorithm as for gravity anomaly and gravity gradient data can be used for magnetic anomaly data, thus yielding magnetic susceptibility values. Information about the magnetized layer depth can be obtained from analysis of aeromagnetic data.

COMPUTATION OF THE GRAVITY VECTOR  
FROM TORSION BALANCE DATA IN SOUTHERN OHIO

by

Dr. D. Arabelos  
Department of Geodesy and Surveying  
University of Thessaloniki  
Greece

Mr. Christian Tscherning  
Geodætisk Institut  
Geodetic Department I  
Gamlehave Alle 22  
2920 Charlottenlund  
Denmark

ABSTRACT

The method of least squares collocation was used for gravity vector estimation from torsion balance measurements in Southern Ohio. The results were dependent on the covariance function used and on the selection of a proper signal to noise ratio. Here a standard deviation of the noise of 10 E.U. ( $10^{-9} \text{ s}^{-2}$ ) gave the best results. Expressed in terms of standard deviations of observed minus predicted differences, the best results were 0.4" for deflections of the vertical and 2 mgal for gravity anomalies. This compares to signal standard deviations of 4" and 22 mgal for deflections and gravity anomalies, respectively.

# COMPUTATION OF THE GRAVITY VECTOR FROM TORSION BALANCE DATA,

IN SOUTHERN OHIO.

by

D. Arabelos	and	C. C. Tscherning
Department of		Geodaetisk Institut
Geodesy and Surveying		Geodetic Department I
University of Thessaloniki		
Greece		Denmark

Abstract: The method of least squares collocation was used for gravity vector estimation from torsion balance measurements in Southern Ohio. The results were dependent on the covariance function used and on the selection of a proper signal to noise ratio. Here a standard deviation of the noise of 10 E.U. ( $10^{-9} \text{ s}^{-2}$ ) gave the best results. Expressed in terms of standard deviations of observed minus predicted differences, the best results were 0.4" for deflections of the vertical and 2 mgal for gravity anomalies. This compares to signal standard deviations of 4" and 22 mgal for deflections and gravity anomalies, respectively.

## 1. Introduction.

The method of collocation and similar optimal estimation techniques have been proposed as possible methods for gravity vector estimation from gravity gradiometer data, see e.g. Jekeli (1985). Since gravity gradiometer data are not yet available, the estimation procedures have only been tested using simulated data. However, the torsion balance delivers measurements of the same kind as the gradiometer, namely linear combinations of second order derivatives of the gravity potential ( $W$ ).

Using torsion balance data we may then demonstrate how least-squares collocation (LSC) can be used for gravity vector estimation, and also show which type of difficulties one may encounter while using the method.

In order to draw conclusions from the use of torsion balance data to the use of gravity gradiometer data, the data distribution should correspond to the one planned for the gradiometer. Furthermore gravity vector data must also be available in the same area as the torsion balance data. Such an optimal situation is found in a  $0.25 \text{ deg.} \times 0.75 \text{ deg.}$  area in Southern Ohio, where gravity data, deflections of the vertical and torsion balance data were observed and collected in the period prior to 1970. The data is somewhat sparser than the one planned for gradiometry, and the area covered is smaller than the typical area foreseen to be covered by some hours of aerial gradiometer measurements. Furthermore the data is not observed at altitude, but at ground level. Also Southern Ohio is not typical, since the area has no large height variations. However, in an operational situation, topographic effects will in general have to be removed (and restored). In this way all areas from the standpoint of the gravity field variation will look like Ohio (Forsberg, 1984, table 6). Also the gravity variation at an altitude of 0.5 - 2.0 km will not be much different from the variation at ground level, when topographic effects have been removed. Furthermore, as we shall see, an increase in the data density would probably not have improved the quality of the prediction vector.

Deflection of the vertical estimation have been successfully tested in Southern Ohio by Badekas and Mueller (1968), using a simple numerical integration method. With LSC we should be (and have been) able to obtain similar results, the advantage being that the method not only enables the estimation of the gravity vector at points where the measurements have been made, but also in all points within a certain distance from the measurements. LSC permits the estimation of the prediction error as well.

In section 2 we will introduce the available data, and in section 3 we will describe the use of LSC, and the associated process of estimating the so-called empirical covariance function. The results obtained using various combinations of the data as well as different analytic models for the empirical covariance function are described in section 4.

## 2. The Southern Ohio test data set.

Let  $W$  be the gravity potential and  $U$  a corresponding reference (normal) potential. Then the anomalous gravity potential is the difference  $T = W - U$ .

The long-wavelength part of  $W$  ( or  $T$  ) is described down to a 1 deg. resolution by one of the available spherical harmonic expansions complete to degree and order  $N=180$  such as the OSU81 and the GPM2 coefficient sets (see Rapp(1981), Wenzel(1985)).

Free-air gravity anomalies ( $\Delta g$ ) have been published by Heiskanen and Uotila (1956), and deflections of the vertical ( $\xi, \eta$ ) by Mueller and Preuss (1965). They are in spherical approximation related to  $T$  through the following equations (Heiskanen and Moritz, 1967).

$$\Delta g = - \frac{\partial T}{\partial r} - \frac{2}{r} T \quad (1)$$

$$\xi = - \frac{1}{r\gamma} \frac{\partial T}{\partial \phi} \quad (2)$$

$$\eta = - \frac{1}{r \cos \phi \gamma} \frac{\partial T}{\partial \lambda} \quad (3)$$

where  $\phi$  is the latitude,  $\lambda$  the longitude,  $\gamma$  normal gravity and  $r$  the distance from the origin, which in spherical approximation is obtained as the sum of the Earth mean radius and the height. Torsion balance data are published by Badekas(1967), and their relations to  $T$  are

$$T_{xz} = \frac{\partial^2 T}{\partial x \partial z} \quad (4)$$

$$T_{yz} = \frac{\partial^2 T}{\partial y \partial z} \quad (5)$$

$$2T_{xy} = 2 \frac{\partial^2 T}{\partial x \partial y} \quad (6)$$

$$T_{\Delta} = \frac{\partial^2 T}{\partial y^2} - \frac{\partial^2 T}{\partial x^2} \quad (7)$$

where  $(x, y, z)$  are the coordinates of a local-level coordinate system with  $x$  east,  $y$  north and  $z$  up. The distribution of the torsion balance data is shown in Fig. 1.

Digital topographic heights was not available. However, topographic effects have been published for the torsion balance in the same publication as the observations and for the deflections in Badekas and Mueller (1968). The topographic effects on the gravity data may be calculated using the simple Bouguer plate reduction, since the terrain corrections are rather small due to the smooth topography.

The use of the spherical harmonic coefficients within the framework of LSC is equivalent to subtracting the contribution of the coefficients from the data. Since the data used for the determination of the coefficients primarily are free-air gravity anomalies, the coefficients also represent the attraction of the topographic masses down to 1 deg. resolution. Consequently only the effect of a Bouguer plate referring to the mean altitude of the topography (265 m) must be subtracted from the gravity anomalies. However, this creates an inconsistency between the topographic corrections for the gravity data and for the other data types, which as we shall see later will result in biases in the predicted results using topographic reduced data. This problem is easily avoided in practice, if a detailed topographic model is available.

Table 1 shows the statistical characteristics of (1) the "raw" data, (2) the data from which the contribution from a set of spherical harmonic coefficients (GPM2 to maximal degree 180) have been subtracted and (3) the data (2) minus the topographic effects. Also statistics for a subset of the gravity data located in an area close to the torsion balance data is given in the table. These 12 gravity values have also been used in the following when comparing observed and predicted quantities.

Note the striking difference in the mean values. In fact, the area is located on the top and east of a large anomalous mass. Also note, that the deflections of the vertical have been transformed from NAD1927 to the preliminary NAD83 using datum shifts parameters provided by the

U.S. National Geodetic Survey. The gravity values have been transformed from the Potsdam system to GRS1980 using a bias correction of 13.7 mgal. Hence a small bias with respect to IGSN 1971 may still be left.

### 3. Least-squares collocation and covariance functions.

The theory and practice of LSC is described in numerous publications. A recent survey is given in Tscherning(1985b).

Suppose we have given  $n$  observations related to the anomalous gravity field through  $n$  linear functionals (eq. (1) - (7)) ,

$$L_i(T) = y_i + e_i, \quad i = 1, \dots, n.$$

Here  $e_i$  is the noise or error. Then let  $C_{ij}$  denote the covariance between  $L_i(T)$  and  $L_j(T)$  and  $C_{Li}$  the covariance between the value of a linear functional  $L$  applied on the anomalous potential,  $L(T)$ , and  $L_i(T)$ . We then obtain an estimate  $L(\bar{T})$  of  $L(T)$  as

$$L(\bar{T}) = \{C_{Li}\}^T \{C_{ij} + D_{ij}\}^{-1} \{y_j\} \quad (8)$$

where  $D_{ij}$  is the covariance of the noise associated with the  $i$ 'th and  $j$ 'th observations. Let  $\bar{C}$  denote the sum of the  $C_{ij}$  and  $D_{ij}$  matrices. Then an estimate of the mean square error for a linear functional is obtained by

$$\sigma^2(L(\bar{T}) - L(T)) = C_{LL} - \bar{C}_L^T \bar{C}^{-1} C_L \quad (9)$$

where  $C_L$  is the vector of covariances between the observations and the quantity  $L(T)$  and  $C_{LL}$  is the variance of this quantity.

Similar equations are obtained if, instead of the observations  $y$ , we use the values from which we have subtracted the effect of the topography or the contribution from a spherical harmonic expansion. On the right hand side ( of eq. (8) ) the covariance function will be the one associated with these residual observations. The vector of

observations will consist of these residuals and on the left hand side we get the residual potential, to which in the final step we should add back the potential implied by the topography and the spherical harmonic expansion. In the case we only have subtracted the contribution from GPM2, we will associate a superscript "s" with the relevant quantity, and if also the topographic effects have been subtracted we will use the superscript "t", i.e.  $\Delta g^t$ .

The starting point for the use of LSC in a local area is the computation and analytic modelling of the empirical covariance function. Its estimation is discussed in detail in Goad et al. (1984). Numerically the estimation is simply done as the computation of the mean value of products of quantities lying within the same interval of spherical distance. The size of this interval is called the sampling interval. For vector quantities, like components of deflections of the vertical, the components of the horizontal gravity (disturbance) gradient (eq. (4), (5)) and the mixed second order derivatives (eq. (6), (7)), the products are formed between products of "along-track" and "cross-track" components. For details, see Krarup and Tscherning (1984).

The quality of the estimation depends on the size of the sampling error, the regularity of the data distribution and the data error. The size of the area should also be so large that the mean value of the quantities (from which the contribution from the spherical harmonic expansion, here GPM2, have been subtracted),  $y_i^s$ , is zero. For a spherical harmonic expansion to degree 180, this generally will be achieved for a 1.5 - 2 deg. equal angular area, since mean values of 1 deg. blocks have been used for the computation of the coefficients.

For the approximately 1 deg. block surrounding the torsion balance data the mean value of the available 227  $\Delta g$ -values is -3.3 mgal (cf. Table 1). Since the standard deviation is 19.8 mgal, this mean value is not significantly different from zero. The gravity values in this area were therefore used for the estimation of the covariance function, both using  $\Delta g^s$  and  $\Delta g^t$  values (cf. Fig. 2 and 3).

When estimating cross-covariance functions with the torsion balance data, we have the problem that the data covers a much smaller area. Furthermore (cf. Table 1), the gravity variation in the  $0.75 \text{ deg} \times 0.85 \text{ deg}$  area is significantly different from the variation in the area immediately surrounding the torsion balance data. Here the variation is much larger, and the mean values are non-zero. We decided anyway to estimate empirical auto- and cross-covariance functions between the (GPM2 and GPM2 + terrain reduced) gravity and torsion balance data. Figures 4 to 12 show the covariance functions for the GPM2 reduced data. It should be noted that the mean values have not been subtracted from the data.

The modelling of the empirical covariance function is based on the fitting of an analytic expression to the empirical values. We used a model for the gravity anomaly covariance function, developed in Tscherning and Rapp (1974),

$$C(P,Q) = \sum_{i=181}^{\infty} \frac{A(i-1)}{(i-2)(i+4)} \left( \frac{R_B^2}{r r'} \right)^{i+2} P_i(\cos \psi_{PQ}), \quad (10)$$

with the two free parameters  $A$  and  $R_B$ . In this expression  $r'$  is the distance of the point  $Q$  from the origin,  $P_i$  the Legendre-polynomial of degree  $i$ ,  $\psi_{PQ}$  the spherical distance between  $P$  and  $Q$  and  $R_B$  is the radius of the so-called Bjerhammar sphere. The summation starts from 181, since we have subtracted the effect of GPM2 to degree 180. This is equivalent to presupposing that the coefficients are error free, a hypothesis which is certainly not true. However, the consequence of adopting the hypothesis will mainly be seen in predicted geoid heights, see Arabelos(1980). Also the start of the summation from  $i=180$  made it reasonable to introduce a modification, namely the division by  $i+4$  instead of a division by  $i+24$  in eq. (10) as recommended in Ibid. (1974). This modification gives some computational savings.

The factor  $A$  in eq. (9) is linearly related to the value at spherical distance zero, the variance. The value of  $R_B$  is more difficult to estimate due to the uncertainty in the estimation of the covariances

and the weak relationship between  $R_E$  and the covariances, see Tscherning (1985b). We decided to try to find the best one (within the class of functions given by eq. (10)), simply by carrying out prediction experiments with different values of  $R_E$ , and then selecting the one, which gave the best agreement between observed and predicted deflection values. The results are summarized in Fig. 13. The analytic covariance function found using this procedure had a depth to the Bjerhammar-sphere of 3.0 km. Its graph is shown with the empirical values in Fig. 2 - 12.

It should be noted that this procedure of selecting a covariance function model very well could have been used if only torsion balance or gradiometer data had been available. A subset of the observations could have been used as test-quantities and the remaining observations as the given data. The covariance model, which gave the best results in a least squares sense must then be the one in between the used set of models, which is most close to the true empirical covariance function.

#### 4. Prediction tests and results.

For the evaluation of the predictions (eq. (8)) as well as the calculation of error estimated (eq. (9)) the FORTRAN program GEOCOL, (Tscherning, 1985a) was used.

In order to check the consistency of the gravity vector data, we first predicted the deflections at the 8 sites shown in Fig. 1 from the 227 gravity values and subsequently the 12 gravity values in the vicinity of the torsion balance data from 15 pairs of deflection points in the same area as covered by the 227 gravity values. The results are given in Table 2. Note how surprisingly well the gravity anomalies are determined from the deflections. Also note, that the deflections are predicted just as well from the gravity data as from the torsion balance data, as we shall see later.

We then wanted to predict also the torsion balance data from gravity, torsion balance from torsion balance data and gravity and deflections from torsion balance data. We assigned a noise standard deviation of

1.0 E.U. to the torsion balance data, equal to the value given in Badekas and Mueller (1968, p. 6871). However all our results were "bad", in the sense that the error estimates computed using eq. (9) were much smaller than the variance of observed minus computed values. We then spent 14 days intensively checking GEOCOL, but found no significant error. This made us go back to the publication Badekas (1967), which contains detailed maps showing the individual data in vector-like form. This revealed that neighbouring values could be rather different, signifying a much larger error level than we had expected. Also the empirically estimated auto-covariance functions indicated that a rather large noise was present. This can be seen from Figures 8 to 11, where the variance is much larger (around  $100 \text{ E.U.}^2$ ) than the value found by smoothly extrapolating from the first 2 - 3 empirical values to the value at spherical distance zero (the variance).

Then changing the noise variance to  $100 \text{ E.U.}^2$ , we suddenly obtained consistent results. This value is probably too pessimistic, but not impossible (I.I. Mueller, personal communication, 1986). We then tried using changing noise levels. The results are illustrated in Fig. 14 - 16. In fact values of the noise <sup>variance</sup> between 50 and  $150 \text{ E.U.}^2$  all give rather similar prediction results, but  $100 \text{ E.U.}^2$  gave the best results. We then used this value in the following computations.

Having arrived so far, we decided to make a series of computational experiments, which should illustrate the dependence of the prediction result on

- (1) the model selected for the covariance function
- (2) the use or non-use of the topography
- (3) the data type and the combination of various data types
- (4) the data density.

The dependence on the covariance function as mentioned already has been used to select a "best" analytic model. The dependence on the model (the depth to the Bjerhammar-sphere) is illustrated in Fig. 13.

The use of topographic data results in a slight smoothing of the gravity field data (cf. Table 1), and we should expect a similar

improvement of the prediction results. However, as seen from Table 3 not very much is gained, but this is probably due to the high data-density. The topographic information is a-priori well represented by the data.

In order to see the influence of the data density we used either all data points or one value from each  $2' \times 2'$  cell. Using all data gave only a small improvement as seen from Table 3. More interesting is the clear difference in contribution from the various torsion balance components to the components of the gravity vector. We maybe should expect the significant contribution of the horizontal gradient of the gravity disturbance to the deflection components from geometrical reasons and from the results presented in Table 2, where gravity data were used to predict deflections. The mixed second order derivatives contributes little, but anyway something of significance.

It is clear that we can not estimate the absolute values of the gravity vector components from torsion balance data alone. This is also confirmed, since we get relatively large biases (cf. Table 3). However, gravity vector differences are well determined as seen from the small standard deviations in the table. On the other hand, we can easily add observed gravity vector information to the input data in LSC. We selected one of the deflection points, which coincide with one of the points of the torsion balance network, but we had to select a gravity station at some distance ( 1 km ) from the network. The result is given in Table 4. We see that most of the biases have decreased, but the bias in the topographically reduced  $\Delta g$  has increased. The reason for this may as mentioned be due to the inconsistency of the topographic reductions.

Contour plots showing the predicted gravity anomaly and deflection components with the estimated errors of prediction (eq. (9)) are shown in Fig. 17 - 21.

## 5. Conclusion.

We have seen how LSC is suitable for gravity vector estimation in a local area from gradiometer-like data. If the method should be used economically for data distributed over large areas, then the area must be split in sub-areas of reasonable size.

The results obtained in the best cases ( 0.4" for deflections and 1.6 mgal for gravity anomalies) is very encouraging since the gradiometer is supposed to have a noise level below 1 E.U. However, as we have seen it is important to use a reasonable signal to noise ratio.

The proper removal of biases, using observed components of the gravity vector requires some further investigations. Here a data set covering a larger area would be suitable, permitting the proper estimation of all cross-covariance functions.

Acknowledgement: This work was carried out while the first author was a visiting scientist at the Geodaetisk Institut, Denmark.

## References:

Arabelos, D.: Untersuchungen zur gravimetrischen Geoidbestimmung, dargestellt am Testgebiet Griechenland. Wiss. Arb. d. Fachrichtung Vermessungswesen d. Universitaet Hannover, Hannover 1980.

Badekas, J.: Torsion Balance Observations in Southwest Ohio. Report of the Department of Geodetic Science, Report No. 89, The Ohio State University, Columbus, 1967.

Badekas, J. and I.I. Mueller: Interpolation of the Vertical Deflection from Horizontal Gravity Gradients. J.Geophys.Res., Vol. 73, No. 22, pp. 6869-6878, 1968.

Forsberg, R.: A Study of Terrain Reductions, Density Anomalies and Geophysical Inversion Methods in Gravity Field Modelling. Reports of the Department of Geodetic Science and Surveying, No. 355, The Ohio State University, Columbus, Ohio, 1984.

Goad, C.C., C.C.Tscherning and M.M.Chin: Gravity Empirical Covariance values for the Continental United States. J.Geophys.Res., Vol. 89, No. B9, pp. 7962-7968, 1984.

Heiskanen, W.A. and H.Moritz: Physical Geodesy. W.H.Freeman & Co, San Francisco, 1967.

Heiskanen, W.A. and U.A. Uotila: Gravity Survey of the State of Ohio. Institute of Geodesy, Photogrametry and Cartography Publication, No. 6, The Ohio State University, 1956.

Jekeli, C.: On Optimal Estimation of Gravity from Gravity Gradients at Aircraft Altitude. Rev. of Geophysics, Vol. 23, pp. 301-311, 1985.

Krarup, T. and C.C. Tscherning: Evaluation of Isotropic Covariance Functions of Torsion Balance Observations. Bulletin Geodesique, Vol. 58, no. 2, pp. 180-192, 1984.

Mueller, I.I. and H.D. Preuss: Astro-Geodetic Deflections in Southwest Ohio. Rep. No. 61, Department of Geodetic Science, The Ohio State University, 1965.

Rapp, R.H.: The Earth's gravity field to degree and order 180 using SEASAT altimeter data, terrestrial gravity data, and other data. Reports of the Department of Geodetic Science and Surveying No. 322, The Ohio State University, Columbus, Ohio 1981.

Tscherning, C.C.: GEOCOL - A FORTRAN-program for Gravity Field Approximation by Collocation. Technical Note, Geodætisk Institut, 3.ed., 25 MAR 1985a.

Tscherning, C.C.: Local Approximation of the Gravity Potential by Least Squares Collocation. In: K.P. Schwarz (Ed.): Proceedings of the International Summer School on Local Gravity Field Approximation, Beijing, China, Aug. 21 - Sept. 4, 1984. Publ. 60003, Univ. of Calgary, Calgary, Canada, pp. 277-362, 1985b.

x

Wenzel, H.-G.: Hochauflösende Kugelfunktionsmodelle fuer das Gravitationspotential der Erde. Wiss. Arb. Fachrichtung Vermessungswesen der Universitaet Hannover, (in print), 1985.

x Tscherning, C.C. and R.H. Rapp: Global covariance expressions for Gravity Anomalies, Geoid Undulations and Deflections of the Vertical implied by anomaly degree variance models. DGS rep. no. 208, OSU, 1977.

## Figure captions.

- Fig. 1. The distribution of the torsion balance (+), gravity data (•) and deflections of the vertical (o), with the free-air gravity anomaly field contoured at 2.5 mgal interval.
- Fig. 2. Empirical (solid line) and synthetic (broken line) covariance functions for the gravity anomalies in Southern Ohio. GPM2 removed from the original data. Units  $\text{mgal}^2$ .
- Fig. 3. Empirical and synthetic covariance functions for the gravity anomalies in Southern Ohio. GPM2 and topographic (simple Bouguer plate) effect removed from the original data. Units  $\text{mgal}^2$ .
- Fig. 4. Empirical and synthetic cross-covariance functions between  $\Delta g$  and  $T_{xz}$ . Units  $\text{mgal} \cdot \text{E.U.}$
- Fig. 5. Empirical and synthetic cross-covariance functions between  $\Delta g$  and  $T_{\Delta}$ . Units  $\text{mgal} \cdot \text{E.U.}$
- Fig. 6. Empirical and synthetic cross-covariance functions between  $2 \cdot T_{xy}$  and  $T_{\Delta}$ . Units  $\text{E.U.}^2$ .
- Fig. 7. Empirical and synthetic cross-covariance functions between  $\Delta g$  and  $2 \cdot T_{xy}$ . Units  $\text{mgal} \cdot \text{E.U.}$
- Fig. 8. Empirical and synthetic auto-covariance functions for the  $T_{xz}$  component. Units  $\text{E.U.}^2$ .
- Fig. 9. Empirical and synthetic auto-covariance functions for the  $T_{yz}$  component. Units  $\text{E.U.}^2$ .
- Fig. 10. Empirical and synthetic auto-covariance functions for the  $2 \cdot T_{xy}$  component. Units  $\text{E.U.}^2$ .
- Fig. 11. Empirical and synthetic auto-covariance functions for the  $T_{\Delta}$  component. Units  $\text{E.U.}^2$ .

Fig. 12. Empirical and synthetic cross-covariance functions between  $T_{xy}$  and  $T_{\Delta}$ . Units E.U.<sup>2</sup>.

Fig. 13. Dependence of the prediction results (expressed in terms of standard deviations of differences observed minus predicted quantities) on the covariance function (the depth to the Bjerhammar sphere).  $x = \xi$ ,  $\Delta = \eta$ . Topographic reduced data shown.

Fig. 14. The effect of changing of the noise level on the prediction results of gravity anomalies from torsion balance data. (expressed in terms of standard deviation of differences observed minus predicted).  $\Delta$  = unreduced,  $x$  = topographic reduced data.

Fig. 15. The same effect as in figure 14, for the  $\xi$  component of the deflection of the vertical.

Fig. 16. The same effect as in figure 14, for the  $\eta$  component of the deflection of the vertical.

Fig. 17. Prediction of gravity anomalies from torsion balance data. (Contour interval is 5 mgal).

Fig. 18. Error of prediction of gravity anomalies from torsion balance data. (Contour line interval is 0.25 mgal).

Fig. 19. Prediction of  $\xi$  from torsion balance data. (Contour interval is 0.5 arcsec).

Fig. 20. Error of prediction of  $\xi$  from torsion balance data. (Contour interval is 0.25 arcsec).

Fig. 21. Prediction of  $\eta$  from torsion balance data using eq.(9). (Contour interval is 0.5 arcsec).

Fig. 22. Error of prediction of  $\eta$  from torsion balance data. (Contour interval is 0.25 arcsec).

Table 1. Statistical characteristics of the raw and reduced data  
 ( 227 gravity points, 12 gravity points, 8 pairs of deflections  
 of the vertical and 233 points of torsion balance observations)

		Raw data		Data-GPM2		Data-GPM2- topography	
		standard		standard		standard	
		mean	deviation	mean	deviation	mean	deviation
$\Delta g$	(mgal) *	-1.24	22.20	-3.32	19.81	-3.32	16.74
$\Delta g$	(mgal) **	22.64	27.66	16.31	25.98	16.24	22.41
$\xi$	(arcsec)	0.92	1.44	0.98	1.49	-0.12	1.70
$\eta$	(arcsec)	4.41	4.72	4.84	4.74	5.89	4.71
$T_{xz}$	(E.U.)	-0.56	16.20	-0.52	16.24	-1.07	14.2
$T_{yz}$	(E.U.)	-8.69	20.59	-8.73	20.63	-7.89	19.40
$T_{\Delta}$	(E.U.)	-0.35	22.62	-0.37	22.65	-1.12	20.10
$2 \cdot T_{xy}$	(E.U.)	2.38	19.70	2.38	19.74	2.43	17.53

\* 227 points    \*\* 12 points

Table 2.

## Prediction results

of the two components of the deflection at 8 points from 227 gravity points

of 12 gravity values from of deflection values in 15 points

input data	$\xi$		$\eta$		$\Delta g$	
	obs. - pred.		obs. - pred.		obs. - pred.	
	standard mean deviation (arcsec)	standard mean deviation (arcsec)	standard mean deviation (arcsec)	standard mean deviation (arcsec)	standard mean deviation (mgal)	standard mean deviation (mgal)
unreduced topogr.	0.03	0.71	-0.17	0.43	5.20	4.32
reduced	-1.27	0.47	1.56	0.47	-	-

Table 3. Prediction of gravity anomalies and deflections of the vertical from torsion balance observations using least squares collocation

Input components	$\Delta g$ (mgal)		$\xi$ (arcsec)		$\eta$ (arcsec)		remark
	mean	standard deviation	mean	standard deviation	mean	standard deviation	
$T_{xz}$	10.43	22.45	-0.27	0.73	2.70	3.69	a
$T_{yz}$	4.97	4.87	-0.12	0.76	0.40	0.72	-
$T_{\Delta}$	13.74	20.03	-0.95	1.70	2.51	3.17	-
$2 \cdot T_{xy}$	17.28	26.58	0.14	1.21	2.84	4.00	-
$T_{xz}, T_{yz}$	0.79	3.40	-0.31	0.90	0.41	0.70	-
$T_{\Delta}, 2 \cdot T_{xy}$	16.85	14.94	-0.45	0.60	1.71	2.92	-
ALL	5.03	3.41	-0.04	0.74	0.18	0.56	-
$T_{xz}$	10.07	22.66	-0.20	0.91	2.62	3.98	b
$T_{yz}$	4.43	5.44	-0.12	0.50	0.55	0.47	-
$T_{\Delta}$	12.68	19.26	-1.07	1.57	2.57	2.91	-
$2 \cdot T_{xy}$	17.59	24.38	0.28	1.21	2.72	3.98	-
$T_{xz}, T_{yz}$	0.04	3.27	-0.20	1.08	0.68	0.52	-
$T_{\Delta}, 2 \cdot T_{xy}$	15.55	8.28	-0.24	1.07	1.37	2.71	-
ALL	-0.27	2.35	0.48	0.70	0.74	0.31	-
$T_{xz}$	10.89	19.32	-1.54	0.44	3.74	3.64	c
$T_{yz}$	5.14	5.08	-1.32	1.07	1.83	0.87	-
$T_{\Delta}$	14.13	16.13	-1.79	1.50	3.57	3.24	-
$2 \cdot T_{xy}$	16.79	24.03	-1.05	1.22	3.96	3.99	-
$T_{xz}, T_{yz}$	1.51	2.74	-1.64	0.61	1.87	0.77	-
$T_{\Delta}, 2 \cdot T_{xy}$	16.44	13.21	-1.44	1.45	3.08	3.09	-
ALL	3.86	2.47	-1.50	0.58	1.75	0.71	-
$T_{xy}$	10.64	19.37	-1.35	0.63	3.70	3.80	d
$T_{yz}$	4.15	5.37	-1.24	0.79	1.84	0.60	-
$T_{\Delta}$	13.94	15.29	-1.89	1.39	3.65	3.11	-
$2 \cdot T_{xy}$	17.00	21.74	-0.89	1.27	3.88	3.94	-
$T_{xz}, T_{yz}$	0.42	2.41	-1.41	0.80	1.95	0.56	-
$T_{\Delta}, 2 \cdot T_{xy}$	15.91	7.21	-1.18	1.14	2.89	2.96	-
ALL	-0.93	1.71	-1.17	0.44	1.85	0.43	-

a : without topographic reduction, one point per  $2' \times 2'$  cell used

b : without topographic reduction, all points used

c : with topographic reduction, one point per  $2' \times 2'$  cell used

d : with topographic reduction, all points used

Table 4. Prediction results using all torsion balance data and  
in addition one gravity point and one deflection point

input data	$\Delta g$ (mgal)		$\xi$ (arcsec)		$\eta$	
	mean	standard deviation	mean	standard deviation	mean	standard deviation
unreduced topogr.	0.05	2.15	0.26	0.68	0.02	0.30
reduced	-5.13	2.40	-0.06	0.49	0.55	0.61

+ Trans. results

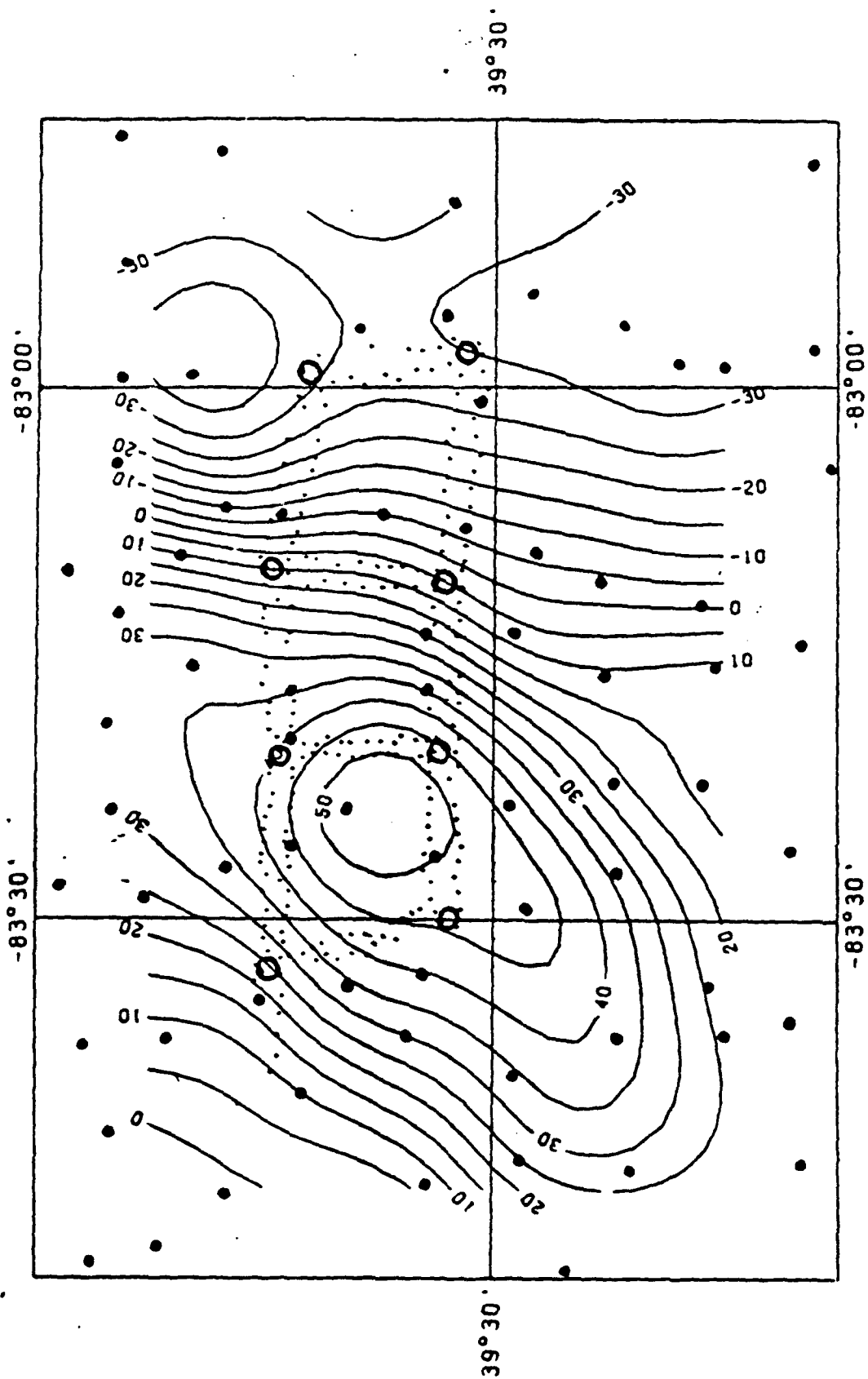


Fig 1.

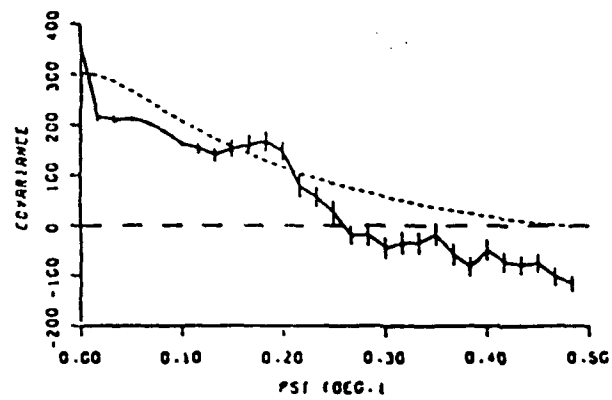


Fig. 2

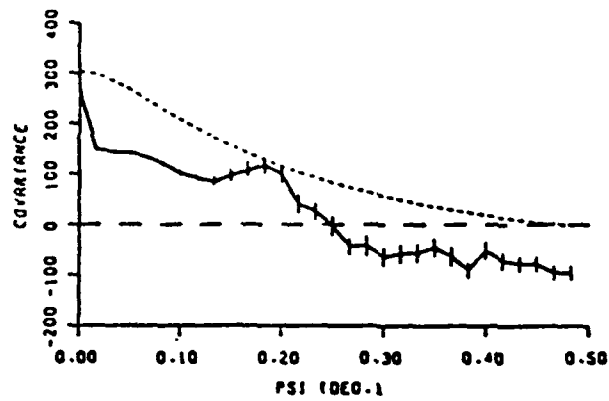


Fig. 3

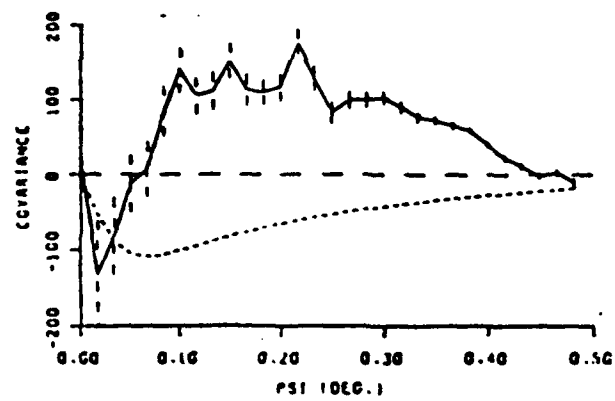


Fig. 4

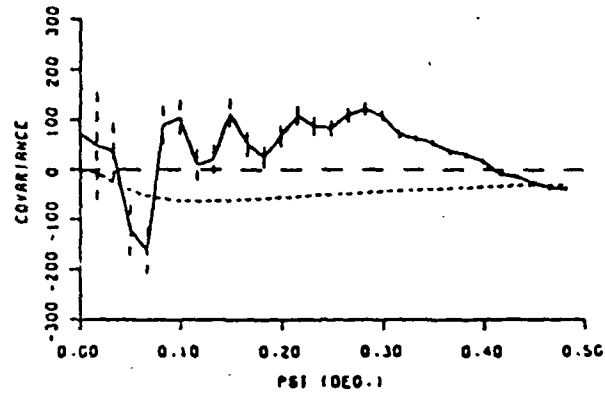


Fig. 5

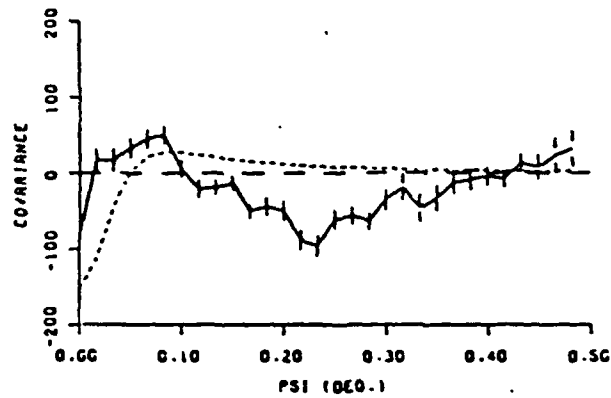


Fig. 6

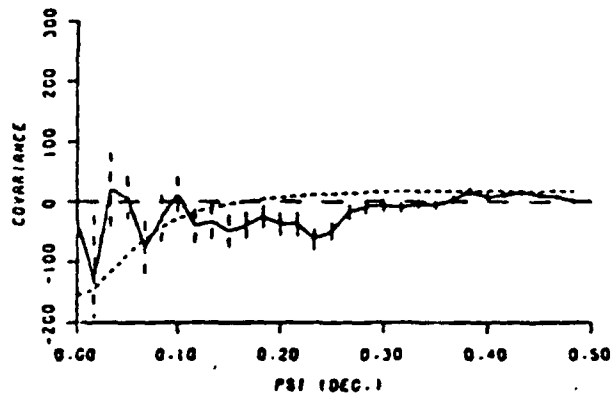


Fig. 7

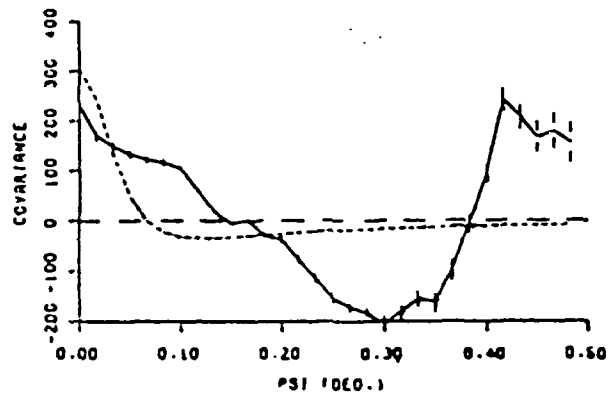


Fig. 8

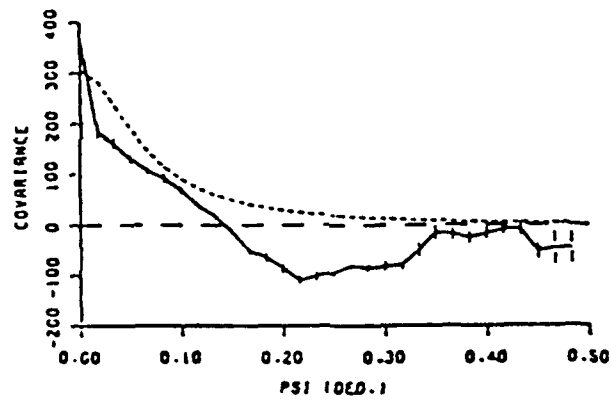


Fig. 9

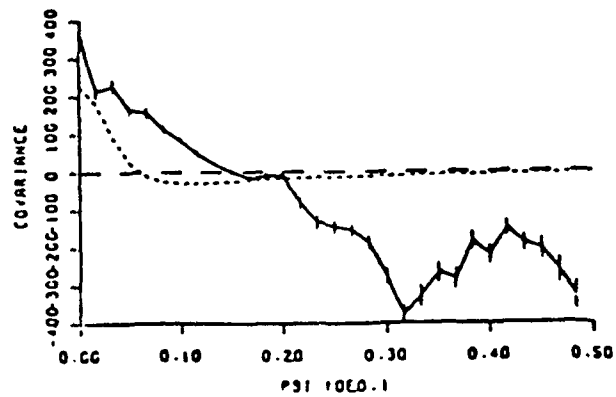


Fig. 10

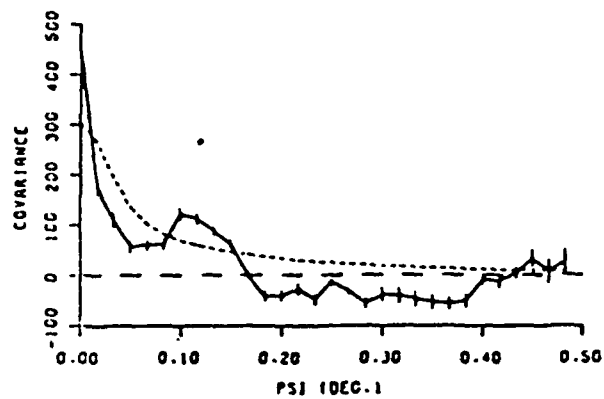


Fig. 11

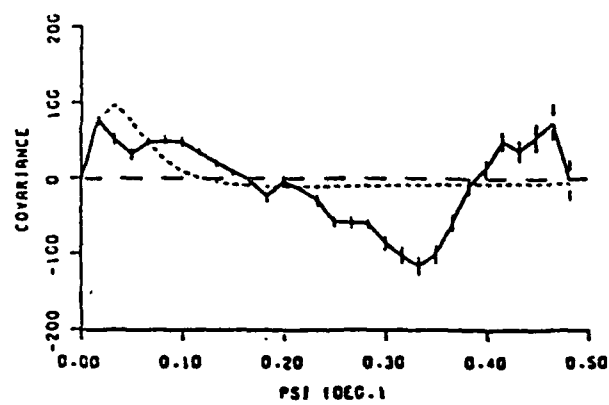


Fig. 12

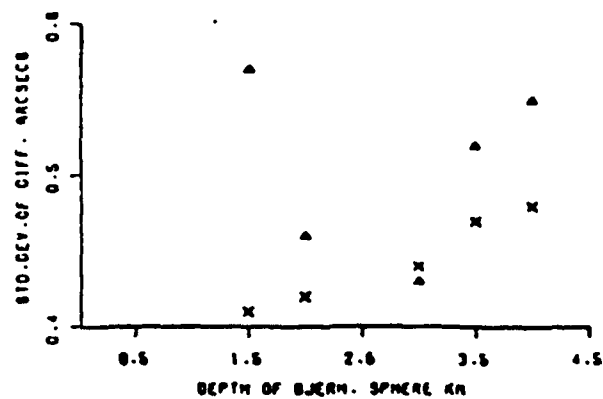


Fig. 13

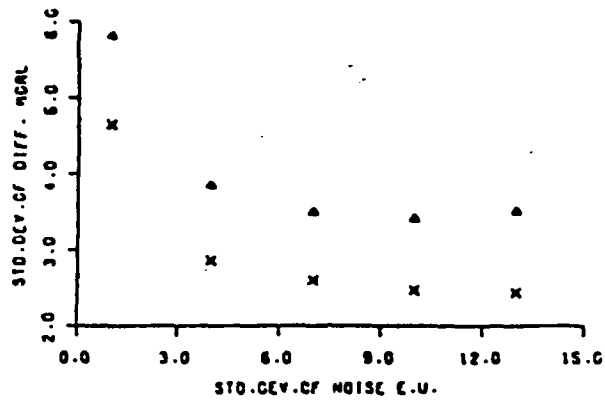


Fig. 14

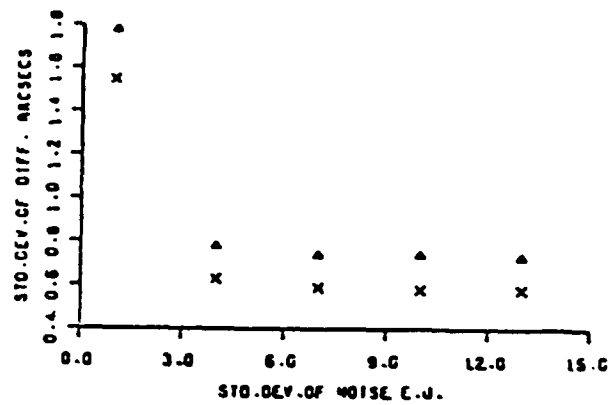


Fig. 15

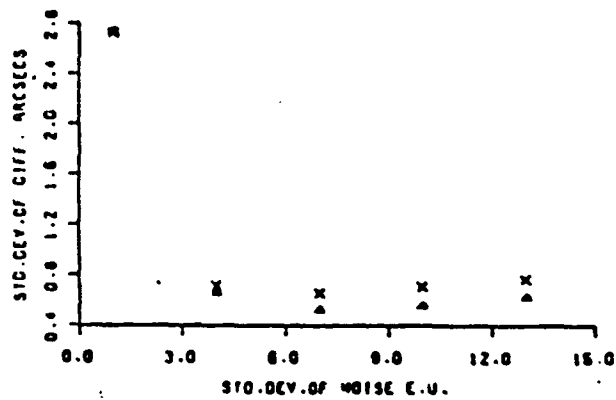


Fig. 16

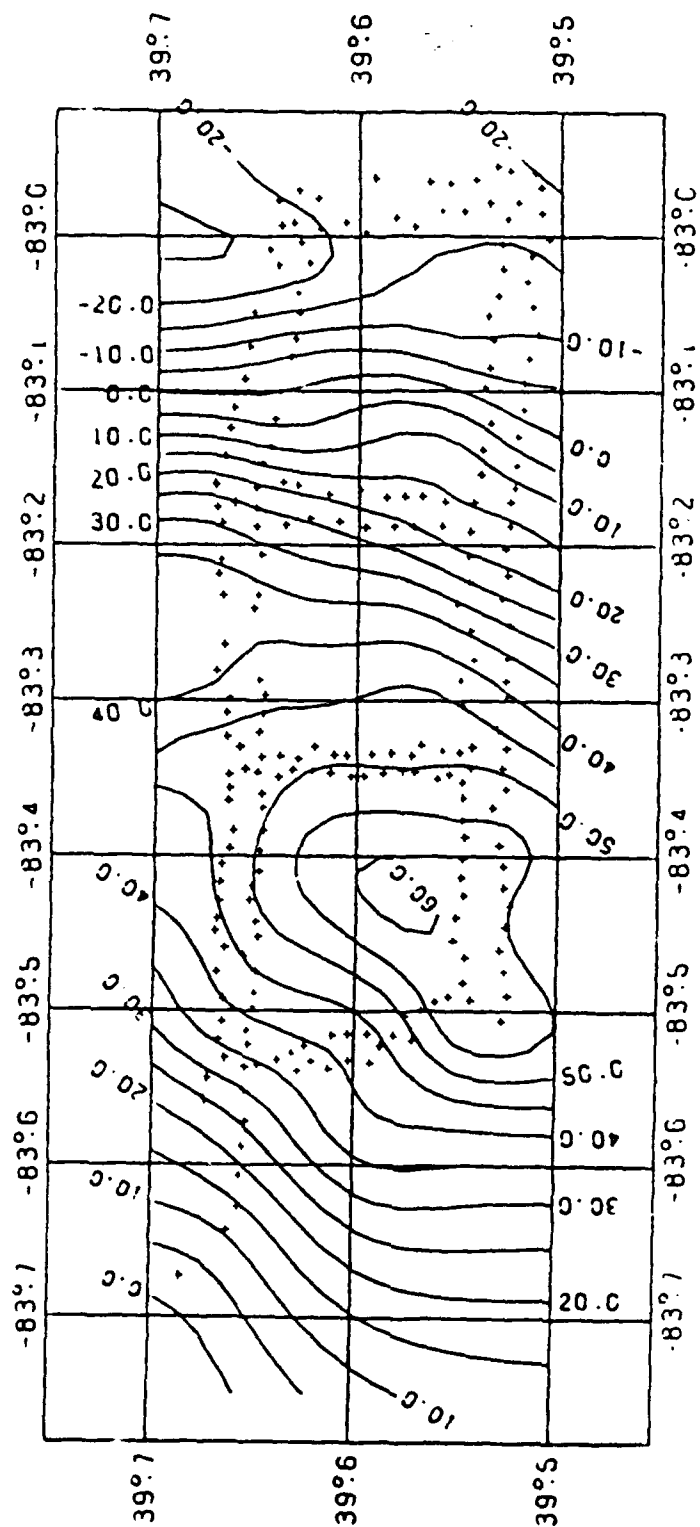


Fig 17

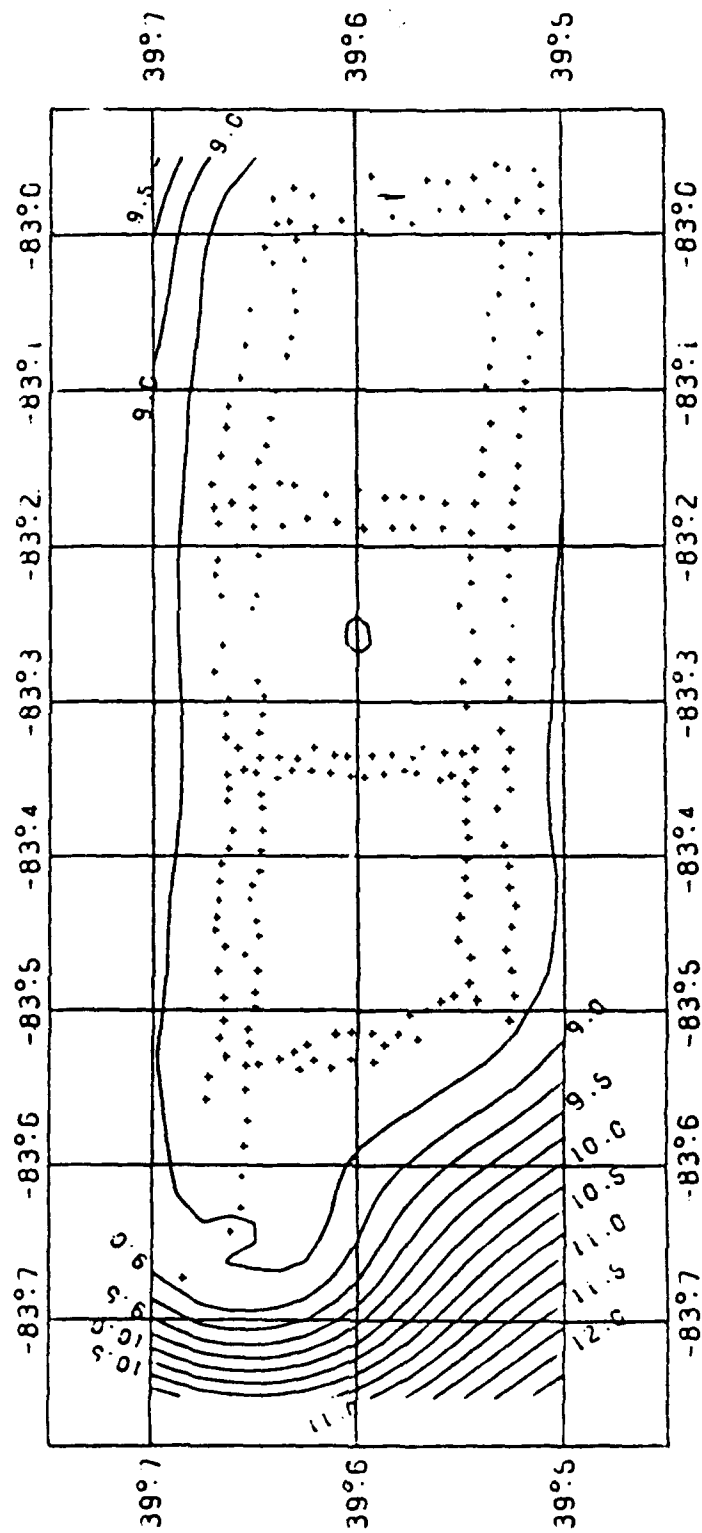


Fig 18

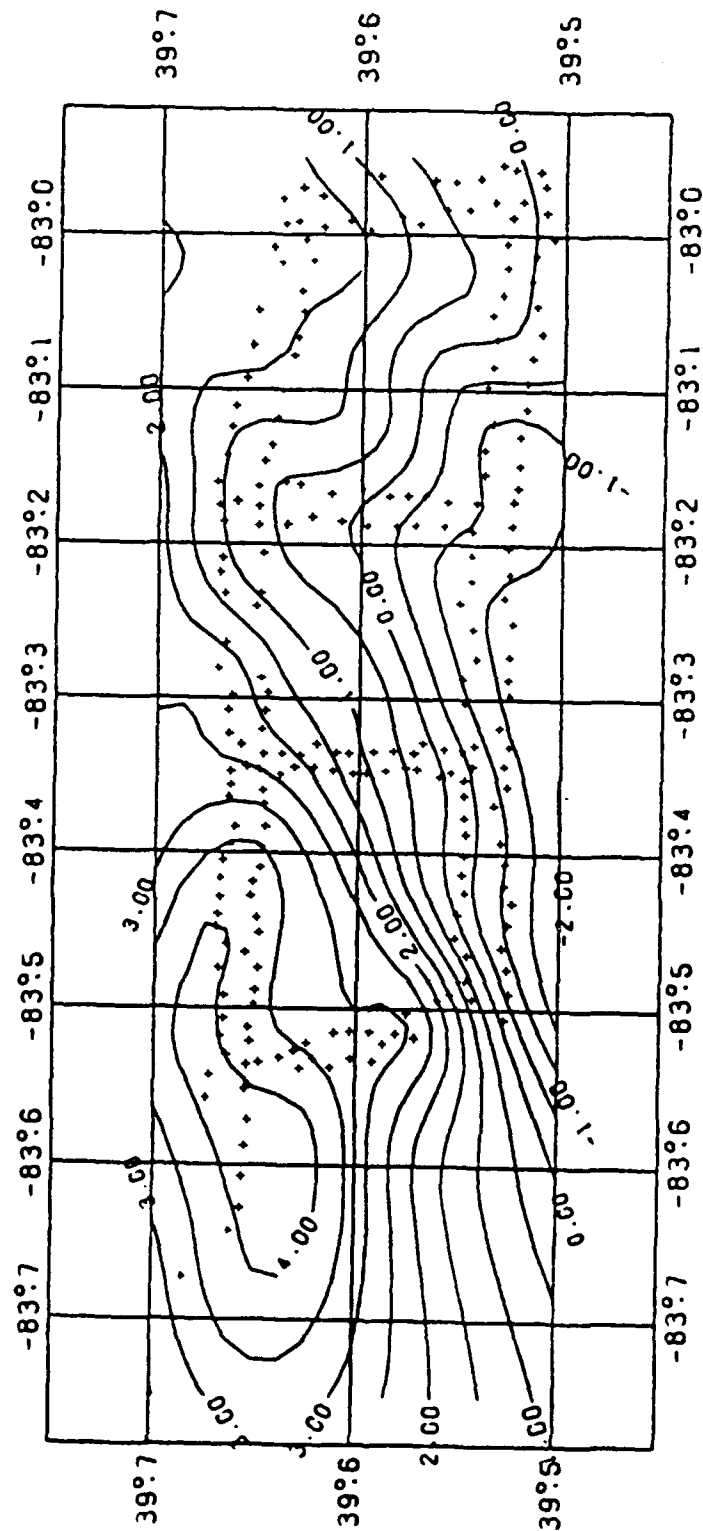


Fig. 19

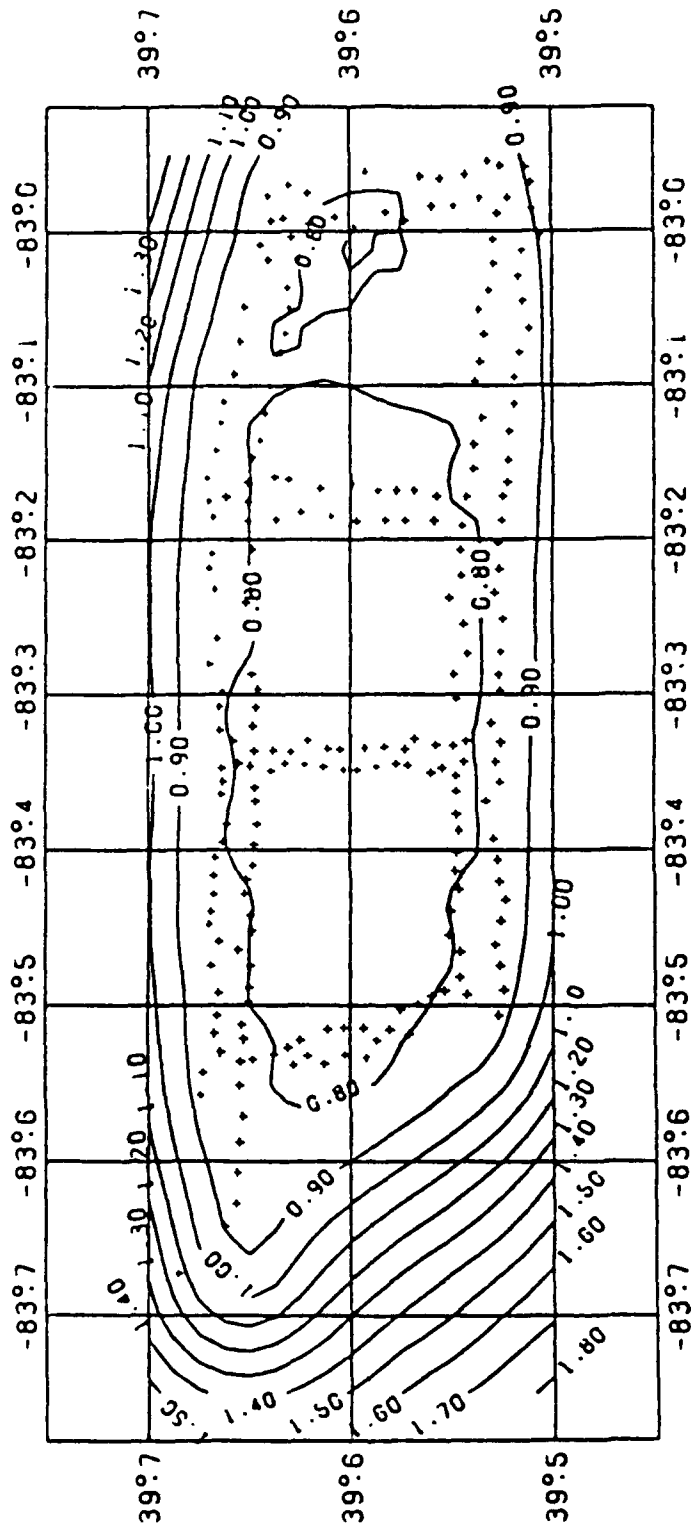
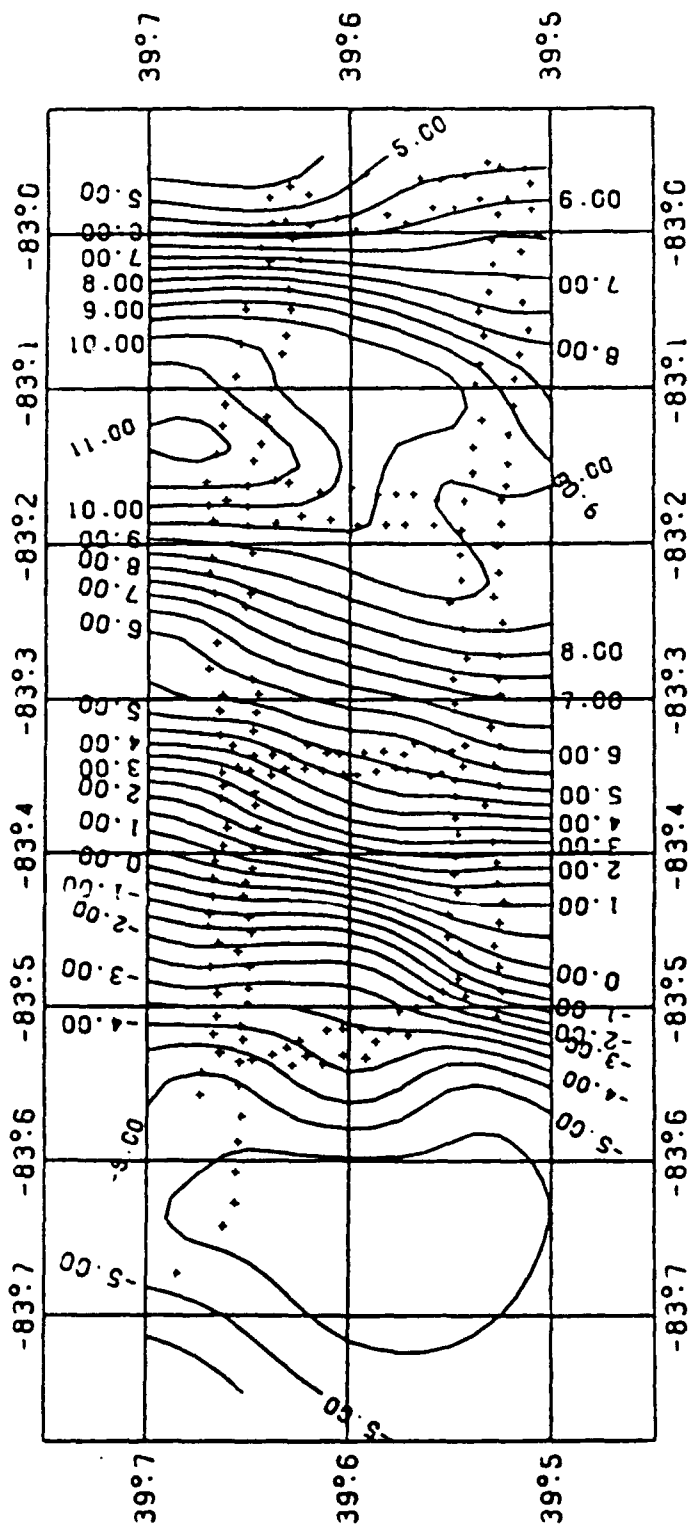


Fig 20



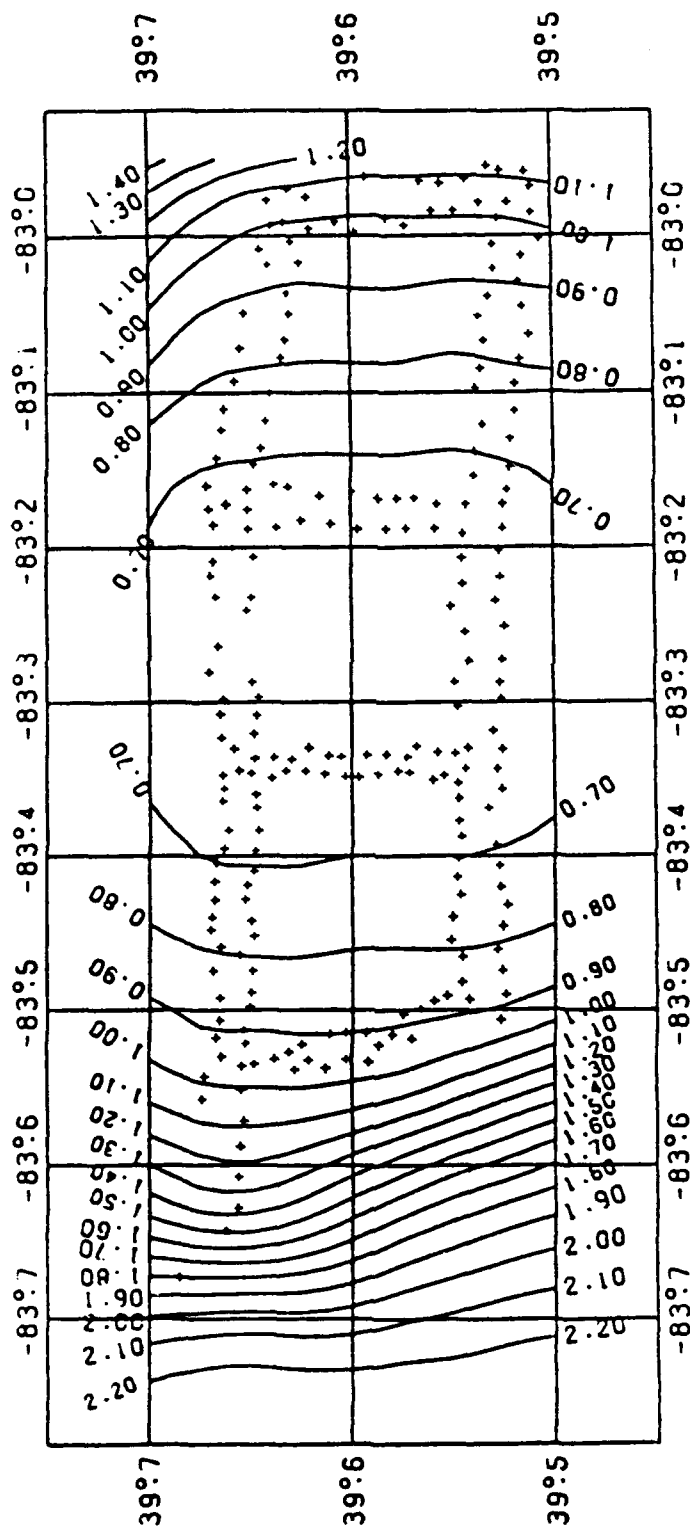


Fig 2d

ESTIMATION OF GRAVITY VECTOR COMPONENTS  
FROM BELL GRADIOMETER AND AUXILIARY DATA  
UNDER CONSIDERATION OF TOPOGRAPHY AND  
ASSOCIATED ANALYTICAL UPWARD CONTINUATION ASPECTS

by .

Dr. Hans Baussus von Luetzow  
Department of the Army  
U.S. Army Engineer Topographic Laboratories  
Fort Belvoir, VA 22060-5546

ABSTRACT

Following an introduction, the paper briefly discusses gravity gradiometer applications. It outlines the estimation of first order derivatives of the anomalous gravity potential from Bell gravity gradiometer and auxiliary data in the context of a Weiner-Kolmogorov optimization scheme under consideration of computable "topographic noise", accomplished on the basis of the Pellinen-Moritz solution of the boundary value problem of physical geodesy. The paper also addresses four different methods of analytical upward continuation of first order derivatives of the anomalous gravity potential under identification of a finite difference method using Laplace's equation as the most economical and efficient one. Relevant conclusions are then presented.

## 1. INTRODUCTION

The estimation of gravity vector components from Bell gravity gradiometer and auxiliary data has been discussed by a number of authors, including Jordan (1982), White and Goldstein (1984), Center, Jordan and Peacock (1985), and Baussus von Luetzow (1985). Apart from gravity gradiometer self noise power spectra or corresponding covariance functions, the collocation theory of physical geodesy was employed to derive spectra and cross-spectra or equivalent covariance functions involving first and second order derivatives of the anomalous gravity potential. The basic covariance functions, pertaining either to a randomized anomalous gravity potential or to a randomized gravity anomaly, accomplished by the subtraction of low frequency harmonic representations of anomalous potential or gravity anomaly data, presuppose the existence of homogeneity and isotropy. The application of collocation theory does not face difficulties in the case of quasi-flat terrain and is a prerequisite to arrive at small estimation errors for gravity vector components in the context of an airborne survey over a square area of  $300 \times 300 \text{ km}^2$ , covered with parallel traverses and cross traverses 5 km apart, conducted at an elevation of 600 m at a speed of about  $360 \text{ km hr}^{-1}$ , and employing only a limited amount of measured gravity vector component data. It is, however, well known that the assumption of homogeneity and isotropy does not satisfactorily hold in the presence of moderate to strong mountainous terrain. Some efforts have been made to apply heuristic topographic corrections to gravity gradiometer measurements. Still, the problem remains to provide for a Wiener-Kolmogorov-type estimation process free of computable topographic noise so that the assumption of homogeneity and isotropy is reasonably fulfilled with respect to modified, signal-type measurements disturbed by gradiometer self noise only. The solution to this problem is possible under application of approaches to the geodetic boundary value problem and the correlated interpolation of gravity anomalies and deflections of the vertical in mountainous terrain by Pellinen (1969), Moritz (1969), and Baussus von Luetzow (1971, 1981). Section 3 as the main section of this paper addresses the solution under consideration of the estimation process and the computation of "topographic noise". The preceding section addresses in a compact way gravity gradiometer applications to place the determination of gravity vector components over relatively large areas and the analytical upward continuation of vertical and horizontal derivatives of the anomalous gravity potential in the proper perspective. The relatively short sections 4-7 discuss different methods of analytical upward continuation, followed by several conclusions.

## 2. GRAVITY GRADIOMETER APPLICATIONS

Geodetic research and the development of associated technology has been considerably stimulated by military requirements and actual or potential military applications with critical funding provided by the U.S. Government. The result thereof was an increase of scientific knowledge, new instrumentation and techniques, and technology transfer to the civilian sector, particularly in navigation and surveying.

The main applications of gravity gradiometers follow:

- Establishment of the spatial gravity field in ICBM<sup>1</sup> launch areas (most important application). This includes gravity vector components on the ground for calibration, local to global coordinate transformations, geodetic azimuth determination, and gravity programmed inertial positioning (beneficial to Small ICBM or Midgetman). An accurate spatial gravity field, extending to

---

<sup>1</sup>Intercontinental Ballistic Missile

a height of 200 km, provides also for comparisons/calibration for the Geopotential Research Mission (GRM) and a Superconducting Gravity Gradiometer Mission (SGGM). Instrument: Bell Gravity Gradiometer.

- ° Accuracy enhancement of SLBM's<sup>2</sup>. Instrument: Bell Gravity Gradiometer.
- ° Improvement of global gravity field for geophysical applications (GRM). Instrument: Superconducting Gravity Gradiometer.  
Byproducts: ICBM target error reduction (not critical), cruise missile navigation, improved satellite ephemeris.
- ° High accuracy space navigation. Instrument: Superconducting Gravity Gradiometer (six axis version).
- ° Gravity vector densification over large areas for gravity programmed inertial navigation and for geodetic network adjustments. Instrument: Bell Gravity Gradiometer.
- ° Subterranean mass detection (cavities, oil, water). Instrument: Superconducting Gravity Gradiometer (vertical axis version).
- ° Test of Newton's square law and tests of Einstein's theory of relativity. Instrument: Superconducting Gravity Gradiometer.

### 3. DETERMINATION OF DERIVATIVES OF THE ANOMALOUS GRAVITY POTENTIAL OVER MOUNTAINOUS TERRAIN USING BELL GRAVITY GRADIOMETER MEASUREMENTS AND AUXILIARY DATA

#### A. Notations and Relations Used

$T$  anomalous gravity potential

$\frac{\partial}{\partial x}, \frac{\partial}{\partial y}$  derivatives taken along the local horizon in a northern and eastern direction

$$\bar{T}_x = \frac{\partial T}{\partial x}$$

$$\bar{T}_{xx} = \frac{\partial^2 T}{\partial x^2}$$

$n = n_1 + n_2$  Bell gravity gradiometer instrument noise with white noise component  $n_1$  and red noise component  $n_2$

$\wedge$  signal variable indicator

$\delta \bar{T}_x$  topographic noise component of  $\bar{T}_x$

$\delta \bar{T}_{xx}$  topographic noise component of  $\bar{T}_{xx}$

$\bar{T}_x$  lower order spherical harmonics representation of  $\bar{T}_x$  used for subtraction

$\bar{T}_{xx}$  lower order spherical harmonics representation of  $\bar{T}_{xx}$  used for subtraction

$\delta \bar{T}_x$  lower order spherical harmonics representation of  $\delta \bar{T}_x$  used for subtraction

---

<sup>2</sup> Sea Launched Ballistic Missile

lower order spherical harmonics representation of  
used for subtraction

$$\hat{T}_x = \bar{T}_x - \delta T_x$$

$$\hat{\bar{T}}_x = \hat{T}_x - \overline{\hat{T}_x} = \bar{T}_x - \delta \bar{T}_x - (\bar{\bar{T}}_x - \delta \bar{\bar{T}}_x)$$

$$\hat{\bar{T}}_{xx} = \bar{T}_{xx} - \delta \bar{T}_{xx}$$

$$\hat{\bar{\bar{T}}}_{xx} = \hat{\bar{T}}_{xx} - \overline{\hat{\bar{T}}_{xx}} = \bar{T}_{xx} - \delta \bar{T}_{xx} - (\bar{\bar{T}}_{xx} - \delta \bar{\bar{T}}_{xx})$$

$a_{iK}$  weight factor with measurement index  $i$  and computation index  $K$ , applicable to  $\bar{T}_x$  in Wiener-Kolmogorov estimation

$b_{jK}$  weight factor with measurement index  $j$  and computation index  $K$ , applicable to  $\bar{T}_{xx}$  in Wiener-Kolmogorov estimation

$R$  earth's mean radius

$\sigma$  unit sphere (full solid angle)

$r$  length of radius vector from earth's center to a moving point on earth's surface

$r_p$  length of radius vector from earth's center to a fixed point on earth's surface

$r_A$  length of radius vector from earth's center to a fixed point on a level surface above earth's surface

$\psi$  angle between radius vectors  $\vec{r}$  and  $\vec{r}_p$  or  $\vec{r}_A$

$$l = (r^2 + r_A^2 - 2rr_A \cos \psi)^{1/2}$$

$\alpha$  azimuth angle counted clockwise from north

$S_g = S(r_A, \psi, r)$  generalized Stokes Function

$h$  elevation of terrain referring to a movable point on earth's surface

$h_p$  elevation of terrain referring to a fixed point on earth's surface

$h_A$  elevation of level surface above terrain

$$\Delta h = h_A - h_p$$

$$\ell_0 = 2 R \sin \frac{\psi}{2}$$

$$\ell_1 = [\ell_0^2 + (h - h_A)^2]^{1/2} \quad \text{planar approximation to } \ell$$

$\Delta g$	gravity anomaly on earth's surface
$C$	topographic correction to gravity anomaly
$\Delta g_F = \Delta g + C$	Faye anomaly
$b$	Bouguer gradient
$k$	gravitational constant
$\rho$	standard density

$$\delta T = 4\pi k \rho h_p R + k \rho R^2 \iint_{\sigma} \ln \frac{\ell_1 + h - h_p}{\ell_0} d\sigma$$

potential of the topographic masses

$$G_1(v) = \frac{R^2}{2\pi} \iint_{\sigma} \frac{v(h - h_p)}{\ell_0^3} d\sigma \quad \text{with } v \text{ as an arbitrary variable}$$

$\phi$	geographic latitude
$\lambda$	geographic longitude

$$\Theta = \frac{\pi}{2} - \phi$$

#### B. Estimation Process

A Wiener-Kolmogorov estimation can, under consideration of  $T_x$  and  $T_{xx}$  only, be characterized by

$$T_{xK} = \sum a_{iK} T_{xi} + \sum b_{jK} (T_{xxj} + n_j) \quad (1)$$

The derivatives  $\bar{T}_{xi}$ , also called truth data, are, of course, also associated with measurement errors. With respect to deflections of the vertical, proportional to  $\bar{T}_x$  and  $\bar{T}_y$ , efforts are being made to determine them astrogeodetically with an error of 0.1 arcsec rms. Gravity anomalies can be measured with a relatively greater accuracy. In order to compute the vertical derivative  $\frac{\partial \bar{T}}{\partial r} = \bar{T}_r$ , high degree spherical harmonic expansions presented by Rapp (1987) or the GRIM3-L1 Model described by Reigber, Balmino, Müller, Basch and Moynot (1985) may be employed. These models are also useful for the subtraction of lower harmonics components from measured first and second order derivatives of  $\bar{T}$ .

Regarding eq. (1), it is assumed that all measured quantities refer to a level surface. In the case of quasi-flat terrain,  $\bar{T}_{xK}$ -estimates have been made from  $\bar{T}_{xi}$  on the earth's surface and from airborne  $\bar{T}_{xx}$ -measurements, employing spatial covariance functions. This is not possible in the presence of pronounced topography. In this case, it is

$$\bar{T}_{xK}(h_p) = \bar{T}_{xK}(h_A) + \frac{\partial \bar{T}_{xK}}{\partial z}(h_p - h_A) \quad (2)$$

where  $\frac{\partial \bar{T}_{xK}}{\partial z}$  is a representative gradient obtained from gravity gradiometer measurements. There is no significant degradation in accuracy if eq. (2) is used.

For simplicity, eq. (1) presupposes the prior application of quasi-systematic corrections obtained from lower harmonic expansions. In the presence of pronounced mountainous terrain, eq. (1) is reformulated as

$$\bar{T}_{xK}^0 = \sum a_{iK}^{(0)} \bar{T}_{xi} + \sum b_{jK}^{(2)} (\bar{T}_{xxj}^0 + \eta_j) \quad (3)$$

### C. Computation of "Topographic Noise"

The essential task is the computation of topographic noise components of the derivatives  $\bar{T}_x$ ,  $\bar{T}_y$ ,  $\bar{T}_z$ . In this respect, the solution nomenclature employed by Moritz (1969)<sup>3</sup> is applied. In order to obtain solutions at elevation  $h_A$  instead of solutions at elevation  $h = h_p$ , Stokes generalized function  $S_g$  replaces Stokes function  $S(\psi)$  in the solutions where applicable.<sup>4</sup>

First, the solution for  $\bar{T}$  at a point  $P_A$  is written as

$$\bar{T} = \sum_i^3 \bar{T}_i \quad (4)$$

<sup>3</sup> Moritz (1969), p. 31.

<sup>4</sup>  $S_g$  is explicitly formulated by Moritz (1966). See p. 49.

The solution components are

$$\bar{T}_1 = \frac{R}{4\pi} \iint_{\sigma} [\Delta g_F + G_1(\Delta g_F)] S_g d\sigma \quad (5)$$

$$\bar{T}_2 = \frac{R}{4\pi} \iint_{\sigma} G_1(-bh_p + \frac{3}{2R} \delta T) S_g d\sigma \quad (6)$$

$$\bar{T}_3 = k_s R^2 \iint_{\sigma} \left( \ln \frac{l_1 + h - h_p + \Delta h}{l_0} - \frac{h - h_p + \Delta h}{l_0} \right) d\sigma \quad (7)$$

$\bar{T}_1$  represents the "signal" term of  $\bar{T}$  since its structure is compatible with the existence of a reproducible kernel in the sense of Krarup, a prerequisite for the application of the collocation method of physical geodesy.

$\bar{T}_2$  and  $\bar{T}_3$  are clearly "noise" terms which do not permit the establishment of a statistical estimation structure.  $\bar{T}_2$  appears to be a more slowly varying function. Moritz (1969) states that the term  $\delta T$  may be neglected in the context of a planar approximation.<sup>5</sup> Accordingly,  $\bar{T}_3$  appears to be mainly responsible for fluctuations of a non-stationary nature.

An improvement of the above analysis is possible by the replacement of  $\Delta g_F$  by the isostatic anomaly  $\Delta g_i$ , provided that isostatic conditions prevail. Neglecting a second order improvement involving consideration of  $\sigma_1$ -terms, the additional "topographic noise" can be written as

$$\bar{T}_4 = \frac{R}{4\pi} \iint_{\sigma} (\Delta g_F - \Delta g_i) S_g d\sigma \quad (8)$$

Without consideration of the term  $\bar{T}_4$ , the "topographic noise" terms involving vertical and horizontal derivatives of  $\bar{T}_2$  and  $\bar{T}_3$  can be formulated as

$$\frac{\partial \bar{T}_2}{\partial z} = \frac{\partial \bar{T}_2}{\partial x_A} = \frac{R}{4\pi} \iint_{\sigma} G_1(-bh_p + \frac{3}{2R} \delta T) \frac{\partial S_g}{\partial x_A} d\sigma \quad (9)$$

<sup>5</sup> Moritz (1969), p. 32.

$$\frac{\partial T_3}{\partial z} = k R^2 \iint_{\sigma} \frac{\partial}{\partial h_p} \left( \ln \frac{l_1 + i - h_p + \Delta h}{l_0} - \frac{h - h_p + \Delta h}{l_0} \right) d\sigma \quad (10)$$

$$\left\{ \frac{\partial T_2}{\partial x} \right\} = \frac{R}{4\pi} \iint_{\sigma} G_1 (-b h_p + \frac{3}{2R} \delta T) \frac{\partial S_0}{\partial \psi} \begin{Bmatrix} \cos \alpha \\ \sin \alpha \end{Bmatrix} d\sigma \quad (11)$$

$$\left\{ \frac{\partial T_2}{\partial x} \right\} = k R^3 \iint_{\sigma} \frac{h - h_p + \Delta h}{l_0^2} \left( \frac{1}{l_1} - \frac{1}{l_0} \right) \sin \psi \begin{Bmatrix} \cos \alpha \\ \sin \alpha \end{Bmatrix} d\sigma \quad (12)$$

#### D. Averaged Second Order Derivatives

Because of the application of a moving average of gravity gradiometer measurements over a time interval  $\Delta t$  of about 10 seconds, it is not necessary to compute second order derivatives with respect to  $x, y, z$  of  $T_2$  and  $T_3$ . As an example, the averaged second order derivative of  $T_3$  with respect to  $x$  is

$$\frac{\partial^2 T_3}{\partial x^2} = \frac{1}{\Delta x} \left[ \left( \frac{\partial T_3}{\partial x} \right)_{t_2} - \left( \frac{\partial T_3}{\partial x} \right)_{t_1} \right] \quad (13)$$

In eq. (13) it is  $\Delta x = v_A (t_2 - t_1) = v_A \cdot \Delta t$ ,  $v_A$  being the horizontal aircraft speed.

#### 4. STANDARD ANALYTICAL UPWARD CONTINUATION

Assuming that the three first order derivatives of the anomalous gravity potential have been estimated from gradiometric surveys at rectangular grid points of a level surface at elevation  $h_A = \text{const.}$ , Poisson's integral formula

$$\bar{T}_p = \frac{R(r^2 - R^2)}{4\pi} \iint_{\sigma} \frac{\bar{T}}{r^3} d\sigma \quad (14)$$

can be used for the analytical upward continuation of  $T$  or of its derivatives  $\frac{\partial T}{\partial r}$ ,  $\frac{\partial T}{\partial \phi}$ ,  $\frac{\partial T}{\partial \lambda}$ . According to Heiskanen and Moritz (1967), for elevations smaller than 250 km, the planar form of eq. (14) is sufficiently accurate. For elevations up to 150 km, which apply in ICBM launch areas, the horizontal integration distance has to be ten times the elevation to assure good accuracy, i.e., a very large information base is required. Additionally, rectangular grid data has to be interpolated to conform with circular zone data to be employed in the computation.

##### 5. IMMEDIATE SPATIAL WIENER KOLMOGOROV ESTIMATION

The three derivatives of the anomalous gravity potential may be estimated directly for grid points at higher elevations in the context of a Wiener-Kolmogorov scheme, using spatial covariance functions or equivalent power spectra. For higher elevations, data derived from a greater number of adjacent surveys would be required, and matrix inversions would become very complicated. Further complications would arise in the presence of pronounced topography because of the non-applicability of effective collocation methods.

##### 6. SPATIAL COLLOCATION UPWARD CONTINUATION OF $T_r, T_\phi, T_\lambda$

If  $T_r, T_\phi, T_\lambda$  are first estimated at grid points of a level surface with elevation  $h_A$ , a collocation upward continuation would be a replacement of the Poisson integral formula approach by statistical methods. Again, a large information base would be required, inversions of matrices associated with higher elevations would become complicated, and complications would exist in the presence of pronounced topography. It would be possible though to apply the collocation extrapolation only to signal quantities  $T_r, T_\phi, T_\lambda$  and to compute the "topographic noise" components separately for higher elevations by means of eqs. (9) - (12).

##### 7. NUMERICAL UPWARD CONTINUATION USING LAPLACE'S DIFFERENTIAL EQUATION

The upward continuation methods discussed in sections 4-6 are characterized by the use of a specific derivative of the anomalous gravity potential, given at a level surface, by the requirement of a large information base for extrapolations to higher elevations, by associated large inversion matrices in collocation approaches, and by the inadequacy of these in the presence of mountainous terrain in the absence of a separation into signal estimation and "topographic noise" computation. Fortunately, the availability of three vector components at a level surface makes it possible to use information at two adjacent level surfaces as a prerequisite for applying Laplace's equation. Hereby, the information base can be reduced significantly, and inversions of matrices are not needed.

In Cartesian coordinates, the availability of  $\frac{\partial T}{\partial x} = T_x, \frac{\partial T}{\partial y} = T_y, \frac{\partial T}{\partial z} = T_z$  at the level  $Z_0$  makes it possible to compute  $T_x, T_y, T_z$  at the level  $Z_1 = Z_0 + \Delta Z$  since

$$\frac{\partial}{\partial z} \frac{\partial T}{\partial x} = \frac{\partial}{\partial x} \frac{\partial T}{\partial z} \quad (15a)$$

$$\frac{\partial}{\partial z} \frac{\partial T}{\partial y} = \frac{\partial}{\partial y} \frac{\partial T}{\partial z} \quad (15b)$$

$$\frac{\partial}{\partial z} \frac{\partial T}{\partial z} = - \left( \frac{\partial}{\partial x} \frac{\partial T}{\partial x} + \frac{\partial}{\partial y} \frac{\partial T}{\partial y} \right) \quad (15c)$$

The derivative  $\frac{\partial^2 f}{\partial z^2}$  can, of course, be determined separately through use of gradiometer information, and a representative value can be employed for analytical upward continuation.

If a variable  $f$  satisfying Laplace's equation is given at two adjacent levels separated by  $\Delta Z$ , Laplace's equation

$$\frac{\partial^2 f}{\partial z^2} = -\Delta^2 Z = -\left(\frac{\partial^2 f}{\partial x^2} + \frac{\partial^2 f}{\partial y^2}\right) \quad (16)$$

permits application of the numerical algorithm

$$f_2 = 2f_1 - f_0 - (\Delta Z)^2 (\Delta^2 f)_1 \quad (17)$$

In more appropriate spherical coordinates  $r, \theta, \lambda$ , eq. (17) has to be replaced by

$$f_2 = 2f_1 - f_0 - \frac{(\Delta r)^2}{r_1^2} \left( 2r \frac{\partial f}{\partial r} + \cot \theta \frac{\partial f}{\partial \theta} + \frac{\partial^2 f}{\partial \theta^2} + \frac{1}{\sin^2 \theta} \frac{\partial^2 f}{\partial \lambda^2} \right)_{r_1} \quad (18)$$

where the derivatives in the bracketed term are to be evaluated by finite differences. Higher order finite difference algorithms may be applied if considered advantageous.

It is possible to use eq. (18) only for "signal" components and to compute the "topographic noise" effects separately, using grid lengths of 1 km instead of 5 km.

## 8. CONCLUSIONS

Wiener-Kolmogorov-type estimation of gravity vector components or of related first order derivatives of the anomalous gravity potential from Bell gravity gradiometer and auxiliary data in the context of an airborne area survey can also be accomplished in the presence of pronounced mountainous terrain. A specific solution of the boundary value problem of physical geodesy permits the determination of "signal" and "topographic noise" solution terms. "Topographic noise" terms can be computed for each first derivative of the anomalous gravity potential, and their consideration permits the application of algorithms, including numerical weight factors, valid in the case of quasi-flat terrain. A slight degradation in accuracy may be expected. The standard analytical upward continuation method and two spatial collocation methods for the estimation of first order derivatives of the anomalous gravity potential can be replaced by numerical upward continuation using Laplace's equation because of the availability of three gravity vector components at the information base level surface. In this case, the standard information base can be reduced considerably, and no matrix inversions are required. Analytical upward continuation of "topographic noise" components may also be accomplished separately, using a higher resolution grid. The computation of "topographic noise" effects is mathematically laborious, can,

however, be achieved by means of high speed computers. The alternative in the presence of mountainous terrain is to reduce flight traverses from 300 km to about 100 km, to use highly accurate "truth" data at both ends of the traverse, and to repeat single traverse surveys.

#### REFERENCES

Baussus von Luetzow, H. 1971. New Solution for the Anomalous Gravity Potential J. Geoph. Research, Vol. No. 20. pp. 4884-4891.

Baussus von Luetzow, H. 1981. On the Interpolation of Gravity Anomalies and Deflections of the Vertical in Mountainous Terrain. Proc. Internatl. Symp. on Geodetic Networks and Computations, Munich. Publications of the German Geodetic Commission at the Bavarian Academy of Sciences, Reihe B, Heft Nr. 258/VII.

Baussus von Luetzow, H. 1985. Aerial Astrogeodetic-Gradiometric Vertical Deflection Determination. Proc. Third Internatl. Symp. on Inertial Technology for Surveying and Geodesy, Vol. 2, Banff, The University of Calgary, Publication 60005.

Center, J.L., Jordan, S.K., and Peacock, G.S. 1985. Post-Mission Adjustment of Gravity Gradiometer Data (U). TR-139-1, Geospace Systems Corporation, Wellesley, MA (Confidential). Unclassified report available from U.S. Army Engineer Topographic Laboratories, Fort Belvoir, VA 22060-5546.

White, J.V. and J.D. Goldstein. 1984. Gravity Gradiometer Survey Data Processing. AFGL-TR-84-0198, The Analytical Sciences Corporation, Reading, MA 01867.

Heiskanen, W.A. and H. Moritz. 1967. Physical Geodesy. W.H. Freeman and Company, San Francisco and London.

Moritz, H. 1966. Linear Solutions of the Geodetic Boundary-Value Problem. Scientific Report No. 11, The Ohio State University Research Foundation, Columbus, Ohio 43212.

Moritz, H. 1969. Nonlinear Solutions of the Geodetic Boundary-Value Problem. Scientific Report No. 2, The Ohio State University Research Foundation, Columbus Ohio 43212.

Pellinen, L.P. 1969. On the Computations of Plumblin Deflections and Quasigeoidal Heights in Highlands (in Russian with English Abstract). Tr. ZNIGAIK, 176, Nedra Press, Moscow.

Rapp, R. 1987. Gradient Information in New High Degree Spherical Harmonic Expansions. Proc., 15th Gravity Gradiometer Conference, Colorado Springs, CO. Air Force Geophysics Laboratory, Hanscom Air Force Base, MA 01731-5000.

Reigber, C., Balmino, G., Mueller, H., Basch, W., and Moynot, B. 1985. GRIM Gravity Model Improvement Using LAGEOS (GRIM3-L1). J. Geoph. Research, Vol. 90, pp. 9285-9299.

DEVELOPMENT OF A THREE-AXIS SUPERCONDUCTING GRAVITY GRADIOMETER  
AND A SIX-AXIS SUPERCONDUCTING ACCELEROMETER

by

Dr. Hinghung A. Chan  
Dr. Q. Kong  
Dr. Martin Vol Moody  
Dr. Ho Jung Paik  
Mr. Joel W. Parke

University of Maryland  
College Park Campus  
Department of Physics and Astronomy  
College Park, MD 20742

ABSTRACT

A three-axis superconducting gravity gradiometer which measures the three in-line components of the gravity gradient tensor is under development at the University of Maryland. The instrument is being developed under a NASA contract for the purpose of precision gravity experiments and gravity field mapping from an orbiting platform. The design of the gradiometer employs a number of recently devised techniques which rely on certain properties of superconductors to obtain a fundamental noise level of  $10^{-4}$  Eotvos  $\text{Hz}^{-1/2}$ , as well as the high degree of stability necessary for such extreme sensitivity. In order to compensate for errors associated with angular motions, the gradiometer will be integrated with a six-axis superconducting accelerometer which is being developed at the University of Maryland under an AFGL contract. The accelerometer will sense the rotational and translational motions of the gradiometer platform. The principle and design of the instruments will be discussed. In addition, the results of tests on the first axis of the gradiometer will be presented.

Development of  
a Three-Axis Superconducting Gravity Gradiometer  
and a Six-Axis Superconducting Accelerometer \*

M. V. Moody, H. A. Chan, Q. Kong  
H. J. Paik, and J. W. Parke

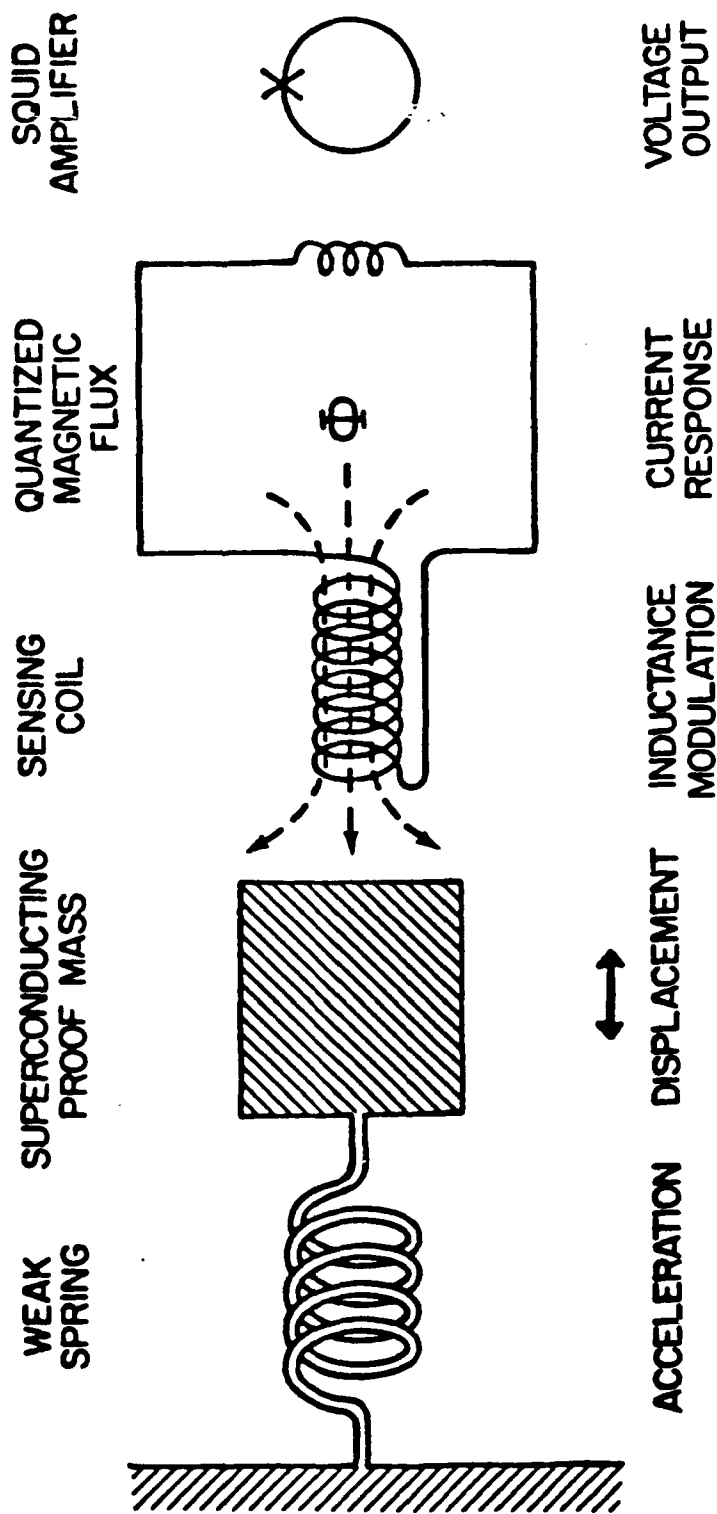
Dept. of Physics, Univ. of Maryland

\* Supported by AFGL and NASA contracts

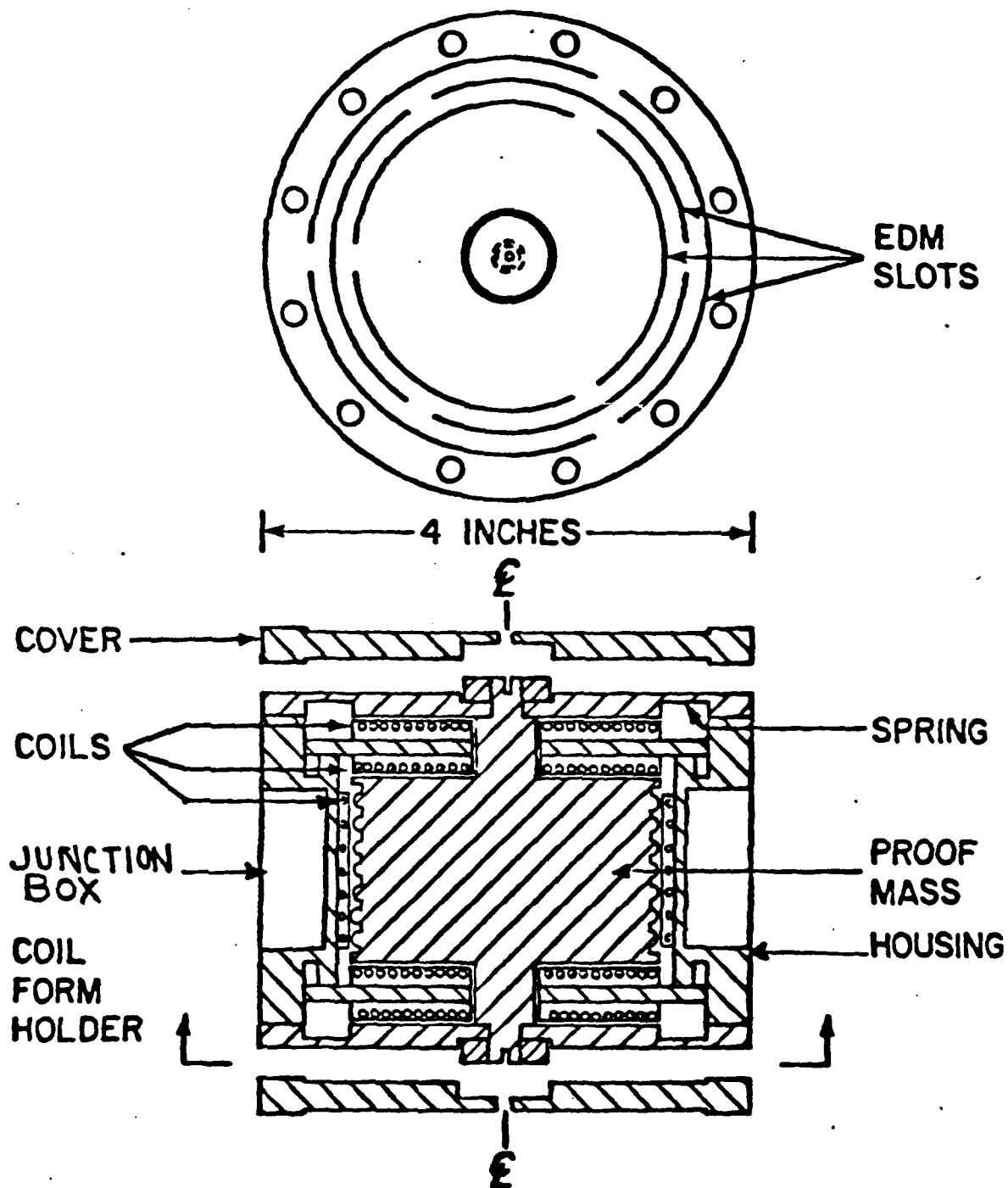
## History of Maryland Superconducting Gravity Gradiometer Program

- I. Outgrowth of Stanford Gravitational Wave Detection Program - early 1970's - Paik
- II. First versions completed - late 1970's - Paik, Mapoles;
  - a) displacement differencing -  
adjust resonance frequencies to balance,
  - b) current differencing -  
adjust ratios of persistent currents.
- III Maryland 1-axis prototype - 1979-1983:
  - a) fundamental sensitivity =  $0.03 \text{ E Hz}^{-1/2}$ ,
  - b) demonstrated in laboratory,  
 $0.3 - 1 \text{ E Hz}^{-1/2}$  from 0.05 to 1 Hz.
- IV Maryland 3-axis gravity gradiometer:
  - a) fundamental sensitivity =  $2 \times 10^{-4} \text{ E Hz}^{-1/2}$ ,
  - b) recently began testing 1<sup>st</sup> axis.

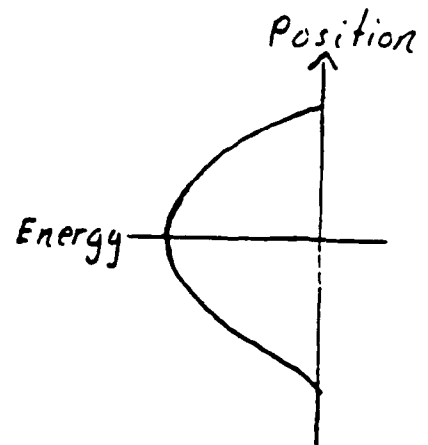
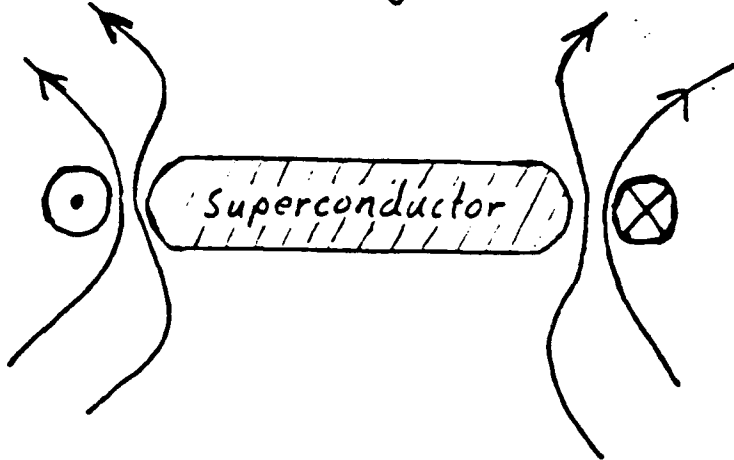
# *Superconducting Accelerometer*



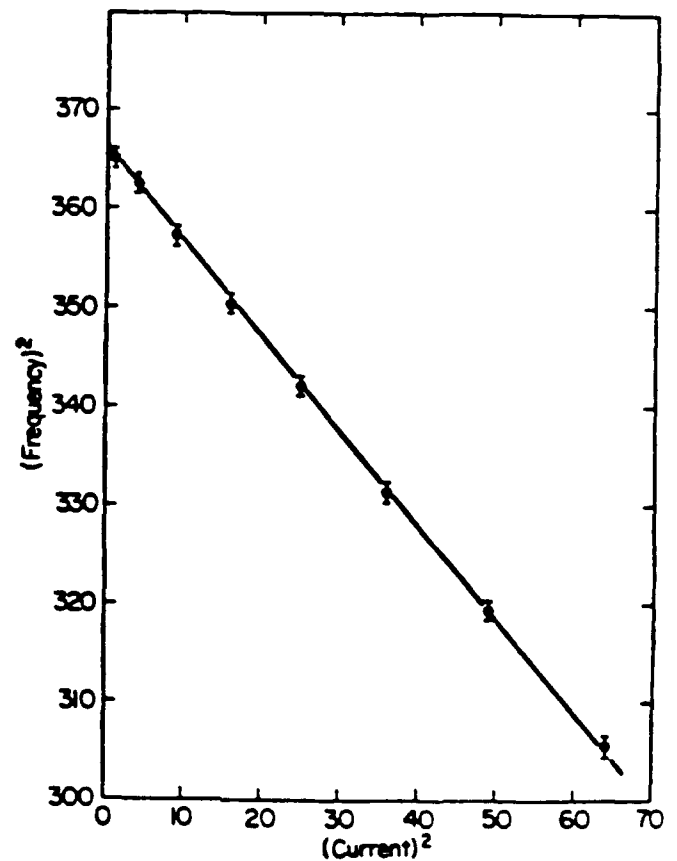
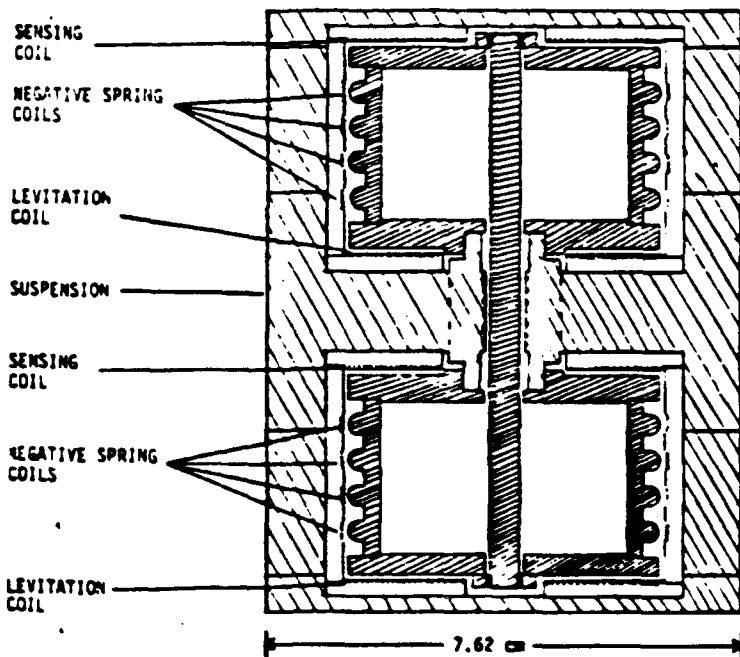
3-AXIS SUPERCONDUCTING GRAVITY GRADIOMETER  
DESIGN FOR ONE OF SIX IDENTICAL UNITS



# Superconducting Negative Spring



$$\text{Energy} = -\frac{1}{2} k x^2 + c x^4 + \dots$$



### Intrinsic Spectral Noise

$$S_r(f) = \frac{8}{m l^2} \left[ K_B T \frac{2\pi f}{Q(f)} + \frac{(2\pi f_0)^2}{2\beta\eta} E_A(f) \right]$$

### Design parameters

proof mass	$m$	1.3 kg
base line	$l$	0.19 m
resonance frequency	$f_0$	< 7 Hz
temperature	$T$	1.5 K
quality factor	$Q$	$\geq 10^5$
amplifier noise (SHE de SQUID)	$E_A$	$3 \times 10^{-30} \text{ J Hz}^{-1}$
energy coupling factor	$\beta\eta$	$\sim 0.5$

### Gravity Gradient Noise

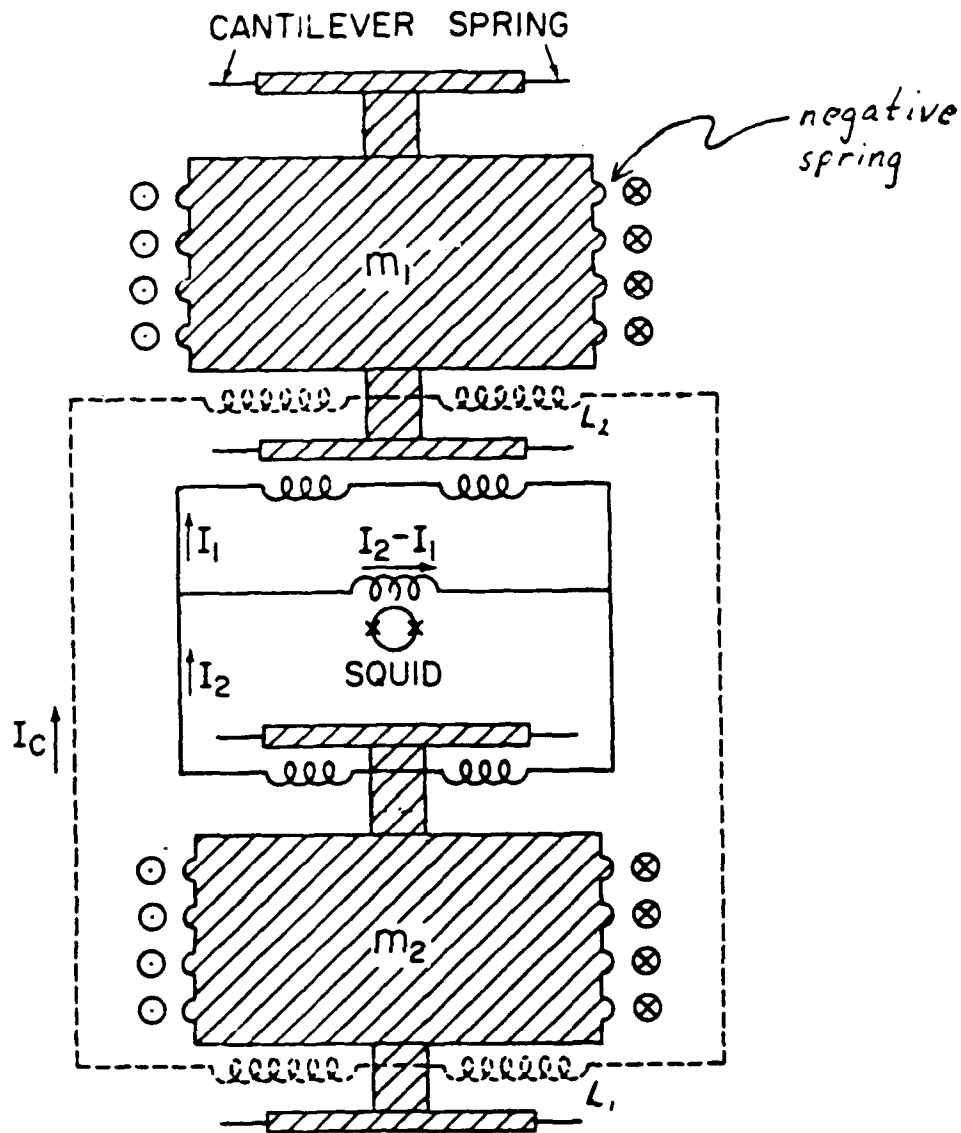
Without negative spring

$$S_r^{1/2}(f) = 1 \times 10^{-3} \text{ E Hz}^{-1/2} \text{ at } 0.1 \text{ Hz}$$

With negative spring ( $f_0 = 1 \text{ Hz}$ )

$$S_r^{1/2}(f) \leq 2 \times 10^{-4} \text{ E Hz}^{-1/2} \text{ at } 0.1 \text{ Hz}$$

Goal set by 1983 workshop  $\rightarrow 3 \times 10^{-4} \text{ E Hz}^{-1/2}$



Sensing circuit —

adjust ratio of  $I_1$  to  $I_2$  to balance out common mode accelerations.

Levitation circuit ----

$$E_L = \frac{\Phi_L^2}{2L}, \quad L = L_1 + L_2, \quad L_i = \mu_0 n_i^2 A_i (d_i + x_i)$$

$\therefore$  increases only common mode resonance frequency ( $\sim 40$  Hz)

## Additional Functions of Superconducting Circuit

### I. Feedback

- a. cold damping
- b. force rebalance
- c. high frequency rejection

### II. Three dimensional balance

### III. Passive rejection of temperature drift

## Feedback Functions

### Force rebalance

Maintains null position of proof masses.

Reduces nonlinearities.

Increases dynamic range.

Reduces cross coupling

### Cold damping

Reduces amplitude of high  $Q$  resonance peak.

Prevents amplifier overload.

Increases signal to noise ratio by permitting high coupling.

### High frequency rejection

Reduces amplitude of peaks above resonance frequency.

## Primary Error Sources

Temperature sensitivity (penetration depth)

Partially cancelled by common mode balance.

Temperature stability of liquid helium.  
(lambda point operation)

Passive rejection by penetration depth thermometer.

Sensitive Axis Misalignment

Linear motion  $\rightarrow$  three dimensional balance

Angular motion  $\rightarrow$  interface with six-axis accelerometer.

Centrifugal acceleration

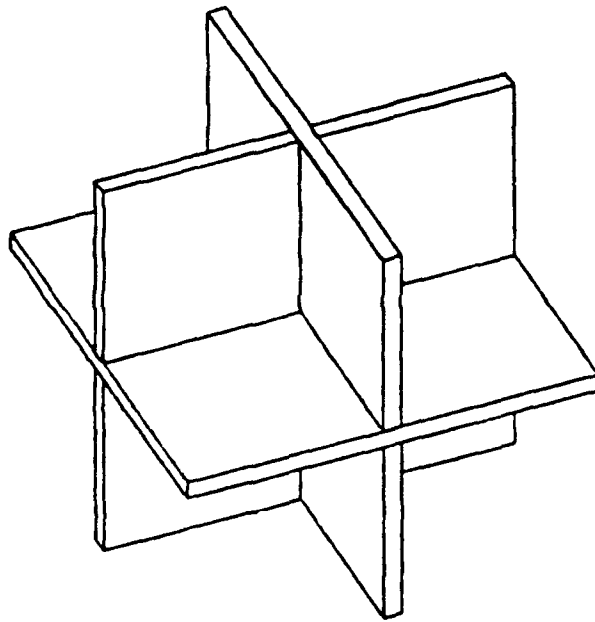
Interface with six-axis accelerometer.

## II. Basic Design

4.

- If we monitor the motion of a single Proof mass, we can measure accelerations in all six degrees of freedom.

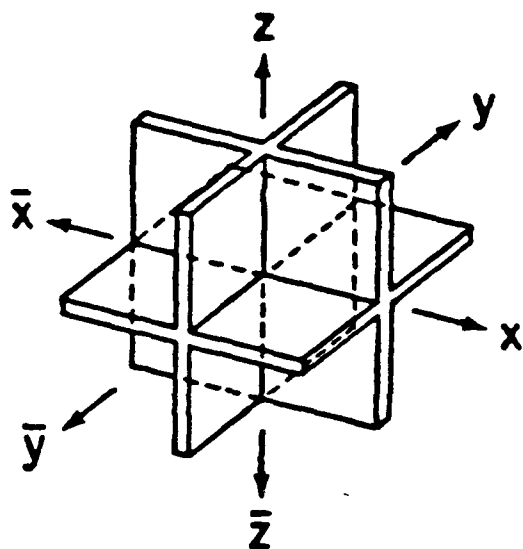
In order to maximize the number of control surfaces, a Nb Proof mass is constructed:



Each face of the proof mass has a levitation/feedback coil and a sensing coil in close proximity.

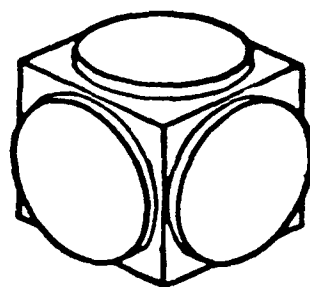
- These coils are mounted on 8 cubes that sit in each one of the 8 quadrants of the proof mass.

# Superconducting Six-axis Accelerometer



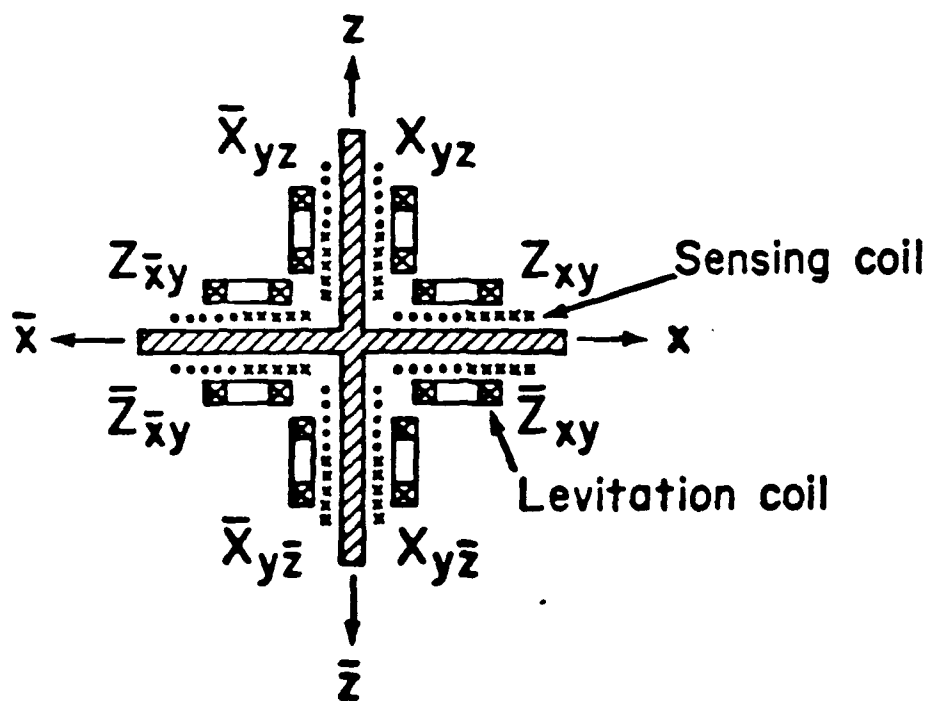
Proof mass (Niobium)

(a)



Coil form (Macor ceramic)

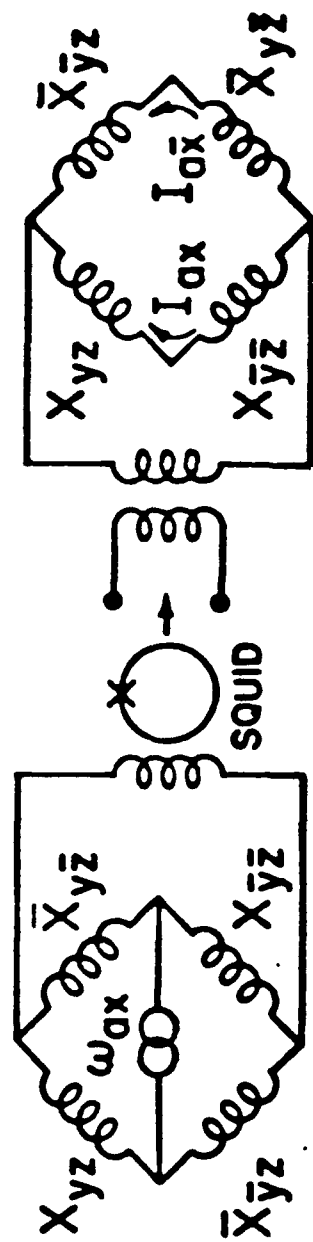
(b)



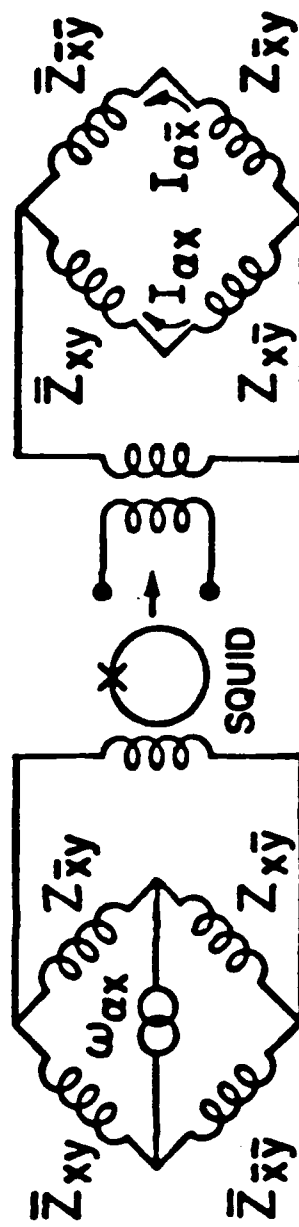
Coils (24 sensing coils + 24 levitation coils)

(c)

# Superconducting Circuit



(a)



(b)

Sensing coils  $\longrightarrow$  Feedback  $\longrightarrow$  Levitation coils

### Intrinsic Spectral Noise

$$S_g(f) = \frac{4}{m} \left[ K_B T \frac{2\pi f}{Q(f)} + \frac{(2\pi f_0)^2}{2\beta} E_A(f) \right]$$

$$S_a(f) = \frac{4}{I} \left[ K_B T \frac{2\pi f}{Q(f)} + \frac{(2\pi f_0)^2}{2\beta} E_A(f) \right]$$

### Design Parameters

proof mass	$m$	0.1 kg
resonance frequency	$f_0$	1 Hz
temperature	$T$	1.5 K
quality factor	$Q$	$10^4$
amplifier noise	$E_A$	$3 \times 10^{-30} \text{ JHz}^{-1}$
energy coupling factor	$\beta$	$\sim \frac{1}{2}$
moment of inertia	$I$	$3 \times 10^{-5} \text{ kg m}^2$

### Acceleration Noise

$$S_g^{1/2}(f) = 4 \times 10^{-14} g_E \text{ Hz}^{-1/2}, \quad f = 0.1 \text{ Hz}$$

$$S_a^{1/2}(f) = 3 \times 10^{-11} \text{ rad s}^{-2} \text{ Hz}^{-1/2}, \quad f = 0.1 \text{ Hz}$$

## LEVITATION CIRCUIT

Equations of Motion:

$$\ddot{X}_1 + (\omega_{10}^2 + \omega_{1L}^2)(X_1 + X_{10}) + \left(\frac{m_1}{m_2}\right)^{1/2} \omega_{1L} \omega_{2L} X_2 = g_1$$

$$\ddot{X}_2 + (\omega_{20}^2 + \omega_{2L}^2)(X_2 + X_{20}) + \left(\frac{m_2}{m_1}\right)^{1/2} \omega_{1L} \omega_{2L} X_1 = g_2$$

$m_i \omega_{i0}^2 = K_{i0} \equiv$  mechanical spring constant

$$K_{iL} = \frac{\partial^2 E_L}{\partial X_i^2} = \frac{\partial^2}{\partial X_i^2} \left( \frac{\Phi^2}{2(L_1 + L_2)} \right) = \frac{\Phi^2}{L^3} \left( \frac{\partial L}{\partial X_i} \right)^2 - \frac{1}{2} \frac{\Phi^2}{L^2} \frac{\partial^2 L}{\partial X_i^2}, \quad L = L_1 + L_2$$

Eigenfrequencies:

$$\begin{aligned} \omega_{\pm}^2 &= \frac{1}{2} \left\{ \omega_{10}^2 + \omega_{1L}^2 + \omega_{20}^2 + \omega_{2L}^2 \pm \left[ (\omega_{10}^2 + \omega_{1L}^2 - \omega_{20}^2 - \omega_{2L}^2)^2 + 4 \omega_{1L}^2 \omega_{2L}^2 \right]^{1/2} \right\} \\ &\approx \frac{1}{2} \left\{ \omega_{10}^2 + \omega_{20}^2 + \omega_{1L}^2 + \omega_{2L}^2 \pm (\omega_{1L}^2 + \omega_{2L}^2) \left[ 1 + \frac{(\omega_{10}^2 - \omega_{20}^2)(\omega_{1L}^2 - \omega_{2L}^2) + \frac{1}{2}(\omega_{10}^2 - \omega_{20}^2)^2}{\omega_{1L}^2 + \omega_{2L}^2} \right] \right\} \end{aligned}$$

$$\omega_+^2 \approx \frac{1}{2} \left[ \omega_{10}^2 + \omega_{20}^2 + 2(\omega_{1L}^2 + \omega_{2L}^2) \right]$$

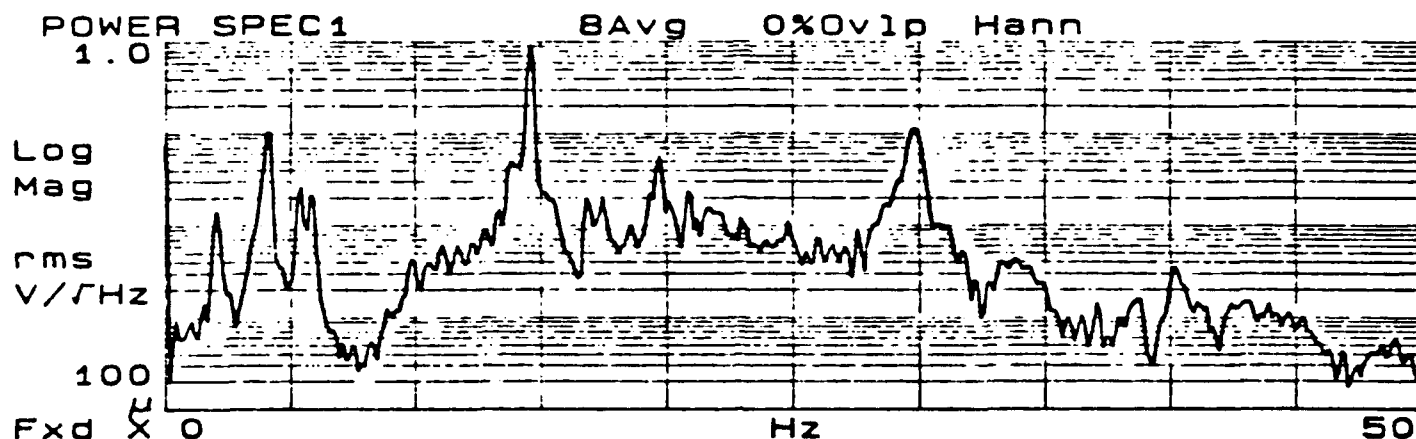
$$\omega_-^2 \approx \frac{1}{2} (\omega_{10}^2 + \omega_{20}^2)$$

For this design,

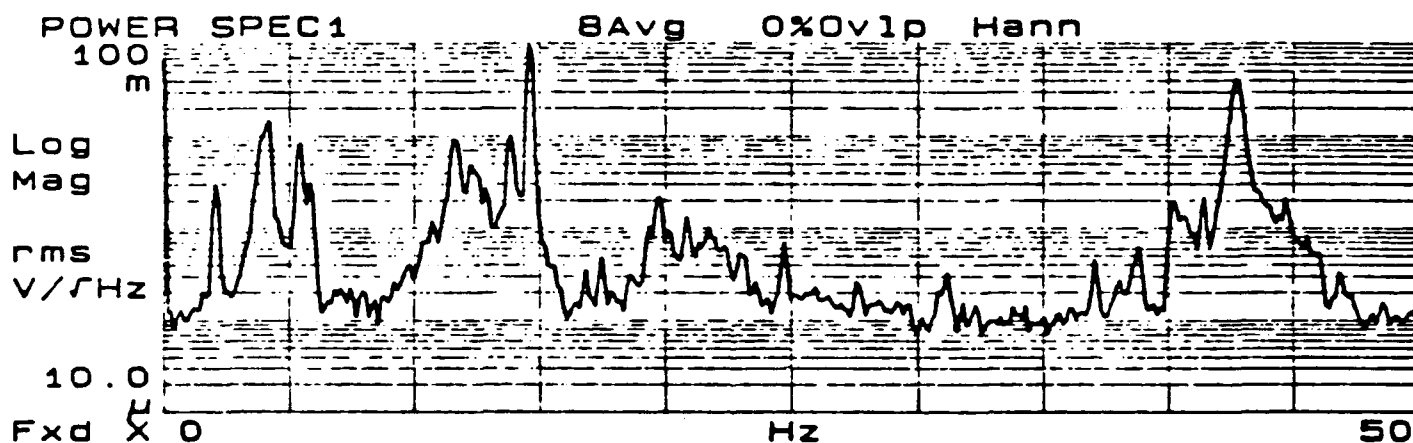
$$\omega_{10} \approx \omega_{20} \approx 2\pi(4.5 \text{ Hz}), \quad \omega_{1L} \approx \omega_{2L} \approx 2\pi(29 \text{ Hz})$$

$$\omega_+ \approx 2\pi(40 \text{ Hz}), \quad \omega_- \approx 2\pi(4.5 \text{ Hz})$$

A. 1 mass levitated ,  $I_L = 10.6 A$



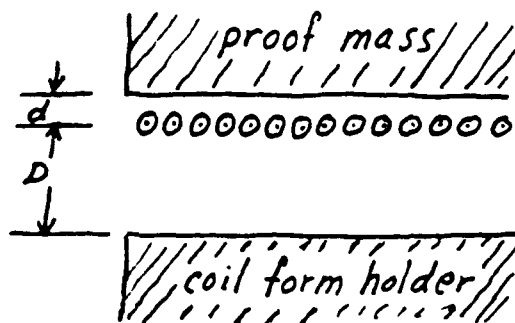
B. Both masses levitated ,  $I_L = 10.7 A$



$A \div B$



Modified inductance due to superconducting plane:



$$\frac{1}{L_i} = \frac{1}{\lambda_i} \left( \frac{1}{d_i} + \frac{1}{D_i} \right), \quad d_i = d_0 + x_i, \quad \lambda_i = \mu_0 n_i A_i$$

Expand to 2<sup>nd</sup> order

$$L_i = L_{i0} \left[ 1 + x_i \frac{L_{i0}}{d_{i0}} - x_i^2 \frac{L_{i0}^2}{\lambda_i^2 D_i d_{i0}^3} \right]$$

Modified equations of motion:

$$\ddot{x}_i + (\omega_{i0}^2 + \omega_{ip}^2 + \omega_{il}^2 (x_i - x_{i0}) + \left( \frac{m_i}{m_j} \right)^{1/2} \omega_{il} \omega_{jl} x_j) = g_i$$

$$\omega_{-}^2 \approx \frac{1}{2} (\omega_{i0}^2 + \omega_{j0}^2 + \omega_{ip}^2 + \omega_{jp}^2)$$

$$\omega_{-} = 2\pi(11.5 \text{ Hz})$$

# Gradiometer Development Schedule

79 80 81 82 83 84 85 86 87 88 89 90 91  
 | | | | | | | | | | | | |

Prototype I  
(Single-axis)

Design Construction Test



Ancillary  
Technologies

S/c therm. S/c joint

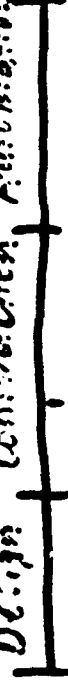
Neg. Spring Coil wind.



Prototype II  
(three-axis)

Design Construction Automation

Test



1-axis  
Test

Design Construction Automation

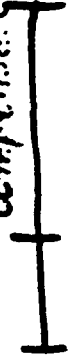
Test



6-axis  
Accelerometer

Integrated  
System

Integrate Error  
Compensate



TITLE OF PAPER: Development of A Three-Axis Superconducting Gravity Gradiometer  
and A Six-Axis Superconducting Accelerometer

SPEAKER: Martin Vol Moody

QUESTIONS AND COMMENTS:

1. Question: Charles F. Martin

The non-linear effects of levitation at 11.5 Hz caused by "d" and "D" dimensions can be ignored in space. Can you adjust adequately for surface or near earth use?

Response:

Yes, that distance can be adjusted and should present no problem in near earth operation.

2. Question: Anthony R. Barringer

Is the six axis accelerometer applicable in a 1 "g" environment?

Response:

Yes. We plan to test it in a 1 "g" environment. It will levitate at 1 "g".

3. Question: James E. Fix

What Q (quality factor) did you achieve?

Response:

Q is pressure limited. Achieved  $Q = 10^5$  in tests at Stanford.

THE GRAVITATIONAL MAGNETIC FIELD OF THE EARTH  
AND THE POSSIBILITY OF MEASURING IT  
USING AN ORBITING GRAVITY GRADIOMETER

by

Dr. Bahram Mashhoon  
Department of Physics and Astronomy  
University of Missouri-Columbia  
Columbia, MO 65211

ABSTRACT

Einstein's theory of gravitation predicts that a rotating body such as the Earth carries the local inertial frames around it ("dragging of the inertial frames"). This results in an effective gravitational "magnetic" field due to mass current in addition to the usual - i.e., essentially Newtonian - gravitational "electric" field, in close analogy with the electromagnetic field around a rotating charged body. This fundamental prediction of general relativity has not yet been tested. A gravity gradiometer in Earth orbit measures mostly the components of the tidal field (i.e., curvature tensor) of the Earth. The gravitational "electric" and "magnetic" fields of the Earth are reflected in the tidal tensor. The tidal accelerations due to a rotating system have been studied and the relativistic corrections to the Newtonian results have been determined (Mashhoon and Theiss, Phys. Rev. Lett. 49, 1542-1545, 1982). The possibility of measuring relativistic effects using Paik's superconducting gravity gradiometer currently under development is investigated.

# Gravitational "Magnetic" Field

## ● Analogy with Electrodynamics

G. Holzmüller 1870

F. Tisserand 1872, 1890

E. Wiechert 1920 "Electrodynamic Theory of  
Gravitation"

F. Hund 1948

D. Sciama 1953

● Einstein's Theory of Gravitation 1916 : GR explains excess  
perihelion precession of Mercury ( $\sim 42''/\text{century}$ )

1918 H. Thirring, J. Lense and H. Thirring :  
Gravitational "Magnetic" Field in GR

"Dragging of the Local Inertial Frames"

References : B.M., F.W. Hehl, D.S. Theiss : Gen. Rel. Grav. 16, 711 (1984)

B.M., Found. Phys. 15, 497 (1985).

● This Aspect of General Relativity Has Never Been Tested!

Analogy :

Gravity

E+M

$$\dot{m} \quad \leftarrow \frac{Gm}{r^2} \hat{r}$$

$$\dot{q} \quad \leftarrow \frac{q}{r^2} \hat{r}$$

$$Gm \leftrightarrow q$$

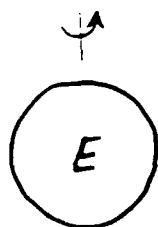
$$J \uparrow \quad \underline{G} \approx -2 \frac{G \underline{J} \times \hat{r}}{r^2}$$

$$\uparrow \underline{\mu} \quad \underline{A} = \frac{\underline{\mu} \times \hat{r}}{r^2}$$

$${}^{\prime\prime}\underline{B}_g{}^{\prime\prime} \approx \underline{\nabla} \times \underline{G}$$

$$\underline{B} = \underline{\nabla} \times \underline{A}$$

$$\underline{\Omega}_D = -\frac{1}{2} \underline{\nabla} \times \underline{G} = \frac{G \underline{J}}{r^3} [3(\hat{r} \cdot \hat{J}) \hat{r} - \hat{J}]$$



$$\frac{d\underline{S}}{d\tau} = \underline{\Omega}_D \times \underline{S}$$

# General Theory of Relativity

## Best Theory of Gravitation Available at Present

- (i) The results of measurements should not depend on the choice of coordinates assigned to events.

"Observables are Scalar Invariants"

- (ii) Einstein's Principle of Equivalence

"Inertial Mass = Gravitational Mass"

Gravitation : Curvature of Spacetime  
( "gravity gradient" )

"Test Particles and Light Rays Follow Geodesics"

$$ds^2 = g_{\mu\nu} dx^\mu dx^\nu$$

Metric  $g_{\mu\nu} \sim \phi$  (Newtonian Potential)

Connection  $\Gamma^\mu_{\nu\rho} \sim \partial\phi$  (Newtonian Force)

Curvature  $R^\mu_{\nu\rho\sigma} \sim \partial^2\phi$  ("Tidal Field")

$$R_{\mu\nu} - \frac{1}{2} g_{\mu\nu} R = -\frac{8\pi G}{c^4} T_{\mu\nu}$$

$$\nabla^2\phi = -4\pi G\rho$$

Gravitational Field Equations

# Newtonian Gravity :



$$\xi(t) = x_2(t) - x_1(t)$$

Global Inertial Frame :  $i=1,2,3$

$$\frac{d^2 x_1^i}{dt^2} = -(\nabla_i \phi)_1$$

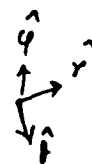
$$\frac{d^2 x_2^i}{dt^2} = -(\nabla_i \phi)_2$$

$$\frac{d^2 \xi^i}{dt^2} = -(\nabla_j \nabla_i \phi)_1 \xi^j + \dots$$

To first order :  $\frac{d^2 \xi^i}{dt^2} + K^i_j(t) \xi^j = 0$

$$K_{ij} = \frac{\partial^2 \phi}{\partial x^i \partial x^j} = \text{Tidal Matrix}$$

(M)

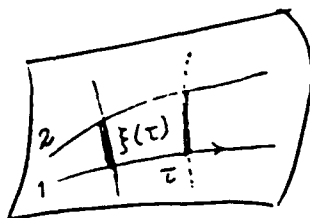


$$\text{Tr } K = \nabla^2 \phi = -4\pi G \rho$$

$$K_{rr} = -\frac{2GM}{r^3}$$

$$K_{\theta\theta} = K_{\phi\phi} = \frac{GM}{r^3}$$

General Relativity :



Jacobi Equation :

$$\frac{d^2 \xi}{d\tau^2} + R \xi = 0$$

$R = \text{Gaussian Curvature of the Surface}$

$$\text{GR : } \frac{d^2 \xi^i}{d\tau^2} + R_{0i0j} \xi^j = 0$$

$R_{\mu\nu\rho\sigma} = \text{Riemann Curvature Tensor}$

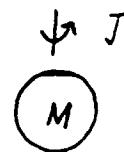
$\text{Tr } R_{\mu\nu\rho\sigma} \approx R_{\mu\rho}$  Ricci Tensor ;  $\text{Tr } R_{\mu\rho} \approx R$

Scalar Curvature

$$R_{\mu\nu} - \frac{1}{2} g_{\mu\nu} R = -\frac{8\pi G}{c^4} T_{\mu\nu}$$

# Gravity Gradiometry in GR:

(i) Gravitational Field of the Earth ( $g_{\mu\nu}$ )



(ii) Calculate  $R_{\mu\nu\rho\sigma}$

(iii) Choose an Orbit  $t = t(\tau)$ ,  $x^i = x^i(\tau)$

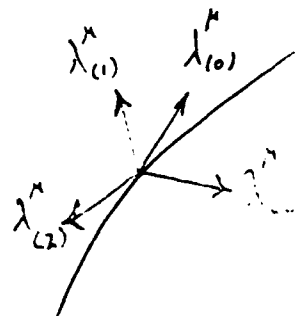
Geodesic Path  $\lambda_{(0)}^\mu = \frac{dx^\mu}{d\tau}$ ,  $\lambda_{(i)}^\mu$  ("gyroscopes")

$\lambda_{(a)}^\mu$ : orthonormal frame parallel propagated along the path  
("Local Inertial Frame")

$$(iv) K_{ij}(\tau) = R_{\mu\nu\rho\sigma} \lambda_{(0)}^\mu \lambda_{(i)}^\nu \lambda_{(0)}^\rho \lambda_{(j)}^\sigma$$

Tidal Matrix

$$\frac{d^2 \xi^i}{d\tau^2} + K_{ij}(\tau) \xi^j = 0.$$



(v) Any other set of local axes:

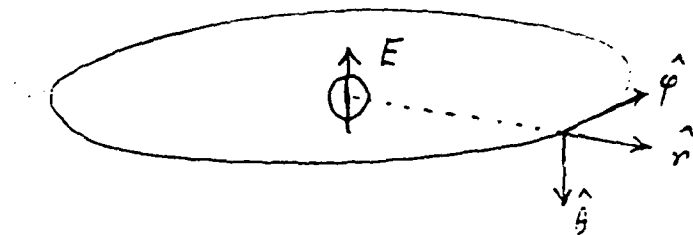
$$\xi'^i = M_{ij}(\tau) \xi^j, \quad \lambda_{(i)}'^\mu = M_{ij}(\tau) \lambda_{(j)}^\mu$$

$$\left[ \frac{d^2 \xi'}{d\tau^2} + 2 \underline{\Omega} \times \frac{d \xi'}{d\tau} + \underline{\Omega} \times (\underline{\Omega} \times \xi') + \frac{d \underline{\Omega}}{d\tau} \times \xi' \right]^i + K'_{ij} \xi'^j = 0$$

$$K' = M K M^\dagger$$

B. M. + D. S. Theiss : *phys. Rev. Lett.* 49, 1542 (1982).

Equatorial Orbit :



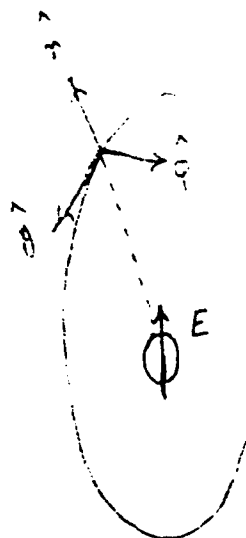
$$K' = \omega_o^2 \begin{bmatrix} -2 & 0 \\ 0 & 1 \\ & 1 \end{bmatrix} + \frac{GM}{c^2 r} \omega_o^2 \begin{bmatrix} -3 & 0 \\ 0 & 3 \\ & 0 \end{bmatrix} + 2 \frac{GJ}{c^2 r^3} \omega_o \begin{bmatrix} -3 & 0 \\ 0 & 3 \\ & 0 \end{bmatrix}$$

$$\omega_o^2 \approx 10^{-6} \text{ sec}^{-2}$$

$$6 \times 10^{-10} \omega_o^2$$

$$\mp 3 \times 10^{-11} \omega_o^2$$

Polar Orbit :



$$K' = \omega_o^2 \begin{bmatrix} -2 & 0 \\ 0 & 1 \\ & 1 \end{bmatrix} + \frac{GM}{c^2 r} \omega_o^2 \begin{bmatrix} -3 & 0 \\ 0 & 3 \end{bmatrix} + \omega_o^2 \begin{bmatrix} 0 & 0 & X \\ 0 & 0 & Y \\ X & Y & 0 \end{bmatrix}$$

$$\omega_o^2 X \approx 9 \frac{GJ}{c^2 r^3} \omega_o (\cos \omega_o \tau - \frac{1}{2} \omega_o \tau \sin \omega_o \tau)$$

$$\omega_o \tau \ll \left( \frac{GM}{c^2 r} \right)^{-1} \approx 10^9$$

$$\omega_o^2 Y \approx 3 \frac{GJ}{c^2 r^3} \omega_o \sin \omega_o \tau$$

Can Pohl's Experiment Measure Gravitational Magnetic Field of the Earth?

TITLE OF PAPER: The Gravitational Magnetic Field of the Earth and the Possibility of Measuring it Using an Orbiting Gravity Gradiometer

SPEAKER: Bahram Mashhoon

QUESTIONS AND COMMENTS:

1. Question: Dan Long

Have the gravitational magnetic effects been derived classically as can be done in Electricity and Magnetism?

Response:

One would get about the same results but that theory has defects and I have not used it.

2. Question: Alan Zorn

Your satellite examples show that the relativistic correction terms are both conservative and harmonic (symmetric and traceless). Is this true in general?

Response:

Yes, general relativity implies this in general.

3. Question: Charles Finley

Does the orientation of the spacecraft, i.e., the orientation of the SGG within the Spacecraft (inertial vs. earth pointing) make a difference for this experiment? If so, which would be preferred?

Response:

In theory, it would not matter which orientation were used since the deviation from true gyroscopic inertial orientation would have to be measured and/or determined. However, in practice this is an important question in that they would want the orientation to be such as to minimize the difficulty in measuring the deviation from the true inertial.

4. Question: Warren Heller

What is the size of the quadrilateral/magnetic effect in ordinary terms?

Response:

$3 \times 10^{-11}$  of an orbit time.

TESTS OF GENERAL RELATIVITY IN EARTH ORBIT  
USING A SUPERCONDUCTING GRAVITY GRADIOMETER

by

Dr. Ho Jung Paik  
Department of Physics and Astronomy  
University of Maryland  
College Park, MD 20742

ABSTRACT

A gravity gradiometer measures a component of the Riemann curvature tensor which is the fundamental gravitational field in General Relativity. Both the mass  $M$  and the angular momentum  $J$  of a spinning object contribute to the Riemann tensor. For the Earth, the relativistic corrections due to  $M$  and  $J$  amount to  $7 \times 10^{-10}$  and  $8 \times 10^{-11}$  of the Newtonian gravity gradient, respectively. These effects could be resolved with a signal-to-noise ratio of 10 in one year by a three-axis superconducting gravity gradiometer of  $10^{-4} \text{ E Hz}^{-1/2}$  sensitivity in a low-altitude polar orbit. We discuss the experimental strategy and the requirements that these experiments put on the orbit and the altitude control of the spacecraft.

# TESTS OF GENERAL RELATIVITY IN EARTH ORBIT USING A SUPERCONDUCTING GRAVITY GRADIOMETER

Ho Jung Paik  
Department of Physics and Astronomy  
University of Maryland, College Park

2/12/87

1. Earth's Gravity Field in General Relativity
2. Null Test of Einstein's Field Equations  
(Search for a Fifth Force)
3. Detection of Gravitational "Magnetic" Field
4. Instrument, Spacecraft and Orbit Requirements

# 1. Earth's Gravity Field in General Relativity

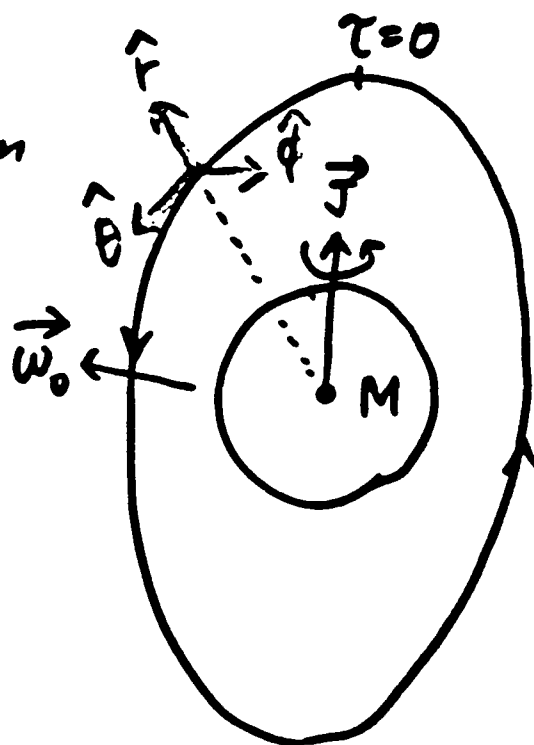
$M$ : Earth's mass

$\vec{J}$ : Earth's angular momentum

$r$ : radius of orbit

$\omega_0 = \sqrt{\frac{GM}{r^3}}$ : Keplerian frequency

$\tau$ : proper time



Tidal matrix (Mashhoon)

Polar Orbit

$$\Gamma_{ij} = \frac{GM}{r^3} \begin{pmatrix} -2 - 3 \frac{GM}{rc^2} & 0 & \frac{9GJ}{r^3 c^2 \omega_0} (\cos \omega_0 \tau - \frac{1}{2} \omega_0 \tau \sin \omega_0 \tau) \\ 0 & 1 & \frac{3GJ}{r^3 c^2 \omega_0} \sin \omega_0 \tau \\ \boxed{\phantom{0}} & \boxed{\phantom{0}} & 1 + \frac{3GM}{rc^2} \end{pmatrix}$$

"Electric" correction:  $\frac{3GM}{rc^2} \cong 2 \times 10^{-9}$

"Magnetic" correction:  $\sim \frac{3GJ}{r^3 c^2 \omega_0} \cong 2 \times 10^{-10}$

+ secular term?

(3)

## Magnitudes of Effects

Newtonian term:

$$\frac{GM}{r^3} \cong 1400 E$$

(dc in rotating frame)

Relativistic "electric" term:

$$\left(\frac{GM}{r^3}\right)\left(\frac{GM}{rc^2}\right) \cong 3 \times 10^{-6} E$$

(dc in rotating frame)

Relativistic "magnetic" term:

$$\left(\frac{GM}{r^3}\right)\left(\frac{3GJ}{r^3 c^2 \omega_0}\right) \cong 3 \times 10^{-7} E \quad \begin{array}{l} \text{(orbital frequency)} \\ \text{in rotating frame} \end{array}$$

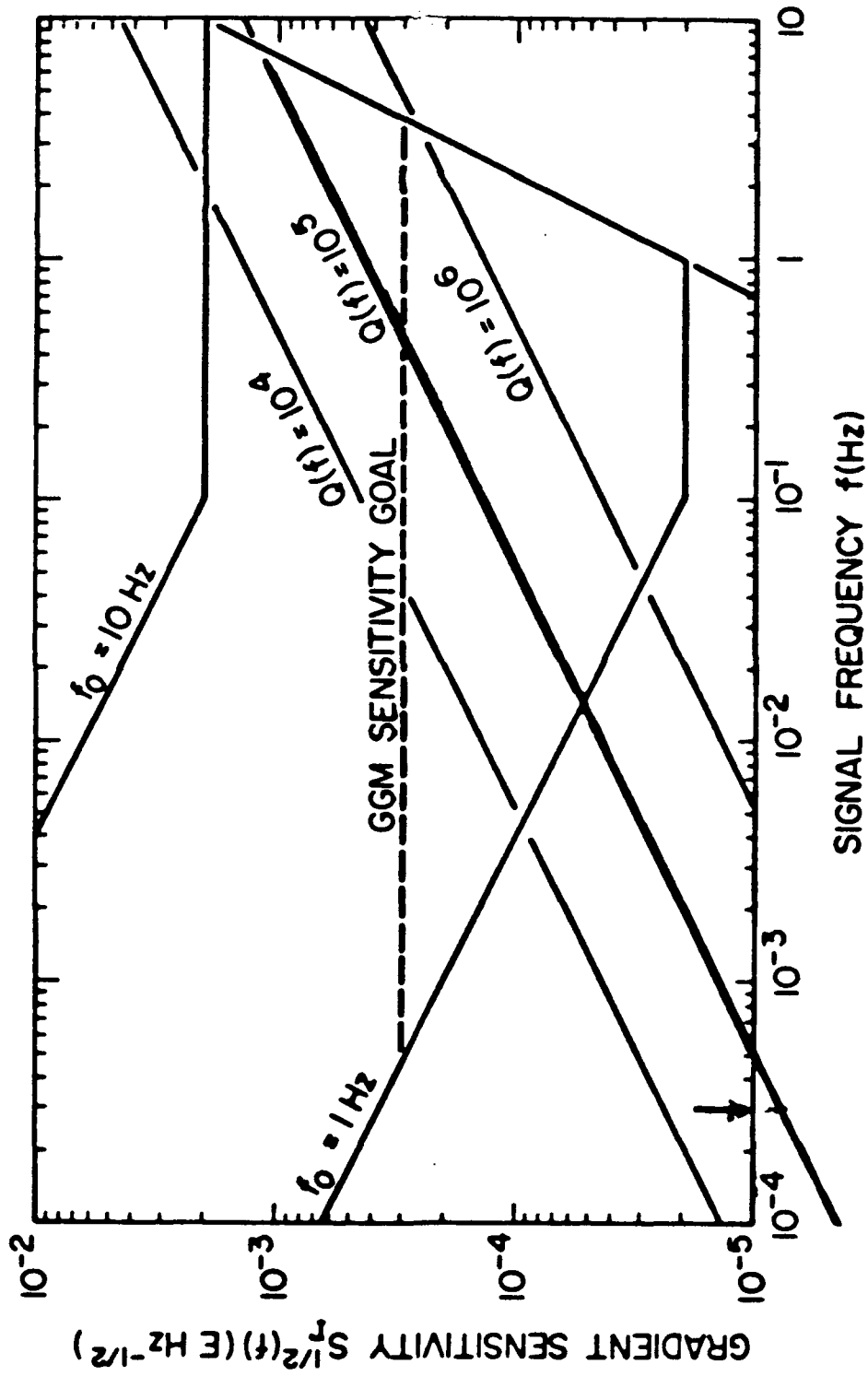
## Instrument Sensitivity

Instrument noise :  $10^{-4} E Hz^{-1/2}$

Integration time:  $T = \pi \times 10^7 s$  (1 year)

$$\Rightarrow \Gamma_N \cong 10^{-4} E Hz^{-1/2} \frac{1}{\sqrt{\pi \times 10^7 s}} \cong 2 \times 10^{-8} E$$

# Expected Sensitivity of S/C Gradiometer



$$1.5 \times 10^{-9} \text{ m/s}^2$$

## 2. Null Test of Einstein's Field Equations

By summing the outputs of a three-axis gradiometer,

$$\sum_{i=1}^3 \Gamma_{ii} = \frac{GM}{r^3} (-2 - 3\chi + 1 + 3\chi + 1) = 0.$$

$$\left( \begin{array}{l} \text{Consequence of Field Equations:} \\ R_{\mu\nu} - \frac{1}{2} g_{\mu\nu} R = 8\pi T_{\mu\nu} \end{array} \right)$$

Main sources of error:

1) Non-orthogonality of three sensitive axes

$\Rightarrow$  Earth-pointing orientation

2) Mismatch of three scale factors

$\Rightarrow$  Interchange of axes  
or continuous cross calibration

Error = scale factor mismatch  $\times$  pointing error

3) Centrifugal acceleration

$\Rightarrow$  Attitude stabilization or compensation  
with the aid of six-axis accelerometer

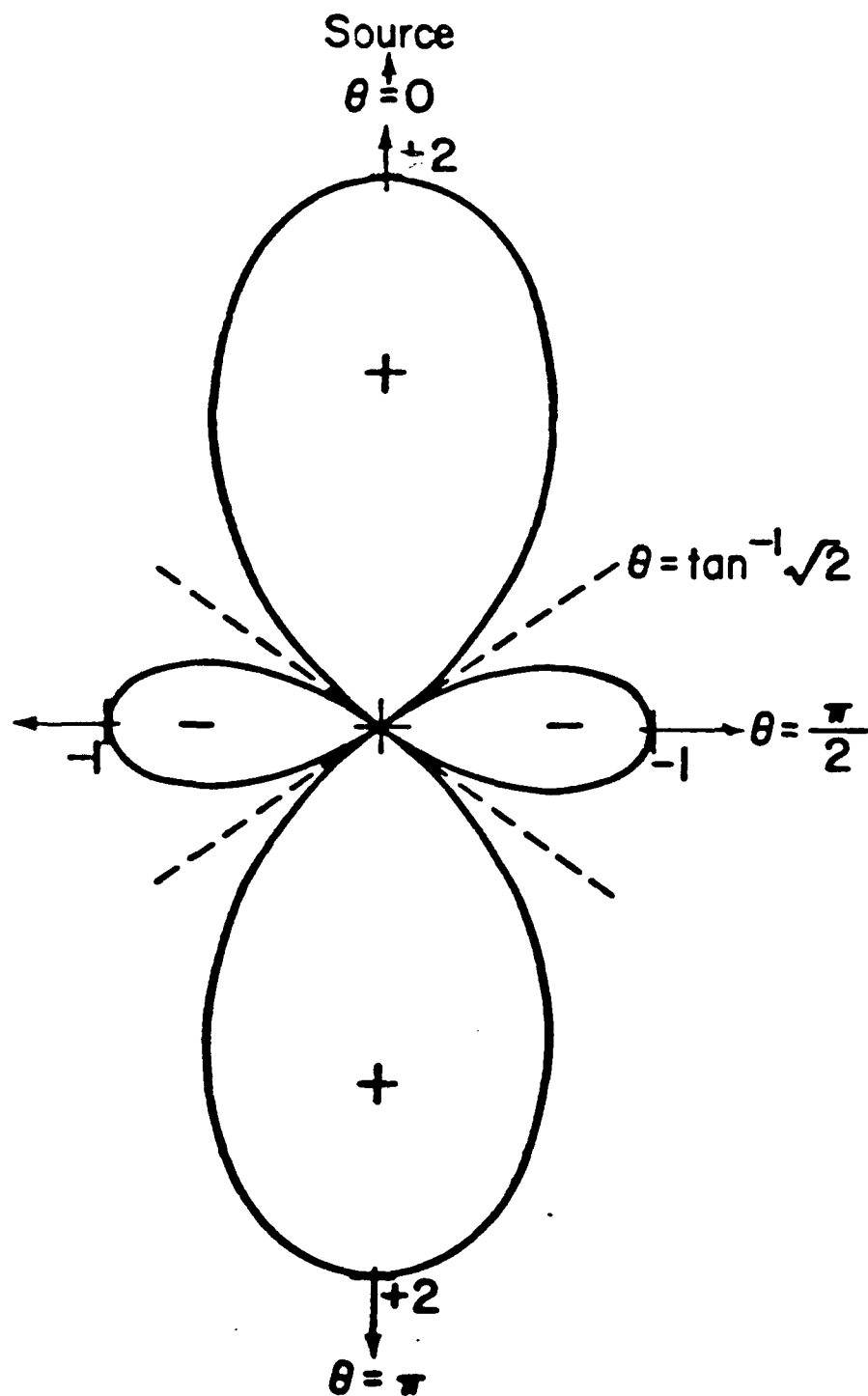


Fig. 3.3. Angular pattern of the gravity gradiometer response to a point mass.

# Forces in Nature

Classical Theory      Quantum Theory      Unified Theory

Long Range  
1. Gravity

General Relativity

?

2. Electro-magnetism

Maxwell's Theory

QED

Short Range

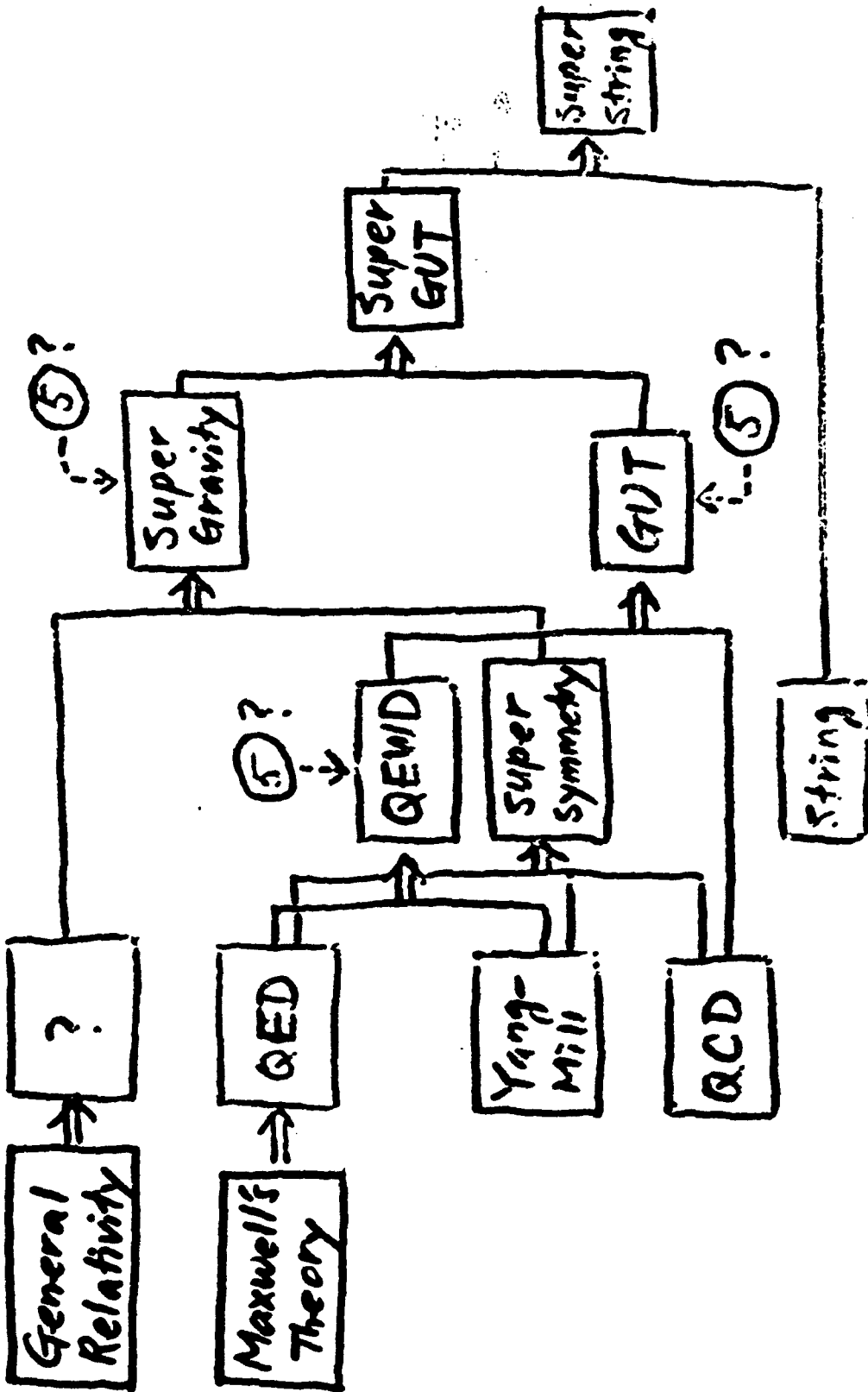
3. Weak

Yang-Mills

4. Strong

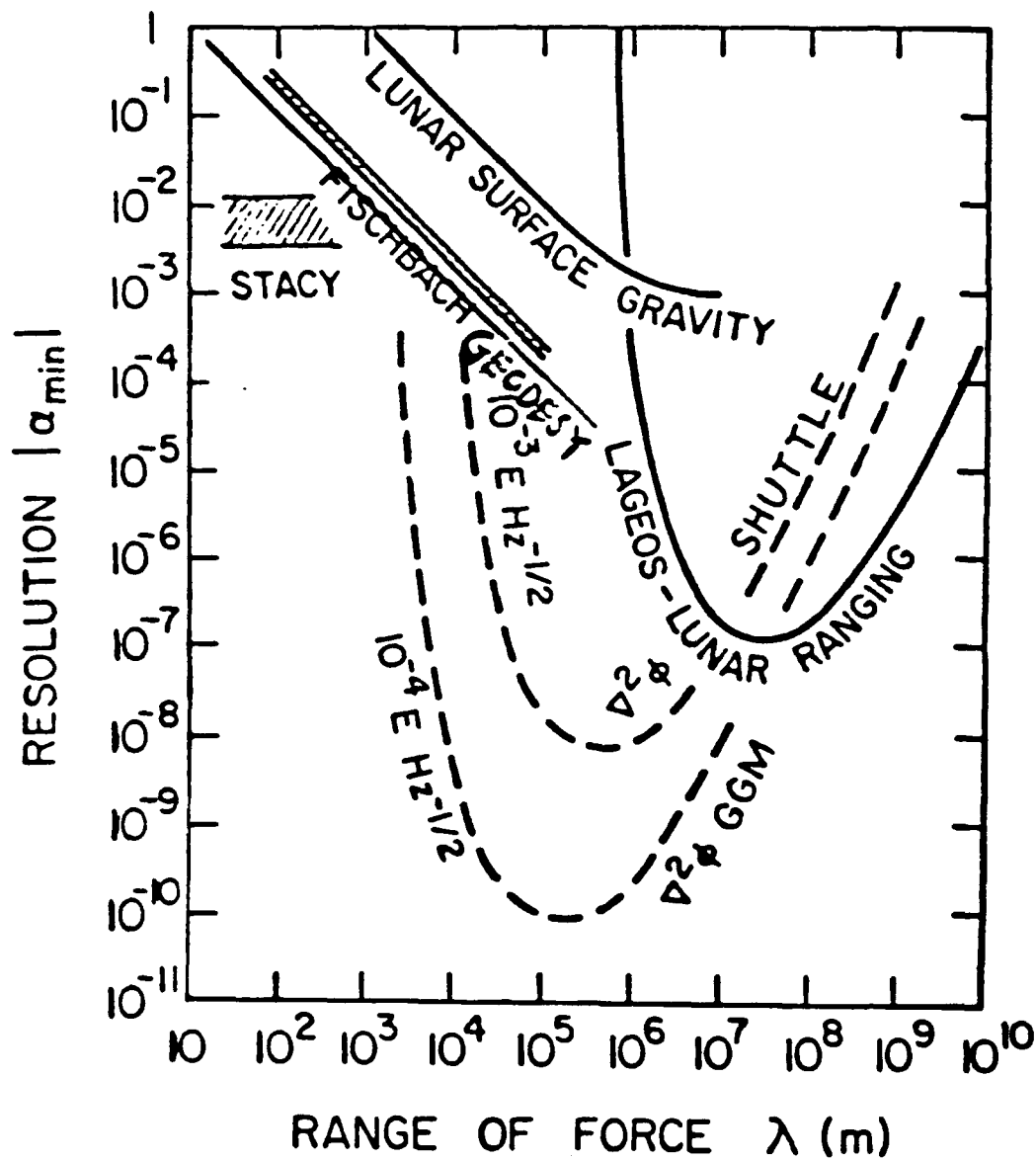
QCD

Medium Range  
5. 5th Force?



# Inverse Square Law Tests

$$\nabla^2 \phi = -4\pi G \rho$$



$$\phi = -\frac{GM}{r} (1 + \alpha e^{-r/\lambda})$$

(5)

### 3. Detection of Gravitational "Magnetic" Field

Orient the gradiometer axes along

$$\hat{r}, \frac{1}{\sqrt{2}}(\hat{\theta} + \hat{\phi}), \frac{1}{\sqrt{2}}(\hat{\theta} - \hat{\phi}).$$

Then,

$$\Gamma_{11} = \Gamma_{rr} = \frac{GM}{r^3} \left( -2 - \frac{3GM}{rc^2} \right)$$

$$\begin{aligned} \Gamma_{22} &= \frac{1}{2}(\Gamma_{\theta\theta} + 2\Gamma_{\theta\phi} + \Gamma_{\phi\phi}) \\ &= \frac{GM}{r^3} \left( 1 + \frac{3}{2} \frac{GM}{rc^2} + \frac{3GJ}{r^3 c^2 \omega_0} \sin \omega_0 \tau \right) \end{aligned}$$

$$\begin{aligned} \Gamma_{33} &= \frac{1}{2}(\Gamma_{\theta\theta} - 2\Gamma_{\theta\phi} + \Gamma_{\phi\phi}) \\ &= \frac{GM}{r^3} \left( 1 + \frac{3}{2} \frac{GM}{rc^2} - \frac{3GJ}{r^3 c^2 \omega_0} \sin \omega_0 \tau \right) \end{aligned}$$

Therefore, the "magnetic" component can be separated out by

$$\Gamma_{22} - \Gamma_{33} \equiv 2\Gamma_{\theta\phi} = \frac{GM}{r^3} \frac{6GJ}{r^3 c^2 \omega_0} \sin \omega_0 \tau.$$

Main sources of error:

1) Non-orthogonality of sensitive axes

⇒ Earth-pointing orientation

2) Eccentricity of orbit

⇒ Subtraction between two horizontal axes

$$\text{Newtonian term} = \frac{GM}{r^3} \times \text{Ellipticity}$$

× (scale factor mismatch  
+ pointing error)

3) Centrifugal acceleration

⇒ Subtraction between two horizontal axes,  
±45° from the along-track direction

Centrifugal acceleration error

$$= \omega_0 \delta \omega_0 \times (\text{pointing error} + \text{scale factor mismatch!})$$

This appears to be an easier experiment  
than the null test of General Relativity!

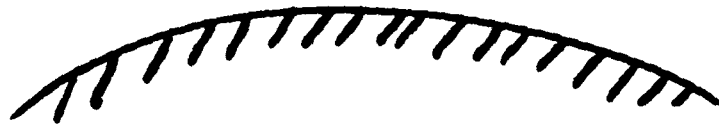
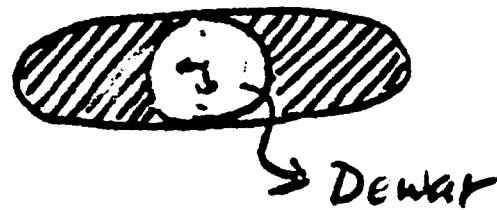
# 4. Instrument, Spacecraft and Orbit Requirements

Error Source	Error Mechanism	Required Control/Knowledge	
		Null Test	"Magnetic" Field
Instrument Noise	$S_p^{1/2}(f)$	$10^{-4} E Hz^{-1/2}$	$10^{-4} E Hz^{-1/2}$
Dynamic Range	$4\Gamma_{E,max} / S_p^{1/2} \Delta f$	$10^5$	$10^5$
Scale Factor Match	$\delta\sigma_i \Gamma_{ii}$	$10^{-10}$	$10^{-5}$
Orthogonality	$\delta\phi_{ij} \Gamma_{ij}$	$10^{-5}$	$10^{-5}$
Pointing	$\delta\theta_{ij} \Gamma_{ij}$	$10^{-5}$	$10^{-5}$
Attitude Rate	$2\vec{\Omega}_0 \cdot \vec{\Omega} - 2(\hat{n} \cdot \vec{\Omega}_0)(\hat{n} \cdot \vec{\Omega})$	$4 \times 10^{-11} s^{-1} Hz^{-1/2}$	$4 \times 10^{-11} s^{-1} Hz^{-1/2}$
Attitude Acceleration	$-\delta\hat{n}_i \times \hat{n} \cdot \vec{\alpha}$	$10^{-9} s^{-2} Hz^{-1/2}$	$10^{-9} s^{-2} Hz^{-1/2}$
Linear Acceleration	$-\frac{1}{2} \delta\hat{n}_i \cdot \vec{a}$	$10^{-8} g Hz^{-1/2}$	$10^{-8} g Hz^{-1/2}$
Altitude	$(\hat{n} \cdot \vec{v}) \hat{n} \cdot \vec{v}_E \cdot \delta\vec{h}$	$0.1 m Hz^{-1/2}$	$10^4 m Hz^{-1/2}$
Orbit Ellipticity	$3[(a-b)/a] \cdot \Gamma_E$	—	$3 \times 10^{-6} (\pm 10 m)$
Instrument Temp	$(d\Gamma/dT) S_T^{1/2}(f)$	$10^{-4} K Hz^{-1/2}$	$10^{-4} K Hz^{-1/2}$

⑧

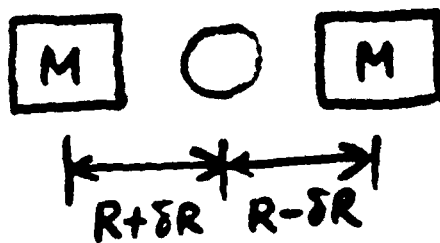
1) Co-rotating satellite

⇒ nearly perfect vibration isolation



2) Symmetric design of satellite with dewar at the center

⇒ self-gravity error becomes a second order effect.



$$\delta \Gamma_s = \frac{12GM}{R^3} \left( \frac{\delta R}{R} \right)^2$$

$$M = 100 \text{ kg}, R = 1 \text{ m}, \delta R = 1 \text{ mm}$$

$$\Rightarrow \delta \Gamma_s \approx 10^{-4} \text{ E}$$

3) Sun-synchronous orbit

⇒ minimizes once-per-orbit disturbances

4) Higher altitude, longer duration preferred

⇒ EOS? (500 km,  $\approx 1$  yr)

Problem: astronauts!

TITLE OF PAPER: Tests of General Relativity in Earth Orbit Using A Superconducting Gravity Gradiometer

SPEAKER: Ho Jung Paik

QUESTIONS AND COMMENTS:

1. Question: Richard Hansen

What about interference to dragging of inertial frames from higher moments of the earth?

Response:

These appear at higher multiples of the orbital frequency. The only effects which can interfere are those with components at orbital frequency.

2. Question: Alan Zorn

Can you comment on the relationship between the current state of scale factor mismatch that you expect on your current instrument and how the requirements for null test ( $10^{-10}$ ) and magnetic field ( $10^{-5}$ ) experiments can be met?

Response:

We expect  $10^{-5}$  on the current 3-axis instrument, so the magnetic field experiment can be done pretty easily. We recognize that the null test experiment will be much harder. However, post processing of the data will help us reach this goal, we believe.

# MAGNETIC ISOLATION-CLOSING THE LOOP

by

Dr. Dave Sonnabend  
Mr. A. Miguel San Martin

Jet Propulsion Laboratory  
California Institute of Technology

## ABSTRACT

Progress on the design, construction, and testing of the JPL single axis magnetic isolation test facility has been previously reported. Our more recent work has been to close the loop with a digital computer, in order to try out various vibration isolation and semi drag free control laws. The status of this work will be reported. For vibration isolation, we will discuss both the theoretical limitations of the technique, and the test limitations imposed by the facility. Finally, for semi drag free operation, we will look at shaping of the current impulses, to minimize the excitation of vibration modes of the floated instrument.

# Magnetic Isolation—Closing the Loop

Dave Sonnabend and A. Miguel San Martin

Jet Propulsion Laboratory  
California Institute of Technology

8 February 1987

## Abstract

Progress on the design, construction, and testing of the JPL single axis magnetic isolation test facility has been previously reported. Our more recent work has been to close the loop with a digital computer, in order to try out various vibration and semi drag free control laws. The status of this work will be reported. For vibration isolation, we will discuss both the theoretical limitations of the technique, and the test limitations imposed by the facility. Finally, for semi drag free operation, we will look at shaping of the current impulses, to minimize the excitation of vibration modes of the floated instrument.

## 1 Introduction

Previous work on magnetic eddy current isolation of gradiometers was reported in Refs. 1 and 2. A single axis torsion pendulum facility was described, on which vibration isolation and semi drag free operation ideas could be tested. The facility characteristics, and initial testing of the magnetic forcers was reported in Ref. 2. The abstract above tells what we would like to have said today; but, as we have not made that much progress, I'll discuss only what we've actually accomplished. Mostly, this will cover our efforts to close a digital control loop around the magnetic test facility. At the end I'll also mention some parallel analytical work, at Arizona State University, on the physics of eddy currents.

## 2 Hardware Description

The plant (the original facility) comprises the torsion pendulum, four eddy current actuators, and two sensors. A photo, from Ref. 1, is shown in Fig. 1. The actuators are mounted externally, on brackets, positioned at opposite faces of the box (where the gradiometer would reside), two on each side. The coil axes are normal to the box faces, along the direction of the box motion. The design and implementation of the torsion pendulum and actuators are described in Ref. 2. A condensed theoretical treatment of eddy current forcing is given in Ref. 1; and a substantial generalization in Ref. 3. A synopsis of the latter work is presented here, in the final section.

The two sensors measure the displacement between the box and the brackets. They are Kaman Instrument Co. eddy current sensors, Model KD-2400. Each sensor consists of two subassemblies—the sensor head and a signal conditioning module. The proximity of the sensor to the box controls a variable gain oscillator within the conditioning module. The oscillator amplitude is detected to provide an analog signal proportional to displacement. Among the sensor features are low cost, no contact, 10 kHz frequency response, adjustable gauge factor, and 0.25 mm resolution.

The function of the control loop is to execute a control law, designed to achieve certain performance objectives. The controller samples analog data from the sensors, converts these to digital form, computes actuator commands according to the trial control law, converts back to analog, and finally doles out power to the actuators. All these operations are carried out periodically, in real time. The two most important requirements of this hardware are at least 12 bit resolution, and a sampling frequency of at least 10 Hz.

Fig. 2 shows the block diagram of the control loop. The computer is a PC's Limited IBM AT compatible; and its characteristics are listed in Table 1. The function of the computer is to carry out the calculations dictated by the control law, control the overall timing of the loop, and generate test evaluation data.

The input/output interface board is located in one of the expansion slots of the computer, and is connected to the computer output bus. Its function is to perform A/D and D/A input and output conversions. Table 2 lists the functions of the interface board. The board consists of a multiplexer, one

A/D and two D/A converters, a clock, and a microprocessor that controls the operation of these elements and communicates with the computer microprocessor in a high level command language. The analog outputs are of the sample and hold type. Purely digital input and output lines are also provided.

The signal generator provides an analog sinusoidal constant amplitude and frequency signal. We are presently operating at 40 kHz. The amplitude modulator regulates the amplitude of the sinusoid according to the control signal from the interface board. At the time of the talk, this was a multiplying D/A converter (see Fig. 3); requiring a digital output from the interface board. However, due to the unavailability of the DAC1220 micro-chip, this approach was changed to using an analog modulator, as shown in Fig. 4.

Finally, the function of the power amplifier is to amplify the signal from the amplitude modulator to provide the desired current to the forcing coils. It is a standard stereo audio amplifier, a Phase Linear Model 400, Series Two. It can put out 205 watts rms into 8  $\Omega$  loads, and has a bandwidth of 50 kHz. Since the talk, these loops have all been closed; and simple control laws have been demonstrated.

### 3 Eddy Current Analysis

In a parallel effort to achieve a better understanding of the physics of eddy current interactions, a contract was let to Arizona State University. Earlier work, summarized in Ref. 1, examined a conductive spherical shell on the axis of a circular coil, carrying a sinusoidal current. The force and dissipation were calculated. The newer work, reported in Ref. 3, extends this to off-axis cases, and computes the torque on the sphere. The analytical results are much too complicated to be presented here; however, the qualitative results are summarized in Fig. 5. As might be expected from symmetry considerations, the axial repelling force does not depend on displacement from the axis, to first order in this displacement; and there is no torque on-axis. However, off-axis, to first order in the displacement, there is a force tending to restore the sphere to the axis, and a torque tending to roll the sphere toward the coil, both proportional to the displacement. The dissipation in the sphere was shown not to vary, to first order in displacement. Future work is planned in this area to develop an electrical model of

the coil-sphere combination, that will serve as a basis for design of practical isolation systems.

#### References

- 1) Seaman, C. H., and Sonnabend, D.; "Semi Drag Free Gravity Gradiometry"; J. Astron. Sci.; Vol. 33, No. 4; 1985.
- 2) Seaman, C. H., and Sonnabend, D.; "A Laboratory Single Axis Magnetic Isolator"; JPL EM 343-1004; 3-21-86.
- 3) Bergman, J., and Hestenes, D.; "Eddy Currents in a Conducting Sphere"; Dept. of Physics, Ariz. St. Univ. Final Report; 10-86; JPL No. 9950-1269.



## COMPUTER

### BRAND AND MODEL:

- PC'S LIMITED IBM AT COMPATIBLE

### FUNCTIONS:

- IMPLEMENT DIGITAL CONTROL LAWS IN REAL TIME
- CONTROL OPERATION OF INPUT/OUTPUT INTERFACE BOARD
- GENERATE TEST EVALUATION DATA

### FEATURES:

- 640KB RAM
- 1.2MB FLOPPY DISK AND 360KB FLOPPY DISK
- 30MB HARD DISK
- 8MHz CLOCK SPEED
- 80287 MATH CO-PROCESSOR

### INTERFACE BOARDS:

- HERCULES GRAPHICS CARD
- PARALLEL/SERIAL PORT
- DATA TRANSLATION IN-OUT INTERFACE BOARD

### PERIPHERALS:

- MONOCHROME DISPLAY
- EPSON FX 85 PRINTER

### SOFTWARE:

- OPERATING SYSTEM: DOS
- PROGRAMMING LANGUAGE: STSC APL\*PLUS



## INPUT/OUTPUT INTERFACE BOARD

### BRAND AND MODEL:

- DATA TRANSLATION DT2801

### FUNCTIONS:

- INTERFACES COMPUTER WITH SENSORS AND ACTUATORS
  - HANDLES MULTIPLE ANALOG/DIGITAL INPUTS AND OUTPUTS
  - PERFORMS A-TO-D AND D-TO-A DATA CONVERSIONS
- PROVIDES TIMING FOR THE CONTROL LOOP

### FEATURES:

- 16SE/8DI ANALOG INPUTS WITH 12-BIT A/D CONVERSION
- 2 ANALOG OUTPUTS WITH 12-BIT D/A CONVERSION
- 16 LINES OF DIGITAL INPUT AND OUTPUT
- INTERNAL PROGRAMMABLE CLOCK
- EXTERNAL TRIGGER
- EXTERNAL CLOCK

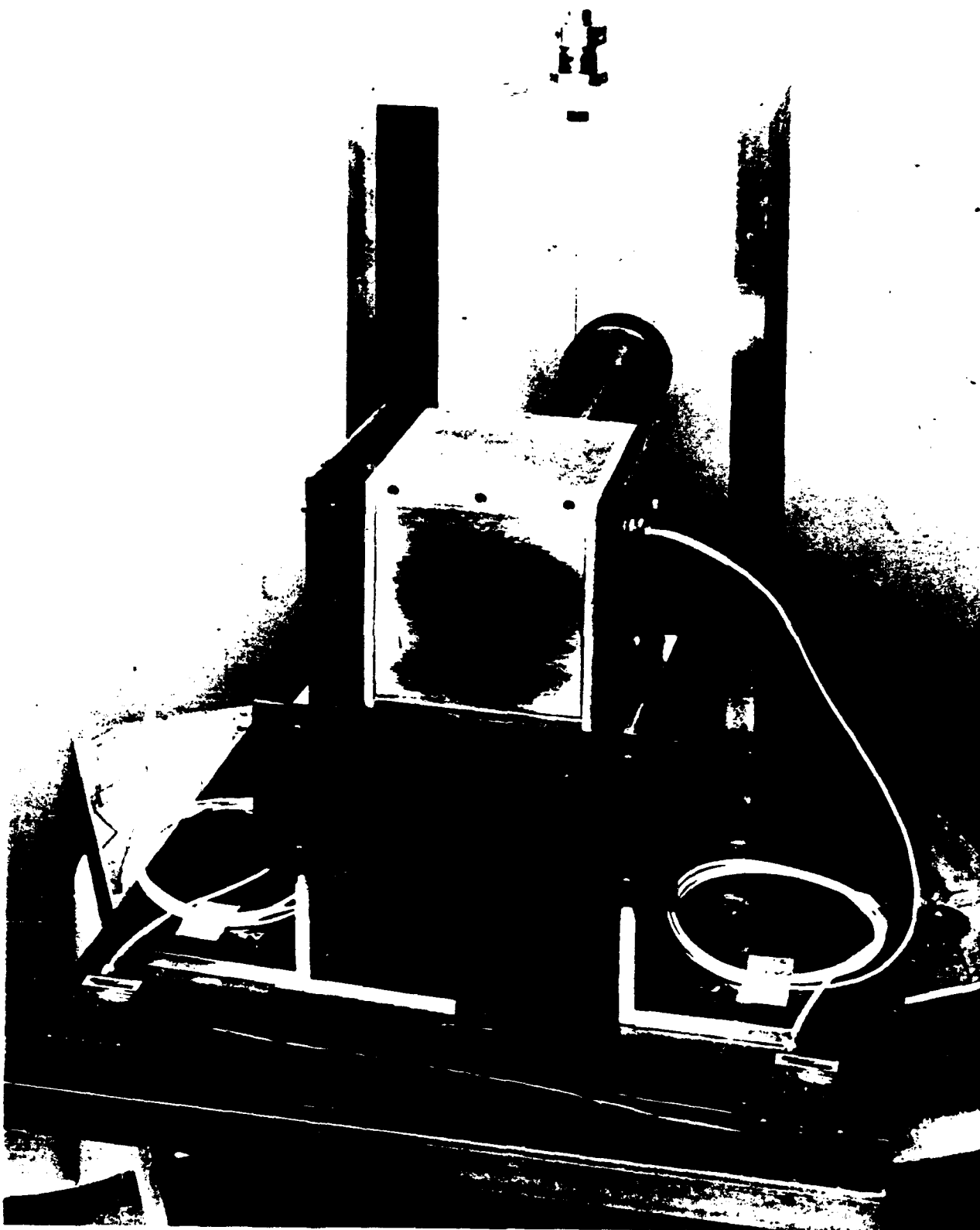


Fig. 1. Magnetic Isolation Test Facility

**SYSTEM BLOCK DIAGRAM**

Figure 2.

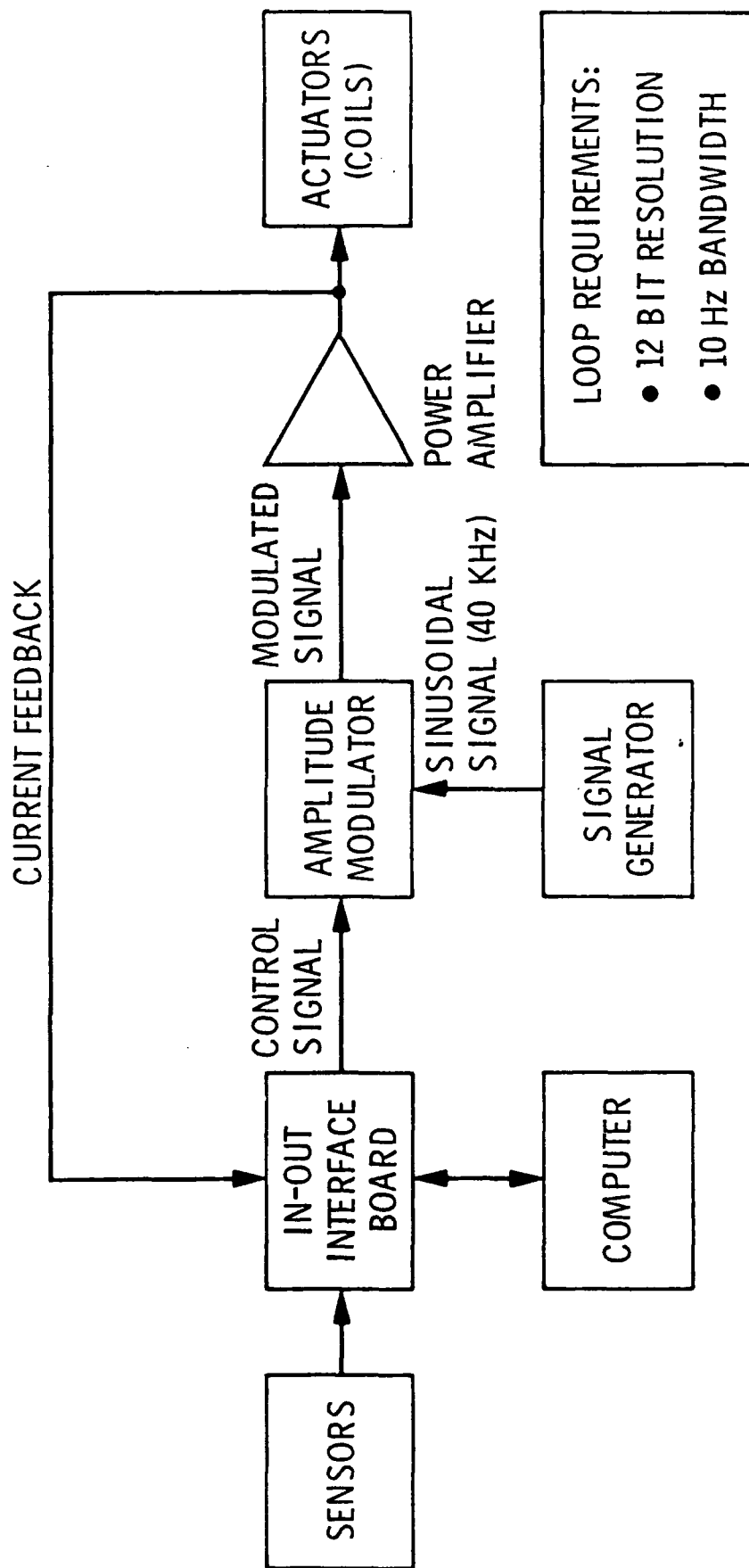


Figure 2.



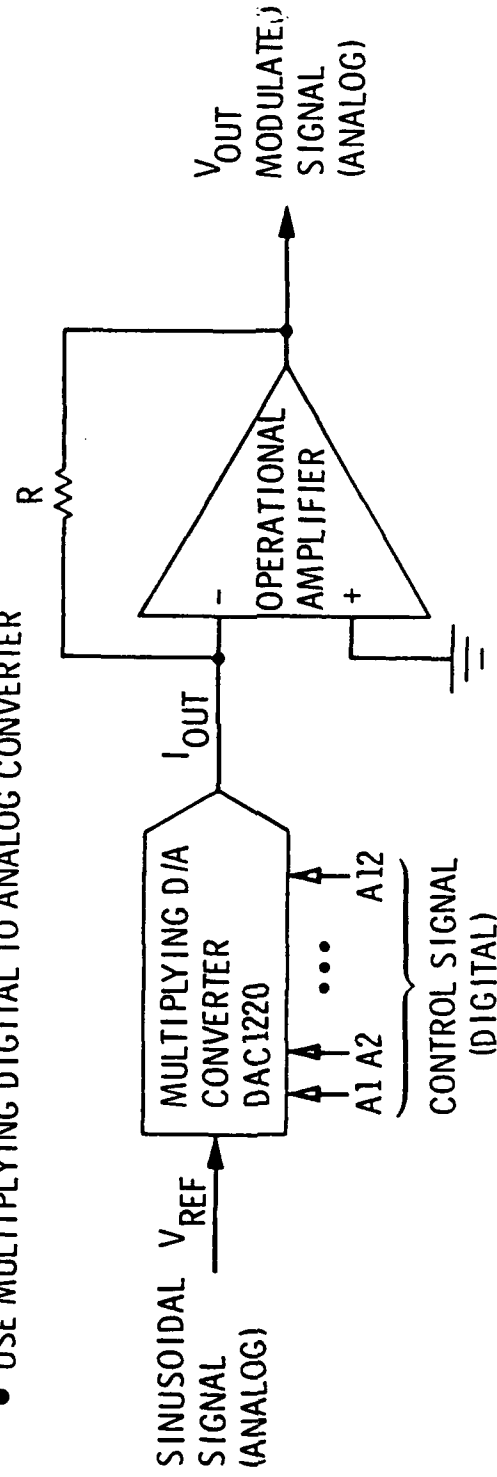
## AMPLITUDE MODULATOR

### FUNCTION:

- PERFORMS THE FOLLOWING PRODUCT:  
(MODULATED SIGNAL) = (CONTROL SIGNAL) x (CONSTANT AMPLITUDE SINUSOIDAL SIGNAL)

### APPROACH:

- USE MULTIPLYING DIGITAL TO ANALOG CONVERTER



$$V_{OUT} = -V_{REF} \left( \frac{A1}{2} + \frac{A2}{4} + \frac{A3}{8} + \dots + \frac{A12}{4096} \right)$$

$$-10V \leq V_{REF} \leq 10V$$

WHERE  $A_N = 1$  IF AN DIGITAL INPUT IS HIGH  
 $A_N = 0$  IF AN DIGITAL INPUT IS LOW

Figure 3.

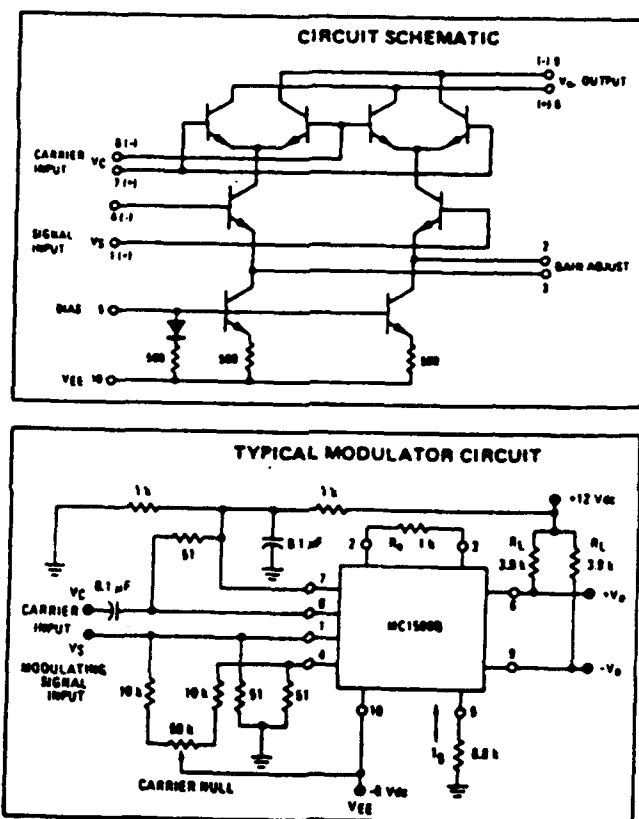
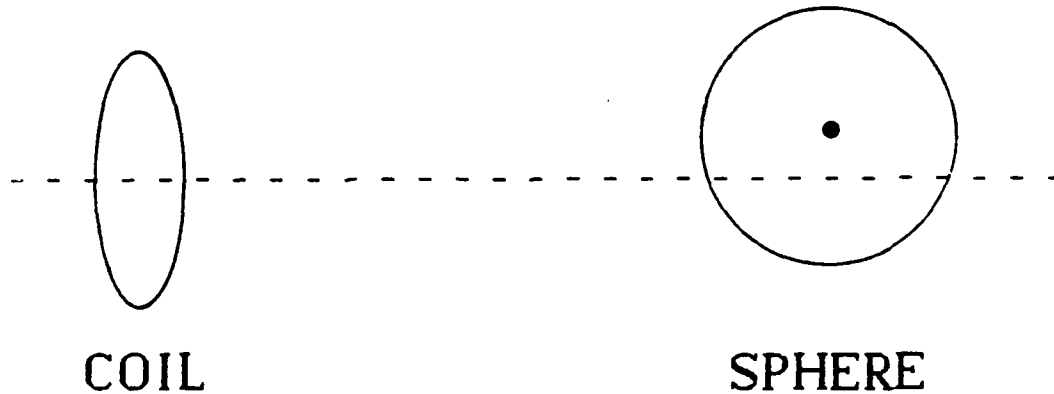


Figure 4.  
Analog Modulator

Figure 5.

## EDDY CURRENT ANALYSIS



Force: Zero Order - Away from Coil  
First Order - Toward Axis

Torque: Zero Order - None  
First Order - Roll Toward Coil

Dissipation: No First Order

LABORATORY G(R) EXPERIMENT - PROGRESS REPORT\*

by

Dr. Dan Long  
Department of Physics  
Eastern Washington University  
Cheney, WA 99004

ABSTRACT

I report on progress in the three areas of vibrations, the optical lever, and the isothermal environment. All vibrating machinery has been decoupled from the laboratory floor and supported from the second floor above. The apparatus table has been rigidified against low frequency vibrations. Preliminary measurements indicate a reduction of about a factor of 4 of unwanted vibrations coupling into the torsion pendulum. The new optical lever is now fully operational. It appears to have a 5 part per ten thousand per hour drift which cannot be traced to a particular cause such as the light source power supply. I suspect long term deformation of the light bulb filament is taking place. This drift should present no measurement problem, but is disappointing. Construction of a new (fireproof) isothermal insulation jacket for the apparatus is now in progress along with the construction of the thermal regulation device. I hope to report on a fully operational signal to noise ratio at the conference.

\* Work supported by AFGL Contract No. F19628-86-K-0014.

LABORATORY G(R) EXPERIMENT - PROGRESS REPORT

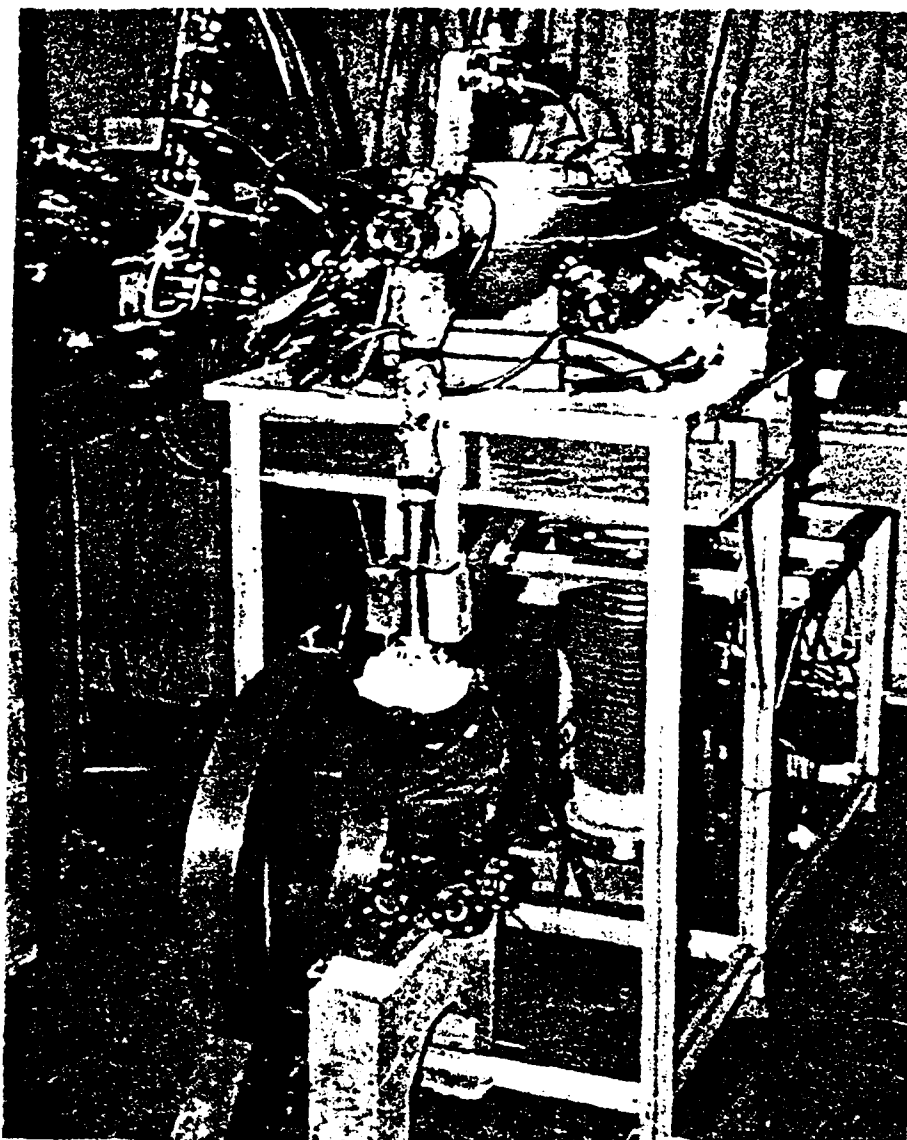
February 1987

DANIEL R. LONG, Ph.D  
Professor of Physics  
Eastern Washington University  
Cheney, Washington 99004

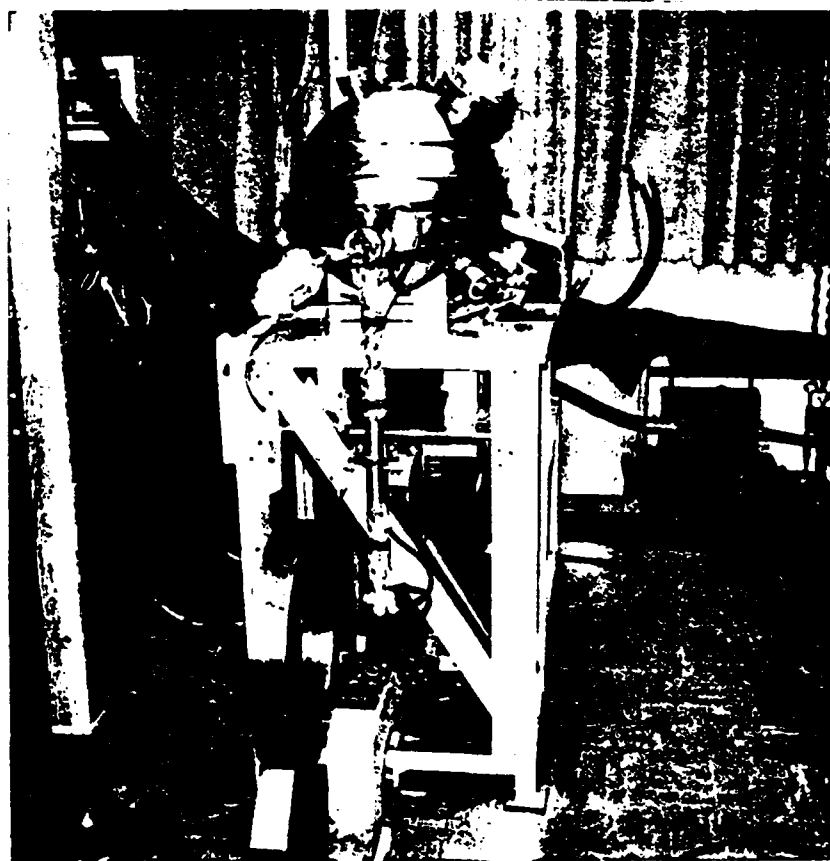
Work supported by AFGL

Contract No. F 19628-86-K-0014

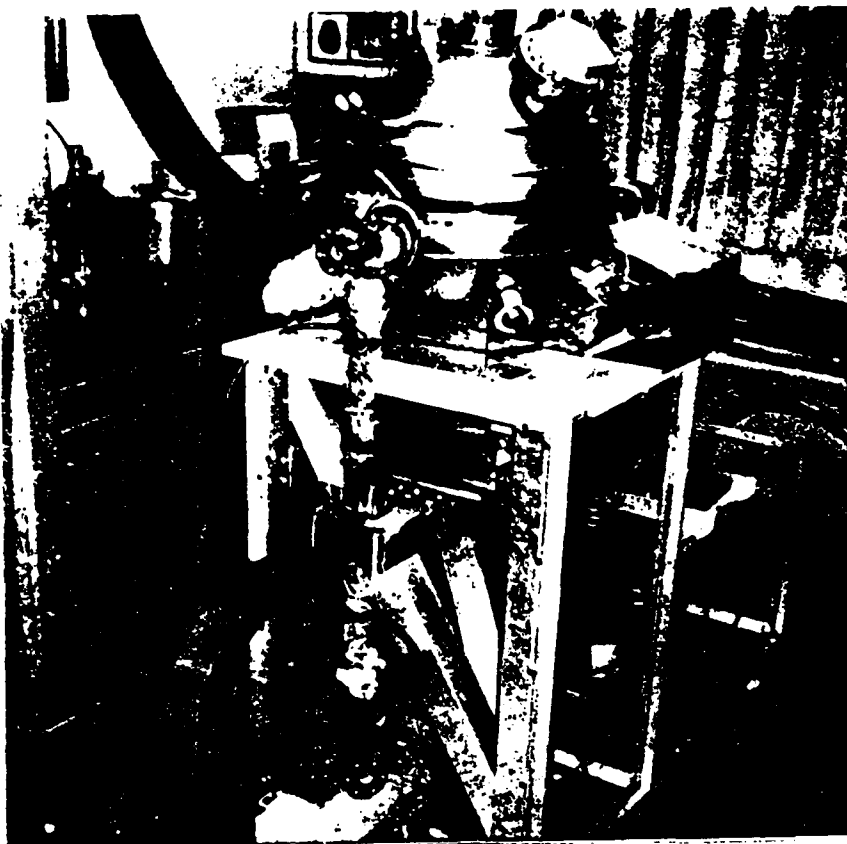
I report on progress in overhauling and improving the Eastern Washington University Cavendish Torsion Balance. Recent improvements, mainly funded by AFGL, are illustrated in the following slides presented at the conference. These substantial modifications addressed reducing the effects of tilt on the output signal, reducing vibrations, and improving thermal stability. The last illustration shows the gravitational force signal now put out by the apparatus. It indicates about a 2 part per ten thousand torque signal stability. This is about a factor of 10 improvement over previous work.



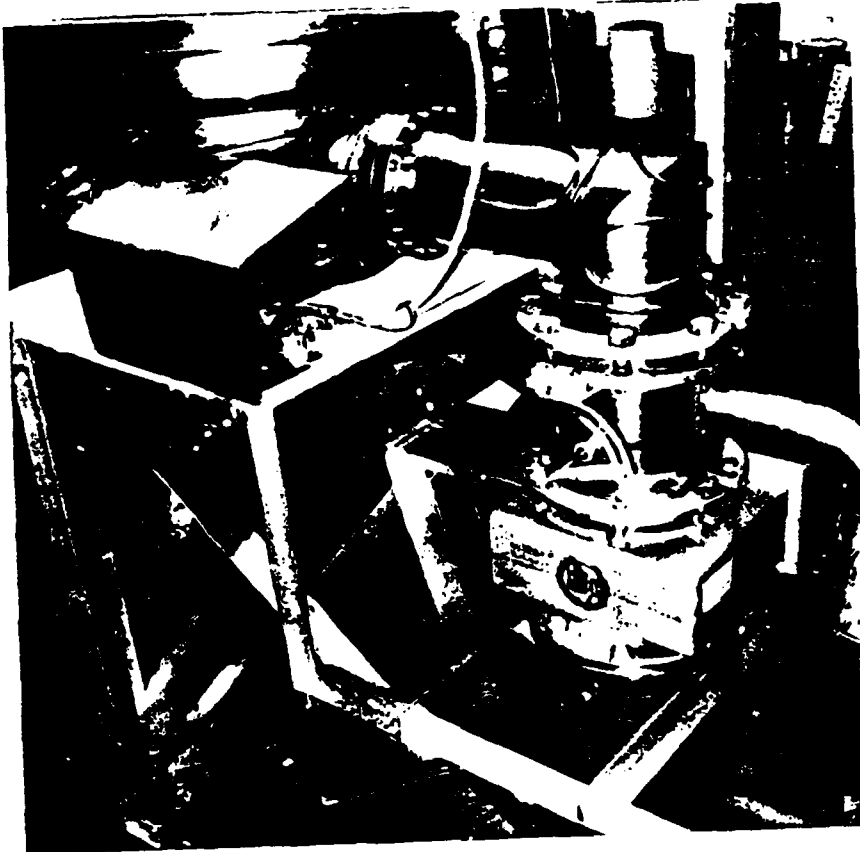
View (1) The entire apparatus with ring masses in view. Note the thin aluminum legs which are reinforced in the next picture.



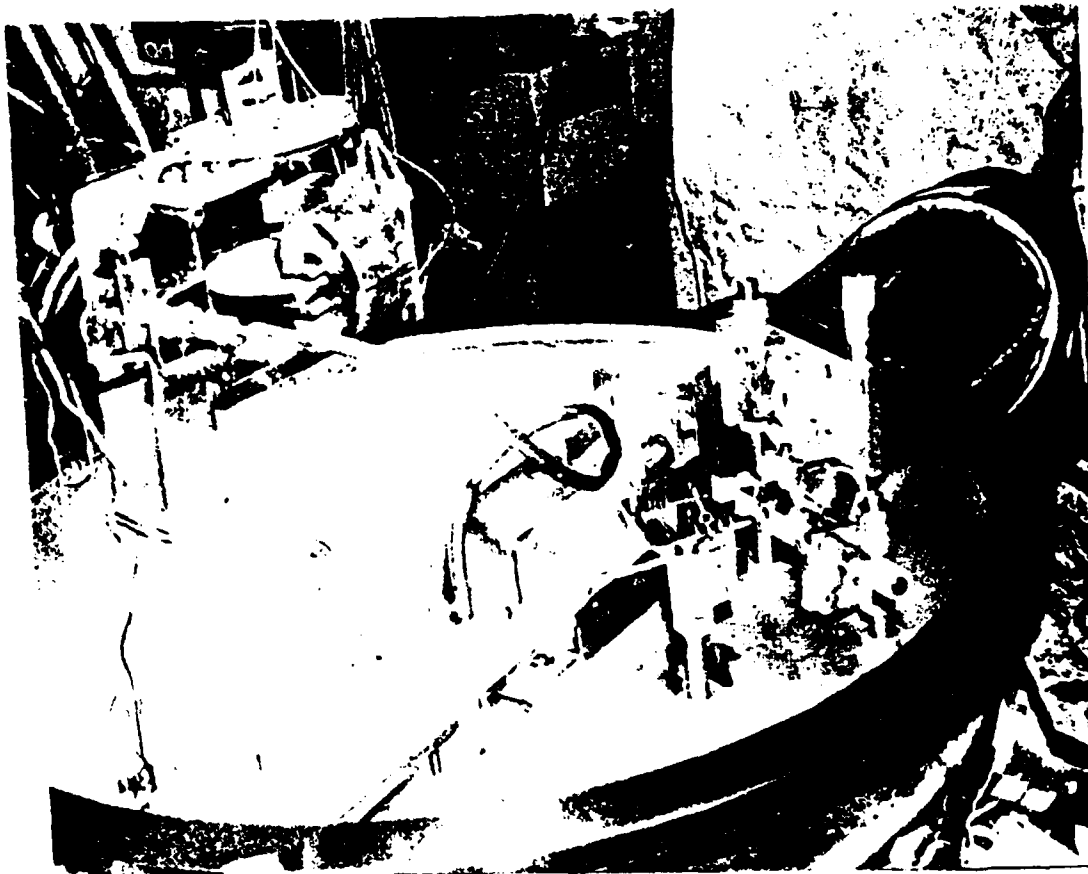
View (2) 3 x 3 x 1/2 aluminum angle has been used to reinforce the frame. The 1/2" aluminum plate below the main table was later loaded with 200 lbs of lead.



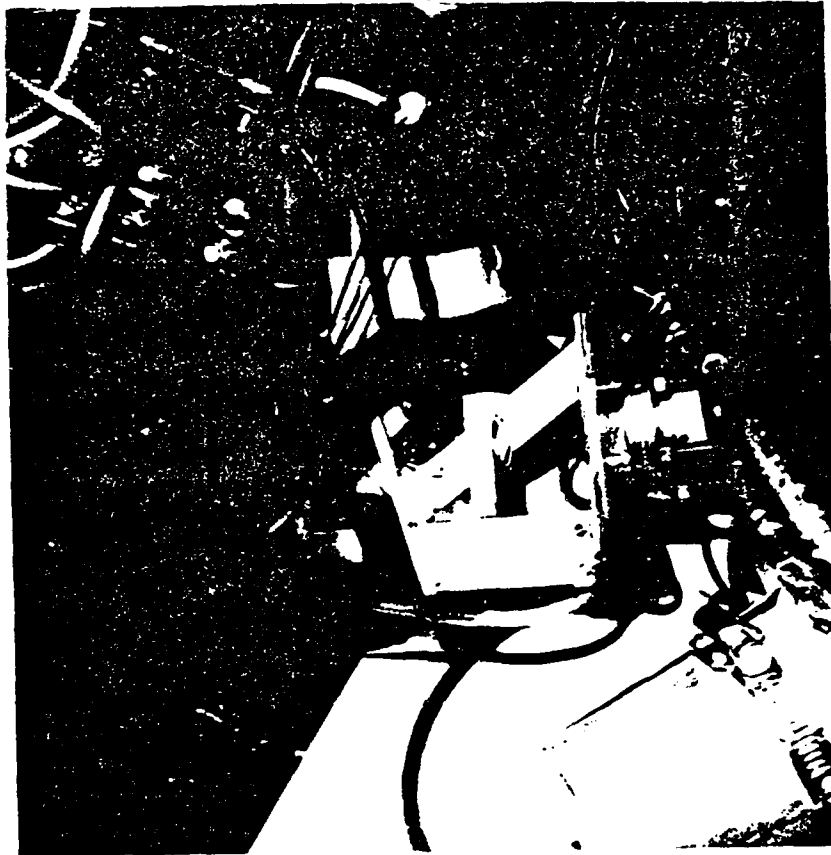
View (3) A view of the frame showing the cross reinforcing.



View (4) A further view from the rear showing the cross reinforcing.



View (5) The new, tilt proof, optical lever of quasi auto collimator design can be seen in the right portion of the photo.



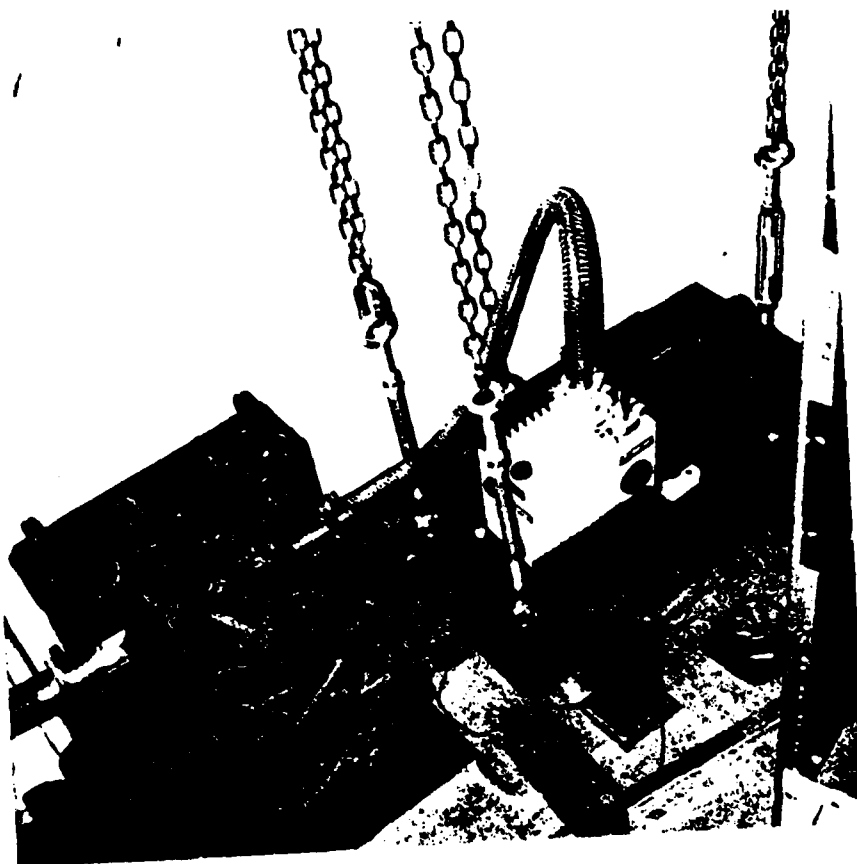
View (6) The new optical lever features a newly constructed external light source and fiber optics. This reduces temperature drift in the vacuum chamber.



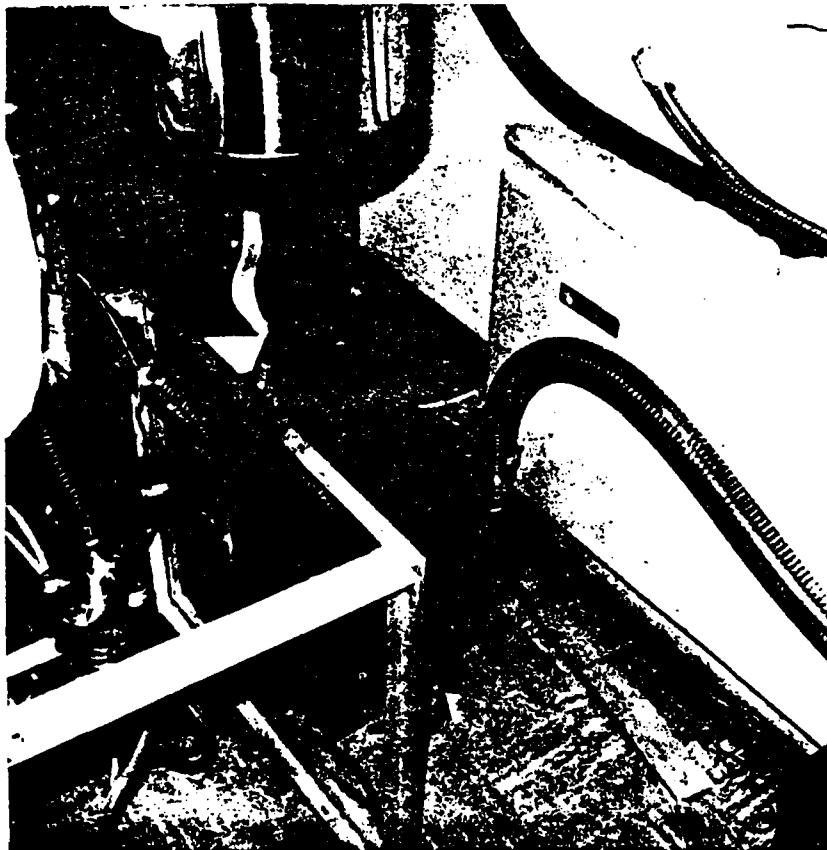
View (7) The fan for cooling the optical lever light source is mounted on the I beams of the second floor above to provide vibrational isolation. The 4 x 4 in the picture can exert a few tons against the second floor to tilt the floor and apparatus at will, without introducing further gravitational masses near the apparatus.



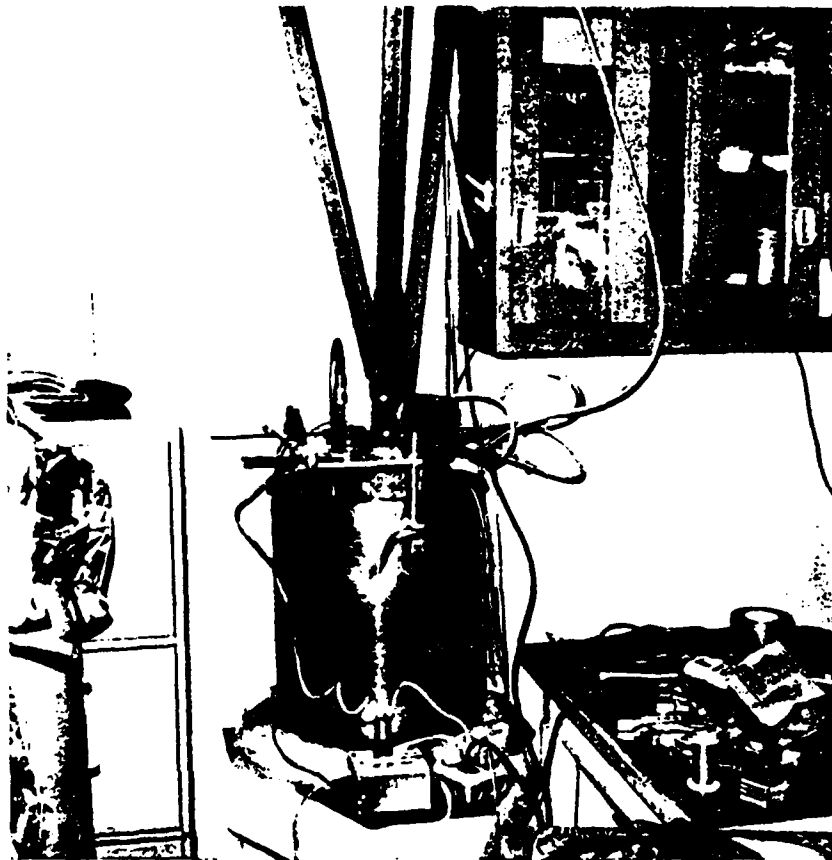
View (8) The newly constructed, thermally, and electrically shielded output box for the optical lever.



View (9) The fore pump is mounted on 300 lbs of steel suspended from the second floor above by chains. The vacuum hose goes to 500 lbs of scrap steel which markedly reduces vibrations.



View (10) After leaving the 500 lbs inertial block mass, the fore-line hose goes to a 400 lbs mass mounted on lead bricks.



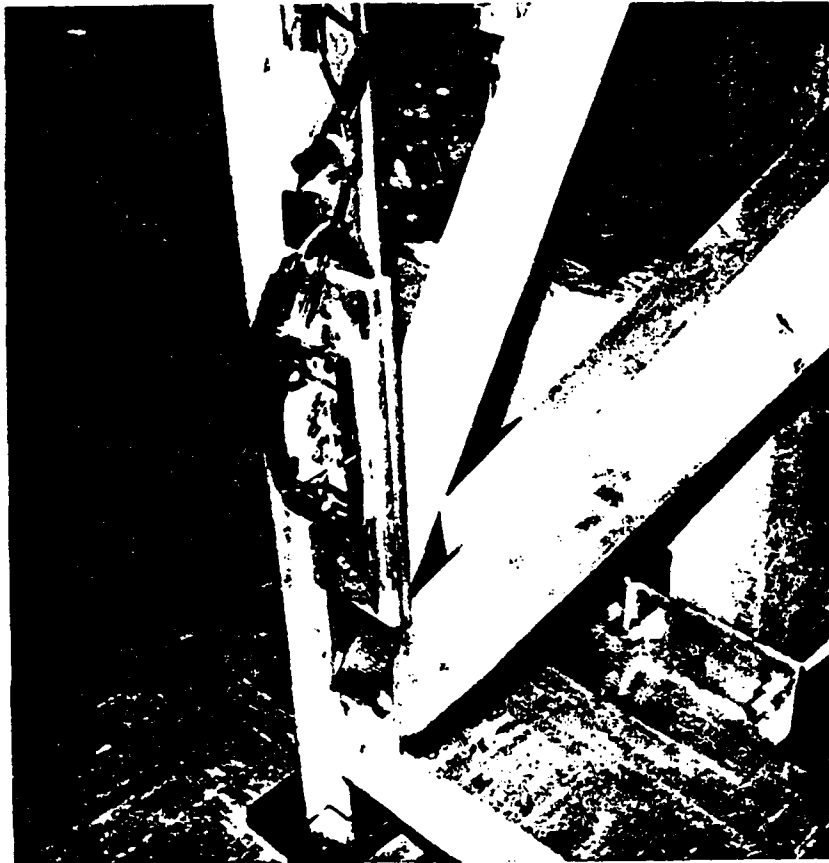
View (11) The newly constructed isothermal water bath needed to supply the diffusion pump with constant temperature water has several vibrating components. These are mounted on the angle iron seen hanging down.



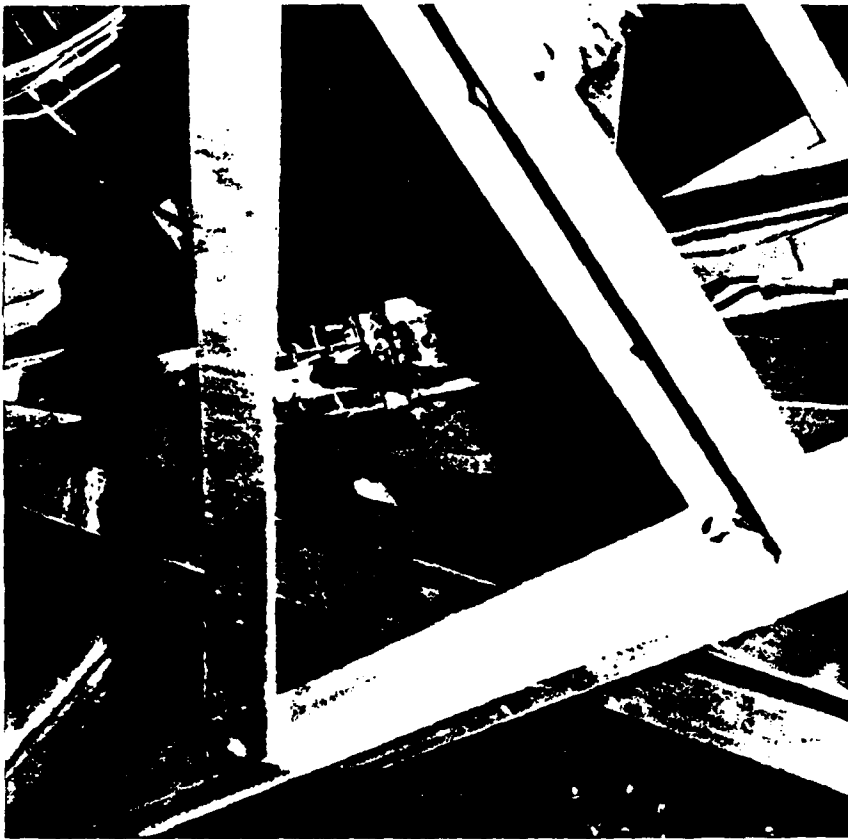
View (12) The water bath angle iron proceeds through the ceiling to the second floor I beams above.



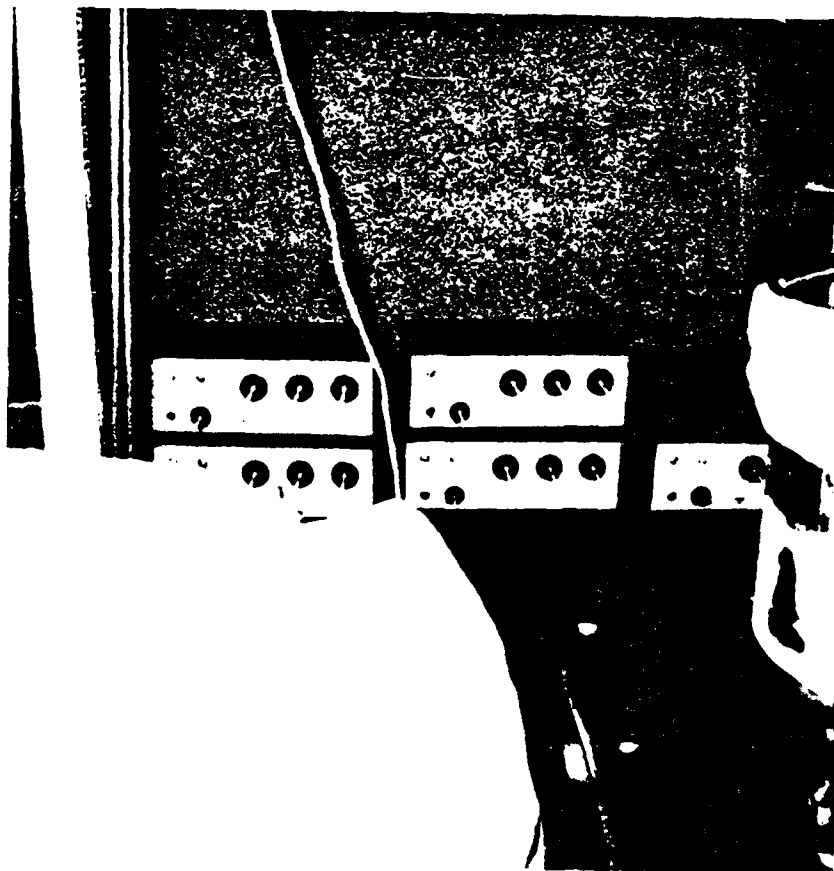
View (13) Heater and control thermister with fail-safe thermostat mounted on the 6 inch exhaust pipe of the main vacuum chamber.



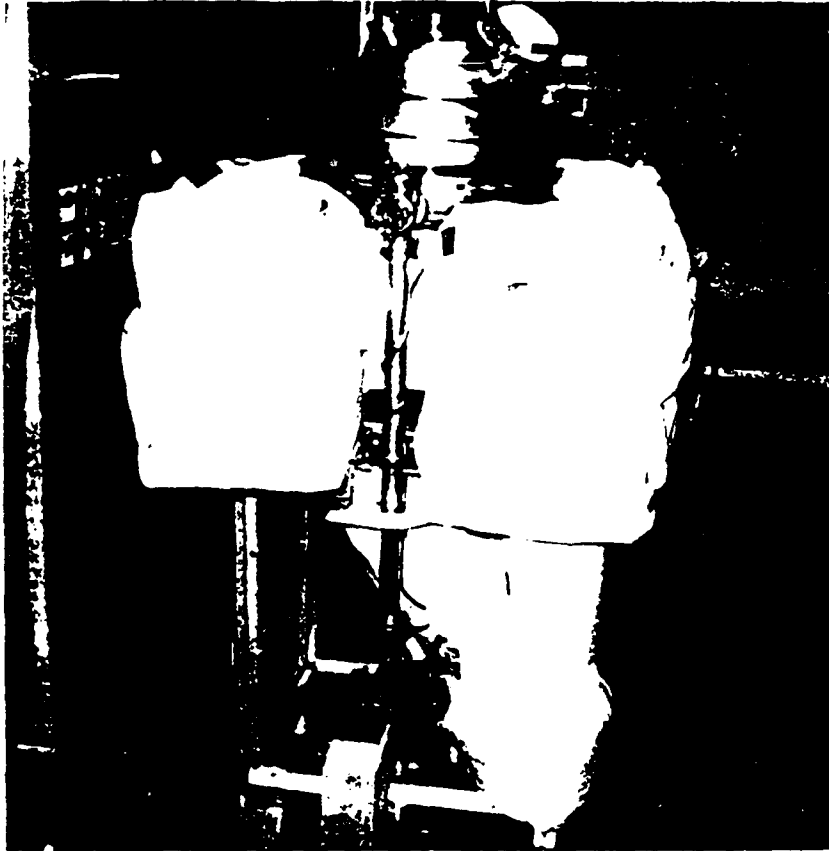
View (14) Heater and control thermister with fail-safe thermostat mounted on the North-East leg.



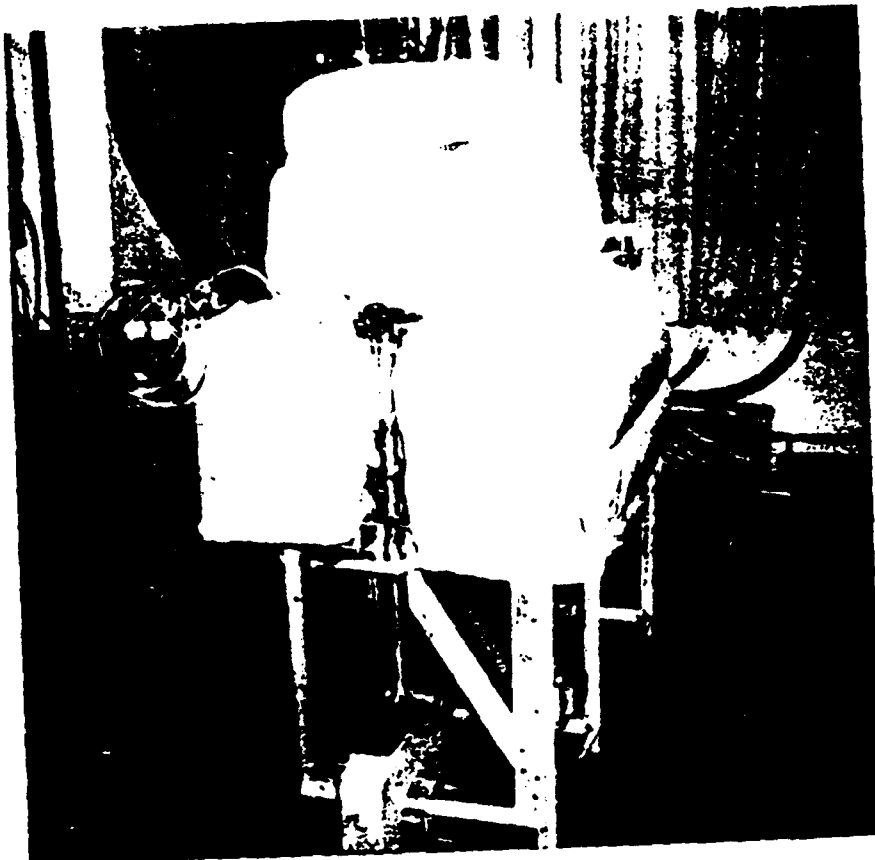
View (15) Heater and control thermister with fail safe  
thermostat mounted on the West leg.



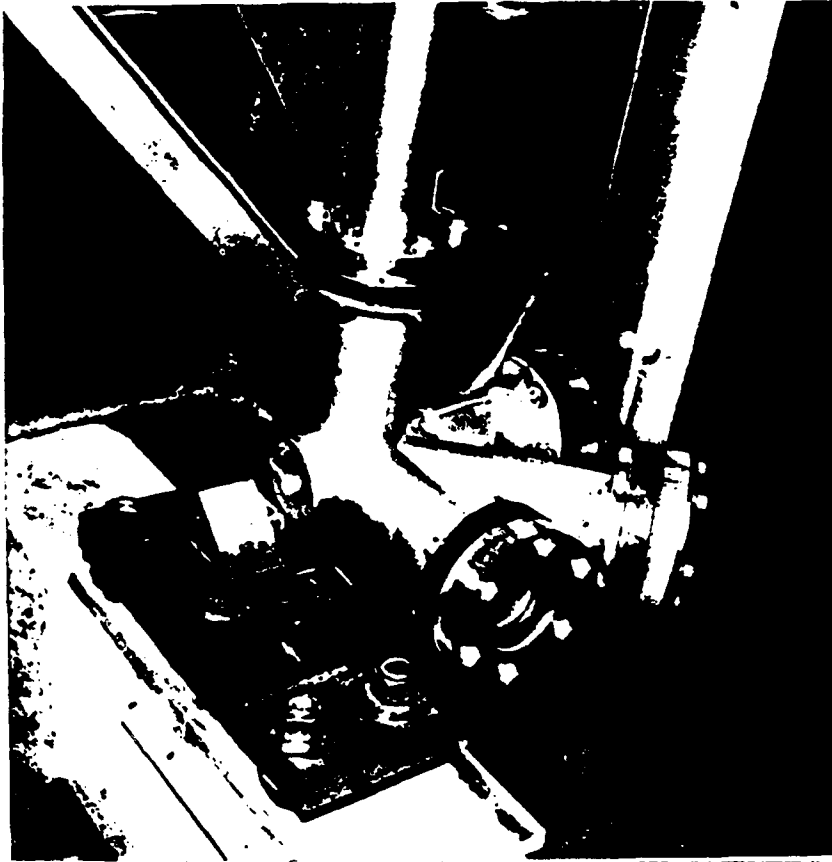
View (16) The five  $0.01^{\circ}\text{C}$  Yellow Springs Instrument Company thermal controllers used to control power to the heaters.



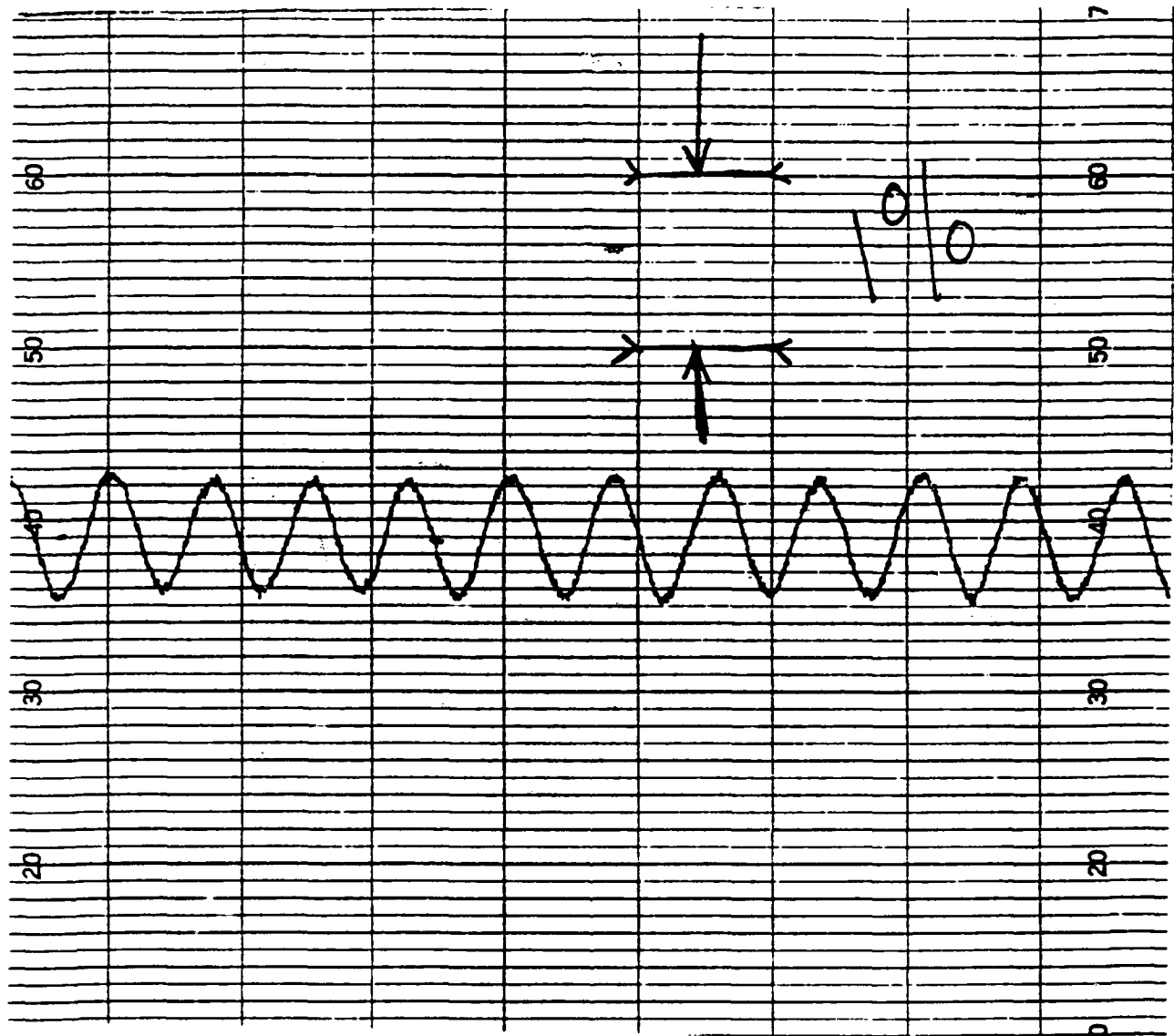
View (17) Newly constructed, fire proof, fitser glass fabric and  
fitser glass felled insulation.



View (18) Insulation of the sphere top. An additional 6 inch hood covers what is seen. Preliminary results suggest  $0-001^{\circ}\text{C}$  stability over a few hours.



View (19) A thermister shown on the side of the attracted ball chamber. This thermister will monitor any changes in temperature produced by introducing the attracting masses near the chamber. 18 thermisters have been mounted on the apparatus.



View (20) Strip chart trace of the optical lever output of the gravitational signal. 10 intervals is 1% of the ring torque signal. The centroid of the sine wave seems stable to 2 or 3 parts per ten thousand of the ring torque.